



HAL
open science

Kinetics of transport influenced reactions in complex media: from memory effects to compartmentalized environments

Toni Vieira Mendes

► **To cite this version:**

Toni Vieira Mendes. Kinetics of transport influenced reactions in complex media: from memory effects to compartmentalized environments. Physics [physics]. Université de Bordeaux, 2023. English. NNT: 2023BORD0303 . tel-04501039

HAL Id: tel-04501039

<https://theses.hal.science/tel-04501039v1>

Submitted on 12 Mar 2024

HAL is a multi-disciplinary open access archive for the deposit and dissemination of scientific research documents, whether they are published or not. The documents may come from teaching and research institutions in France or abroad, or from public or private research centers.

L'archive ouverte pluridisciplinaire **HAL**, est destinée au dépôt et à la diffusion de documents scientifiques de niveau recherche, publiés ou non, émanant des établissements d'enseignement et de recherche français ou étrangers, des laboratoires publics ou privés.



THÈSE PRÉSENTÉE
POUR OBTENIR LE GRADE DE
DOCTEUR
DE L'UNIVERSITÉ DE BORDEAUX

ÉCOLE DOCTORALE SCIENCES PHYSIQUES ET DE L'INGÉNIEUR
SPÉCIALITÉ LASERS, MATIÈRE ET NANOSCIENCES

Par **Toni VIEIRA MENDES**

Cinétique des réactions influencées par le
transport en milieu complexe :
des effets de mémoire aux environnements compartimentés

Sous la direction de : **Thomas GUÉRIN**

Soutenue le 13 novembre 2023

Membres du jury :

M. GREBENKOV, Denis	Directeur de recherche, CNRS, LPMC	Rapporteur
M. RANDON-FÜRLING, Julien	Professeur, ENS Paris-Saclay	Rapporteur
M. BICKEL, Thomas	Professeur, Université de Bordeaux	Examineur
M. FOURNIER, Jean-Baptiste	Professeur, Université Paris-Cité	Examineur
M. MAJUMDAR, Satya	Directeur de recherche, CNRS, LPTMS	Examineur
M. GUÉRIN, Thomas	Chargé de recherche, CNRS, LOMA	Directeur de thèse

Cinétique des réactions influencées par le transport en milieu complexe :
des effets de mémoire aux environnements compartimentés

Résumé : Dans cette thèse, nous caractérisons les propriétés du temps de réaction (défini comme le temps mis par un marcheur aléatoire pour trouver un cible potentiellement partiellement réactive) dans trois situations rendues complexes soit par les propriétés de transport (marches aléatoires à mémoire) ou par la géométrie du problème (espaces avec compartiments, cibles multiples). En premier lieu, nous étudions les réactions dites imparfaites, pour lesquelles de multiples rencontres avec la cible peuvent être nécessaires avant d'obtenir une réaction. Nous développons un formalisme qui détermine le temps moyen de réaction pour un marcheur aléatoire à mémoire cherchant une cible imparfaite, décrite soit par un taux de réaction dépendant de l'espace ou par le fait que la cible n'est réactive que de manière intermittente. Nous trouvons que, pour des processus suffisamment sous-diffusifs, la première contribution du transport au temps de réaction diverge pour les faibles réactivités, à cause des effets de mémoire. Cette divergence est associée à un exposant non-trivial que nous calculons analytiquement et vérifions par des simulations numériques. Ensuite, dans le cas de réactions parfaites, nous étudions les effets de mémoire pour les réactions compétitives, à deux cibles. Nous développons une théorie pour calculer la probabilité de splitting (définie comme la probabilité de toucher une cible avant l'autre cible). Nous vérifions les résultats de notre théorie en la comparant à des observations expérimentales de trajectoires de billes se mouvant dans des fluides viscoélastiques. Ces expériences prouvent que, à l'instant du temps de réaction, le système est hors de l'équilibre, à cause des effets de mémoire. Finalement, nous étudions les réactions parfaites dans des milieux compartimentés. Nous calculons le temps moyen de premier passage d'un marcheur aléatoire Markovien cherchant une cible au centre d'un compartiment fractal, où le mouvement est sous-diffusif, immergé dans un domaine où le mouvement est diffusif. Nous validons nos résultats théoriques par des simulations stochastiques et déterminons dans quelles conditions le temps moyen de réaction peut être optimisé par la présence du compartiment.

Mots-clés : processus stochastiques, temps de premier passage, réactions imparfaites, marches non-Markovien, milieux viscoélastiques, diffusion en milieu fractal

Kinetics of Transport-Influenced Reactions in Complex Media:
from memory effects to compartmentalized environments

Abstract: In this thesis, we characterize the properties of the reaction time (defined as the time needed by a random walker to find a target that is potentially partially reactive) in three situations that are complex, either due to the transport properties (non-Markovian random walks) or due to the geometry of the problem (compartmentalized spaces, multiple targets). First, we study imperfect reactions, where many encounters with the target might be necessary before a reaction happens. We develop a general formalism that provides the mean reaction time for non-Markovian processes searching for imperfect targets, where imperfectness comes from sink reactivity and/or gated reactions. We find that, if a process is strongly subdiffusive, the first transport contribution to the mean reaction time diverges for small reactivity, as a consequence of memory. This divergence is characterized by a non-trivial exponent that we analytically identify and verify with simulations. Then, in the case of perfect reactions, we study the effect of memory in competitive reactions with two targets. We develop a theory to calculate the splitting probability (the probability to touch one target before the other) for non-Markovian Gaussian processes. We validate our theoretical results by comparing them to the experimental observation of beads moving in a viscoelastic fluid. These experiments prove that, at the reaction time, the system is out-of-equilibrium, due to memory effects. Finally, we study perfect reactions in crowded compartmentalized media. We calculate the mean first passage time for a Markovian random walker to a target located in the center of a fractal compartment, in which the motion is subdiffusive, embedded into a domain where the motion is diffusive. We verify that our theory is consistent with stochastic simulations and determine in which conditions the mean reaction time can be optimized by the presence of a compartment.

Keywords: stochastic processes, first passage times, imperfect reactions, non-Markovian walks, viscoelastic media, diffusion in fractals

ACKNOWLEDGMENTS

In first place, I would like to express my deepest gratitude to my supervisor Thomas Guérin for the continuous support and invaluable guidance throughout this thesis. Your enthusiasm, motivation, availability, and patience were without a doubt essential to the success of these three years.

I would also like to extend my deepest gratitude to the members of the jury for agreeing to participate in the evaluation process: Denis Grebenkov, Julien Randon-Fürling, Thomas Bickel, Jean-Baptiste Fournier and Satya Majumdar.

I could not have undertaken this journey without the support of my friends from Portugal, to whom I express my warmest thanks: Daniela, Ângela, Bia, Mara, and all the others, from the choir, from the orchestra, from the school. Equally important, was the support from inside the office, Bhavesh and Maryam (yes, I am including you in our office), you were a fundamental key during these last three years. To all the other friends and colleagues that I have made and met in Bordeaux, Adeline, Arthur, Benjamin, Jonny, Juliette, Pascale, Sotiris, Thibaut, at some point or another, all of you have been important for me to call Bordeaux “home”.

Finally, but certainly not the least, I have to thank my parents and my brother. Mami, Papi, André, é escusado dizer que sem vocês não teria sido possível. Sou-vos grato por tudo.

RÉSUMÉ DES RÉSULTATS

This thesis summary, in French, is placed here to comply with the instructions of the doctoral school. An english version of the summary can be found in Chapter 2 (Section 2.3).

Considérons un marcheur aléatoire, qui, à chaque fois qu’il passe à proximité d’une cible, a une probabilité d’induire un événement, ou de “réagir”. Cette situation est, au sens large, celle des réactions influencées par le transport. Elle est pertinente pour la description des réactions chimiques (les réactants doivent se rencontrer avant de réagir, et ne réagissent pas nécessairement à chaque contact) mais aussi dans d’autres contextes comme la recherche d’une cible sur l’ADN, la captation de nutriments par des récepteurs membranaires, le calcul du risque d’être ruiné avant d’atteindre un certain profit, la cinétique la décharge d’un neurone une fois que le voltage dépasse un seuil, etc. Lorsque la réaction a lieu chaque fois que la cible est atteinte, elle est dite parfaite, et le problème est celui d’un premier passage.

Le but de cette thèse est de comprendre comment les propriétés de transport et de réactivité influencent les cinétiques de réaction pour trois exemples de situations complexes, pour des mouvements complexes du marcheur lui-même (mouvement à mémoire) ou en présence de géométrie complexe (plusieurs cibles, compartiments). De nombreuses études ont porté sur les propriétés de premier passage de processus stochastiques complexes dans les dernières décennies ([Redner, 2001](#); [Bray et al., 2013](#); [Metzler et al., 2014](#)), motivées en partie par les nombreuses observations de mouvement aux propriétés anormales dans les milieux biologiques ou les fluides complexes ([Bressloff and Newby, 2013](#); [Höfling and Franosch, 2013](#)), posant la question de comprendre si ces propriétés de transport complexe se transfèrent aux propriétés de réactivité. Cependant, certains aspects demeurent inexplorés et seront l’objet de cette thèse.

Le premier problème considéré est celui de l’effet de la mémoire et de la réactivité imparfaite sur les cinétiques de réaction. La mémoire apparaît dès lors que le marcheur aléatoire interagit avec d’autres variables, et peut être considérée comme la règle plutôt que l’exception ([van Kampen, 1998](#)). Le fait que la réaction ne soit pas parfaite semble aussi une propriété usuelle ([Grebekov, 2019](#)), et pourtant il n’existe pas de théorie prédisant les cinétiques de réactions imparfaites pour des variables à mémoire. Ce sera l’objet de la première partie de cette thèse.

Dans la seconde partie, nous étudions le problème des réactions compétitives (en présence de deux cibles) pour les processus à mémoire. Pour les processus à mémoire, les théories existantes reposent sur des développements perturbatifs (faible mémoire) ([Wiese, 2019](#)) ou des lois d’échelles pour des processus invariants d’échelle ([Majumdar et al., 2010](#)), et nous allons décrire une théorie non-perturbative permettant de prédire la probabilité d’atteindre une cible plutôt qu’une autre. Nous allons aussi étudier cette situation expérimentalement, ce qui nous permettra d’établir expérimentalement que l’état d’un système au premier passage n’est pas un état d’équilibre.

Enfin, la troisième partie sera consacrée à l'étude des réactions en présence de compartiments. Bien que la présence de compartiments dans les cellules soit couramment observée, les théories existantes de premier passage supposent des mécanismes de transport diffusifs au sein de ces compartiments, et nous les généraliserons au cas de transport anormal (fractal, nous nous limiterons au cas de processus sans mémoire, l'espace lui-même présentant déjà un certain degré de complexité).

Influence de la mémoire sur la cinétique de réactions imparfaites en confinement

Dans un premier temps, nous étudions les cinétiques de réaction imparfaites pour des processus aléatoires à mémoire. La mémoire est une propriété importante qui apparaît dès lors que la dynamique du marcheur considéré résulte de l'interactions avec d'autres degrés de liberté, cachés ou non, dans son environnement. Un exemple classique est celui du mouvement d'un monomère, les variables cachées étant les autres monomères. Comme la mémoire provient des interactions avec d'autres variables, sa présence pourrait être pensée comme la règle plutôt que l'exception. Pourtant, la majorité des théories de premier passage s'est concentrée sur les processus sans mémoire. Récemment, des théories ont été proposées pour décrire l'effet de la mémoire sur les premiers passages; cependant ces théories décrivent uniquement des réactions parfaites. Pourtant, le fait qu'une cible possède une réactivité finie, de telle sorte qu'une réaction ne se passe pas nécessairement au premier contact, pourrait également être pensé comme la règle plutôt que l'exception. L'effet de la réactivité imparfaite sur les cinétiques de réaction a jusqu'à présent été exploré uniquement pour des processus sans mémoire. Dans la première partie de cette thèse, nous nous attachons à décrire une théorie qui tienne compte à la fois des effets de mémoire et de la réactivité finie, afin de déterminer si la combinaison de la mémoire finie et réactivité finie donne des propriétés particulières aux cinétiques de réaction.

Dans le chapitre 3, *Kinetics of Imperfect Reactions for non-Markovian Walkers in Confinement*, nous nous intéressons au problème du temps que met un marcheur aléatoire se mouvant dans un espace à une dimension $x(t)$, pour réagir avec une cible en position $x = 0$ qui est imparfaitement réactive, ce que nous décrivons par un taux de réaction dépendant de l'espace $k(x) = \kappa \delta(x)$ qui est pris comme étant ponctuel dans un premier temps. Nous supposons que le marcheur, en l'absence de cible, est en espace confiné, de telle sorte qu'il existe une probabilité de présence à l'état stationnaire $p_s(x)$, permettant de définir un volume effectif $V = 1/p_s(0)$ (égal au volume géométrique lorsque p_s est uniforme).

Notre premier résultat est une expression générale du temps moyen de réaction, valide lorsque la trajectoire de x est continue mais "rugueuse" ($\langle \dot{x}^2 \rangle = \infty$), auquel cas le temps moyen de réaction (noté $\langle RT \rangle$), étant donné que RT représente le "Reaction Time" en anglais)

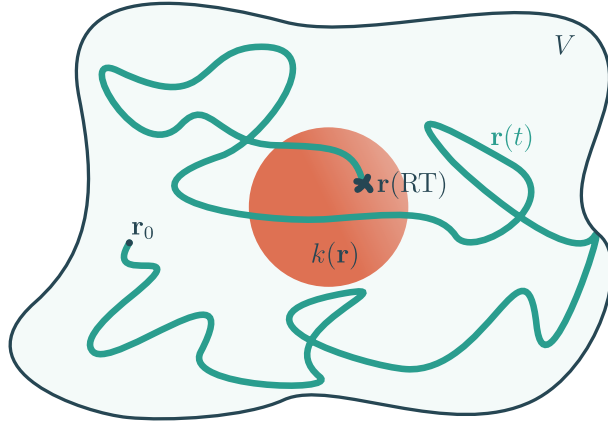


Figure 1: **Schéma du problème de réactivité imparfaite.** Un marcheur aléatoire $\mathbf{r}(t)$ se déplace dans un espace confiné de volume V en présence d'une cible imparfaitement réactive, présentant un taux de réaction $k(\mathbf{r})$. Combien de temps doit-on attendre avant d'obtenir une réaction ? Ce temps est connu comme le temps de réaction.

est donné par la formule exacte

$$\frac{\langle \text{RT} \rangle}{V} = \frac{1}{\kappa} + \int_0^\infty dt [p_\pi(0, t) - p(0, t)], \quad (1)$$

où $p(x, t)$ est la densité de probabilité de présence à la position x à t en l'absence de réaction, et $p_\pi(x, t)$ est la densité de probabilité de présence du processus stochastique $x_\pi(t) = x(t + \text{RT})$ dans le futur de la réaction.

Pour être plus explicite, nous supposons que, loin des bords du volume, la marche aléatoire est à incrément stationnaires (pas de vieillissement) et suit une statistique Gaussienne. L'hypothèse de Gaussiannité est forte, mais de nombreux exemples de processus non-Markoviens sont néanmoins Gaussiens (en dynamique des polymères ou d'interfaces, ou pour des billes traceurs en milieu viscoélastique par exemple). Les propriétés de transport sont alors spécifiées par le déplacement quadratique moyen $\psi(\tau) = \langle (x(t + \tau) - x(t))^2 \rangle$. Nous supposons que $\psi(t) \simeq Kt^{2H}$ aux temps longs, avec $0 < H < 1$, ce qui signifie que le marcheur, en l'absence de confinement, ne reste pas piégé près de la cible mais s'éloigne en explorant l'espace de manière diffusive ($H = 1/2$), sous-diffusive ($H < 1/2$) ou super-diffusive ($H > 1/2$). Dans la limite de grand volume, l'expression du temps de réaction peut être évaluée en supposant que le processus $x_\pi(t)$ est Gaussien, décrit par une moyenne $\mu(t)$ et une covariance approximée par la covariance du processus initial $x(t)$. En utilisant ces hypothèses dans l'équation (1), le temps moyen de réaction devient

$$\frac{\langle \text{RT} \rangle}{V} = \frac{1}{\kappa} + \int_0^\infty \frac{dt}{\sqrt{2\pi\psi(t)}} \left[\exp\left(-\frac{\mu(t)^2}{2\psi(t)}\right) - \exp\left(-\frac{x_0^2}{2\psi(t)}\right) \right], \quad (2)$$

où $x_0 = x(0)$ est la position initiale. Dans cette équation, toutes les variables sont connues, à l'exception de la trajectoire $\mu(t)$. Cependant, il est possible d'obtenir une équation qui

définit $\mu(t)$ de manière auto-cohérente, et qui s'écrit

$$0 = \frac{\mu(\tau)}{\kappa} + \int_0^\infty \frac{dt}{\sqrt{2\pi\psi(t)}} \left[(\mu(t+\tau) - \mu(t)M(t,\tau))e^{-\frac{\mu^2(t)}{2\psi(t)}} - x_0(1 - M(t,\tau))e^{-\frac{x_0^2}{2\psi(t)}} \right], \quad (3)$$

avec

$$M(t,\tau) = \frac{\psi(t+\tau) + \psi(t) - \psi(\tau)}{2\psi(t)}. \quad (4)$$

La résolution de l'équation intégrale (3) permet d'obtenir $\mu(t)$, ce qui donne accès au temps de réaction dans l'équation (2). Jusqu'à présent, cette équation n'avait été obtenue que dans le cas de réactions parfaites ($\kappa \rightarrow \infty$), pour le problème de premier passage.

Plusieurs remarques générales peuvent être faites à partir des équations pour $\langle \text{RT} \rangle$ et $\mu(t)$. Par exemple, le terme $T_{\text{RC}} \equiv V/\kappa$ peut être vu comme un temps de réaction contrôlé par la réaction (RC, "Reaction Controlled"). Pour un processus Markovien, pour une cible ponctuelle, $\langle \text{RT} \rangle - T_{\text{RC}}$ serait directement égal au temps de premier passage. Cependant, notre formalisme indique clairement que cette propriété additive ne tient pas pour les processus à mémoire, car $\mu(t)$ dépend de κ , comme cela peut être vu dans l'équation (3). C'est clairement un effet de mémoire, venant du fait que l'état des degrés de liberté "cachés" (qui sont responsables de la non-Markovianité du marcheur) n'est pas le même à chaque passage du marcheur sur la cible.

Sur la figure 2, nous présentons les résultats de simulations de temps de réaction pour trois processus stochastiques définis par leur déplacement quadratique moyen $\psi(t)$. Nous comparons ces simulations aux prédictions numériques de notre théorie, ainsi qu'aux résultats de l'approximation pseudo-Markovienne (appelée approximation de Wilemski-Fixman dans la littérature), où $\mu(t)$ est approximée par $\mu(t) = 0$. Notre théorie prédit quantitativement les temps moyens de réaction, y compris lorsque l'approche pseudo-Markovienne prédit un temps moyen de réaction infini.

Dans le but de mieux comprendre analytiquement les équations (2) et (3), nous avons obtenu les comportements asymptotiques des trajectoires réactives $\mu(t)$ dans le cas où la marche aléatoire (loin de la cible) est un mouvement Brownien fractionnaire, i.e., $\psi(t) = Kt^{2H}$, et nous trouvons

$$\mu(t) \underset{t \rightarrow \infty}{\sim} \begin{cases} x_0 - \frac{A(\kappa)}{t^{1-2H}}, & H \leq \frac{1}{2} \\ -A(\kappa)t^{2H-1}, & H > \frac{1}{2} \end{cases} \quad \text{et} \quad \mu(t) \underset{t \rightarrow 0}{\sim} \begin{cases} \kappa A(x_0, K, \kappa) t^{2H}, & H \leq \frac{1}{2} \\ \kappa B(x_0, K, \kappa) t, & H > \frac{1}{2} \end{cases}. \quad (5)$$

Il est intéressant de noter que, aux temps longs, pour un processus sous-diffusif $H < 1/2$, la position initiale n'est jamais oubliée, et ce même pour des valeurs très faibles de la réactivité κ . Aux temps courts, pour une particule passive avec $H < 1/2$, $\mu(t) \propto \psi(t)$, un comportement qui est formellement équivalent à la trajectoire moyenne d'une particule que l'on aurait soumise à une force la faisant revenir près de sa position initiale. Pour $H > 1/2$, aux temps courts la particule traverse la cible avec une trajectoire de vitesse moyenne finie.

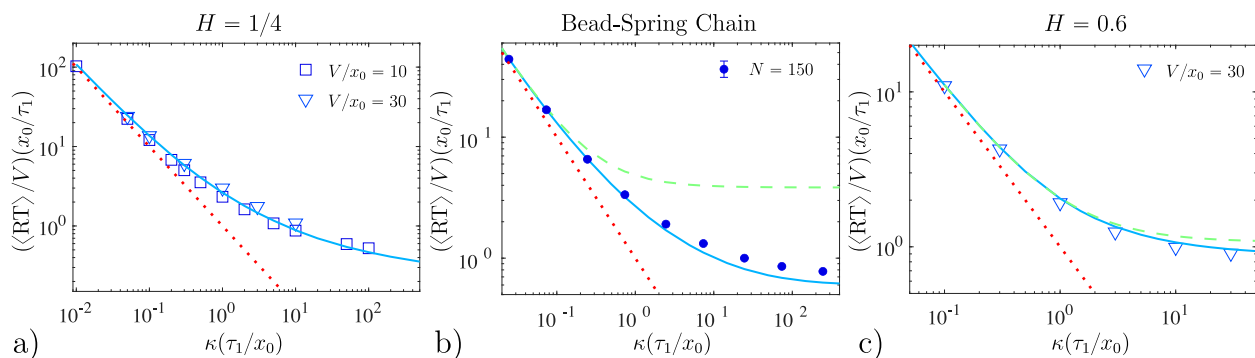


Figure 2: **Comparaison des prédictions théoriques de l'équation $\langle RT \rangle$ avec les résultats de simulations.** Pour les cas a) et c), le processus est invariant d'échelle $\psi(t) = Kt^{2H}$ avec les valeurs respectives $H = 1/4$ et $H = 0.6$. Pour le cas b), le processus est le premier monomère d'une chaîne flexible de $N = 150$ billes reliées par des ressorts, un exemple physique qui donne un mouvement sous-diffusif $\psi(t) = K\sqrt{t}$ pour $N \rightarrow \infty$, avec $K\sqrt{\tau_R}/l_R^2 = 4/\sqrt{\pi}$, où l_R est la taille d'une liaison et τ_R est le temps de relaxation d'un monomère. Les paramètres sont $x_0 = 5l_R$, $V = 30x_0$. Les symboles représentent les résultats de simulations, les lignes continues bleues sont le résultat de notre théorie non-Markovienne, les lignes pointillées rouges sont le résultat asymptotique $\langle RT \rangle = V/\kappa$, et les tirets verts sont le résultat de l'approche pseudo-Markovienne, où $\mu(t) = 0$. Notons que cette approximation prédit un temps moyen de réaction infini pour $H < 1/3$. Ici, $\tau_1 = (x_0^2/K)^{1/2H}$ est le temps de transport typique pour un mouvement Brownien fractionnaire.

Un autre cas limite notable est la limite de faible réactivité, $\kappa \rightarrow 0$. Dans ce cas, nous trouvons que le temps apparent contrôlé par la diffusion, défini comme $\langle RT \rangle - T_{RC}$, est donné par une loi de puissance non-triviale et diverge pour $\kappa \rightarrow 0$:

$$\frac{\langle RT \rangle}{V} - \frac{1}{\kappa} \underset{\kappa \rightarrow 0}{\sim} \left(\frac{1}{\kappa} \right)^{\frac{1-3H}{1-H}} \frac{x_0^2}{K^{\frac{1}{1-H}}} \nu_H, \quad (6)$$

où $H < 1/3$, et ν_H est une fonction de H qui peut être calculée à partir de notre théorie. Cette loi d'échelle indique que le temps de réaction est une fonction non-analytique de la réactivité, et le régime où le temps de réaction est contrôlé par la réaction est atteint de manière beaucoup plus lente pour un processus sous-diffusif fortement non-Markovien ($H < 1/3$) que pour un processus Markovien. Cette loi d'échelle est l'un des principaux résultats de cette thèse et a été observée dans nos simulations numériques.

Ensuite, le chapitre 4, *Imperfect Reactions for Gated Reactions, Finite Targets and Higher Dimensions*, présente plusieurs extensions de notre formalisme, pour être en mesure de prédire le temps de première réaction pour des espaces à plusieurs dimensions (nous traitons le cas de la dimension 2), pour des cibles étendues avec un taux de réaction $k(x)$ non-localisé. Dans ce cas, nous établissons des équations d'autocohérence qui prédisent la valeur de la trajectoire après la réaction, mais aussi la distribution de positions du marcheur à l'instant où la réaction a lieu.

Dans ce même chapitre, nous étendons également le formalisme pour traiter un autre type de réactions imparfaites, celui de réactions où la cible peut se trouver dans un état

ouvert (ou la réaction peut avoir lieu) ou fermé. Ce mécanisme de “*gated reactions*”, où la cible est ouverte de manière intermittente. Si nous appelons ω_i le taux avec lequel la cible devient inactive, et ω_a le taux auquel elle devient active, notre théorie peut être étendue et donne des équations pour $\langle RT \rangle$ qui sont similaires à l’équation (2). Lorsque les transitions entre les états ouverts et fermés sont rares, dans la limite $\omega = \omega_i + \omega_a \rightarrow 0$, la réaction peut être décrite avec un taux effectif de réaction que nous avons calculé,

$$\frac{\langle RT \rangle}{V} \underset{\omega \rightarrow 0}{\sim} \frac{1}{\kappa_{\text{eff}}}, \quad \kappa_{\text{eff}} = \omega^{1-H} \frac{q_s}{1 - q_s} \frac{\sqrt{2\pi K}}{\Gamma(1 - H)}, \quad (7)$$

où $q_s = \omega_a/\omega$ est la probabilité stationnaire que la cible soit active. Ce résultat indique que le taux effectif de réaction dépend aussi des propriétés de transport K et généralise des résultats obtenus pour le cas Markovien (Mercado-Vásquez and Boyer, 2019).

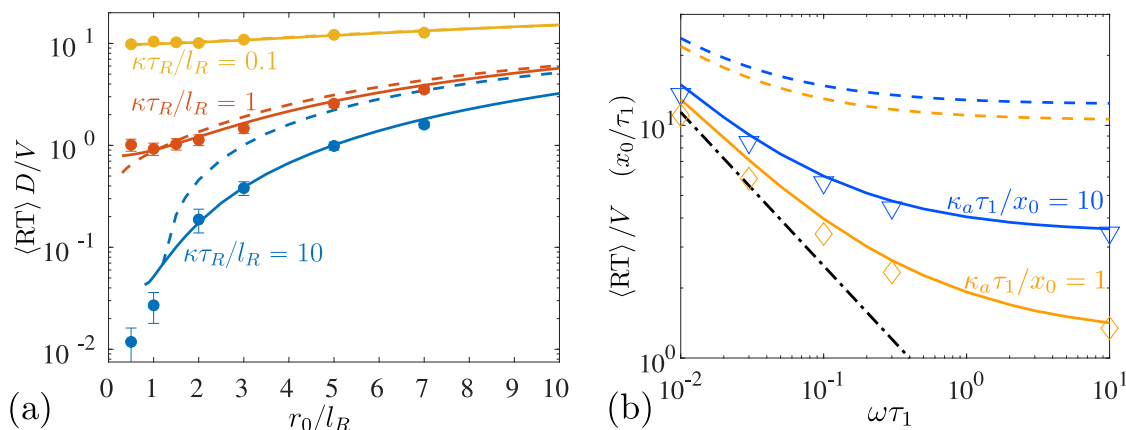


Figure 3: Temps moyen de réaction pour des réactions en deux dimensions et des cibles intermittentes. Les prédictions théoriques sont représentées par des lignes continues, celles obtenues avec l’approximation pseudo-Markovienne par des lignes pointillées, et les simulations sont représentées par des symboles. Sur la figure (a) nous traçons le temps moyen de réaction pour une chaîne de billes et de ressorts de 40 monomères en fonction de la distance initiale, r_0 au centre d’une cible de réactivité Gaussienne. La réactivité totale est $\kappa = \int d\mathbf{x}k(\mathbf{x})$ et nous utilisons les unités naturelles du modèle de polymère, τ_R est le temps de relaxation d’une liaison et l_R la longueur typique d’une liaison. Sur la figure (b), nous traçons le temps moyen de réaction pour une cible intermittente, de réactivité κ_a lorsqu’elle se trouve dans l’état actif, lorsque $x(t)$ est un mouvement Brownien fractionnaire d’exposant $H = 0.34$. ω est la somme des taux de transition dans les états actifs et inactifs. L’unité de temps $\tau_1 = (x_0^2/K)^{1/2H}$ est le temps typique de transport pour un mouvement Brownien fractionnaire.

Observation expérimentale de l'impact de la mémoire sur les événements compétitifs

Dans le chapitre 5, *Competitive First Passage Events in Viscoelastic Fluids and Confrontation with Experiments*, nous étudions le problème des événements compétitifs pour des marcheurs aléatoires non-Markoviens. Dans ce cas, un marcheur aléatoire est mis en présence de deux cibles, et le problème est de trouver quelle est celle qui est atteinte en premier, ce qui est décrit en calculant la *probabilité de splitting* (la probabilité de toucher la première cible plutôt que la deuxième). Il s'agit d'un problème récurrent dans plusieurs domaines (Espenson, 1981; Bouchaud et al., 2018; Hansen et al., 2019), mais il n'est bien compris que pour des processus Markoviens. Pour les processus à mémoire, il existe des lois d'échelle (Majumdar et al., 2010) ou des résultats perturbatifs pour des marcheurs faiblement non-Markoviens (Wiese, 2019). Une autre motivation pour étudier ce problème est que la situation est idéale pour observer expérimentalement une quantité de premier passage: la présence de deux cibles permet de ne pas avoir à suivre une particule pendant des trajectoires longues qui pourraient aller loin de la cible. Dans ce chapitre, nous introduisons une théorie qui permet de prédire quantitativement les probabilités de "splitting" pour un marcheur Gaussien non-Markovien à incrément stationnaire, et nous comparons explicitement avec des résultats expérimentaux.

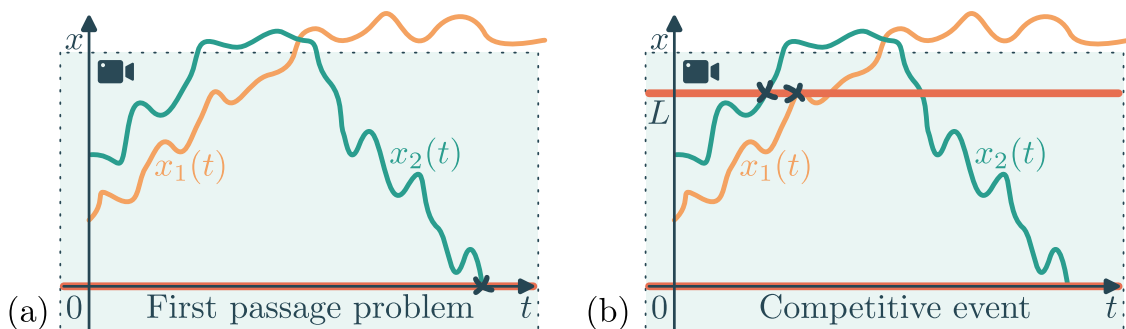


Figure 4: **Différence expérimentale entre l'observation de premier passage à une cible et les événements compétitifs.** Expérimentalement, les trajectoires $x_1(t)$ et $x_2(t)$, en présence de cibles en rouge, peuvent seulement être vues à l'intérieur de la région délimitée par les lignes pointillées (correspondant au champ de vision enregistré par la caméra). Dans le cas du premier passage sur une cible, (a), certaines trajectoires sont perdues. Dans le cas d'événements compétitifs, (b), il n'est pas possible de perdre des particules avant qu'elles n'atteignent une des deux cibles.

Nous considérons un marcheur aléatoire $x(t)$, symétrique ($\langle x(t) \rangle = x_0$), continu (et rugueux) à incrément stationnaire, de déplacement quadratique moyen $\psi(t)$, en présence de deux cibles, la première étant à l'origine $x_1 = 0$, et l'autre à $x_2 = L > x_0 > 0$, avec x_0 la position initiale du marcheur aléatoire. Nous dérivons une équation pour la probabilité de splitting π_1 , défini comme la probabilité de toucher x_1 avant x_2 :

$$x_0 = \lim_{t \rightarrow \infty} [\pi_1 \mu_1(t) + (1 - \pi_1) \mu_2(t)], \quad (8)$$

où $\mu_i(t)$ est la trajectoire moyenne après avoir touché la cible x_i pour la première fois, étant donné que x_i est touchée avant l'autre cible. Notons que cette équation est générale et

n'implique aucune autre approximation. Pour trouver les trajectoires μ_i , nous supposons que le processus dans le futur d'un premier passage sur la cible i est Gaussien, avec la même covariance que le processus initial. En utilisant cette approximation, nous trouvons un set de deux équations intégrales

$$\int_0^\infty \frac{dt}{\sqrt{2\pi\psi(t)}} \left[\sum_{j=1,2} \pi_j [\mu_j(t+\tau) - (\mu_j(t) - x_i)M(t,\tau)] \exp\left(-\frac{(x_i - \mu_j(t))^2}{2\psi(t)}\right) - [x_0 - (x_0 - x_i)M(t,\tau)] \exp\left(-\frac{(x_i - x_0)^2}{2\psi(t)}\right) \right] = 0, \quad \forall_{i=1,2}, \quad (9)$$

où $M(t, \tau)$ est défini comme auparavant par l'équation (4). En résolvant ces équations, les fonctions $\mu_1(t)$ et $\mu_2(t)$ peuvent être obtenues numériquement, donnant accès à $\pi_1(x_0)$ avec l'équation (9).

Ensuite, nous décrivons un système expérimental qui nous permet d'obtenir des trajectoires non-Markoviennes à partir desquelles nous pouvons tester cette théorie non-Markovienne d'événements compétitifs. Les trajectoires sont obtenues à partir du suivi du mouvement de billes immergées dans un fluide contenant des polymères de grand poids moléculaire. Nous vérifions que ces trajectoires sont Gaussiennes, à incréments stationnaires, rugueuses (à l'échelle des pas de temps expérimentaux), et symétriques, comme supposé dans la théorie. Le mouvement des billes peut être décrit comme sous-diffusif aux temps courts et diffusif aux temps longs, ce qui nous conduit à considérer une équation de Langevin généralisée

$$\int_0^t dt' K(t') \dot{x}(t-t') = F(t), \quad \langle F(t)F(t') \rangle = k_B T K(|t-t'|), \quad (10)$$

où le noyau de friction $K(t)$ combine un comportement en loi de puissance et une décroissance exponentielle:

$$K(t) = \frac{\gamma_0}{\tau_0} f_H\left(\frac{t}{\tau_0}\right), \quad f_H(x) = \frac{1}{\Gamma(1-2H)} \frac{e^{-x}}{x^{2H}}, \quad (11)$$

où H est l'exposant de Hurst aux temps courts, $\gamma_0 = \int_0^\infty K(t)dt$ est le coefficient de friction à temps longs, et τ_0 est un temps de mémoire.

A partir des trajectoires obtenues, nous pouvons extraire les probabilité de splitting et les trajectoires moyennes après la "réaction" (le premier passage sur l'une des cibles). Sur la Figure 5, nous montrons que la mémoire, dans ce système viscoélastique, tend à augmenter la probabilité de toucher la cible la plus proche avant la plus lointaine. Cet effet, qualitativement présent dans les lois d'échelle présentes dans la littérature, est quantitativement décrit par notre théorie. De plus, les trajectoires dans le futur d'un premier passage sur une cible x_i ne restent clairement pas sur cette cible mais tendent à revenir dans l'espace entre les cibles. C'est clairement un effet non-Markovien, montrant que les degrés de liberté externes à la bille, qui rendent le mouvement non-Markovien (et sont inconnus dans le cas présent), ne sont pas à l'équilibre au moment du premier passage. Cette observation est la première

preuve expérimentale directe qu'un système n'est pas à l'équilibre à l'instant du premier passage. Ces trajectoires sont également bien décrites par notre théorie.

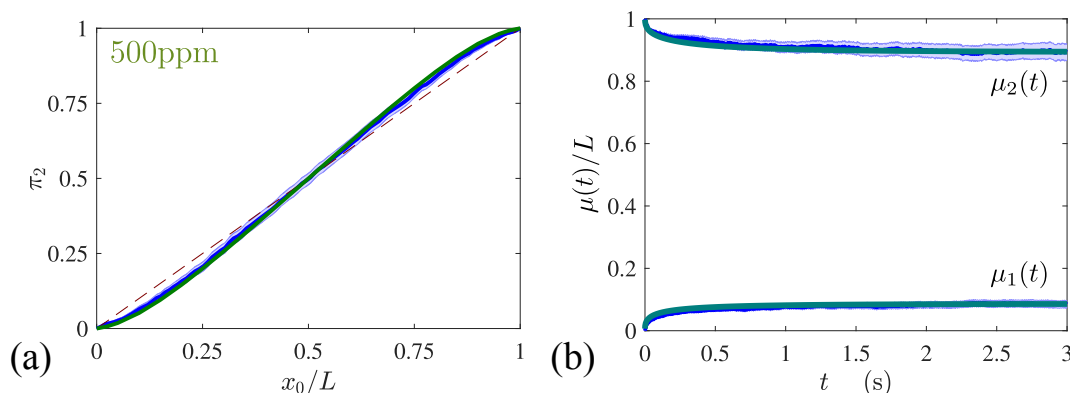


Figure 5: **Comparaison de la théorie non-Markovienne des réactions compétitives avec des données expérimentales.** En vert, nous représentons les prédictions théoriques, en bleu, les observations expérimentales, et en lignes rouges pointillées la prédiction pseudo-Markovienne, où $\mu_i(t) = x_i$ et $\pi_2 = x_0/L$. Les trajectoires ont été enregistrées avec une résolution temporelle de 500 images par seconde, dans une solution de polymères concentrée à 500ppm. (a) Courbes de probabilité de splitting π_2 , avec $L = 1\mu\text{m}$, (b) trajectoires moyennes après un premier passage $\mu_1(t)$ et $\mu_2(t)$, avec $L = 1\mu\text{m}$ et $x_0 = 0.2L$, comparé avec les résultats expérimentaux.

Cinétique de réactions dans des milieux compartimentés

Le dernier problème étudié dans cette thèse est la détermination du temps de premier passage sur une cible localisée à l'intérieur d'un compartiment où les propriétés de transport sont complexes (sous-diffusives), ce compartiment étant lui-même immergé dans un milieu où le transport est diffusif. Ce problème est inspiré par l'existence d'organelles sans membranes dans les cellules, où le mouvement est sous-diffusif. Notre objectif est de déterminer le temps de premier passage pour une telle situation, et de rechercher si une optimisation du temps de réaction est possible, dans un modèle simple. Ce chapitre 6, *First Passage in Complex Compartmentalized Media*, est le seul qui ne traite pas de processus stochastiques non-Markoviens. Ceci est dû à la difficulté d'implémenter le concept d'interface entre compartiments dans des approches théoriques. A la place, nous utilisons un modèle plus simple où l'espace à l'intérieur du compartiment est supposé avoir une architecture fractale, créant un effet d'encombrement forçant le mouvement à être sous-diffusif. Dans la littérature, les temps de premier passage dans les compartiments ont été étudiés seulement dans le cas de mouvement diffusif au sein du compartiment.

Nous considérons le mouvement d'un marcheur aléatoire dont la position initiale est dans un volume de confinement V , où le mouvement est diffusif avec diffusivité D , à l'extérieur d'un compartiment fractal de rayon R et dimension fractale d_f . Le mouvement à l'intérieur du compartiment est supposé sous-diffusif, avec un déplacement quadratique moyen $\psi(t) \propto (Kt)^{2/d_w}$, où K est un coefficient de transport et d_w est la dimension de la marche. Nous avons

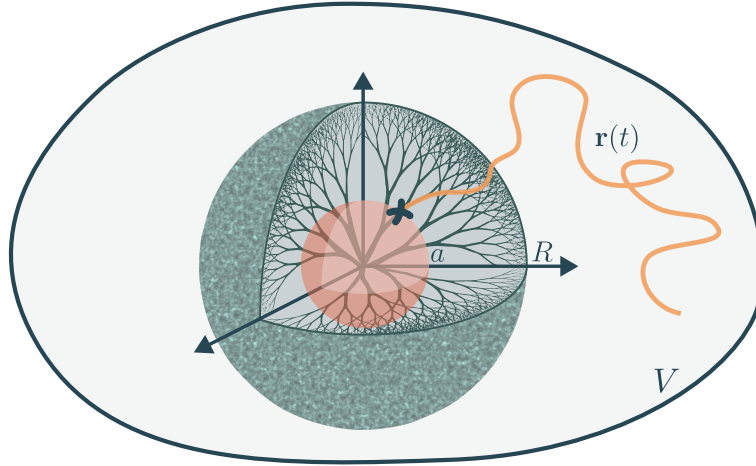


Figure 6: **Schéma du problème de premier passage à l'intérieur d'un compartiment fractal.** In marcheur aléatoire $\mathbf{r}(t)$, commençant à $\mathbf{r}_0 = \mathbf{r}(0)$, se déplace dans un volume de confinement V , et cherche une cible de rayon a à l'intérieur d'un compartiment fractal de rayon R .

développé un formalisme pour prédire le temps moyen de premier passage pour atteindre une cible de rayon a au centre du compartiment, obtenant

$$\frac{\langle T \rangle (a | r_0 > R)}{V} = \begin{cases} \frac{e^{-\beta E_0}}{\eta d_f K} \frac{R^{d_w - d_f} - a^{d_w - d_f}}{d_w - d_f} + \frac{1}{4\pi D} \left(\frac{1}{R} - \frac{1}{r_0} \right) & (d = 3) \\ \frac{e^{-\beta E_0}}{\eta d_f K} \frac{R^{d_w - d_f} - a^{d_w - d_f}}{d_w - d_f} + \frac{1}{2\pi D} \ln \left(\frac{r_0}{R} \right) & (d = 2) \end{cases}, \quad (12)$$

où η est une mesure de l'encombrement à l'intérieur du compartiment (défini de telle sorte que le volume accessible dans une boule de rayon R est ηR^{d_f}), r_0 est la distance initiale au centre de la cible $\beta = 1/k_B T$ avec k_B la constante de Boltzmann et T la température, et E_0 est la valeur d'un gain énergétique que le marcheur a à être dans le compartiment. Ce résultat est obtenu en utilisant l'opérateur de O'Shaughnessy-Procaccia, qui est une description macroscopique approximative du mouvement au sein d'une fractale (O'Shaughnessy and Procaccia, 1985).

Nous avons vérifié que notre description prédit correctement le temps de premier passage en comparant avec des simulations numériques en dimension $d = 2$, dans le cas où le compartiment à l'intérieur de la fractale est un réseau de percolation critique. Les résultats sont présentés sur la figure 7, où notre théorie prédit de façon quantitative le temps moyen de premier passage pour plusieurs rayons de compartiment, sans aucun paramètre ajustable.

Ensuite, après avoir vérifié que notre théorie est vérifiée par des simulations, nous avons cherché les conditions dans lesquelles le temps moyen de premier passage peut être optimisé par la présence du compartiment, c'est à dire pour lequel la cible est plus rapidement atteinte qu'une cible de même taille dans un milieu non-compartimenté. Pour ce faire, nous nous restreignons au cas où le mouvement au sein du compartiment est plus lent qu'à l'extérieur, du fait de l'encombrement, ce qui impose la condition

$$K a^{2-d_w} \ll D. \quad (13)$$

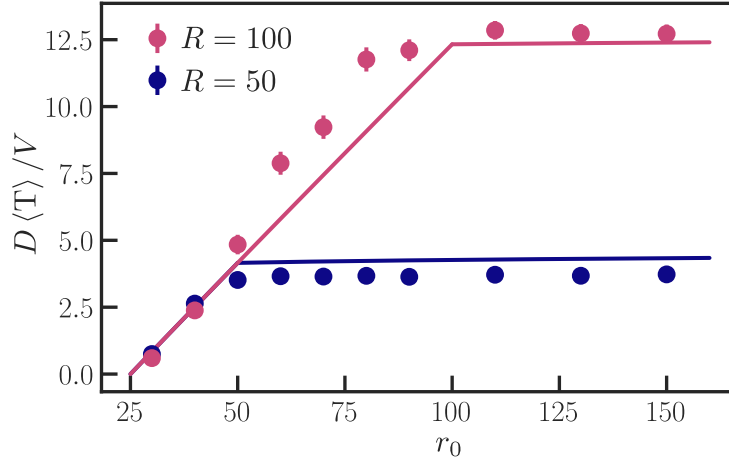


Figure 7: **Prédictions théoriques (lignes) et résultats de simulations (symboles) pour le temps de premier passage sur une cible dans un milieu compartimenté.** Les simulations ont été effectuées sur un réseau carré bidimensionnel avec $V = 2.5 \cdot 10^5$ (où la taille d'une liaison est $\ell = 1$), à l'intérieur du compartiment de taille $R = 50$ et $R = 100$ les liaisons ont été retirées aléatoirement (avec probabilité $p = 0.5$) pour obtenir un réseau de percolation critique.

Nous avons montré que, si $E_0 = 0$, il n'y a aucune optimisation possible qui respecte cette condition. Ceci est dû au fait qu'il y a une barrière entropique qui s'oppose à l'entrée du compartiment. Ensuite nous avons autorisé une valeur non-nulle de E_0 , avec la contrainte que la probabilité stationnaire de trouver le marcheur dans le compartiment n'est pas plus grande que celle que l'on aurait de le trouver dans une sphère de rayon R dans un milieu non-compartimenté, signifiant qu'il n'y a pas de sur-concentration de réactants dans le compartiment, ce qui implique que

$$E_0 \sim k_B T \ln \left(R^{d-d_f} / \eta \right), \quad (14)$$

où d est la dimension du volume de confinement externe. Dans ces conditions, si $d = 3$, nous trouvons que la présence du compartiment peut réduire considérablement le temps de recherche par rapport à un milieu non-compartimenté à la condition $d_w < 3$, impliquant que la marche aléatoire n'est pas trop sous-diffusif. Cette optimisation est possible car une marche diffusive peut trouver une cible infiniment petite en temps fini, alors que le temps d'une recherche diffusive en dimension 3 diverge pour une petite cible. En dimension $d = 2$, aucune optimisation n'est possible.

CONTENTS

1	Introduction	1
2	Introductory Chapter: Kinetics of Transport-Influenced Reactions and Non-Markovian Processes	3
2.1	Random walks and the problem of search processes	4
2.1.1	Some properties of the kinetics of transport-influenced reactions . . .	5
2.1.2	The mean reaction-controlled time for point-like targets	7
2.1.3	Mean reaction time for a three-dimensional diffusive process	8
2.1.4	Mean reaction time in scale invariant media	9
2.2	The importance of memory and its existence in Gaussian processes	10
2.2.1	Gaussian processes with stationary increments	11
2.2.2	Transport-influenced reactions for non-Markovian processes	13
2.3	Outline of the thesis and summary of results	14
2.3.1	Influence of memory in the kinetics of imperfect reactions in confinement	14
2.3.2	Experimental observation of the effects of memory in competitive events	18
2.3.3	Kinetics of reactions in compartmentalized media	20
3	Kinetics of Imperfect Reactions for Non-Markovian Walkers in Confinement	23
3.1	Mean reaction time for a point-like target	27
3.1.1	Finding the mean reaction time	27
3.1.2	Self-consistent equation for the mean trajectory after reaction	31
3.1.3	Simulation results and numerical methods	33
3.2	Asymptotics of the mean trajectory after reaction, $\mu(t)$	35
3.2.1	Long time asymptotics for a long time fractional Brownian motion . . .	36
3.2.2	Short time asymptotics for a fractional Brownian motion	37
3.3	Weakly non-Markovian regime	38
3.3.1	General solution	38
3.3.2	Long time diffusive process	39
3.3.3	Perturbative fractional Brownian motion	40
3.3.4	Mean reaction time in the weakly non-Markovian limit	41
3.4	Matched asymptotic expansions for a fractional Brownian motion with limit reactivities	42
3.4.1	Weakly reactive targets	43

3.4.2	Strongly reactive targets	47
3.5	Conclusion	51
4	Imperfect Reactions for Gated Reactions, Finite Targets and Higher Dimensions	53
4.1	The mechanism of gated reactions.	54
4.1.1	Dynamics of the target activity.	54
4.1.2	Mean reaction time to an intermittent target.	55
4.2	One-dimensional extended targets	57
4.3	Imperfect reactions in two dimensions.	61
4.4	Conclusion	66
5	Competitive First Passage Events in Viscoelastic Fluids and Confrontation with Experiments	69
5.1	Non-Markovian motion in viscoelastic fluids and the generalized Langevin equation	72
5.1.1	The Generalized Langevin Equation for a Rouse Chain	72
5.1.2	Calculation of the mean square displacement	75
5.1.3	Developing an experiment to see non-Markovian effects	77
5.2	Predicting the splitting probabilities for Gaussian random walkers	82
5.3	Testing the theory with experiments	86
5.3.1	Choosing appropriate experimental parameters	86
5.3.2	Experimental mean trajectories after reaction	87
5.3.3	Experimental Splitting Probabilities	88
5.4	Conclusion	89
6	First Passage in Complex Compartmentalized Media	91
6.1	Theory of diffusion in fractals	93
6.2	Transport in a medium with a fractal compartment	96
6.2.1	Dynamics in free (infinite) space	96
6.2.2	Introduction of a confining volume: the stationary distribution	97
6.3	Calculation of the mean first passage time	98
6.4	The bond-percolation network and simulations	101
6.4.1	Parameters of the fractal	102
6.4.2	Simulation scheme	104
6.4.3	Simulation results	105

6.5	Does the compartment facilitate reactions?	107
6.5.1	Compartment with no energetic bonding	108
6.5.2	Compartment with energetic bonding	108
6.5.3	Is optimization still possible in two-dimensional space?	109
6.6	Conclusion	110
7	Conclusion and Perspectives	111
A	Conditioned Gaussian Processes and Projection Formulas	115
B	Solution to a Class of Second Kind Volterra Integral Equations	117
C	Asymptotics of the Mean Trajectory After Reaction for the Fractional Brownian Motion in the Weakly non-Markovian Regime	119
D	Self-Consistent Equations for Competitive First Passage Events	123

INTRODUCTION

Consider a random walker that, at each passage through a reactive region (or a target), has some probability of undergoing a transformation, which we call a “reaction”. When studying these situations, one says that there is a transport-influenced reaction. If many passages through the target are required for a reaction to happen, the target is said to be “imperfect”, whereas, if reactions happen instantaneously at first passage, the target is “perfect”. At first glance, one would say that these situations corresponds to chemical reactions; where reactants must first meet, and then, if an energetic barrier is overcome, react. However, the study of transport-influenced reactions is not restricted to chemistry and it is useful to study (many) diverse phenomena as DNA transcription (where transcription factors search for specific DNA sequences), cell signaling (where extracellular molecules: hormones, neurotransmitters, etc. search for receptor proteins on the membranes), neurone firing (that happens after a specific voltage threshold is reached), risk analysis (where an investment might bring the investor to ruin before reaching a given profit), etc. The purpose of this thesis is to understand how each of the steps of a transport-influenced reaction is altered in the presence of three complex situations: reactants with complex transport (characterized by the existence of memory), multiple targets and compartmentalized media.

First, in Chapter 3, we treat the case of a one dimensional non-Markovian random walker that is searching for an imperfect point-like target inside a confining volume. So far, theoretical approaches have either described perfect reactions for non-Markovian random walks or imperfect reaction for Markovian. To our knowledge, the only approaches that attempt to take into account memory effects for imperfect reactions rely on the Wilemski-Fixman approximation, which, as we proceed to show, leads to quantitatively incorrect predictions. Our theory, which is valid for large confining volumes, enables us to find the mean reaction time as a function of the reactivity, through the intrinsic reaction rate of the target, the geometry, through the initial condition and the confining volume, and the transport properties, through the mean square displacement. To find the mean reaction time, one first has to find the mean trajectory after reaction, for which our theory finds a closed equation that can be solved numerically. Notably, we find that, for weakly reactive targets, a non-trivial exponent emerges as a consequence of memory.

Then, as an extension of Chapter 3, we develop a non-Markovian theory for gated reactions, a different mechanism of imperfect reactivity, and extend the formalism of imperfect reactions to finite targets and two dimensional random walkers. These three extensions are described in Chapter 4. Gated reactions are imperfect reactions where the imperfect target is also

allowed to exist in either an active or an inactive state. The switch between active and inactive states happens as a stochastic process with some transition rate to go from inactive to active and vice versa. We obtain a closed set of equations for the mean reaction time that, when extended to low transition rates, generalizes previous results obtained for Brownian motion. In the second section, we first extend the theory of Chapter 3 to finite targets, which are necessary to the study two dimensional imperfect reactions, where, to have finite mean reaction times (in the sense that the time scales with the confining volume), the target must be of finite size. We develop the theory for Gaussian targets and obtain a closed set of equations for the mean reaction time, the mean trajectory after reaction and the mean reactive position.

Next, though many theories have been developed to study first passage problems (corresponding to perfect targets), experimental observations of the effect of memory in first passage problems are scarce. In Chapter 5, we describe an experimental setup that can directly detect the influence of memory on competitive events (the first passage problem with two targets) and develop a theory that predicts the outcome of such competitive events for non-Markovian random walkers. Our theory deals with non-Markovian Gaussian random walkers that are moving between two targets. The goal is to find the probability of touching one of the targets before the other. Then, by tracking the movement of a bead in a dense long polymer solution, we can measure the probability for a particle to reach one target before the other one, with which we can confirm that the theoretical predictions of our theory are quantitatively correct.

Finally, in Chapter 6, motivated by the existence of small (complex) membraneless organelles in cells where movement is generally subdiffusive, we study the effect of compartments in the problem of first passage. Though the ideal would be to study this case in a non-Markovian framework (to better incorporate the complex interior of the organelles), we argue that this is not yet possible and proceed by assuming that the interior of the compartments is fractal, thus creating a crowded compartment where many positions are not available for diffusion. We develop a theory that gives us the mean first passage time for a random walker that starts its motion outside a fractal compartment (but inside a large confining volume) and has to find a target inside the compartment. Then, we study the possibility of reaction optimisation caused by the fractal compartment. We find that, if there is an energetic gain inside the compartment that compensates the decrease of available sites (thus making stationary concentration continuous in the interface), then, it is possible to have a faster reaction time even when movement inside the compartment is slower.

We complete this manuscript by adding an introductory chapter, Chapter 2, where we briefly review some properties of first passage quantities, reaction times (corresponding to the imperfect reactivity case) and Gaussian random walks. Then, in the last chapter, Chapter 7, we present some conclusions and discuss the perspectives and future paths that our research can take.

INTRODUCTORY CHAPTER: KINETICS OF TRANSPORT-INFLUENCED REACTIONS AND NON-MARKOVIAN PROCESSES

2.1	Random walks and the problem of search processes	4
2.1.1	Some properties of the kinetics of transport-influenced reactions	5
2.1.2	The mean reaction-controlled time for point-like targets	7
2.1.3	Mean reaction time for a three-dimensional diffusive process	8
2.1.4	Mean reaction time in scale invariant media	9
2.2	The importance of memory and its existence in Gaussian processes	10
2.2.1	Gaussian processes with stationary increments	11
2.2.2	Transport-influenced reactions for non-Markovian processes	13
2.3	Outline of the thesis and summary of results	14
2.3.1	Influence of memory in the kinetics of imperfect reactions in confinement	14
2.3.2	Experimental observation of the effects of memory in competitive events	18
2.3.3	Kinetics of reactions in compartmentalized media	20

The purpose of this chapter is to introduce some concepts on transport-influenced reactions, non-Markovian processes and diffusion in scale-invariant spaces (fractals) that will be useful for the rest of the thesis. We start by defining the problem of transport-influenced reactions, in the case of Markovian processes. In a second stage, we focus on processes with memory, i.e., non-Markovian, and specify in which conditions Gaussian processes are Markovian. Finally, we announce the main results of this thesis with a brief summary of the results.

2.1 | Random walks and the problem of search processes

When the movement of a body results from a large number of interactions, it is (in general) not possible to describe the system in a deterministic way, which means that another approach must be used to study the dynamics of these bodies. By observing such systems, e.g., the movement of microscopic spheres suspended in water (where the interactions correspond to collision with water molecules), one can see that the movement is irregular, with no clear explanations as to why the body moves in one direction rather than the other. The trajectories taken by these bodies are called *random walks*, and, in fact, their motion is so irregular that it can only be described with a probabilistic framework, the framework of *stochastic processes* (Gardiner, 1985; Van Kampen, 1992). Examples of these walks can be found in multiple situations: electrical noise, population dynamics, the value of a stock, the charge of a neuron, etc. Due to their wide range of applications, these random walks have been an important topic of physics research in the last century. Recent decades have seen a considerable amount of work on anomalous random walks, i.e., walks $\mathbf{r}(t)$ where $\langle \mathbf{r}^2(t) \rangle \underset{t \rightarrow \infty}{\sim} t^\alpha$, with $\alpha \neq 1$ (Metzler and Klafter, 2000; Sokolov, 2012). Notably in the field of Biology, where anomalous walks that result from crowded environments have been used to model the movement inside cells (Höfling and Franosch, 2013).

One relevant question associated with these random walks is the question of how much time it takes for such a walk to reach a predetermined position, or a *target* (Redner, 2001). This time is commonly known as the first passage time, and, given the stochastic nature of the walks, it must be itself a stochastic variable. The study of first passage events is motivated in part by the existence of processes that only happen after a certain threshold is reached, e.g., the discharge of a neuron after a certain tension is reached, the predator that only stops hunting after a pray is caught or the investor that only sells a stock once it reaches a certain profiting value.

However, not all search problems end with a simple passage through a target. One can imagine a situation where, after reaching said target, some other stochastic process decides if a transformation (or a *reaction*) happens or not, see the example in Figure 2.1. This secondary process introduces an extra step to the kinetics of reaction, thus driving these problems out of the reach of first passage processes. In fact, one calls such processes *imperfect* or *transport-influenced reactions*, to emphasise the importance of the two steps involved in the kinetics of these reactions: the transport towards the target and the intrinsic reaction process at the target (Grebekov, 2019). Naturally, we call the time that it takes for a reaction to happen the reaction time, noted RT. Many mechanisms can be at the origin of such intrinsic reaction processes, ranging from gated reactions, where reactants switch between reactive and non-reactive states (thus allowing for encounters that do not lead to a reaction), to the cases where reactions only happen if reactants meet with a prescribed orientation or energy (corresponding to “entropic” and energetic activation barriers). If the reaction step in a transport-influenced reaction is instantaneous (corresponding to a first passage process) one says that the target (and the reaction) is *perfect*.

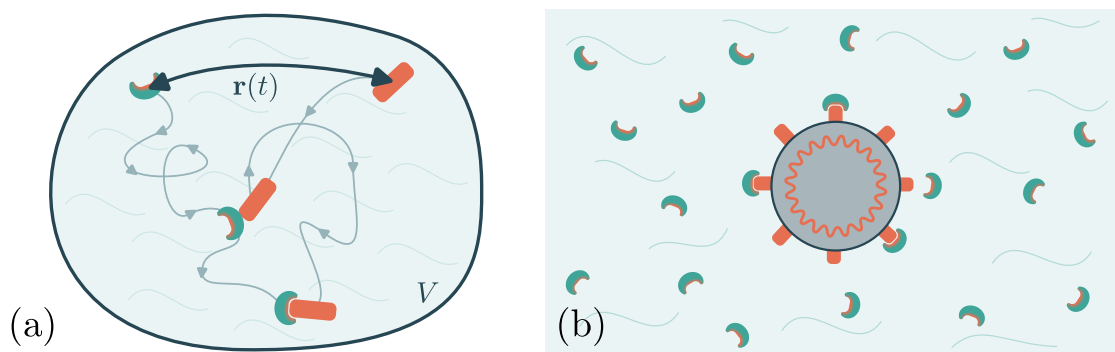


Figure 2.1: **Example of a transport-influenced reaction and application.** (a) Two random walkers are searching for each other. However, meeting is not enough for them to bond as this only happens if they meet with a certain orientation. (b) Schematic representation of a virus immersed in a fluid with antibodies that can make the surface proteins (represented by the orange blocks) inactive, thus inactivating the virus. The rate of protein-antibody bonding can be obtained by studying the problem of transport-influenced reactions in (a).

2.1.1 | Some properties of the kinetics of transport-influenced reactions

In the last decades, much effort has been put into understanding how reactivity influences the kinetics of imperfect reactions (Grebekov, 2019). However, most of this work has been performed for a specific subset of stochastic processes: the Markovian random walks.

A process is Markovian if the statistics of the future steps only depend on the current state of the process and not on the past trajectory taken by this process. The Markov property, for a random walker $x(t)$, can be mathematically expressed as

$$p(x_3, t_3 | x_2, t_2; x_1, t_1) = p(x_3, t_3 | x_2, t_2), \quad \text{with } t_3 > t_2 > t_1, \quad (2.1)$$

where $p(x_3, t_3 | x_2, t_2; x_1, t_1)$ is the probability density of finding $x(t_3) = x_3$ given that $x(t_2) = x_2$ and $x(t_1) = x_1$. Markovian processes are also called memoryless processes as they do not carry any knowledge of the past trajectory into the consideration of the next steps. Though the Markov property might seem simple, it allows us to develop many useful tools. For example, if a process is Markovian, then, one can write a partial differential equation that determines the dynamics of the propagator, i.e., the probabilistic dynamics of a random walker. This equation, commonly known as the Fokker-Planck equation, is arguably one of the most important tools to deal with Markovian processes, and it can be written as (Van Kampen, 1992):

$$\partial_t p(x, t | x_0) = \mathcal{L}_x p(x, t | x_0), \quad (2.2)$$

where the dynamics of the propagator for a particle to go from x_0 to x in a time t , $p(x, t | x_0)$, is connected to the transport operator \mathcal{L}_x . In the transport operator, one typically introduces the properties of the transport and the medium where the transport happens. Though Eq. (2.4) might be solvable or not, depending on the geometry specific boundary conditions, it is an essential tool to the calculation of the first passage time and, in a wider sense, the kinetics of transport-influenced reactions.

One can incorporate imperfect reactivity into the Fokker-Planck equation in two ways, with each method characterizing a different mechanism of imperfect reactivity. First, one might consider that the target influences the motion of $x(t)$ even if the reaction does not happen, e.g., partially reflective targets. In this case, imperfect reactivity can be introduced by adding a Robin boundary condition to the Fokker-Planck equation. For a diffusive process, $\mathcal{L}_x = D\partial_x^2$, with diffusive coefficient D , this corresponds to the boundary condition:

$$D\partial_n p(x, t|x_0)\Big|_{x \in \partial\mathcal{R}} = \kappa_n p(x, t), \quad (2.3)$$

where $\partial_n p(x, t|x_0)\Big|_{x \in \partial\mathcal{R}}$ is the derivative taken in the (outwards) normal direction to the border (∂) of the reactive region \mathcal{R} , and κ_n is a parameter that quantifies the reactivity of the surface with dimensions of length per time (even if the reaction problem happens at a space of d dimensions).

The other mechanism of imperfect reactivity that we present here is the mechanism of sink reactivity, characterized by a reaction rate $k(x)$ that is spatially localized. When imperfect reactivity comes from sink reactivity, the trajectory of the random walker is not changed by a passage through the target without a reaction. In this case, one can rewrite the Fokker-Planck equation and introduce the reaction rate as an absorbing sink term:

$$\partial_t p(x, t|x_0) = \mathcal{L}_x p(x, t|x_0) - k(x)p(x, t|x_0). \quad (2.4)$$

In principle, both situations could be analytically solved to find the full distribution of reaction times.

Let us now give some basic properties for the mean reaction time when the reactants are confined to an arbitrary large volume V with a reaction rate $k(x) = \kappa\delta(x)$, where κ is called the reactivity. Due to the lack of memory, it is natural to write the mean reaction time, $\langle\text{RT}\rangle(x_T|x_0)$, as the sum of the mean first passage time to the target $\langle\text{T}\rangle(x_T|x_0)$, corresponding to the time necessary to reach the target (the mean first passage time), and a time $\langle T_{\text{RC}}\rangle$, that we call the mean reaction-controlled time, corresponding to the time necessary for a reaction to happen once the random walker is started at the target. It is natural to assume that the reaction-controlled time does not depend on the initial conditions. However, as we argue in the next section that, for point-like targets, this reaction-controlled time only depends on the volume and on the reactivity. Therefore, one can write the mean reaction time as a sum of two (independent) terms:

$$\langle\text{RT}\rangle(x_T|x_0) = \langle T_{\text{RC}}\rangle + \langle\text{T}\rangle(x_T|x_0). \quad (2.5)$$

In fact, this additivity property is exact for point-like targets in one dimension, reactions on a network and for small finite targets (as long as the target is so small that reactions happen uniformly in the surface of the target) (Grebekov, 2019; Grebekov and Oshanin, 2017; Grebekov et al., 2017; Gu erin et al., 2021). Additionally, the additivity property is approximately verified in other situations, as the case where the target is a partially reflective patch placed in the boundary of a confining volume (Gu erin et al., 2023).

2.1.2 | The mean reaction-controlled time for point-like targets

Let us focus on the mean reaction-controlled time for a random walker, $x(t)$, with $x(0) = 0$, to react at a target with reaction rate $k(x) = \kappa\delta(x)$, inside a confinement with volume V . It is easy to show that the reaction-controlled time only depends on V and κ for $\kappa \rightarrow 0$ with the hypothesis of fast transport but it is much less obvious to state that it holds for all κ . For simplicity we work within the framework of dynamics on a discrete lattice.

If a random walker is at the site i at time t it has a probability $\nu_{ij}dt$ to jump to a neighbouring site j between t and $t + dt$. We assume that there is only one reactive site $i = 0$ where there is a reaction rate κ . Let us call P the probability that the reaction happens during one passage at the site $i = 0$. If $S_0(t)$ is the probability of not having jumped to a neighbour and not having reacted at time t , given that one starts at $i = 0$ at $t = 0$, i.e., the probability of staying at the target without a reaction, then

$$S_0(t) = e^{-\kappa t - \sum_j \nu_{0j} t}, \quad (2.6)$$

where the sum runs over the neighbouring sites of $i = 0$. Using $S_0(t)$ one can write the probability density $p(t)$ that the reaction happens at each passage after being at the target for time t :

$$p(t) = S_0(t)\kappa = \kappa e^{-\kappa t - \sum_j \nu_{0j} t}. \quad (2.7)$$

Hence, the probability that the reaction happens during one passage at the target is

$$P = \int_0^\infty dt p(t) = \frac{\kappa}{\kappa + \nu_0}, \quad (2.8)$$

where we have introduced $\nu_i = \sum_j \nu_{ij}$, which is the inverse waiting time at the site i (in the dynamics without reaction at the target).

Let us call τ_1 the first return time to the target (including the waiting time on the target when one starts on it). Now, since the number of passages n to obtain a reaction and the return time τ_1 are independent variables, we can write the mean reaction-controlled time as

$$\langle T_{\text{RC}} \rangle = \langle n\tau_1 \rangle = \langle n \rangle \langle \tau_1 \rangle. \quad (2.9)$$

The probability that the reaction happens during the passage number n at the target is exactly $P(1 - P)^n$, so that

$$\langle n \rangle = \sum_{n=1}^\infty P(1 - P)^n n = \frac{1 - P}{P}. \quad (2.10)$$

Therefore, one can write

$$\langle T_{\text{RC}} \rangle = \frac{1 - P}{P} \langle \tau_1 \rangle, \quad (2.11)$$

which has been obtained, for example in [Guérin et al. \(2021\)](#).

Now, if we note p_i^s the stationary probability to be at site i in absence of reaction at the target, we may note that

$$p_0^s = \nu_0^{-1} / \langle \tau_1 \rangle, \quad (2.12)$$

which follows from *ergodicity*: the stationary probability can be computed by counting the amount of time spent at some site in a long period of time. This is actually Kac's lemma (from ergodic theory) applied to our situation. Using Eqs. (2.8) and (2.12) into the formula for the mean reaction-controlled time, Eq. (2.11), one finds

$$\langle T_{\text{RC}} \rangle = \frac{1}{\kappa p_0^s}. \quad (2.13)$$

In the continuous dynamics limit one can write:

$$\frac{\langle T_{\text{RC}} \rangle}{V} = \frac{1}{\kappa}, \quad (2.14)$$

showing that the mean reaction-controlled time, $\langle T_{\text{RC}} \rangle$, does not depend on transport properties, which is true for all values of reactivity and not only for small ones. Note that this derivation could easily be extended to higher dimensions with the same result.

With this mean reaction-controlled time we are now left to find the mean first passage time, $\langle T \rangle (x_T | x_0)$. However, before moving onwards, let us first note that deriving the reaction-controlled time for low reactivity (assuming that dynamics is fast) does not require the Markov property, suggesting that the scaling $\langle \text{RT} \rangle / V \sim 1/\kappa$ should remain valid for the low reactivity limit of non-Markovian processes (processes that do not verify the Markov property).

2.1.3 | Mean reaction time for a three-dimensional diffusive process

Let us combine the results of the two previous sections to compute the mean reaction time for a three-dimensional random walker that diffuses to react at a target of radius a . We assume that the random walker is started far from the target.

If imperfect reactivity comes from a semi-reflective target that is spherically symmetric, then, we may see the Robin boundary condition, Eq. (2.3), as an effective sink reaction rate $k(\mathbf{x}) = \kappa_n \delta_s(\mathbf{x})$, where $\delta_s(\mathbf{x})$ is a surface delta function, such that the reactivity can be written as $\kappa \equiv \int d\mathbf{x} k(\mathbf{x}) = 4\pi a^2 \kappa_n$. Therefore, one can write the mean reaction-controlled time for a spherical target of radius a as

$$\frac{\langle T_{\text{RC}} \rangle}{V} = \frac{1}{4\pi a^2 \kappa_n}. \quad (2.15)$$

Combining this result with the mean first passage time for a three-dimensional random walker that diffuses and is started far from the target of radius a , $\langle T \rangle (a|\infty) = 1/(4\pi aD)$ (Redner, 2001), one can write the mean reaction time as

$$\frac{\langle RT \rangle}{V} = \frac{1}{4\pi a^2 \kappa_n} + \frac{1}{4\pi aD} = \frac{1}{\kappa_{\text{eff}}}, \quad \text{with } \kappa_{\text{eff}} = \frac{4\pi a^2 \kappa_n D}{a\kappa_n + D}. \quad (2.16)$$

The effective reaction rate found here corresponds to the (steady-state) results of Collins and Kimball (1949).

2.1.4 | Mean reaction time in scale invariant media

Assume that a random walker moves in a scale invariant space of dimension d_f , and that it describes a random walk of dimensions d_w , meaning that the mean square displacement is $\langle \Delta r^2 \rangle \sim t^{2/d_w}$. In this case, one can write the mean first passage time as (Condamin et al., 2007)

$$\frac{\langle T \rangle (a|r_0 = \|\mathbf{x}_0\|)}{V} = \begin{cases} A(r_0^{d_w-d_f} - a^{d_w-d_f}) & \text{for } d_w > d_f : \text{ (compact)} \\ B \ln(r_0/a) & \text{for } d_w = d_f : \text{ (marginally-compact)} \\ C(1/a^{d_f-d_w} - 1/r_0^{d_f-d_w}) & \text{for } d_w < d_f : \text{ (non-compact)} \end{cases}, \quad (2.17)$$

where $A, B, C > 0$ are numerical constants that do not depend on r_0 or a . From this result one can see that, if the search process is compact, $d_w > d_f$, then the time for the random walker to find a target of infinitesimal size remains finite and it is proportional to $V r_0^{d_w-d_f}$. One example of such a process would be the movement of a Brownian particle ($d_w = 2$) that is searching for a target in a one-dimensional space, in which case the mean first passage time is $\sim V r_0$. Then, in the non-compact case, $d_f > d_w$ one can see that infinitesimal targets require, on average, an infinite amount of time to be reached. This means, for example that a Brownian motion in three dimensions would find it much harder to find a small target, even though it covers the space with a similar walk dimension. Note as well that for random walkers that start far from the target their initial distance to the target will not influence the mean first passage time.

Using Eq. (2.14) with this mean first passage time and the mean reaction-controlled time from Section 2.1.2, one can write the mean reaction time for a random walker (of walk dimension d_w) that searched for a target of radius a and reactivity κ inside a confining volume of volume V and of dimension d_f .

$$\frac{\langle RT \rangle (a|r)}{V} = \frac{1}{\kappa} + \begin{cases} A(r^{d_w-d_f} - a^{d_w-d_f}) & \text{for } d_w > d_f : \text{ (compact)} \\ B \ln(r/a) & \text{for } d_w = d_f : \text{ (non-compact)} \\ C\left(\frac{1}{a^{d_f-d_w}} - \frac{1}{r^{d_f-d_w}}\right) & \text{for } d_w < d_f : \text{ (non-compact)} \end{cases}. \quad (2.18)$$

This result generalizes the results of last section to the case of scale invariant media and was studied in Guérin et al. (2021).

2.2 | The importance of memory and its existence in Gaussian processes

Though the Markov property is assumed quite generally when developing stochastic models, it must be noted that this is not always the case. In fact, as soon as a random walker interacts with an environment that does not relax instantaneously, one must consider that the resulting process is non-Markovian, as the slow relaxation of the environment acts as a reminder of the previous positions taken by the process. In general, one can track non-Markovianity to some hidden or forgotten degrees of freedom that act as memory storage. One example of these processes is the case of a bead that moves inside a dense solution of long polymers. Due to the dense and complex networks that long polymers create, any movement of the bead will create a perturbation on the state of the network, which will eventually (but not instantly) relax to an equilibrium state. In this case, the polymer network stored the movement of the bead “in memory” for some time. Yet, during the time that it remained out of equilibrium, it might have influenced the movement of the bead, thus providing a memory of a past point in the bead’s trajectory, see Figure 2.2 for a schematic representation of this phenomenon.

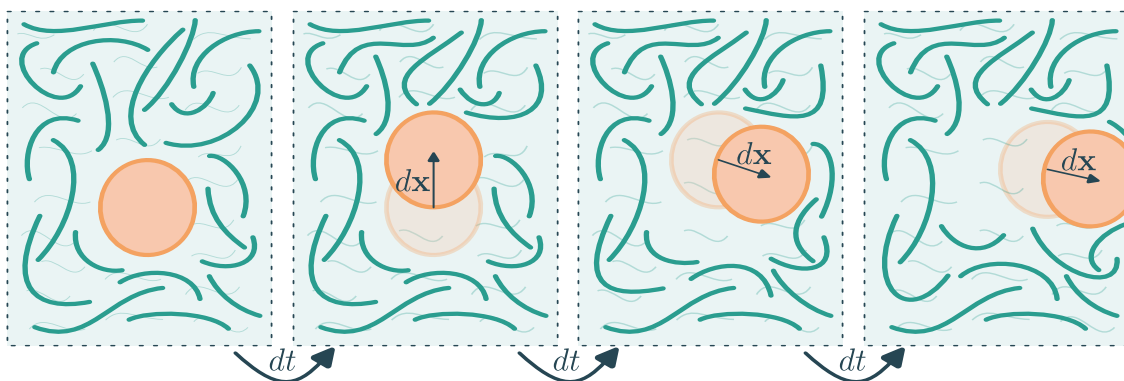


Figure 2.2: **Schematic representation of a bead moving in a fluid with long polymers as a simplistic example of a non-Markovian process.** Here one can see that after one time step the bead moved dx thus creating a place of low polymer density. Then, after another time step, the bead moves again but now influenced by the trail of low polymer density that the last move created. This means that some memory of the previous trajectory was stored in the network of polymers and it influenced the future steps of the bead. In the last frame, the polymers that were influenced by the initial perturbation starts to relax to equilibrium.

Many of the known examples of non-Markovian processes in nature appear to be Gaussian processes (with stationary increments), as is the cases of single file diffusion (Wei et al., 2000), the movement of beads in viscoelastic fluids (Mason et al., 1997) or the dynamics of protein components (Min et al., 2005). It is then natural to raise the question of non-Markovianity of Gaussian processes, as the most famous of all stochastic processes, the Brownian motion, is Gaussian, with stationary increments and Markovian.

2.2.1 | Gaussian processes with stationary increments

A Gaussian process is a stochastic process $x(t)$, where the statistics of all sets $\{x(t_i)\}_{i=1,\dots,N}$ is characterized by a multivariate Gaussian function. These processes are uniquely defined by a mean, $m(t) = \langle x(t) \rangle$, and covariance, $\sigma(t, t') \equiv \text{Cov}(x(t), x(t')) = \langle x(t)x(t') \rangle - m(t)m(t')$.

Influence of stationary increments on the covariance of Gaussian processes

Let us first characterize the covariances of Gaussian processes with stationary increments. Take a symmetric Gaussian process with stationary increments that is started at x_0 at time $t = 0$. The mean of this process is x_0 (due to the symmetry of the process) and the covariance is $\sigma(t, t')$, with $\sigma(t, 0) = 0$, due to the fact that the process is conditioned at $t = 0$. If a process displays stationary increments, then, by definition, the statistics of $y_\tau(t) = x(t + \tau) - x(t)$ is stationary, meaning that it does not depend on t . The process $y_\tau(t)$ is also Gaussian with mean zero and covariance

$$\text{Cov}(y_\tau(t), y_\tau(t')) = \sigma(t + \tau, t' + \tau) - \sigma(t + \tau, t') - \sigma(t, t' + \tau) + \sigma(t, t'). \quad (2.19)$$

Expanding the covariance in Eq. (2.19) for small τ one can write

$$\text{Cov}(y_\tau(t), y_\tau(t')) \underset{\tau \rightarrow 0}{\sim} \tau^2 \partial_t \partial_{t'} \sigma(t, t'), \quad (2.20)$$

which, since $y_\tau(t)$ is stationary, must only depend on the distance between t and t' , $|t - t'|$. Therefore, there must be a function $f(t)$ such that

$$\partial_t \partial_{t'} \sigma(t, t') = f(|t - t'|). \quad (2.21)$$

Then, one can integrate this equation to obtain the covariance of the original process,

$$\sigma(t, t') = h(t) + h(t') + g(|t - t'|), \quad (2.22)$$

where we have used the fact that $\sigma(t, t') = \sigma(t', t)$ and h, g are two functions of a single variable. Since the process $x(t)$ is conditioned to the initial position x_0 at time $t = 0$ one must have $\sigma(0, t') = \sigma(t', 0) = 0$, which gives us a condition for h and g , $h(t) = -g(t)$. Moreover, by definition, the mean square displacement of $x(t)$ is $\psi(t) = \sigma(t, t)$, which gives us the function h , $h(t) = \psi(t)/2$.

Therefore, the covariance of a process that is (i) Gaussian, (ii) symmetric, (iii) with stationary increments and (iv) with an initial condition that is fixed, $x(0) = x_0$, is given by

$$\sigma(t, t') = \frac{1}{2} [\psi(t) + \psi(t') - \psi(|t - t'|)]. \quad (2.23)$$

What is the condition for a Gaussian process with stationary increments to be Markovian?

Let us now study the Markovianity of Gaussian processes. We start by assuming that $x(t)$, with $x(0) = x_0$, is a symmetric Gaussian process that displays stationary increments. The covariance of these processes, as shown in Eq. (2.23) can be written as a function of the mean square displacement, $\psi(t)$.

If a process $x(t)$ is Markovian two conditions must be true. First, the conditioned probability distributions $p(x, t|x', t')$, with $t > t'$, must be written as

$$p(x, t|x', t') = \frac{1}{\sqrt{2\pi\psi(t-t')}} \exp\left(-\frac{(x-x')^2}{2\psi(t-t')}\right), \quad (2.24)$$

Then, the probability distribution of a Markovian process must also verify the Chapman-Kolmogorov equation (derived by using the Markovian property in Eq. (2.1)),

$$p(0, t|x_0, 0) = \int_{-\infty}^{\infty} dy p(0, t|y, t')p(y, t'|x_0, 0). \quad (2.25)$$

Combing these two conditions one obtains the equation,

$$\frac{e^{-x_0^2/2\psi(t)}}{\sqrt{\psi(t)}} = \frac{e^{-x_0^2/2(\psi(t-t')+\psi(t'))}}{\sqrt{\psi(t-t')+\psi(t')}} \quad (2.26)$$

which is only possible if

$$\psi(t) = \psi(t-t') + \psi(t'). \quad (2.27)$$

The only (non-trivial) mean square displacement that obeys this condition is the linear one, $\psi(t) = At$, corresponding to Brownian motion. This proves that the only process that is (i) symmetric (ii) Gaussian (iii) with stationary increments and (iv) Markovian is the Brownian motion, characterized by a mean square displacement that grows linearly with time.

This proof is similar to that of Doob's theorem (Doob, 1942), where it is stated that the only stationary Gaussian process that is Markovian is the Ornstein-Uhlenbeck process, corresponding to a Brownian particle that is moving inside an harmonic potential. Note that it is possible to draw a correspondence between these two theorems, as ours can be seen as an integrated version of the original Doob's theorem.

2.2.2 | Transport-influenced reactions for non-Markovian processes

In the last decades, first passage properties have been a focus of research for processes with memory. In the current literature, one can categorize the study of first passage properties into four categories. First, in a category that we can call the pseudo-Markovian approaches, we have all the studies that rely on the Wilemski-Fixman approximations, stating that, at the reaction moment, the system is at equilibrium (Wilemski and Fixman, 1974a,b). As we show in the next chapters, this approaches are not great and, in some cases, predict wrong scalings. Then, in a category that can be named perturbative approaches, we have all the studies that assume weak memory, usually obtained by considering a small perturbation around the Brownian motion (Delorme and Wiese, 2015; Sadhu et al., 2018; Wiese, 2019; Walter et al., 2021). Next, we have a category that focuses on the persistence exponents, that directly gives us the long times scaling laws related to the first passage time, (Bray et al., 2013; Krug et al., 1997). Finally, we have the category where non-Markovian results are derived by studying the trajectories in the future of a first passage (Guérin et al., 2016; Levernier et al., 2020, 2019, 2022).

Interestingly, with the exception of the pseudo-Markovian approaches, none of the methods described above has been applied to the case of imperfect reaction. In fact, the exceptions to this observation are only two, the pseudo-Markovian approaches, that sometimes predicts incorrect scalings, and the case of the random acceleration process, that, due to its particular properties, allows for theoretical developments that are not possible for any other non-Markovian process. This is the goal of the first part of this thesis, the study of imperfect reactions for non-Markovian random walkers. We note that, for non-Markovian processes, one cannot define a Fokker-Planck equation, so that the Robin boundary condition and the sink reactivity method are not available when processes display memory. Additionally, the additivity property, Eq. (2.14), cannot be used when there is memory, as the time for a reaction to happen once the random walker is at the target must depend on the specific path that it has taken to reach the target in the first place. Therefore, the results for the mean first passage time of non-Markovian processes cannot be directly used to deduce the kinetics of imperfect reactions as in the Markovian case.

Moreover, apart from scaling arguments and perturbative approaches, the classical methods to deal with memory apply only to single target problems. In a second stage of the thesis, we apply the method of studying trajectories after a first passage to study the case of the two target problem.

Last, most methods to treat first passage problems, including the Markovian ones, assume homogeneous spaces. In the final stage of this thesis, we consider the effect of compartments (where transport is altered) in the first passage times.

2.3 | Outline of the thesis and summary of results

In this thesis, we study the reaction kinetics of three complex situations. First, we consider the case of imperfect reactions with memory. Then, for perfect reactions, we analyze the case of competitive reactions with memory (theoretically and experimentally). Finally, we study targets that are immersed in complex compartments.

2.3.1 | Influence of memory in the kinetics of imperfect reactions in confinement

In Chapter 3, *Kinetics of Imperfect Reactions for non-Markovian Walkers in Confinement*, we study the time that it takes for a one-dimensional random walker, $x(t)$, to react at a target at $x = 0$ that is imperfect and point-like, with reaction rate $k(x) = \kappa\delta(x)$. We assume that the walker is confined to a space of volume V that can be connected to the stationary probability in the absence of a target, $V = 1/p_s(0)$.

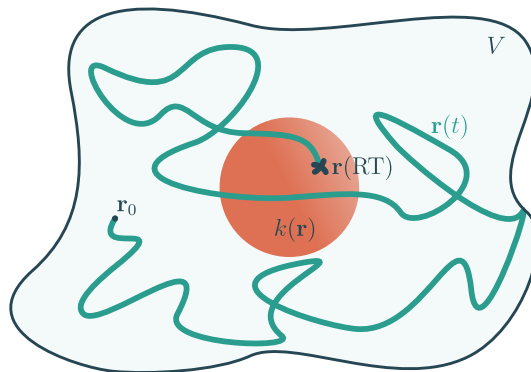


Figure 2.3: **Scheme of the problem of imperfect reactivity.** A random walker, $\mathbf{r}(t)$, moves in a confining space V in the presence of an imperfectly reactive target, $k(\mathbf{r})$. How much time does it take for the random walker to react at the target? This time is known as the reaction time, RT.

Our first result is a general expression for the mean reaction time, RT, for any stochastic process that is continuous but non-smooth ($\langle \dot{x}^2 \rangle = \infty$):

$$\frac{\langle \text{RT} \rangle}{V} = \frac{1}{\kappa} + \int_0^\infty dt [p_\pi(0, t) - p(0, t)], \quad (2.28)$$

where $p(x, t)$ is the probability density of finding a particle at position x at time t when there is no target and $p_\pi(x, t)$ is the probability density of finding the process $x_\pi(t) \equiv x(t + \text{RT})$, known as the process after reaction, at position x at time t .

Though the generality of the previous equation is remarkable, to proceed further, one has to assume one specific subset of stochastic process. We assume that, far from the boundaries of the confining volume, the process is Gaussian and displays stationary increments. As mentioned in the previous section, many non-Markovian processes are Gaussian, thus

suggesting that studying Gaussian processes is not an assumption too restrictive. Since the process displays stationary increments, the covariance of the process, $\sigma(t, t')$, is uniquely characterized by the mean square displacement $\psi(\tau) = \langle (x(t + \tau) - x(t))^2 \rangle$, see Eq. (2.23). We assume that $\psi(t) \simeq Kt^{2H}$ at long times, with $0 < H < 1$, meaning that the random walker does not remain in the initial position and it moves (at long times) in a diffusive way ($H = 1/2$), a subdiffusive way ($H < 1/2$) or in a superdiffusive way ($H > 1/2$). In the large volume limit, Eq. (2.28) can be simplified by assuming that the process after reaction, $x_\pi(t)$, is Gaussian with mean $\mu(t)$ and covariance that is approximately equal to the covariance of the original process $x(t)$. Using these hypothesis in Eq. (2.28), one can write the mean reaction time as

$$\frac{\langle \text{RT} \rangle}{V} = \frac{1}{\kappa} + \int_0^\infty \frac{dt}{\sqrt{2\pi\psi(t)}} \left[\exp\left(-\frac{\mu(t)^2}{2\psi(t)}\right) - \exp\left(-\frac{x_0^2}{2\psi(t)}\right) \right], \quad (2.29)$$

where $x_0 = x(0)$ is the initial position. In this equation, all variables are known except for the mean trajectory after reaction $\mu(t)$. However, it is possible to obtain a self-consistent integral equation for $\mu(t)$:

$$0 = \frac{\mu(\tau)}{\kappa} + \int_0^\infty \frac{dt}{\sqrt{2\pi\psi(t)}} \left[(\mu(t + \tau) - \mu(t)M(t, \tau))e^{-\frac{\mu^2(t)}{2\psi(t)}} - x_0(1 - M(t, \tau))e^{-\frac{x_0^2}{2\psi(t)}} \right], \quad (2.30)$$

with

$$M(t, \tau) = \frac{\psi(t + \tau) + \psi(t) - \psi(\tau)}{2\psi(t)}. \quad (2.31)$$

Solving the integral equation in Eq. (2.30), one obtains $\mu(t)$ that can then be introduced in Eq. (2.29) to obtain the mean reaction time.

Many remarks can be made from the equations for $\langle \text{RT} \rangle$ and $\mu(t)$. For instance, the term $\langle T_{\text{RC}} \rangle \equiv V/\kappa$ can be seen as a Reaction Controlled time since it dominates for small κ , and does not depend on the dynamics. For Markovian processes looking for a point-like target, $\langle \text{RT} \rangle - \langle T_{\text{RC}} \rangle$ would be equal to the mean first passage time. However, our formalism clearly shows that this additivity property does not hold for non-Markovian processes, because $\mu(t)$ depends on κ , as can be seen in Eq. (2.30). This is clearly a non-Markovian effect, physically coming from the fact that the state of the hidden degrees of freedom (responsible for the memory of the process) is not the same at each passage at the target.

In Figure 2.4, we present the mean reaction times obtained from the simulation of three different stochastic processes defined by their distinct mean square displacements. We compare the simulation results to our theoretical predictions and to the results obtained with pseudo-Markovian approximations (also known as Wilemski-Fixman approximations in literature), corresponding to the approximation $\mu(t) = 0$. Our theory quantitatively predicts the correct mean reaction times, even when the pseudo-Markovian approach predicts infinite reaction times, Figure 2.4.a.

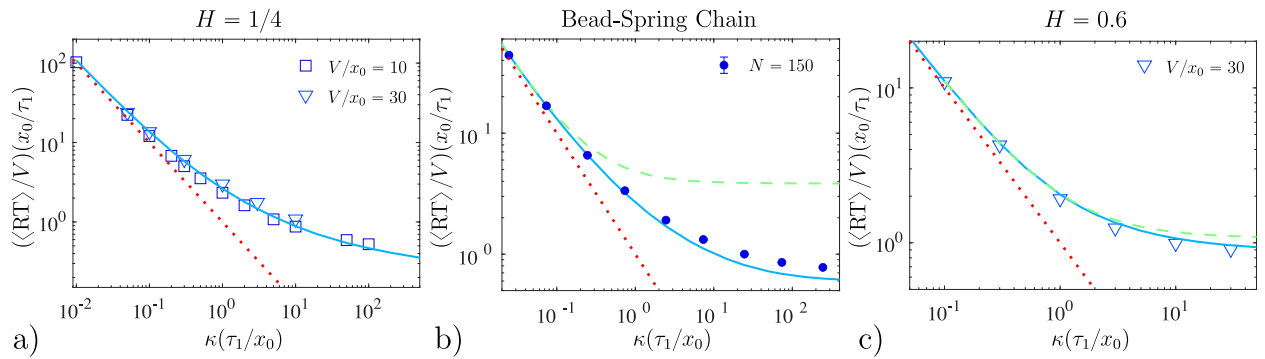


Figure 2.4: **Comparing our theoretical predictions of $\langle \text{RT} \rangle$ to the results of simulations.** In a) and c), the process is a fractional Brownian motion with Hurst exponents $H = 1/4$ and $H = 0.6$ respectively. In b), the process simulated is the movement of the first monomer in a bead-spring chain with $N = 150$ monomers, an example of a physical realization of a subdiffusive fractional Brownian motion with $\psi(t) = K\sqrt{t}$ for $N \rightarrow \infty$, where $K\sqrt{\tau_R}/l_R^2 = 4/\sqrt{\pi}$, l_R is the typical size of one bond and τ_R is the relaxation time of one monomer. The parameters of the simulations are $x_0 = 5l_R$, $V = 30x_0$. The symbols represent the simulation results, the continuous lines (in blue) represent our theoretical predictions, the dashed lines (in green) represent the pseudo-Markovian predictions (only represented when it is finite, i.e., in b and c) and the dotted lines (in red) correspond to the asymptotic behaviour for small κ : $\langle \text{RT} \rangle = V/\kappa$. The time unit $\tau_1 = (x_0^2/K)^{1/2H}$ is the typical time scale of a fractional Brownian motion.

With the hope of obtaining a better understanding of the analytic solutions of Eqs. (2.29) and (2.30), we study the asymptotic behaviours of $\mu(t)$ for random walkers that perform fractional Brownian motion, i.e., $\psi(t) = Kt^{2H}$, finding

$$\mu(t) \underset{t \rightarrow \infty}{\sim} \begin{cases} x_0 - \frac{A(\kappa)}{t^{1-2H}} & \text{for } H \leq \frac{1}{2} \\ -A(\kappa)t^{2H-1} & \text{for } H > \frac{1}{2} \end{cases} \quad \text{and} \quad \mu(t) \underset{t \rightarrow 0}{\sim} \begin{cases} \kappa A(x_0, K, \kappa) t^{2H} & \text{for } H \leq \frac{1}{2} \\ \kappa B(x_0, K, \kappa) t & \text{for } H > \frac{1}{2} \end{cases}. \quad (2.32)$$

It is interesting to realize that, at long times, for a subdiffusive process ($H < 1/2$), the initial position is never forgotten, even for small reactivities (where reactions take more time to happen). At short times, for subdiffusive particles, $\mu(t) \propto \psi(t)$, corresponding to the movement of a particle that is being pushed back to the initial position by an external force. For superdiffusive particles, at short times, the particles cross the target describing trajectories that have finite mean velocities.

Another interesting limit case is the limit of weak reactivity, $\kappa \rightarrow 0$. In this case, we find that the apparent diffusion-controlled time, $\langle \text{RT} \rangle - \langle T_{\text{RC}} \rangle$, is dominated by a divergent non-trivial exponent of κ :

$$\frac{\langle \text{RT} \rangle}{V} - \frac{1}{\kappa} \underset{\kappa \rightarrow 0}{\sim} \left(\frac{1}{\kappa} \right)^{\frac{1-3H}{1-H}} \frac{x_0^2}{K^{\frac{1}{1-H}}} \nu_H, \quad (2.33)$$

where $H < 1/3$ and ν_H is a function of H that can be calculated from our theory. This new, non-trivial, scaling law tells us that the mean reaction time is a non-analytical function of the reactivity and that the regime where the reaction-controlled time dominates the mean reaction time is reached much slower for non-Markovian process than for the Markovian ones.

This scaling law is one of the main results of this thesis and it has been observed in our simulation.

Then, in Chapter 4, *Kinetics of Imperfect Reactions for Non-Markovian Walkers in Confinement*, we present three extensions of our formalism. First, in the case of gated reactions, then, in the case of finite Gaussian-shaped targets in one dimension and, finally, in the case of two-dimensional Gaussian-shaped targets. The mechanism of gated reactions is characterized by a target that might be active, with reaction rate $k(x) = \kappa_a \delta(x)$, or inactive, with $k(x) = 0$. The target randomly switches from active to inactive and vice versa, with rates ω_i and ω_a respectively. Our theory can be extended to this case obtaining equations for the mean reaction time of gated reactions that are similar to those of the point-like target. When transition in the target are rare, corresponding to $\omega = \omega_a + \omega_i \rightarrow 0$, reactions are rare and the mean reaction time can be written as

$$\frac{\langle \text{RT} \rangle}{V} \underset{\omega \rightarrow 0}{\sim} \frac{1}{\kappa_{\text{eff}}}, \quad \kappa_{\text{eff}} = \omega^{1-H} \frac{q_s}{1 - q_s} \frac{\sqrt{2\pi K}}{\Gamma(1 - H)}, \quad (2.34)$$

where $q_s = \omega_a/\omega$ is the stationary probability of finding an active target. This result suggests that the effective reaction rate depends on the transport properties, K , and generalizes the results obtained for Markovian processes (Mercado-Vásquez and Boyer, 2019). Additionally, we find the equations that enable us to calculate the mean reaction time for Gaussian-shaped targets in one and two dimensions. In Figure 2.5, we compare our theoretical predictions for gated reactions and two-dimensional Gaussian-shaped targets to the results of simulations. We find that our theories quantitatively agree with the simulations.

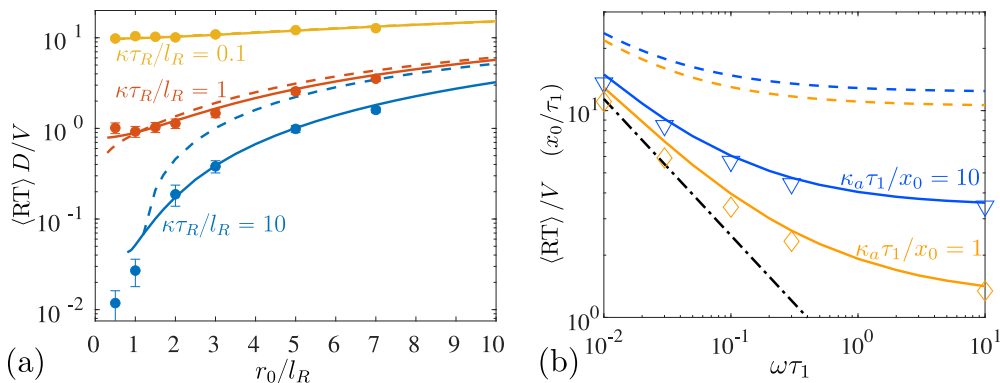


Figure 2.5: Mean reaction times for two-dimensional and gated targets. We represent our theoretical predictions with continuous lines, the pseudo-Markovian predictions with dashed lines and the simulations with symbols. In (a) we represent the mean reaction time (for a bead-spring chain with 40 monomers) as a function of the initial distance to the center of a Gaussian-shaped target, r_0 . The reactivity of the target is $\kappa = \int d\mathbf{x}k(\mathbf{x})$ and we use the natural units of the bead-spring chain model, τ_R is the relaxation time of one monomer and l_R is the typical size of one bond. In (b) we represent the mean reaction time for a fractional Brownian motion, with $H = 0.34$, in the case of a gated target with reactivity κ_a when it is active. The target, that can be active or inactive, switches from one state to the other at a rate ω . The time unit $\tau_1 = (x_0^2/K)^{1/2H}$ is the typical time scale of a fractional Brownian motion.

2.3.2 | Experimental observation of the effects of memory in competitive events

In Chapter 5, *Competitive First Passage Events in Viscoelastic Fluids and Confrontation with Experiments*, we study the problem of competitive events for non-Markovian processes. In this problem, a random walker is placed in between two targets, and the objective is to find the probability of touching one of the targets before the other, i.e., the splitting probability. As shown in Figure 2.6, the problem of competitive events is the ideal configuration for an experimental study of first passage properties. In that chapter, we develop a theory that quantitatively predicts the correct splitting probabilities for Gaussian processes with stationary increments, and compare these predictions to the experimental results.

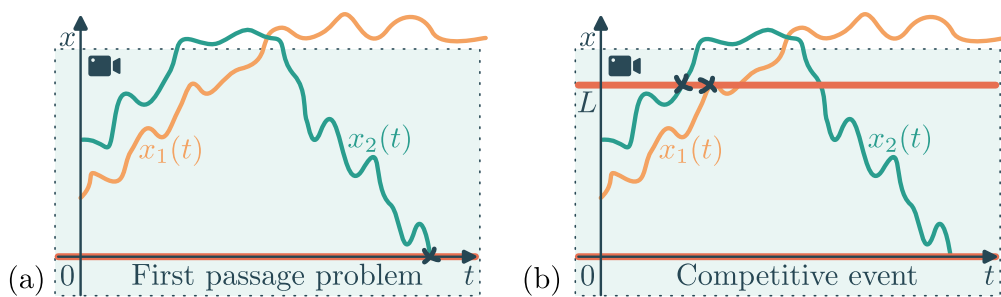


Figure 2.6: **Experimental difference between observing first passage to one target and competitive events.** Experimentally, the trajectories $x_1(t)$ and $x_2(t)$ that are searching for the red targets can only be seen inside the dotted region (corresponding to the space that is recorded by the camera). In the case of a first passage to one target, (a), many trajectories are lost. In the case of competitive events, (b), it is not possible to lose particles from the recorded region, as trajectories must touch one of the targets before leaving this region.

We consider a random walker $x(t)$ that is symmetric ($\langle x(t) \rangle = x_0$, with $x(0) = x_0$), continuous, non-smooth, with stationary increments and mean square displacement $\psi(t)$. This walker is searching for one of two targets, one at the origin $x_1 = 0$ and one at a distance L , $x_2 = L > x_0 > 0$. We derive the equation for the splitting probability π_1 , defined as the probability to reach x_1 before reaching x_2 :

$$x_0 = \lim_{t \rightarrow \infty} [\pi_1 \mu_1(t) + (1 - \pi_1) \mu_2(t)], \quad (2.35)$$

where $\mu_i(t)$ is the mean trajectory after touching x_i for the first time, and before touching the other target. We note that this equation is exact and general, it is true for any process that has long time mean square displacement Kt^{2H} with $H > 0$. To find the limits of $\mu_i(t)$, we assume that the process in the future of touching one of the target for the first time (and before touching the other targets) is Gaussian with mean $\mu_i(t)$ and covariance is approximately equal to that of the original process. Using these approximations, it is

possible to find the set of integral equations that gives us $\mu_i(t)$

$$\int_0^\infty \frac{dt}{\sqrt{2\pi\psi(t)}} \left[\sum_{j=1,2} \pi_j [\mu_j(t+\tau) - (\mu_j(t) - x_i)M(t,\tau)] \exp\left(-\frac{(x_i - \mu_j(t))^2}{2\psi(t)}\right) - [x_0 - (x_0 - x_i)M(t,\tau)] \exp\left(-\frac{(x_i - x_0)^2}{2\psi(t)}\right) \right] = 0, \quad \forall_{i=1,2}, \quad (2.36)$$

where $M(t, \tau)$ is defined as in Eq. (2.31). By solving these equations numerically, it is possible to obtain the splitting probability $\pi_1(x_0)$.

Moreover, we describe an experimental setup that enables us to obtain non-Markovian trajectories, where one can test competitive first passage theories. The trajectories are obtained by tracking the movement of a bead in a fluid with concentrated long polymers. Then, we verify that the trajectories obtained are symmetric, Gaussian, with stationary increments and non-smooth (at the scale of temporal resolution), thus corresponding to the assumptions of the theory. The movement of the beads can be described as subdiffusion that becomes diffusion after some crossover time τ_0 , which leads us to consider a generalised Langevin equation

$$\int_0^t dt' K(t') \dot{x}(t-t') = F(t), \quad \langle F(t)F(t') \rangle = k_B T K(|t-t'|), \quad (2.37)$$

with a memory kernel, $K(t)$, that combines power law and exponential decays:

$$K(t) = \frac{\gamma_0}{\tau_0} f_H\left(\frac{t}{\tau_0}\right), \quad f_H(x) = \frac{1}{\Gamma(1-2H)} \frac{e^{-x}}{x^{2H}}, \quad (2.38)$$

where $H < 1/2$ is the Hurst exponent at short times and $\gamma_0 = \int_0^\infty K(t)dt$ is the long time friction coefficient.

From the trajectories obtained, one can extract the splitting probability and the mean trajectory after reaction. In Figure 2.7, we show that memory, in this viscoelastic system, does influence the splitting probability by making targets that are close easier to reach first. This effect, qualitatively described by the scaling laws present in the literature, is quantitatively described by our theory. Additionally, the mean trajectories in the future of a first passage clearly return from the targets to the space between targets. This is clearly a non-Markovian effect that shows that the hidden degrees of freedom (corresponding to the memory) are not at equilibrium at the first passage moment. This observation is the first direct experimental proof that a non-Markovian system is out-of-equilibrium at the first passage moment.

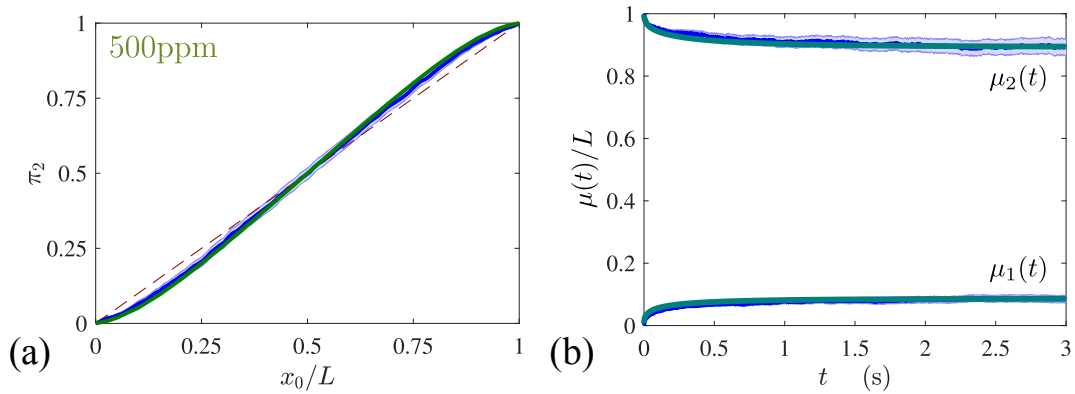


Figure 2.7: **Comparing the predictions of the non-Markovian theory for competitive event to the experimental results.** In green, we represent the theoretical predictions, in blue, the experimental observations and, in red (dashed) the pseudo-Markovian prediction, where $\mu_i(t) = x_i$ and $\pi_2 = x_0/L$. The trajectories used were recorded at 500fps in a solution of long polymers with concentration 500ppm. (a) Curves of the splitting probability π_2 as a function of the initial position x_0 with $L = 1\mu\text{m}$, (b) mean trajectories after first passage $\mu_1(t)$ and $\mu_2(t)$, with $L = 1\mu\text{m}$ and $x_0 = 0.2L$, compared to the experimental results.

2.3.3 | Kinetics of reactions in compartmentalized media

The last problem that we study in this thesis is the determination of the mean first passage time for a target that is inside a compartment that is immersed in a regularly diffusive confining volume. This problem is inspired by the existence of membraneless organelles in cells, inside which movement is subdiffusive. Our objective is to determine the mean first passage time in such situations and then, by tuning the parameters of the system, investigate if it is possible to optimize reactions. This chapter, Chapter 6, *First Passage in Complex Compartmentalized Media*, is the only one that does not deal with non-Markovian processes. This is due to the difficulty of implementing interfaces in the theory of non-Markovian random walkers. To produce a subdiffusive compartment, we suppose that the space inside the compartment is fractal. This creates a crowding effect in the compartment that forces the movement to be subdiffusive. In the literature, the problem of first passage problem mediated by compartments is restricted to the case of diffusive walks.

We consider a random walker started outside the compartment but inside a confinement of volume V , where movement is diffusive with diffusivity D . Inside the compartment of radius R and fractal dimension d_f movement is subdiffusive, characterized by the mean square displacement $\psi(t) \propto (Kt)^{2/d_w}$, where K is a transport coefficient and d_w is the walk dimension. We developed a formalism to predict the mean first passage time to reach a target of radius a in the center of the fractal compartment

$$\frac{\langle T \rangle (a|r_0 > R)}{V} = \begin{cases} \frac{e^{-\beta E_0}}{\eta d_f K} \frac{R^{d_w-d_f} - a^{d_w-d_f}}{d_w-d_f} + \frac{1}{4\pi D} \left(\frac{1}{R} - \frac{1}{r_0} \right) & (d = 3) \\ \frac{e^{-\beta E_0}}{\eta d_f K} \frac{R^{d_w-d_f} - a^{d_w-d_f}}{d_w-d_f} + \frac{1}{2\pi D} \ln \left(\frac{r_0}{R} \right) & (d = 2) \end{cases}, \quad (2.39)$$

where η is a measure of the crowding inside the compartment (defined such that the ac-

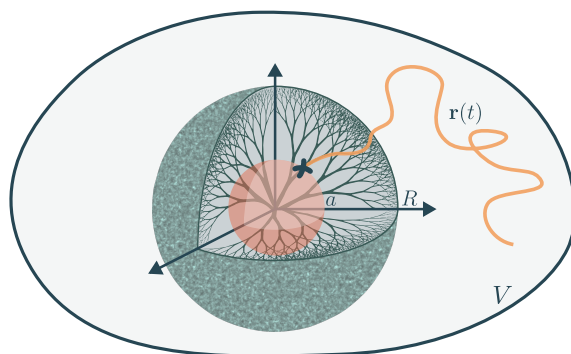


Figure 2.8: **Scheme of a first passage problem to a target that is inside a fractal compartment.** A random walker $r(t)$, started at $\mathbf{r}_0 = \mathbf{r}(0)$, moves in a confining volume, V , searching for a target of radius a inside a fractal compartment of radius R .

cessible volume inside a sphere of radius r is ηr^{d_f}), r_0 is the initial distance to the center of the compartment, $\beta = 1/k_B T$, with k_B the Boltzmann constant and T the temperature, and E_0 is an energetic gain given to the walker when it enters the compartment. This results is obtained by using the O’Shaughnessy-Procaccia operator, that is an approximative macroscopic description of the movement inside a fractal (O’Shaughnessy and Procaccia, 1985).

We have verified that our theory quantitatively predicts the mean first passage times obtained from simulations in the two dimensional case (with no fitting parameters). The simulations are performed with a compartment that is a critical bond percolation network. Our results are represented in Figure 2.9

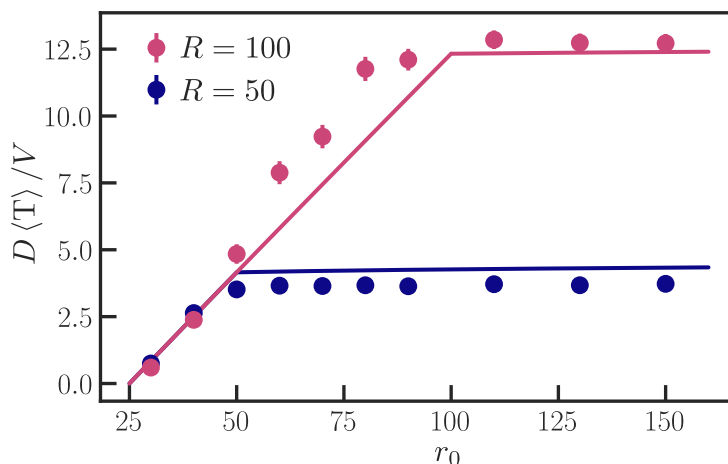


Figure 2.9: **Theoretical predictions (lines) and simulations results (symbols) for the first passage time to target in the center of a fractal compartment.** The simulations were performed in a two-dimensional square lattice with $V = 2.5 \cdot 10^5$ and lattice spacing $\ell = 1$. Inside the compartment, of radius $R/\ell = 50$ and $R/\ell = 100$, bond are removed with probability $p = 0.5$ to obtain a critical percolation network.

Then, after verifying that our theory agrees with simulations, we search for the conditions that minimize the mean first passage time in the presence of a subdiffusive compartment.

However, we do not want an optimisation that comes from fast subdiffusion inside the compartment, as crowding should impose slower movement than outside the compartment. Therefore, we are looking for optimisations that obey the condition

$$Ka^{2-d_w} \ll D. \quad (2.40)$$

We have shown that, if $E_0 = 0$ (no energetic gain inside the compartment), then it is not possible to optimize the mean first passage problem while keeping movement slower inside compartment. This is due to an entropic barrier that prevents the entrance inside the compartment. Then, we allow for an energetic gain inside the compartment such that the stationary probability to find the walker inside the compartment is the same as if there was no compartment. This acts as a compensation to the entropic barrier created by the fractal environment. The energetic gain must then be

$$E_0 \sim k_B T \ln \left(R^{d-d_f} / \eta \right), \quad (2.41)$$

where d is the dimension of the confining volume. In this case, if $d = 3$, we find that the presence of a compartment can considerably reduce the mean first passage time if the walk dimension inside the fractal is $2 < d_w < 3$, implying that the random walker is not too subdiffusive. This optimisation is made possible because the compartment allows for an infinitesimal target to be found in finite time, whereas, in three dimensional space, the mean first passage diverges for small targets. In two dimensions, $d = 2$, we find that it is not possible to optimise the mean first passage time.

KINETICS OF IMPERFECT REACTIONS FOR NON-MARKOVIAN WALKERS IN CONFINEMENT

3.1	Mean reaction time for a point-like target	27
3.1.1	Finding the mean reaction time	27
3.1.2	Self-consistent equation for the mean trajectory after reaction . . .	31
3.1.3	Simulation results and numerical methods	33
3.2	Asymptotics of the mean trajectory after reaction, $\mu(t)$	35
3.2.1	Long time asymptotics for a long time fractional Brownian motion	36
3.2.2	Short time asymptotics for a fractional Brownian motion	37
3.3	Weakly non-Markovian regime	38
3.3.1	General solution	38
3.3.2	Long time diffusive process	39
3.3.3	Perturbative fractional Brownian motion	40
3.3.4	Mean reaction time in the weakly non-Markovian limit	41
3.4	Matched asymptotic expansions for a fractional Brownian motion with limit reactivities	42
3.4.1	Weakly reactive targets	43
3.4.2	Strongly reactive targets	47
3.5	Conclusion	51

When considering chemical reactions, understanding the way reactants move from their initial positions to reach reactive distance is crucial to determine the time it takes for the reaction to happen (Rice, 1985; Berg and von Hippel, 1985). This is true in general for any kind of reaction, i.e., any process where random walkers (reactants) meet and undergo some transformation. However, this transformation might also depend on other degrees of freedom of the system and not only on the distance between reactants. When a reaction only depends on the distance between reactants and happens as soon as reactants reach some threshold distance, the problem is reduced to a first passage problem (*perfect* reaction) and

the transport is the only relevant step of these reactions. These reactions are usually called *diffusion-controlled* (or, in a more general way, *transport-controlled*) reactions (Redner, 2001; Berg and von Hippel, 1985). However, in some cases the fact that the reactants are within reactive distance might not be the only condition for the reaction to happen, in this case the reaction is called an *imperfect* reaction (Grebekov, 2019). Imperfect reactions are also known in the literature as *transport-influenced* reactions, due to the fact that both transport and the reactivity play an important role in the reaction process.

The main characteristic of imperfect reactions is that it is not sufficient to have the reactants within reactive distance for the reaction to occur. There are many mechanisms in the origin of imperfect reactivity. Here, we will distinguish them into three main classes. First, some reactions are imperfect due to an entropic barrier, i.e., even when the reactants are within reactive distance, there is only a small number of configurations where the reaction is possible (Berg and von Hippel, 1985; Zhou and Zwanzig, 1991). Two examples of entropic barriers would be: (i) a target coated with absorbing patches outside, so that reactions can only happen by reaching those patches, see Fig. 3.1.a (Berg and Purcell, 1977); (ii) particles that require a prescribed orientation to pass through a slit, Fig. 3.1.b (Shoup et al., 1981; Schmitz and Schurr, 1972). A second mechanism of imperfect reactivity is when an energetic barrier has to be overcome for the reaction to happen. Chemical reactions are a typical example of this mechanism, Fig. 3.1.c (Shoup and Szabo, 1982; Hänggi et al., 1990). Finally, there is also the case of gated reactions, where reactants switch between reactive and non-reactive states (Reingruber and Holcman, 2009; Bénichou et al., 2000; Mercado-Vásquez and Boyer, 2019; Scher and Reuveni, 2021b,a; Scher et al., 2022; Spouge et al., 1996). One example of this would be the capture a firefly on video, where the first passage time (or the moment the firefly goes in frame) is not necessarily the time where we start seeing the firefly in the video, Fig. 3.1.d). Another example is the passage through a biological channel that can be open or closed.

Determining the kinetics of imperfect reactions has attracted considerable attention in the past years. In the recent literature, one can identify two ways of dealing with imperfect reactivity. First, one might consider that reactivity does not influence the movement of the random walkers (as in, not reacting does not change the future steps of walker), which is the case we consider in this chapter. In this case one says that the imperfect reaction is characterized by sink reactivity, expressed by a spatially dependent reaction rate (Doi, 1975; Wilemski and Fixman, 1974a; Guérin et al., 2021; Isaacson et al., 2016). Note that the case of sink reactivity includes gated reactions, as the random walker does not change its motion when it passes through an inactive target (Scher and Reuveni, 2021a,b; Mercado-Vásquez and Boyer, 2019; Reingruber and Holcman, 2009). Then, one might consider the case where movement is somehow altered by a missed reaction. This would be the case of a particle trying to react at a partially reactive target, where, if a reaction does not happen, the random walker is reflected by the target (instead of crossing the target with an unaltered trajectory). In this case one says that the target is semi-reflective, or that the problem is characterized by a Robin boundary condition (Grebekov, 2019; Bressloff, 2022; Grebekov, 2020, 2010; Grebekov et al., 2017, 2018a,b, 2019; Grebekov and Oshanin, 2017; Lindsay et al., 2017; Grebekov,

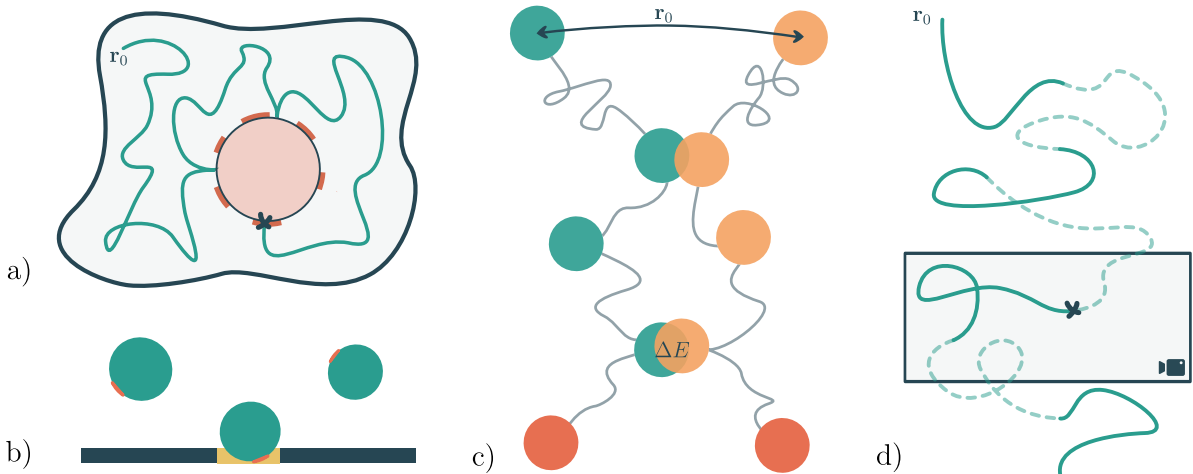


Figure 3.1: **Examples of reactions that can be modeled as imperfect reactions.** On the left, a) and b), we represent reactions that can be seen as imperfect due to an “entropic barrier”. In a) a random walker (green curve started at r_0) searches for a reaction at the circular target that is coated with absorbing patches (thick orange sections of the target). In b) the particles try to pass through a slit, but can only do so if they touch the slit with the small orange patch. In c) we represent a chemical reaction where two species, green and orange, have to meet with energy ΔE (at least) for the chemical reaction to happen, then producing two particles of the species red. In d) we represent an example of a gated reaction where one is trying to catch a firefly in video, the reaction here is when the firefly is glowing inside the frame of the camera.

2022; Grebenkov and Skvortsov, 2022; Chaigneau and Grebenkov, 2022; Grebenkov et al., 2018a; Lindsay et al., 2015). However, the study of imperfect reactions in the literature is restricted to *Markovian* (i.e., memoryless) transport processes. This is usually due to the fact that Markovian processes allow for many mathematical tools that are not available in the case of non-Markovian processes. A notable example of these tools is the Fokker-Planck equation, a partial differential equation governing the dynamics of the propagators of Markovian processes. Moreover, the main characteristic of Markovian processes is that they have no memory of the past states of the system, meaning that imperfect reaction problems can be reduced into two sub problems, one to obtain the time needed for the reactants to be within reactive distance (usually called a diffusion-controlled step) and one to obtain the time it takes for a reaction to happen once the reactants are within reactive distance (usually called a reaction-controlled step). In the Markovian case, these two problems can be solved independently since there is no memory, at least in networks or for point-like targets.

However, non-Markovian motion should be considered as “the rule rather than the exception” (van Kampen, 1998). In a non-Markovian walk, the step taken at time t depends on all the previous steps, and so the process has some intrinsic memory. It is then obvious that the Markovian reasoning of splitting imperfect reactions into two independent problems is no longer possible. In the last decade, progress has been made to describe first passage statistics for non-Markovian processes (Wiese, 2019; Sadhu et al., 2018; Delorme and Wiese, 2015; Levernier et al., 2022, 2020, 2019; Guérin et al., 2016; Walter et al., 2021; Bray et al., 2013). However, with the exception of the randomly accelerated process (Burkhardt, 2000; De Smedt et al., 2001), these approaches are limited to perfect reactions. So far, the only

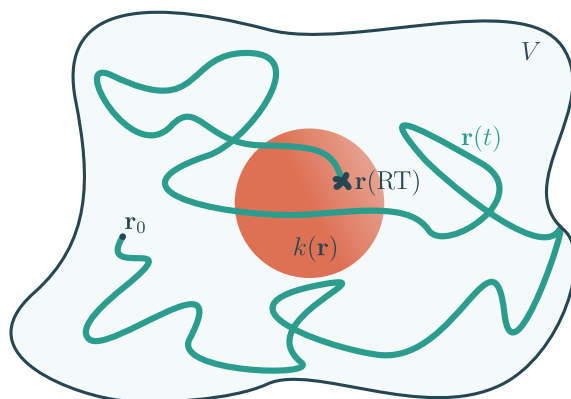


Figure 3.2: **Question investigated in this Chapter.** A random walker, $\mathbf{r}(t)$, moves in a confining space V in the presence of an imperfectly reactive target, $k(\mathbf{r})$. What is the mean time, $\langle \text{RT} \rangle$, that the random walker has to search for a reaction before the reaction happens?

theoretical methods that describe the effect of memory on the kinetics of imperfect reactions are based on quasi-static (pseudo-Markovian) approximations, also known in the literature as Wilemski-Fixman approximations (Wilemski and Fixman, 1974a,b). In these approximations one assumes that, at the moment of reaction, all degrees of freedom of the system (that are usually the origin of memory) are at equilibrium, effectively “resetting” the memory. Using this pseudo-Markovian approximation often leads to incorrect scalings and sometimes even divergent results when one knows that the results should be finite.

In this chapter, we characterize how the interplay between memory and reactivity impacts the reaction kinetics. We present a general formalism that predicts the mean reaction time for a non-Markovian random walker in confinement looking for an imperfectly reactive site, modeled by a spatially localized reaction rate. Our formalism holds in the limit of large confining volume, when the dynamics near the target is Gaussian. One of our main results is the impossibility to decompose the mean reaction time as a the sum of a transport controlled time (the mean first passage time) and a reaction controlled time (which would not depend on transport properties). This non-additivity holds for point-like targets and is a purely non-Markovian effect coming from the fact that the state of the system, i.e., the previous trajectory “stored” in memory, is not the same at successive encounters. This property is clearly illustrated for strongly subdiffusive processes in the weakly reactivity limit, for which we find that the deviation to the reaction controlled limit is a non-trivial power-law of the reactivity and therefore strongly differs from the mean first passage time.

The outline of the chapter is as follows. In Section 3.1, we develop the theory that gives us the mean reaction time for non-Markovian random walkers in confinement that is searching for a point-like imperfect target, and compare the theoretical predictions to stochastic simulations. Then, in Section 3.2, we find the typical behaviour of the random walkers right after a reaction has happened and a long time after the reaction. Finally, with the aim of better understanding the analytic solutions of the problem, we study three perturbative regimes: the weakly non-Markovian regime in Section 3.3; the weakly reactive regime in Section 3.4.1; and the strongly reactive regime in Section 3.4.2.

3.1 | Mean reaction time for a point-like target

3.1.1 | Finding the mean reaction time

Consider a one-dimensional Gaussian stochastic process, $x(t)$, moving in an arbitrary volume, V , in continuous time t , with initial position $x(0) = x_0$. Here, we assume that, far from the confinement walls, the process is unbiased, $\langle x(t) \rangle = x_0$, non-smooth, $\langle \dot{x}^2(t) \rangle = \infty$, and that the increments are stationary, so that the statistics of $x(t + \tau) - x(t)$ does not depend on t , thus leading to the covariance¹,

$$\sigma(t, t') \equiv \text{Cov}(x(t), x(t')) = \frac{1}{2}(\psi(t) + \psi(t') - \psi|t - t'|), \quad (3.1)$$

where $\psi(t) = \langle (x(t + \tau) - x(t))^2 \rangle$ is the mean square displacement, that is assumed to behave as a fractional Brownian motion at long times, i.e., $\psi(t) \underset{t \rightarrow \infty}{\sim} Kt^{2H}$, where $K > 0$ is a constant and $0 < H < 1$ is the Hurst exponent. Note that this mean square displacement is defined in unconfined space, whereas in confined space the mean square displacement should saturate at times where the random walker reaches the confinement. However, as it will be made clear during this section, the real mean square displacement (the confined one) does not intervene in the calculation of the mean reaction time, and only the unconfined mean square displacement will be used.

The probability distribution function of $x(t)$ is written as $p(\chi, t)$, meaning that the probability to find $x(t)$ in the interval $[\chi, \chi + dx[$ is given by $p(\chi, t)dx$. It is also useful to define the joint probability distribution function of this process $p(\chi, t; x_1, t + t_1)$ so that the probability of having a trajectory that verifies $x(t) \in [\chi, \chi + dx[$ and $x(t + t_1) \in [x_1, x_1 + dx_1[$ is given by $p(\chi, t; x_1, t + t_1)dx dx_1$. In the stationary limit, $t \rightarrow \infty$, this joint probability becomes the joint stationary probability $p_s(x, 0; x_1, t_1)$, with

$$p_s(x, 0; x_1, t_1) \equiv \lim_{t \rightarrow \infty} p(x, t; x_1, t + t_1). \quad (3.2)$$

Our goal here is to find the mean reaction time, $\langle \text{RT} \rangle$, for the random walker to react at a target, located at $x = 0$, that displays a reaction rate $k(x) = \kappa \delta(x)$ with finite reactivity, κ . Here we assume that the target is localized at the origin, an hypothesis that will be released in the next chapter. We start with $p(0, t)$ and write a renewal equation for it, where we split the trajectories into (i) the trajectories that have not yet reacted before t and (ii) the trajectories for which a reaction has already happened at some time $\tau < t$:

$$p(0, t) = p(0, t; \text{RT} > t) + \int_0^t d\tau p(0, t; \text{RT} = \tau), \quad (3.3)$$

where $p(0, t; \text{RT} > t)$ is the joint probability density to find the random walker at the target

¹In Section 2.2.1, we prove that unbiased Gaussian processes with stationary increments must have this covariance.

at time t and that it has not yet reacted, whereas $p(0, t; \text{RT} = \tau)$ is the joint probability density that the random walker is at the target at time t and that it has already reacted at time $\tau < t$, which is then integrated over τ to take into account all possible reactions from time 0 to t .

We define the probability distribution function for the reaction time, $F(t)$, such that $F(t)dt$ is the probability that the reaction time is in the interval $[t, t + dt]$. This probability can be written as

$$F(t)dt = \int_{-\infty}^{\infty} d\chi p(\chi, t; \text{RT} > t) k(\chi) dt = p(0, t; \text{RT} > t) \kappa dt, \quad (3.4)$$

where one takes the probability to reach a reactive position without a reaction, $p(\chi, t; \text{RT} > t)$, and multiplies it by the probability of a reaction at that position, $k(\chi)dt = \kappa\delta(\chi)dt$.

Using Eq. (3.4) in Eq. (3.3) and subtracting $p_s(0) \equiv \lim_{t \rightarrow \infty} p(0, t)$, the stationary probability density of finding the walker at the target, on both sides, one obtains:

$$p(0, t) - p_s(0) = \frac{F(t)}{\kappa} - p_s(0) \int_t^{\infty} d\tau F(\tau) + \int_0^t d\tau F(\tau) [p(0, t | \text{RT} = \tau) - p_s(0)], \quad (3.5)$$

with $p(0, t | \text{RT} = \tau) = p(0, t; \text{RT} = \tau) / F(\tau)$ the conditional probability density of finding the walker at the target at time t given that a reaction has happened at time $\tau < t$.

If one now integrates Eq. (3.5) over t , it is possible to uncover the mean reaction time from the second term of the right hand side,

$$\int_0^{\infty} dt \int_t^{\infty} d\tau F(\tau) = \int_0^{\infty} d\tau \int_0^{\tau} dt F(\tau) = \int_0^{\infty} d\tau \tau F(\tau) = \langle \text{RT} \rangle. \quad (3.6)$$

Performing the same integration in the third term of the right hand side of Eq. (3.5) one can write:

$$\begin{aligned} & \int_0^{\infty} dt \int_0^t d\tau F(\tau) (p(0, t | \text{RT} = \tau) - p_s(0)) \\ &= \int_0^{\infty} d\tau \int_{\tau}^{\infty} dt F(\tau) (p(0, t | \text{RT} = \tau) - p_s(0)) \end{aligned} \quad (3.7)$$

$$= \int_0^{\infty} d\tau \int_0^{\infty} du F(\tau) (p(0, u + \tau | \text{RT} = \tau) - p_s(0)) \quad (3.8)$$

$$= \int_0^{\infty} du \left(\int_0^{\infty} d\tau F(\tau) p(0, u + \tau | \text{RT} = \tau) - p_s(0) \int_0^{\infty} d\tau F(\tau) \right) \quad (3.9)$$

$$= \int_0^{\infty} du (p_{\pi}(0, u) - p_s(0)). \quad (3.10)$$

The steps performed to obtain Eq. (3.10) are the switch of the order of integration, the variable change $t \rightarrow u = t - \tau$ and the integration of $F(t)$ in the term proportional to $p_s(0)$ by using its normalization condition. Then, in the final step, we have identified $p_{\pi}(x, t)$, which we define as

$$p_{\pi}(x, t) = \int_0^{\infty} d\tau F(\tau) p(x, t + \tau | \text{RT} = \tau). \quad (3.11)$$

The function $p_\pi(x, t)$ is the probability distribution function of a new process $x_\pi(t)$, defined as $x_\pi(t) = x(\text{RT} + t)$, where RT is the reaction time (a random variable by itself), so that this process represents the trajectory followed after a reaction has happened. In Fig. 3.3, we represent some realizations of this process for a bead spring chain, and the corresponding average.

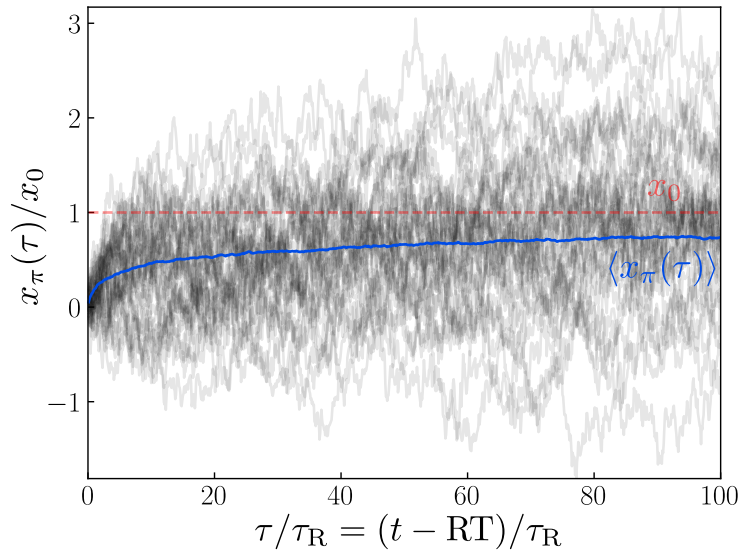


Figure 3.3: **Representation of the resulting process after a reaction, $x_\pi(t)$.** In grey, with some transparency, we represent some trajectories after the reaction has happened, $x_\pi(t) = x(\text{RT} + t)$; in dashed red we represent the initial position of the original process, $x(0) = x_0$, for reference; and in blue we represent the mean trajectory after reaction, $\langle x_\pi(\tau) \rangle$. The simulations were performed by looking at the first monomer of a bead spring chain with 50 monomers, see Section 3.1.3 for a small introduction of the bead spring chain. The time unit, τ_R , is the relaxation time of a single bond.

After the integration over t of Eq. (3.5), one can use Eqs. (3.6) and (3.10) to write the equation that connects the mean reaction time to the propagators (probability distribution functions) of our system:

$$p_s(0) \langle \text{RT} \rangle = \frac{1}{\kappa} + \int_0^\infty dt (p_\pi(0, t) - p(0, t)). \quad (3.12)$$

Note that this equation for the mean reaction time is exact since no approximations have been made up to here and, additionally, no properties of Gaussian processes have been used, so this equation is valid for any non-smooth stochastic process. The main difficulty here, and the reason we have to specifically treat Gaussian processes in what follows, is the fact that the function $p_\pi(x, t)$ is not known for most stochastic processes. Moreover, as expected from Section 2.1.2, we see that the term corresponding to slow reactions and fast diffusion (equivalent to $\kappa \rightarrow 0$), $1/\kappa$, is still present in Eq. (3.12).

If one now takes the large volume limit, it is possible to approximate the propagators in confined space by the free space propagators. Therefore, since $x(t)$ is a Gaussian process

with stationary increments, one can write

$$p(0, t) \approx \frac{1}{\sqrt{2\pi\psi(t)}} \exp\left(-\frac{x_0^2}{2\psi(t)}\right), \quad (3.13)$$

where $\psi(t)$, as mentioned before, corresponds to the unconfined mean square displacement, assumed to behave as $\psi(t) \underset{t \rightarrow \infty}{\sim} Kt^{2H}$. Additionally, we assume that in this limit one can still write the stationary probability as $p_s(0) = 1/V$. Note that, if the confinement is a harmonic potential instead of a solid (hard wall) confinement, it is still possible to write $p_s(0) = 1/V$ where V is an effective volume, with the limit $V \rightarrow \infty$ corresponding to a small harmonic stiffness. Therefore,

$$\frac{\langle \text{RT} \rangle}{V} = \frac{1}{\kappa} + \int_0^\infty dt \left[p_\pi(0, t) - \frac{1}{\sqrt{2\pi\psi(t)}} \exp\left(-\frac{x_0^2}{2\psi(t)}\right) \right]. \quad (3.14)$$

We are now left to find the probability distribution function of the process after reaction, $p_\pi(x, t)$. As an approximation, we assume that the process $x_\pi(t)$ is Gaussian with mean $\mu(t) = \langle x(t + \text{RT}) \rangle$ and covariance $\sigma_\pi(t, t') \approx \sigma(t, t')$. Using this approximation one can write

$$p_\pi(x, t) \approx \frac{1}{\sqrt{2\pi\psi(t)}} \exp\left(-\frac{(x - \mu(t))^2}{2\psi(t)}\right), \quad (3.15)$$

and the final equation for the mean reaction time reads

$$\frac{\langle \text{RT} \rangle}{V} = \frac{1}{\kappa} + \int_0^\infty \frac{dt}{\sqrt{2\pi\psi(t)}} \left[\exp\left(-\frac{\mu(t)^2}{2\psi(t)}\right) - \exp\left(-\frac{x_0^2}{2\psi(t)}\right) \right]. \quad (3.16)$$

Notice that the problem is not yet solved, to use Eq. (3.16) we still need to find the shape of $\mu(t)$, which is not a trivial problem. We also note that this function is the signature of memory in this system. If there were no memory, then $\mu(t)$ should be zero, as a consequence of the fact that $x_\pi(0) = 0$ and the process should not be biased. Note that Eq. (3.16) is remarkably similar to the equation obtained for the perfect case, where $\kappa \rightarrow \infty$ (Guérin et al., 2016). The only difference between our equation and that of the perfect case is the term $1/\kappa$, that, as explained in Section 2.1.2, is inherent to the problem of imperfect reactions. However, one must not think that this similarity means that the problem of imperfect reactions in non-Markovian processes is solved by taking the perfect case and adding a term $1/\kappa$. This would be wrong because one still has to find the function $\mu(t)$, which might depend on the reactivity κ , thus making the problem completely different from that of the perfect case.

3.1.2 | Self-consistent equation for the mean trajectory after reaction

To find the function $\mu(t)$, we have to study the trajectories in the future of a reaction. To do so, we consider a generalized version of the renewal equation, Eq. (3.3), written for the joint probabilities with an extra point in the future of a passage through the target:

$$p(0, t; x_1, t + t_1) = p(0, t; x_1, t + t_1; \text{RT} > t) + \int_0^t d\tau p(0, t; x_1, t + t_1; \text{RT} = \tau), \quad (3.17)$$

which is true for arbitrary x_1 and $t_1 > 0$. Following similar step to the ones used to derive Eq. (3.12), starting by the subtraction of $p_s(x_1, t_1; 0)$ on both sides of Eq. (3.17) and integrating over t from 0 to ∞ , one can write

$$p_s(x_1, t_1; 0) \langle \text{RT} \rangle = \frac{p_\pi(x_1, t_1)}{\kappa} + \int_0^\infty d\tau [p_\pi(0, t; x_1, t + t_1) - p(0, t; x_1, t + t_1)]. \quad (3.18)$$

The first term on the left hand side, with the mean reaction time, is obtained as before by using Eq. (3.6). Similarly, the integral term is obtained with the same steps that led to Eq. (3.10), the sole difference being that the development is done with joint probabilities and one must extend the definition in Eq. (3.11) to

$$p_\pi(x, t; x_1, t + t_1) = \int_0^\infty d\tau F(\tau) p(x, t + \tau, x_1, t + t_1 + \tau | \text{RT} = \tau). \quad (3.19)$$

The term with $p_\pi(x_1, t_1)$ in Eq. (3.18) is not so simple to obtain from the previous development. It comes from the term $p(0, t; x_1, t + t_1; \text{RT} > t)$ in Eq. (3.17). In fact, to relate $p(0, t; x_1, t + t_1; \text{RT} > t)$ to $p_\pi(x_1, t_1)$ one must first introduce the probability P , defined as

$$P \equiv \mathbb{P}[x(t + t_1) \in [x_1, x_1 + dl[\text{ and } \text{RT} \in [t, t + dt[], \quad (3.20)$$

where dl and dt are infinitesimals of space and time. This probability can be written in two different ways. First, we can write it by using the reaction rate:

$$P = \int_{-\infty}^\infty dx k(x) dt p(x, t; x_1, t + t_1; \text{RT} > t) dl = \kappa p(0, t; x_1, t + t_1; \text{RT} > t) dt dl, \quad (3.21)$$

where we write P as the product of the probability of reaching a reactive position without a reaction and the probability of a reaction at that reactive position. Alternatively, one can also write P by using the reaction time probability distribution function, $F(t)$:

$$P = p(x_1, t + t_1 | \text{RT} = t) dl F(t) dt. \quad (3.22)$$

Combining the two ways of writing P generalizes the argument in Eq. (3.4):

$$\kappa p(0, t; x_1, t + t_1; \text{RT} > t) = p(x_1, t + t_1 | \text{RT} = t) F(t), \quad (3.23)$$

which, after integration over t , becomes

$$\int_0^\infty dt p(0, t; x_1, t + t_1; \text{RT} > t) = \frac{p_\pi(x_1, t_1)}{\kappa}, \quad (3.24)$$

thus justifying the term with $p_\pi(x_1, t_1)$ in Eq. (3.18).

After multiplication of Eq. (3.18) by x_1 and integration over the same variable one can write

$$\langle x(t_1)|0 \rangle_s \frac{\langle \text{RT} \rangle}{V} = \langle x(t_1)|0, 0 \rangle_\pi \frac{1}{\kappa} + \int_0^\infty dt [\langle x(t+t_1)|0, t \rangle_\pi p_\pi(0, t) - \langle x(t+t_1)|0, t \rangle p(0, t)], \quad (3.25)$$

where $\langle x(t_1)|0 \rangle_s = 0$ is the stationary average of $x(t_1)$ given that, at time 0, the process is at the target; $\langle x(t+t_1)|0, t \rangle_\pi$ is the mean position after time $t+t_1$ given that, at time t , the particle was at the target and that it has reacted at time 0. Using the formulas for conditional averages of Gaussian random variables² (that we also call projection formulas), one can write (Eaton, 2007):

$$\langle x(t+t_1)|0, t \rangle_\pi = \mu(t+t_1) - \mu(t) \frac{\sigma(t, t+t_1)}{\psi(t)}, \quad (3.26)$$

$$\langle x(t+t_1)|0, t \rangle = x_0 - x_0 \frac{\sigma(t, t+t_1)}{\psi(t)}. \quad (3.27)$$

Collecting the expressions of $\langle x(t+t_1)|0, t \rangle_\pi$, $\langle x(t+t_1)|0, t \rangle$ and $\langle x(t_1)|0 \rangle_s$, we can write the final form of Eq. (3.25), that defines $\mu(t)$ in a self-consistent way,

$$0 = \frac{\mu(\tau)}{\kappa} + \int_0^\infty \frac{dt}{\sqrt{2\pi\psi(t)}} \left[(\mu(t+\tau) - \mu(t)M(t, \tau))e^{-\frac{\mu^2(t)}{2\psi(t)}} - x_0(1 - M(t, \tau))e^{-\frac{x_0^2}{2\psi(t)}} \right], \quad (3.28)$$

with

$$M(t, \tau) = \frac{\sigma(t+\tau, t)}{\psi(t)} = \frac{\psi(t+\tau) + \psi(t) - \psi(\tau)}{2\psi(t)}. \quad (3.29)$$

In principle, we have now a procedure to find the mean reaction time: we have an integral equation giving us $\mu(t)$ that we can insert into Eq. (3.16) thus obtaining the mean reaction time. However, Eq. (3.28) is a non-linear integral equation that is not analytically solvable. Nonetheless, there are analytic results that we can obtain in some limiting cases. These limits will be studied in detail in sections 3.2, 3.3 and 3.4.

As a first remark, we see that the statistics of the trajectories after a reaction depends on the imperfect properties of the target, κ . This is made obvious in Eq. (3.28) where $\mu(t)$ explicitly depends on the reactivity, κ . Therefore, *a priori*, the mean reaction time cannot be decomposed into two independent problems, one for the first passage (which would be the integral term in Eq. (3.16) but now depends on κ) and one for the reaction once the walker is started at the target. This dependence is also seen in simulations, see Fig. 3.4, where it is evident that the statistics of the process $x_\pi(\tau)$ is highly dependent on κ .

²We present these formulas in Appendix A.

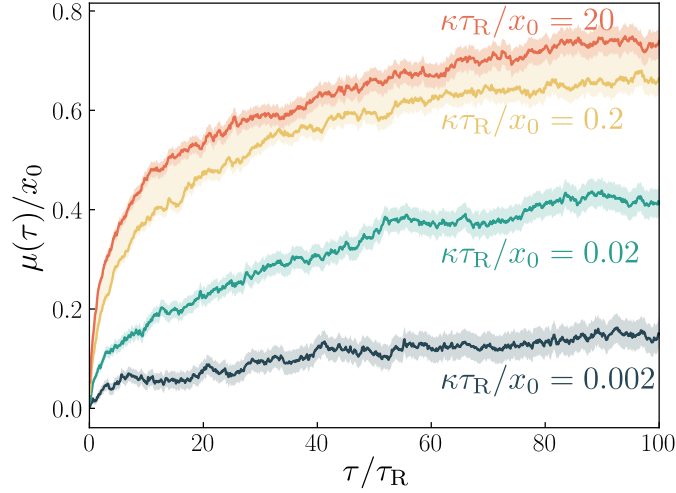


Figure 3.4: **The mean trajectory after reaction depends on the reactivity.** Mean trajectory of the simulated $x(t)$ after reaction, $\mu(\tau) = \langle x(\tau + \text{RT}) \rangle$ (and associated standard error of the mean) for different reactivities, κ . The simulations were performed by looking at the first monomer of a bead spring chain with 50 monomers, whose dynamics is given by the Langevin equation in Eq. (3.34). For each reactivity 1000 runs have been performed. The time unit, τ_R , is the relaxation time of one monomer in the bead spring chain.

3.1.3 | Simulation results and numerical methods

Let us now introduce a numerical method to solve the integral equation in Eq. (3.28) and obtain our theoretical predictions of the mean reaction time. One can write Eq. (3.28) as

$$0 = \mathcal{H}([\mu], \tau) = \frac{\mu(\tau)}{\kappa} + \int_0^\infty dt h(t, \tau), \quad (3.30)$$

which, in principle, can be solved with the iteration scheme

$$\mu_i(t) = \mu_{i-1}(t) - \Delta s \mathcal{H}([\mu_{i-1}], t), \quad (3.31)$$

where $\mu_0(t) = 0$ and Δs is the iteration step. One can see that, as more iterations are made, and if Δs is sufficiently small, a fixed point should be reached. This fixed point is characterized by small values of $\mathcal{H}([\mu_{i-1}], t)$ for all times t . However, this iteration scheme assumes that one is dealing with continuous functions, which is not the case for numerical integrations. Therefore, we discretize time and introduce a cutoff t_M , that allows us to perform the integral in Eq. (3.30) in two parts. First, one computes the integral from 0 to t_M with the trapezoidal method, then, the integral from t_M to ∞ can be analytically computed by assuming that the long time behaviour of $\mu(t)$ is known, which is in fact the case as we will shown in Section 3.2. We choose the following interpolation for $\mu_i(t)$:

$$\mu_i(t) = \begin{cases} [\mu_i(t_j) + \mu_i(t_{j+1})]/2 & \text{for } t_j < t < t_{j+1} \\ x_0 - A_i t^{2H-1} & \text{for } t > t_M \end{cases}, \quad (3.32)$$

where we have used for the long time behaviour the result of next section, Eq. (3.40). The constant A_i satisfies the equality:

$$x_0 - A_i t_M^{2H-1} = \mu_i(t_M). \quad (3.33)$$

Note that the integral from t_M to ∞ can be performed without discretization. After performing the necessary n_s iteration steps, one obtains the numerical solution $\mu_{n_s}(t)$, which one then introduces in Eq. (3.16), thus finding the mean reaction time.

Now that we have a numerical procedure to find the mean reaction time, we would like to test the accuracy of the theory. To do so, we use stochastic simulations. We use two types of physical processes. First, we simulate a pure fractional Brownian motion, characterized by a mean square displacement, $\psi(t) = Kt^{2H}$, where the confining volume is introduced by setting the walker on a ring, i.e., $x(t) = z(t) \bmod V$, where \bmod represents the modulo operator, $z(t)$ is a fractional Brownian motion (unconfined), obtained using the circulant matrix algorithm (Davies and Harte, 1987; Dietrich and Newsam, 1997), and $x(t)$ is our process that is searching for a target at the origin of positions while confined to the volume V .

The second type of stochastic process that we simulate is the bead spring chain (also known as the Rouse chain) (Doi and Edwards, 1988). In these simulations we consider N particles with trajectories $y_i(t)$, that move in a fluid with friction drag γ and are connected in series by springs of stiffness k . Their dynamics is described by the Langevin equations

$$\gamma \dot{y}_i(t) = k(y_{i+1}(t) - 2y_i(t) + y_{i-1}(t)) + f_i(t), \quad (3.34)$$

where $\langle f_i(t) \rangle = 0$ and $\langle f_i(t) f_j(t') \rangle = 2\gamma k_B T \delta_{ij} \delta(t - t')$, with k_B the Boltzmann constant and T the temperature of the surrounding fluid. Note that, for this equation to apply for all monomers, one has to add two fictitious monomers, $y_0(t) = y_1(t)$ and $y_{N+1}(t) = y_N(t)$. We introduce, as natural units, the typical length of one bond, $l_R = \sqrt{k_B T/k}$, and, as the time unit, its typical relaxation time, $\tau_R = \gamma/k$. To “create” a non-Markovian walker one can look at the first monomer of the chain, $x(t) = y_1(t)$. By only looking at one monomer, the others are forgotten and act as hidden variables where memory is stored. The mean square displacement of this monomer displays three behaviours (Khokhlov and Grosberg, 1994):

$$\psi(t) \sim \begin{cases} 2Dt & \text{for } t \ll \tau_R \\ (4l_R^2/\sqrt{\pi})\sqrt{t/\tau_R} & \text{for } \tau_R \ll t \ll \tau_R N^2 \\ 2(D/N)t & \text{for } t \gg \tau_R N^2 \end{cases}, \quad (3.35)$$

where $D = k_B T/\gamma$ is the diffusion coefficient of a single (free) monomer. Therefore, if one simulates bead spring chains with sufficiently large N it is possible to mimic a fractional Brownian motion with $H = 1/4$.

Both types of simulation are not compatible with ideal point-like targets. Consequently, instead of simulating point-like targets, one has to simulate a reactive region of size $2a$ with

reaction rate $\kappa(x) = H(a - |x|)\kappa/(2a)$, such that $\int_0^\infty dx \kappa(x) = \kappa$. To better approximate a point-like target one has to verify that a is sufficiently small so that the mean reaction time converges to the point-like limit.

To find the mean reaction times from these simulations we use two different methods. (i) For the simulations of a Rouse chain, we numerically solve Eq. (3.34) with some time step dt . Then, at each time step, we decide if a reaction occurs or not. If it does, we store the reaction time and create more trajectories. The result of these simulations is the mean value of the different reaction times. (ii) Alternatively, one can build an estimator for the mean reaction time based on one trajectory $x_i(t)$,

$$\hat{\tau}_\kappa[x_i] = \int_0^\infty dt e^{-\kappa \ell_t[x_i]}, \quad (3.36)$$

where $\ell_t[x_i] \equiv \int_0^t d\tau \delta(x_i(\tau))$ is the local time at time t associated to the trajectory $x_i(\tau)$, i.e., the time that the trajectory $x_i(\tau)$ spent in the vicinity of the target up to time t . In practice, for extended targets, the local time is estimated by $\ell_t = (1/2a) \int_0^t d\tau \Theta(a - |x(\tau)|)$, where $\Theta(x)$ is the Heaviside step function. If one assumes that an extensive sampling of trajectories is equivalent to an extensive sampling of the local times, then, using the fact that $S(t) = \langle e^{-\kappa \ell_t} \rangle$ (Grebekov, 2020), it becomes clear that the expected value of $\hat{\tau}[x_i]$ is equal to the mean reaction time³. This method is preferred in comparison to (i), as it converges much faster. We use (ii) when simulating the fractional Brownian motion.

In Figure 3.5, we compare the theoretical prediction of $\langle \text{RT} \rangle$ to simulation results obtained for a bead spring chain and for fractional Brownian motions with $H = 1/4$ and $H = 0.6$. We find that our theory quantitatively predicts the correct mean reaction times. This is specially true when compared to the pseudo-Markovian predictions, where equilibrium is assumed at the reaction time, i.e., $\mu(t) = 0$. By taking a pseudo-Markovian approach, one would find that, for $H < 1/3$, the mean reaction time (over V) should be infinite, which is clearly not true after analyzing the results of the simulations. Even though the pseudo-Markovian approach gives reasonable results for $H = 0.6$ (and in general for $H > 1/3$) we still find that our non-Markovian approach performs better when compared to simulations.

3.2 | Asymptotics of the mean trajectory after reaction, $\mu(t)$

The first analytic results one can get from the theory developed in Section 3.1 is the long and short time behaviour of $\mu(t)$, the mean trajectory after reaction. In this section, we first focus on a schematic derivation of the long time behaviour of $\mu(t)$ for the long time fractional Brownian motion and then, for fractional Brownian motions, we derive the short time behaviour or $\mu(t)$.

³The derivation goes as follows: $\langle \hat{\tau}[x_i] \rangle = \frac{1}{N_{\text{traj.}}} \sum_{i=1}^{N_{\text{traj.}}} \hat{\tau}[x_i] = \int_0^\infty \frac{dt}{N_{\text{traj.}}} \sum e^{-\kappa \ell_t} = \int_0^\infty dt S(t) = \langle \text{RT} \rangle$

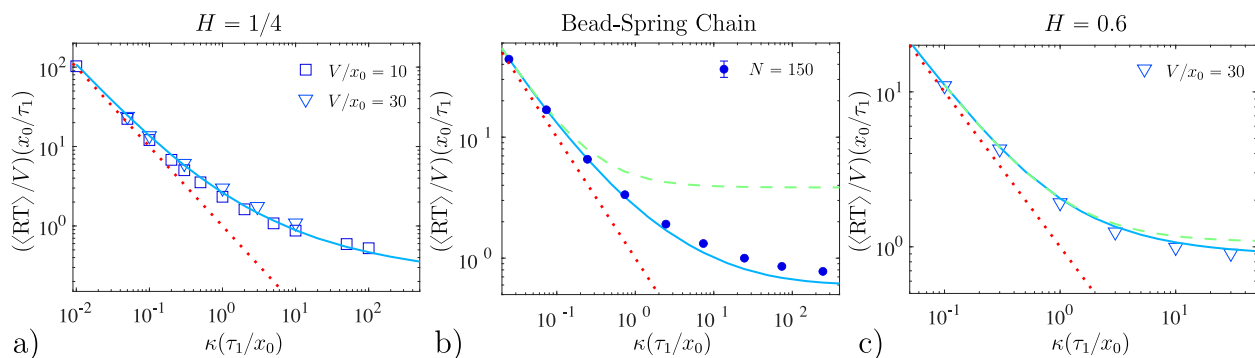


Figure 3.5: **Testing the theoretical predictions of $\langle RT \rangle$ against simulations.** Simulation results, in symbols, for different processes in units of x_0 and $\tau_1 = (x_0^2/K)^{1/2H}$. The continuous blue line is the numerical mean reaction time obtained with our theory, the dotted (red) line is the asymptote $1/\kappa$ and the dashed (green) line is the pseudo-Markovian approach (equivalent to setting $\mu(t) = 0$). Note that the pseudo-Markovian approach predicts infinite mean reaction times for long time fractional Brownian motions with $H < 1/3$. a) and c) are simulations of fractional Brownian motions with $H = 1/4$ and $H = 0.6$ respectively. b) is the simulation of a bead-spring (or Rouse) chain with parameters $x_0 = 5l_R$, $V = 30x_0$ and $N = 150$.

3.2.1 | Long time asymptotics for a long time fractional Brownian motion

Let us start with a long time fractional Brownian motion, i.e., the mean square displacement for large times is $\sim Kt^{2H}$ with $0 < H < 1$. Given the similarity of Eq. (3.28) to the equation obtained in the perfect case (the only difference is the presence of the term $\mu(t)/\kappa$, that goes to zero in the perfect limit) one feels tempted to look for a long time asymptotic behaviour of $\mu(t)$ that is similar to the perfect one:

$$\mu(t) \underset{t \rightarrow \infty}{\sim} x_0 - \frac{A(\kappa)}{t^\alpha}, \quad (3.37)$$

where $A(\kappa) \neq 0$. In comparison to the perfect result, in our ansatz we have added the possibility for A to depend on κ and used a general exponent $\alpha > 0$ instead of the $1 - 2H$ obtained in the perfect case (Guérin et al., 2016).

Inserting our ansatz into Eq. (3.28) for $\tau \rightarrow \infty$, and changing t to $u\tau$, we obtain the following leading order terms

$$0 = \mathcal{H}(\tau) \sim \frac{x_0 - A(\kappa)\tau^{-\alpha}}{\kappa} - A(\kappa) \int_0^\infty \frac{\tau^{1-H-\alpha} du}{\sqrt{2\pi K} u^H} \left(\frac{1}{(u+1)^\alpha} - \frac{1}{u^\alpha} \frac{(u+1)^{2H} + u^{2H} - 1}{2u^{2H}} \right), \quad (3.38)$$

where the exponential terms, $e^{-\mu^2(t)/2\psi(t)}$ and $e^{-x_0^2/2\psi(t)}$ are equal to unity in the limit $t = u\tau \rightarrow \infty$ because, in that limit, $\mu(\tau) \ll \sqrt{\psi(\tau)}$ and $x_0 \ll \sqrt{\psi(\tau)}$.

For the condition $\mathcal{H}(\tau) = 0$ to be true, it must also be true at all orders in τ . However, as we have developed $\mathcal{H}(\tau)$ to only obtain its leading terms, Eq. (3.38) can only give us the equality for the leading term. Looking at Eq. (3.38), since $x_0 \neq 0 \neq A(\kappa)$, the only term that

might be equal to zero is the integral term. Therefore, this must be the leading behaviour of $\mathcal{H}(\tau)$, giving us the condition $\alpha < 1 - H$ and implying the equality:

$$\int_0^\infty \frac{du}{u^H} \left(\frac{1}{(u+1)^\alpha} - \frac{1}{u^\alpha} \frac{(u+1)^{2H} + u^{2H} - 1}{2u^{2H}} \right) = 0, \quad (3.39)$$

which is only verified if $\alpha = 1 - 2H > 0$. Hence, for $H < 1/2$, one must have $\mu(t) \sim x_0 - A(\kappa)/t^{1-2H}$.

We are then left to find the leading behaviour of $\mu(t)$ for $H > 1/2$. To do this, we assume that α might be negative, meaning that $A(\kappa)/t^\alpha$ is now the leading term of $\mu(t)$. Nonetheless, Eq. (3.38) (without the x_0) is still the correct expression of the leading term of $\mathcal{H}(\tau)$ and therefore $\alpha = 1 - 2H$ is still the only solution of $\mathcal{H}(\tau) = 0$, thus giving us the long time behaviour of $\mu(t)$ for $H > 1/2$.

Combining the results for $H < 1/2$ and $H > 1/2$, one obtains the long time asymptotic behaviour of $\mu(t)$:

$$\mu(t) \underset{t \rightarrow \infty}{\sim} \begin{cases} x_0 - \frac{A(\kappa)}{t^{1-2H}} & \text{for } H < \frac{1}{2} \\ x_0 - A(\kappa) & \text{for } H = \frac{1}{2} \\ A(\kappa)t^{2H-1} & \text{for } H > \frac{1}{2} \end{cases}, \quad (3.40)$$

where $A(\kappa)$ is unknown. In Section 3.4, we find the asymptotic of $A(\kappa)$ for $\kappa \rightarrow 0$ and $\kappa \rightarrow \infty$.

In conclusion, we have found that the long time behaviour of the mean trajectory after reaction in the imperfect case is similar to that of perfect reactions. Therefore, the fact that the initial position is never forgotten, seen by the presence of x_0 in Eq. (3.40), remains true when the reactions are imperfect (for any reactivity κ , including very small ones).

3.2.2 | Short time asymptotics for a fractional Brownian motion

In this section, we derive the short time behaviour of $\mu(t)$. Naturally, one has to additionally assume a short time behaviour of the mean square displacement, $\psi(t)$. Let us take a fractional Brownian motion, $\psi(t) = Kt^{2H}$ at all times t . Let us start by expanding the integral equation that gives $\mu(t)$, Eq. (3.28), for small times ($\tau \rightarrow 0$):

$$\begin{aligned} \frac{\mu(\tau)}{\kappa} = & -\tau^{2H} \frac{1}{2\sqrt{2\pi K}} \int_0^\infty \frac{dt}{t^{3H}} \left[\mu(t) e^{-\frac{\mu^2(t)}{2\kappa t^{2H}}} - x_0 e^{-\frac{x_0^2}{2\kappa t^{2H}}} \right] \\ & - \tau \int_0^\infty \frac{dt}{\sqrt{2\pi K} t^H} \left[\left(\mu'(t) - H \frac{\mu(t)}{t} \right) e^{-\frac{\mu^2(t)}{2\kappa t^{2H}}} + x_0 H \frac{1}{t} e^{-\frac{x_0^2}{2\kappa t^{2H}}} \right], \end{aligned} \quad (3.41)$$

where $\mu'(t)$ denotes de time derivative of $\mu(t)$.

From Eq. (3.41), we see that, if the integrals converge, then, there are two possible short time behaviours for $\mu(\tau)$: one for $H < 1/2$ and one for $H > 1/2$. For $H < 1/2$, $\tau^{2H} \gg \tau$ for small τ , meaning that the mean trajectory after reaction for short times is $\sim \tau^{2H}$. Using this behaviour and the one for long times, Eq. (3.40), it is possible to show that the integral in the prefactor of τ^{2H} converges, and, consequently, the short time behaviour is well identified for $H < 1/2$. Similarly, for $H > 1/2$, the integral in the prefactor of the leading term (τ) becomes convergent if the short time behaviour of $\mu(\tau)$ is $\sim \tau$. Therefore, the short time behaviour of $\mu(t)$ is given by

$$\mu(t) \underset{t \rightarrow 0}{\sim} \begin{cases} \kappa A(x_0, K, \kappa) t^{2H} & \text{for } H < \frac{1}{2} \\ \kappa B(x_0, K, \kappa) t & \text{for } H > \frac{1}{2} \end{cases}, \quad (3.42)$$

where A and B are the integral terms in Eq. (3.41), which might depend on x_0 , K and κ .

In conclusion, we find that, when a reaction happens, a superdiffusive (fractional Brownian) particle crosses the target with a finite average speed, whereas a subdiffusive particle behaves as if it were being pulled back to the initial position by a force $F \sim \kappa A(x_0, K, \kappa)$, with $\mu(t) \sim F\psi(t)$, which can be proved by considering a generalized Langevin equation with a force, see for example [Levernier et al. \(2020\)](#).

3.3 | Weakly non-Markovian regime

3.3.1 | General solution

Given that the Markovian case is already well studied, it is interesting to see what happens in its vicinity. To do this, we take a process with a mean square displacement that is the sum of diffusion, $\sim 2Dt$, and a perturbation $\psi_1(t)$, such that $\psi(t) = 2Dt + \varepsilon\psi_1(t) + \mathcal{O}(\varepsilon^2)$, where $\varepsilon \ll 1$ quantifies the deviation from Markovianity (diffusion). We choose the time units such that $D = 1/2$. For Markovian processes the mean trajectory after reaction, $\mu(t)$, should be equal to the position of the target (zero in this case), in this perturbative limit we can write $\mu(t) = \varepsilon\mu_1(t) + \mathcal{O}(\varepsilon^2)$. Introducing these expansions into Eq. (3.28) (the integral equation for $\mu(t)$) and differentiating with respect to τ one obtains, at first order in ε , the linear integral equation:

$$\mu_1'(\tau) + \frac{\kappa}{\sqrt{2\pi}} \int_0^{+\infty} \frac{dt}{\sqrt{t}} \mu_1'(t + \tau) = \frac{\kappa}{\sqrt{2\pi}} g(\tau), \quad (3.43)$$

where the prime denotes temporal differentiation and

$$g(\tau) = -x_0 \int_0^\infty \frac{dt}{\sqrt{t}} \frac{\psi_1'(t + \tau) - \psi_1'(\tau)}{2t} e^{-\frac{x_0^2}{2t}}. \quad (3.44)$$

This equation can be solved analytically, however, instead of solving this particular equation one can solve the general set of second kind Volterra integral equations of the form

$$f(\tau) + \int_0^\infty dt K(t)f(t + \tau) = h(\tau). \quad (3.45)$$

In Appendix B, Eq (B.10), we derive the general solution for the case where $f(t) = y'(t)$. Using this solution and noticing that $K(t) = \kappa/\sqrt{2\pi t}$, $h(t) = g(t)\kappa/\sqrt{2\pi}$ and $\mu_1(0) = 0$, one can write

$$\mu_1(t) = \frac{\kappa}{\sqrt{2\pi}} \int_0^{+\infty} d\zeta W(\zeta)[g(\zeta) - g(\zeta + t)], \quad (3.46)$$

where $W(t) = \mathcal{L}^{-1}\left[\frac{1}{s(1+\tilde{K}(s))}\right](t)$, with $\tilde{f}(s) = \mathcal{L}[f(t)](s) = \int_0^{+\infty} dt f(t)e^{-st}$ the Laplace transform of the function $f(t)$. Using the expression of $K(t)$ it is possible to obtain $W(t) = e^{\kappa^2 \frac{t}{2}} \operatorname{erfc}\left(\kappa\sqrt{\frac{t}{2}}\right)$, where $\operatorname{erfc}(x)$ is the complementary error function⁴. Therefore, the solution to the original integral equation, Eq. (3.43), can be written as

$$\begin{aligned} \mu_1(t) = \frac{x_0\kappa}{2\sqrt{2\pi}} \int_0^{+\infty} d\xi \int_0^{+\infty} d\zeta e^{\frac{1}{2}\kappa^2\xi} \operatorname{erfc}\left(\kappa\sqrt{\zeta/2}\right) \frac{e^{-\frac{x_0^2}{2\xi}}}{\xi^{3/2}} \\ \cdot \left[\psi'_1(\zeta + t + \xi) - \psi'_1(\zeta + t) - \psi'_1(\zeta + \xi) + \psi'_1(\zeta) \right]. \end{aligned} \quad (3.47)$$

This is a very general analytic result that is valid for any function $\psi_1(t)$. If one takes the perfect reaction limit, $\kappa \rightarrow \infty$, it becomes clear that Eq. (3.47) is the generalization of the results in Guérin et al. (2016) to the case of imperfect reactions⁵. In what follows we test two particular cases of perturbations to the Markovian case, the first for diffusion with an exponentially decaying perturbation and the second for a fractional Brownian motion with Hurst exponent $H = \frac{1}{2} + \varepsilon$.

3.3.2 | Long time diffusive process

We start with $\psi(t) = t + \varepsilon(1 - e^{-\lambda t})$, that represents a diffusive process with an effective diffusion constant $2D_{\text{eff}} = 1 + \varepsilon\lambda$ for short times and normal diffusion⁶, t , for long times the transition between these two behaviours happens at $t \sim 1/\lambda$. This perturbative case is the simplest way of adding memory to diffusion, where we only add one relaxation time scale, it is equivalent to having a Markovian walker that is weakly coupled with a variable whose relaxation time is $1/\lambda$. This relaxation time is not assumed to be small, in fact we do not assume fast relaxations of the degrees of freedom here, just weak coupling with this relaxation time.

As an example of this kind of process one can think of a Brownian particle in a Maxwell fluid, which is the simplest description of viscoelastic fluids. This fluid is characterized by a

⁴The complementary error function is defined as $\operatorname{erfc}(x) = 1 - \operatorname{erf}(x) = 1 - \int_0^x dt 2e^{-t^2}/\sqrt{\pi}$

⁵Note that: $\lim_{x \rightarrow \infty} x e^{x^2} \operatorname{erfc}(x) = 1/\sqrt{\pi}$.

⁶Note that we have used time units where $D = 1/2$.

timescale, τ_M that separates the elastic and viscous regimes of the fluid (Grimm et al., 2011).

Introducing this mean square displacement into the equation for $\mu_1(t)$ one obtains

$$\mu_1(t) = \frac{\kappa}{2 + \kappa\sqrt{2/\lambda}} (1 - e^{-\lambda t}) (1 - e^{-\sqrt{2\lambda}x_0}), \quad (3.48)$$

where one notices that the typical time scale with which $\mu_1(t)$ varies is still $1/\lambda$.

3.3.3 | Perturbative fractional Brownian motion

Here we study the case of almost diffusive fractional Brownian motion, where non-Markovianity is seen as a perturbation to normal Brownian motion, $\psi(t) = t$. The way we do this is by introducing $H = \frac{1}{2} + \varepsilon$ in the mean square displacement of a fractional Brownian motion: $\psi(t) = t^{2H} = t + \varepsilon 2t \ln t + \mathcal{O}(\varepsilon^2)$. Therefore, using Eq. (3.47), the mean trajectory after reaction reads

$$\mu_1(t) = \frac{x_0\kappa}{\sqrt{2\pi}} \int_0^{+\infty} d\xi \int_0^{+\infty} d\zeta e^{\frac{1}{2}\kappa^2\zeta} \operatorname{erfc}\left(\sqrt{\frac{1}{2}\kappa^2\zeta}\right) \frac{e^{-\frac{x_0^2}{2\xi}}}{\xi^{3/2}} \ln\left(\frac{(\zeta+t+\xi)\zeta}{(\zeta+t)(\zeta+\xi)}\right). \quad (3.49)$$

Without performing the integrals it is already possible to see that $\mu_1(t) < 0$, for all $t > 0$, and so, if a process is subdiffusive ($\varepsilon < 0$), the mean trajectory after reaction tends to take the walker back to its initial position. However, if the process is superdiffusive, then the mean trajectory after reaction moves away from the initial position, and, in particular, from the target position.

Next, we analyze the asymptotic behaviour of $\mu_1(t)$. In Appendix C we show that, to find the long and short time behaviours of $\mu_1(t)$, one has to consider two time scales, one that is of order 1 and another time scale that depends explicitly on the reactivity. Therefore, one has to look at three different regimes of reactivity to find the asymptotic behaviours of $\mu_1(t)$. First, we look at the case where κ is finite. In this case one finds that

$$\mu_1(t) \underset{\substack{t \rightarrow 0 \\ \kappa \text{ fixed}}}{\sim} \kappa t \ln t \quad \text{and} \quad \mu_1(t) \underset{\substack{t \rightarrow \infty \\ \kappa \text{ fixed}}}{\sim} C - 2x_0 \ln t. \quad (3.50)$$

Then, one also has to check what happens when κ is infinite or infinitesimal, where different behaviours emerge for the short and long time scales, respectively. We do this by taking the limits of κ before searching for the time asymptotics. If $\kappa \rightarrow 0$ then

$$\mu_1(t) \underset{\substack{\kappa \rightarrow 0 \\ t \rightarrow \infty}}{\sim} -2x_0\kappa\sqrt{2\pi t}. \quad (3.51)$$

If $\kappa \rightarrow \infty$,

$$\mu_1(t) \underset{\substack{\kappa \rightarrow \infty \\ t \rightarrow 0}}{\sim} -2\sqrt{2\pi t}. \quad (3.52)$$

These different asymptotic behaviours suggest that there is a time scale $\tau \sim 1/\kappa^\alpha$ with $\alpha > 0$ that is relevant when studying the effects of reactivity on reaction times. One can find the exponent α by looking at the case of high reactivity $\kappa \rightarrow \infty$. In this limit one must have the crossover between the short time behaviour $\sim \kappa t$ and the behaviour in Eq. (3.52), this implies that the relevant crossover time scale is $\tau = 1/\kappa^2$. The same procedure can be made in the limit $\kappa \rightarrow 0$ with the same result.

Figure 3.6.(a) summarizes this section. In this figure it is clear that there are three relevant regions of time for any reactivity κ . In Figure 3.6.(b) it is possible to see that, for $\kappa < 0.01$, the behaviour $\sim t^{1/2}$ becomes visible for $1 \ll t \ll 1/\kappa^2$. Similarly, it is possible to see in Figure 3.6.(b) that, for $\kappa > 200$, the behaviour $\sim \kappa t^{1/2}$ becomes visible for $1/\kappa^2 \ll t \ll 1$.

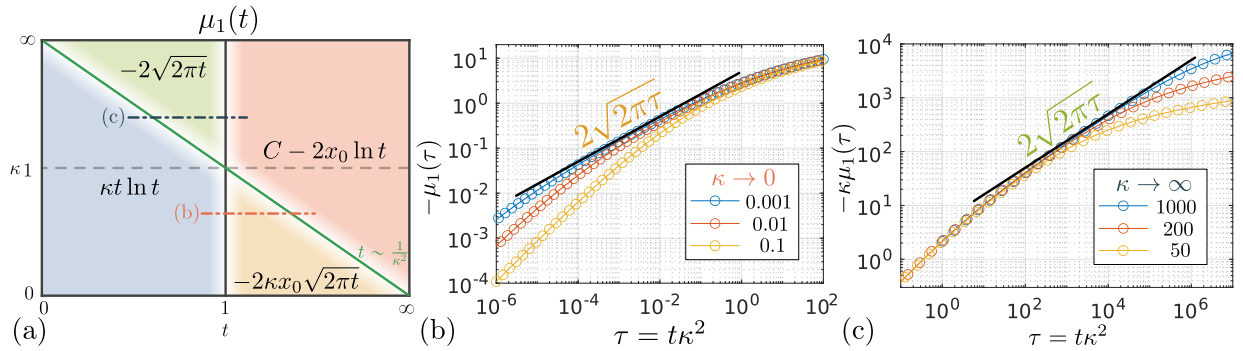


Figure 3.6: **Asymptotics of the mean trajectory after reaction for a perturbative fractional Brownian motion.** (a) Expressions of the asymptotic behaviour of the mean trajectory after reaction (at first order) for the case of almost diffusive fractional Brownian motions. The green line represents the relevant time scale $t \sim 1/\kappa^2$ that appears once one considers imperfect reactions. The orange and black dash-dotted lines represent the regions of that correspond to (b) and (c). In (b), we show the convergence of $\mu(t)$ towards $2\kappa\sqrt{2\pi t}$ for small times in the when $\kappa \rightarrow 0$. In (c) we show the convergence towards $2\sqrt{2\pi t}$ for large times when $\kappa \rightarrow \infty$

3.3.4 | Mean reaction time in the weakly non-Markovian limit

In this final section, we would like to check if these newly derived perturbative memory effects can be seen in the mean reaction time. For this, we introduce the perturbative mean square displacement, $\psi(t) = t + \varepsilon\psi_1(t)$, and the mean trajectory after reaction, $\mu(t) = \varepsilon\mu_1(t)$, in the equation for the mean reaction time (Eq. (3.16)). Doing this it is straightforward to see that, in fact, $\mu_1(t)$ will not intervene in the mean reaction time at first order, since it appears only in the equation as $\mu^2(t)$ thus being neglected. Therefore, at first order, the effect of memory on the mean reaction time would have been well described by a simple pseudo-Markovian (or Wilemski-Fixman) approach where one just assumes equilibrium of all hidden variables in the moment of reaction, equivalent to setting $\mu(t) = 0$. In fact,

$$\frac{\langle \text{RT} \rangle}{V} = \frac{1}{\kappa} + \int_0^\infty dt \frac{1 - e^{-\frac{x_0^2}{2t}}}{\sqrt{2\pi t}} - \varepsilon \int_0^\infty dt \frac{\psi_1(t)}{2\sqrt{2\pi t}^{3/2}} \left(1 - e^{-\frac{x_0^2}{2t}} \left(1 - \frac{x_0^2}{t} \right) \right) + \mathcal{O}(\varepsilon^2). \quad (3.53)$$

It is interesting to notice that, in this limit, one recovers the additivity property expected from Markovian stochastic processes, where there is no memory and one could solve the problems of imperfect reactions by summing two time contributions: one for the time it takes to reach the target (the terms in integrals); and another representing the time it takes for the reaction to happen once the random walker starts at the target ($1/\kappa$). Note that, even though $\mu_1(t)$ does not influence the mean reaction time at first order, it serves as a guide to the development of non perturbative approaches. However, we expect to find a dependence on $\mu_1(t)$ at order ε^2 .

3.4 | Matched asymptotic expansions for a fractional Brownian motion with limit reactivities

Here, we will use the method of matched asymptotics to find the mean trajectory after reaction and the mean reaction time with the two cases. First, we will look at the case of weak reactivity, $\kappa \rightarrow 0$, and then, we will look at the case of strong reactivity (or almost perfect reactions), $\kappa \rightarrow \infty$. We will find these for the specific case of fractional Brownian motions, $\psi(t) = Kt^{2H}$. Our goal is to identify, analytically, how the mean reaction time behaves when κ is close to the limiting cases.

Inspired by the section on weakly non-Markovian walks, Section 3.3, we predict that there will be a relevant, non-trivial, time scale ($\sim 1/\kappa^2$ for $H = 1/2 + \varepsilon$) that will play a role in the scaling laws of the mean trajectory after reaction. Via dimensional analysis it is possible to form two time scales with the parameters of the problem: x_0, K, κ

$$\tau_1 = \left(\frac{x_0^2}{K}\right)^{\frac{1}{2H}} \quad \text{and} \quad \tau_\kappa = \left(\frac{K}{\kappa^2}\right)^{\frac{1}{2-2H}}. \quad (3.54)$$

Note that many other time scales could be constructed using these two. However, we chose the two time scales that match the weakly non-Markovian ones (~ 1 and $\sim 1/\kappa^2$). Additionally, one can physically justify each of these two time scales. The time scale τ_1 has already been shown to be relevant for a fractional Brownian motion in the perfect case (Guérin et al., 2016), we thus believe it should remain relevant here. Then, the time scale τ_κ is the only time scale that depends on reactivity but not on geometry (x_0). In principle, there is no fundamental reason for τ_κ and τ_1 to be the only relevant time scales. On the other hand, if these time scales were not the relevant ones, then, the solutions we find should be ill-defined. This is not the case and all the solutions we find are well defined, thus, indicating that τ_1 and τ_κ are the relevant time scales for the case of weak and high reactivities.

In what follows we choose the units of length and space so that $x_0 = 1$ and $K = 1$. Using these units the relevant time scales become $\tau_1 = 1$ and $\tau_\kappa = 1/\kappa^{\frac{1}{1-H}}$. In some equations, considered to be the main results, we will reestablish homogeneity.

3.4.1 | Weakly reactive targets

Here, we study point targets that are highly imperfect, tending to the inert case, $\kappa \rightarrow 0$. We start with a naive approach, that fails for some value of H , and then perform the complete calculation to obtain the behaviour of $\mu(t)$ for $0 < H < 1$. Then, we introduce this behaviour into the equation for the mean reaction time, and deduce how it behaves when the target is almost inert.

3.4.1.1 | Naive approach

Even though we already expect the solutions to vary in two different time scales, τ_1 and τ_κ , it is interesting to first approach this problem in a naïve way by looking for a mean trajectory after reaction that is a simple power law expansion around the position of the target, $\mu(t) = \kappa g_1(t) + \mathcal{O}(\kappa^2)$. Inserting this power expansion in the integral equation for $\mu(t)$, Eq. (3.28), one can obtain $g_1(t)$:

$$g_1(\tau) = \int_0^\infty dt \frac{\psi(t) + \psi(\tau) - \psi(t + \tau)}{2\psi(t)} \frac{e^{-1/2\psi(t)}}{\sqrt{2\pi\psi(t)}}. \quad (3.55)$$

Therefore the mean reaction time is

$$\frac{\langle \text{RT} \rangle}{V} = \frac{1}{\kappa} + \int_0^\infty \frac{dt}{\sqrt{2\pi\psi(t)}} \left(1 - e^{-\frac{1}{2\psi(t)}} \right). \quad (3.56)$$

We see that, if $\psi(t) \sim t^{2H}$ for large times, then the integrals do not converge for $H < 1/3$ and clearly this naïve approach is incorrect, at least in that regime of highly subdiffusive processes. Additionally, we know that the behaviour of $\mu(t)$ for long times must be the one in Eq. (3.40), which is not possible to obtain with $g_1(\tau)$ as defined in Eq. (3.55), at least for $H < 1/2$.

3.4.1.2 | Mean trajectory after reaction for $H > 1/3$

If the naive approach works for $H > 1/3$, then we will assume that it is also correct in the complete approach, but only for times of order one. To incorporate the other time scale, τ_κ , we introduce another scaling law for $\mu(t)$ that is true once t is of order τ_κ , i.e., when $\kappa \rightarrow 0$: $t/\tau_\kappa = t\kappa^{\frac{1}{1-H}} \sim 1$,

$$\mu(t) \sim \begin{cases} \kappa g_1(t), & \text{for } t \sim \tau_1 \\ \kappa^{\alpha_\kappa} g_\kappa(t/\tau_\kappa), & \text{for } t \sim \tau_\kappa \end{cases}, \quad (3.57)$$

where $g_\kappa(\tau)$ does not depend on κ . Note that, even when homogeneity is reestablished ($x_0 \neq 1$ and $K \neq 1$), the function $g_\kappa(\tau)$ is assumed to not depend on either x_0 or K . In this case one must write $\mu(t) \sim x_0(\tau_1\kappa/x_0)^{\alpha_\kappa} g_\kappa(t/\tau_\kappa)$.

One can introduce an intermediate time scale χ , such that $1 = \tau_1 \ll \chi \ll \tau_\kappa$. Using this

time scale one can write the integral equation, Eq. (3.28), for times of the form $\tau = v\tau_\kappa$, i.e., times of order τ_κ , with v of order one:

$$\begin{aligned} & \frac{\mu(v\tau_\kappa)}{\kappa} + \int_0^\chi \frac{dt}{\sqrt{2\pi\psi(t)}} \left[(\mu(t+v\tau_\kappa) - \mu(t)M(t, v\tau_\kappa))e^{-\frac{\mu^2(t)}{2\psi(t)}} - (1 - M(t, v\tau_\kappa))e^{-\frac{1}{2\psi(t)}} \right] \\ & + \int_\chi^\infty \frac{dt}{\sqrt{2\pi\psi(t)}} \left[(\mu(t+v\tau_\kappa) - \mu(t)M(t, v\tau_\kappa))e^{-\frac{\mu^2(t)}{2\psi(t)}} - (1 - M(t, v\tau_\kappa))e^{-\frac{1}{2\psi(t)}} \right] = 0, \end{aligned} \quad (3.58)$$

where we have divided the integral in Eq. (3.28) into two integrals, one for times of order one: $t < \chi \ll \tau_\kappa$, and one for times of order τ_κ : $t > \chi \gg 1$. One can now perform the change of variables $t = u\tau_\kappa$ in the second integral (and $t = u\tau_1 = u$ in the first one), which enables us to use the scaling laws, $\mu(t) \underset{t \sim 1}{\sim} \kappa g_1(t)$ and $\mu(t) \underset{t \sim \tau_\kappa}{\sim} \kappa^{\alpha_\kappa} g_\kappa(t/\tau_\kappa)$, to evaluate the integrals. Keeping the terms of lowest order in κ (for all possible values of H) one obtains:

$$\begin{aligned} 0 = & \kappa^{\alpha_\kappa} \left[g_\kappa(v) + \int_{\chi/\tau_\kappa}^\infty du \frac{g_\kappa(u+v) - g_\kappa(u)M(u, v)}{\sqrt{2\pi}u^H} \right] \\ & - \int_{\chi/\tau_\kappa}^\infty du \frac{1 - M(u, v)}{\sqrt{2\pi}u^H} + \kappa^{\frac{2-3H}{1-H}} H \int_0^\chi du \left(\frac{u}{v}\right)^{1-2H} \frac{e^{-1/2u^{2H}}}{\sqrt{2\pi}u^H}. \end{aligned} \quad (3.59)$$

Let us start by looking at the terms κ^0 and $\kappa^{\frac{2-3H}{1-H}}$. If $1/3 < H < 2/3$, then, $\kappa^0 \gg \kappa^{\frac{2-3H}{1-H}}$. However, the term κ^0 is not equal to zero (except for $H = 1/2$), which means that it has to be compensated by another term, the remaining term κ^{α_κ} . Therefore, for $1/3 < H < 2/3$, one must have $\alpha_\kappa = 0$. Furthermore, for $H > 2/3$, one has instead that the term $\kappa^{\frac{2-3H}{1-H}}$ is much bigger than the term κ^0 . Since the term $\kappa^{\frac{2-3H}{1-H}}$ is never equal to zero one must have $\alpha_\kappa = -\frac{3H-2}{1-H}$ for $H > 2/3$. Consequently, the equations for $g_\kappa(\tau)$ must be:

$$0 = g_\kappa(v) + \int_0^\infty \frac{du}{\sqrt{2\pi}u^H} (g_\kappa(u+v) - 1 - (g_\kappa(u) - 1)M(u, v)) \quad \text{for } \frac{1}{3} < H < \frac{2}{3}, \quad (3.60)$$

and, for $H > 2/3$,

$$0 = g_\kappa(v) + \int_0^\infty \frac{du}{\sqrt{2\pi}u^H} \left(g_\kappa(u+v) - g_\kappa(u)M(u, v) + H \left(\frac{u}{v}\right)^{1-2H} e^{-1/2u^{2H}} \right), \quad (3.61)$$

where the integration limits χ/τ_κ and χ have been taken to ∞ and 0 respectively, which is allowed because χ is chosen such that $1 \ll \chi \ll \tau_\kappa$ and, if the integrals converge, this is equivalent to say that the integration limits are ∞ and 0 . To show that the integrals do converge, one has to find the behaviour of $g_\kappa(\tau)$ for small τ . This is done by realizing that $\kappa^{\alpha_\kappa} g_\kappa(t/\tau_\kappa \ll 1) \sim \kappa g_1(t \gg 1)$ and therefore, after finding the asymptotic behaviour of $g_1(t)$ from Eq. (3.55), one finds $g_\kappa(\tau \ll 1) \sim \tau^{1-H}$ for $1/3 < H < 2/3$ and $g_\kappa(\tau \ll 1) \sim \tau^{2H-1}$ for $H > 2/3$. With this result it is straightforward to show that all integrals in Eq. (3.59) converge when the limits $\chi \rightarrow \infty$ and $\chi/\tau_\kappa \rightarrow 0$ are taken.

3.4.1.3 | Mean trajectory after reaction for $H < 1/3$

Now, let us look at the more problematic case of strong subdiffusion, $H < 1/3$. Here, we must assume a general scaling law for times of order one,

$$\mu(t) \sim \kappa^{\alpha_1} g_1(t), \quad \text{for } t \sim 1, \quad (3.62)$$

just like before for times of order τ_κ . Independent of the limit $\kappa \rightarrow 0$ one should always have that $\mu(0) = 0$, therefore, α_1 must be positive (or zero). Assuming this, the equation for times of order τ_κ , Eq. (3.59), is still true, as it would just add a term of order $\kappa^{1+\alpha_\kappa}$ that would always be smaller than the other terms. Therefore, the behaviour of $\mu(t)$ for times of order τ_κ is the same for $H < 2/3$, i.e., $\alpha_\kappa = 0$ and $g_\kappa(\tau)$ given by Eq. (3.60)⁷.

To obtain the behaviour of $g_1(\tau)$ and the value of α_1 , we write the integral equation for $\mu(t)$, Eq. (3.28), at times of order one, and divide the integral into $t < \chi \ll \tau_\kappa$ and $t > \chi \gg 1$. The leading term resulting from this behaviour are:

$$0 = \kappa^{\alpha_1} g_1(\tau) + \kappa^{\frac{2H}{1-H}} \int_{\chi/\tau_\kappa}^{\infty} \tau^{2H} \frac{du}{2\sqrt{2\pi}u^{3H}} (g_\kappa(u) - 1). \quad (3.63)$$

Therefore, since we want non trivial solution for $g_1(\tau)$, one must have $\alpha_1 = \frac{2H}{1-H}$ and $g_1(\tau)$ given by:

$$g_1(\tau) = -\tau^{2H} \int_0^\infty \frac{dt}{2\sqrt{2\pi}} \frac{g_\kappa(t) - 1}{t^{3H}} \quad \text{for } H < \frac{1}{3}, \quad (3.64)$$

where we have, once again, taken the limit $\chi/\tau_\kappa \rightarrow 0$, allowed by the fact that, since $g_1(\tau) \sim \tau^{2H}$, then $g_\kappa(\tau \ll 1) \sim \tau^{2H}$.

By analyzing the equations for $g_1(\tau)$ and $g_\kappa(\tau)$, and using the results of Section 3.2, one can find the remaining asymptotic behaviours of these functions. These are summarized in Table 3.1.

	$g_1(\tau \ll 1)$	$g_1(\tau \gg 1) \sim g_\kappa(\tau \ll 1)$	$g_\kappa(\tau \gg 1)$
$H < 1/3$	τ^{2H}	τ^{2H}	$1 - B\tau^{2H-1}$
$1/3 < H < 1/2$		τ^{1-H}	
$1/2 < H < 2/3$	τ	τ^{2H-1}	τ^{2H-1}
$H > 2/3$			

Table 3.1: Asymptotic behaviour of the scaling functions $g_1(\tau)$ and $g_\kappa(\tau)$.

In summary (and after reestablishing homogeneity), the mean trajectory after reaction always displays two scaling laws when $\kappa \rightarrow 0$:

$$\mu(t) \underset{\kappa \rightarrow 0}{\sim} \begin{cases} x_0^{1-\alpha_1} \tau_1^{\alpha_1} \kappa^{\alpha_1} g_1(t/\tau_1) & \text{for } t \sim \tau_1 \\ x_0^{1-\alpha_\kappa} \tau_1^{\alpha_\kappa} \kappa^{\alpha_\kappa} g_\kappa(t/\tau_\kappa) & \text{for } t \sim \tau_\kappa \end{cases}, \quad (3.65)$$

⁷Note that, as we show later, the asymptotic behaviour of $g_\kappa(\tau)$ is $g_\kappa(\tau \ll 1) \sim \tau^{2H}$ and $g_\kappa(\tau \gg 1) \sim 1$, meaning that the integral in Eq. (3.60) is still well defined.

where α_1 and α_κ are exponents that depend only on H :

$$\alpha_1 = \begin{cases} \frac{2H}{1-H} & \text{for } H < \frac{1}{3} \\ 1 & \text{for } H > \frac{1}{3} \end{cases} \quad \text{and} \quad \alpha_\kappa = \begin{cases} 0 & \text{for } H < \frac{2}{3} \\ -\frac{3H-2}{1-H} & \text{for } H > \frac{2}{3} \end{cases}, \quad (3.66)$$

and the functions $g_1(\tau)$ and $g_\kappa(\tau)$ are given by the equations previously derived. For $g_1(\tau)$ we derived the Eqs. (3.64) and (3.55). And, for $g_\kappa(\tau)$, Eqs. (3.60), (3.61). Therefore, the behaviour of $\mu(t)$ in the limit $\kappa \rightarrow 0$ is now completely identified. This asymptotic behaviour is summarized in Table 3.2.

$\mu(t) \underset{\kappa \rightarrow 0}{\sim}$	$t \ll \tau_1$	$\tau_1 \ll t \ll \tau_\kappa$	$t \gg \tau_\kappa$
$H < \frac{1}{3}$	$x_0 K^{-\frac{H}{1-H}} \kappa^{\frac{2H}{1-H}} t^{2H}$		x_0
$\frac{1}{3} < H < \frac{1}{2}$	$x_0^{-\frac{2H-1}{H}} K^{\frac{2H-1}{2H}} \kappa t^{2H}$	$x_0 K^{-1/2} \kappa t^{1-H}$	
$\frac{1}{2} < H < \frac{2}{3}$	$x_0 K^{-1/2} \kappa t^1$		$-x_0 K^{-\frac{2H-1}{2(1-H)}} \kappa^{\frac{2H-1}{1-H}} t^{2H-1}$
$H > \frac{2}{3}$		$-x_0^{\frac{2^{1-H}}{H}} K^{-\frac{1-H}{H}} \kappa t^{2H-1}$	

Table 3.2: Typical behaviour of the mean trajectory after reaction for $\kappa \rightarrow 0$.

3.4.1.4 | Consequences of weak reactivity on the mean reaction time

We would now like to see what is the effect of these scaling laws, Eq. (3.65), on the mean reaction time. It is expected, and seen in simulations, that the main contribution to the mean reaction time is the term $1/\kappa$, but here we want to investigate the new effects coming from the memory, so we will look for the first corrections to $\langle \text{RT} \rangle / V - 1/\kappa$. To do this, one introduces the scaling laws in Eq. (3.16) and, after splitting the integral into the different time scales ($1 \ll \chi \ll \tau_\kappa$), expand it to leading order in κ :

$$\begin{aligned} \frac{\langle \text{RT} \rangle}{V} - \frac{1}{\kappa} \underset{\kappa \rightarrow 0}{\sim} & \int_0^\chi \frac{d\tau}{\sqrt{2\pi}} \frac{1 - e^{-1/2\tau^{2H}}}{\tau^H} - \kappa^{2\alpha_1} \int_0^\chi \frac{d\tau}{\sqrt{2\pi}} \frac{g_1^2(\tau)}{2\tau^{3H}} \\ & + \kappa^{\frac{3H-1}{1-H}} \int_{\chi/\tau_\kappa}^\infty \frac{d\tau}{\sqrt{2\pi}} \frac{1}{2\tau^{3H}} - \kappa^{\frac{3H-1}{1-H} + 2\alpha_\kappa} \int_{\chi/\tau_\kappa}^\infty \frac{d\tau}{\sqrt{2\pi}} \frac{g_\kappa^2(\tau)}{2\tau^{3H}}, \end{aligned} \quad (3.67)$$

where we have kept the leading terms of each expansion so that now we can use the same equation for all possible Hurst exponents, H . Using the expressions of α_1 and α_κ in Eq. (3.66), one finds two possible leading terms, one for $H > 1/3$ and one for $H < 1/3$. The first one reads

$$\frac{\langle \text{RT} \rangle}{V} - \frac{1}{\kappa} \underset{\kappa \rightarrow 0}{\sim} \int_0^\infty \frac{d\tau}{\sqrt{2\pi} K \tau^H} \left(1 - e^{-\frac{x_0^2}{2K\tau^{2H}}} \right) \quad \text{for } H > \frac{1}{3}, \quad (3.68)$$

where we have reestablished homogeneity and the integration limit χ was safely taken to infinity due to the good convergence of the integral. We note that this is the same result as the one obtained with the naive approach introduced in the beginning of this Section, see Eq. (3.56). In fact, this is the same behaviour as the one obtained using the pseudo-Markovian

approach ($\mu(t) \approx 0$). However, for $H < 1/3$, we find a new, interesting, result:

$$\frac{\langle \text{RT} \rangle}{V} - \frac{1}{\kappa} \underset{\kappa \rightarrow 0}{\sim} \left(\frac{1}{\kappa} \right)^{\frac{1-3H}{1-H}} \frac{x_0^2}{K^{\frac{1}{1-H}}} \nu_H \quad \text{for } H < \frac{1}{3}, \quad (3.69)$$

$$\text{with } \nu_H = \int_0^\infty \frac{d\tau}{\sqrt{2\pi}} \frac{1 - g_\kappa^2(\tau)}{2\tau^{3H}}, \quad (3.70)$$

where we have reestablished homogeneity and taken the limit $\chi/\tau_\kappa \rightarrow 0$ in Eq. (3.67), allowed by the fact that $g_\kappa(\tau \gg 1) \sim 1 - Bt^{2H-1}$, and therefore the integral still converges when this limit is taken.

We find that the apparent diffusion-controlled time, $T_{\text{DC}} = \langle \text{RT} \rangle - V/\kappa$, depends on the reactivity in a diverging way, whereas, in a Markovian mindset, one would expect T_{DC} to depend only on the transport properties. This result shows (once again) that, due to the existence of memory, one cannot split a problem of imperfect reactivity into two first passage problems. Moreover, given that the T_{DC} depends on reactivity in a non-trivial and divergent way for small κ , we have found a new, relevant, contribution to the mean reaction time of strongly subdiffusive processes. This is clearly a purely non-Markovian effect, coming from the fact that the process ‘‘remembers’’ the amount of time spent close to the target.

In Figure 3.7 it is possible to see that the scaling in Eq. (3.69) does exist for the two cases that we have simulated (see section 3.1.3 for more details): a fractional Brownian motion with $H = 1/4$ and a Rouse chain (physical realization of fractional Brownian motion with $H = 1/4$ for times $< N^2$). The value of ν_H ($\nu_{1/4} \approx 1.9$) can be computed numerically by solving Eq. (3.60) for $H = 1/4$ and introducing the resulting $g_\kappa(t)$ into Eq. (3.70). Remarkably, in Figures 3.7.a) and 3.7.b), we see that the non-trivial scaling found in Eq. (3.69) is a good fit⁸ to the mean reaction times found in the simulations, even for reactivities that are not so small (it seems to work well up to $\kappa\tau_1/x_0 \approx 10$).

3.4.2 | Strongly reactive targets

In the last section, we have studied what happens when the target is almost inert, here we would like to study what happens when the target is almost perfect $\kappa \rightarrow \infty$, and imperfect reaction are seen as a defect on the normal perfect reactions. The case of non-Markovian perfect reactions was already studied in (Gu erin et al., 2016) so we have a clear idea of what the extreme case looks like, however, we do not know how small imperfections in the target affect the mean reaction time.

We follow a similar approach to the one taken in the previous section (Section 3.4.1), where we introduce two time scales, τ_1 and τ_κ , and expand the theory for $\kappa \rightarrow 0$ taking into account the two time scales. Note that in Section 3.3 we have already seen the second time scale, τ_κ , appearing for short times. In fact the two time scales used before are now changed,

⁸Note that it is not a fit in the sense that no parameters are adjusted to *fit* the simulation data.

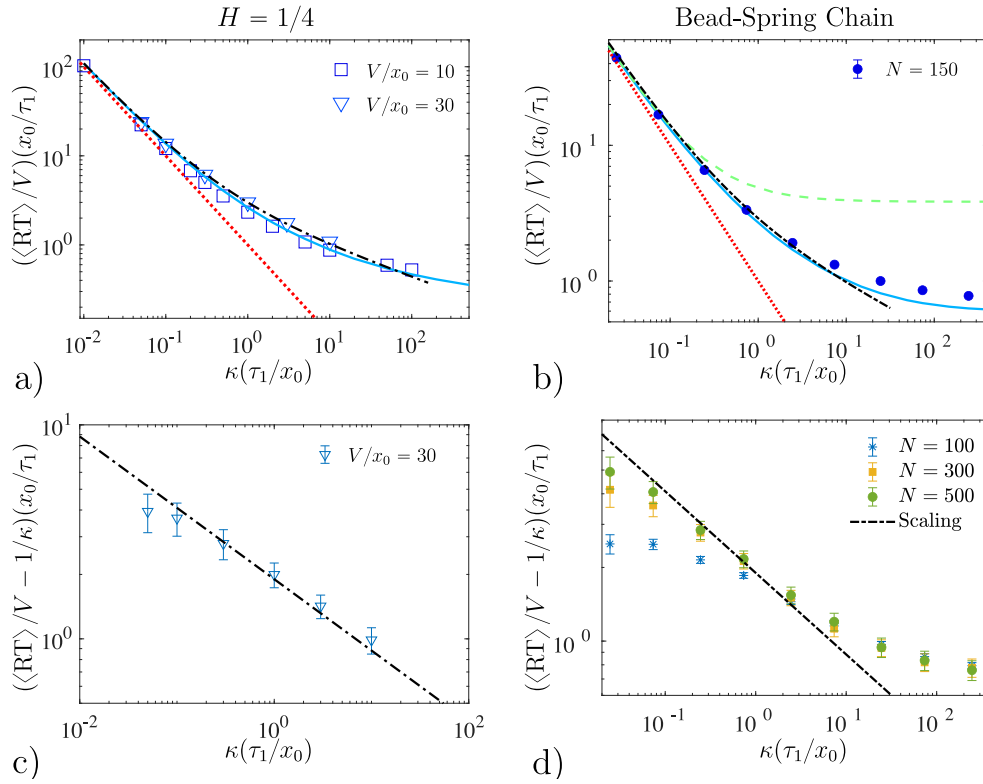


Figure 3.7: **The non-trivial low reactivity scaling found is compatible with simulations.** Simulation results, in symbols, for different processes. The continuous blue line is the numerical mean reaction time obtained with our theory, the dotted (red) line is the asymptote $1/\kappa$, the dashed (green) line is the pseudo-Markovian approach (equivalent to setting $\mu(t) = 0$) and the scaling from Eq. (3.69) is in dash-dotted line (black). Note that the pseudo-Markovian approach is divergent for long time fractional Brownian motions with $H < 1/3$. a) and c) are simulations of fractional Brownian motions with $H = 1/4$. b) and d) are simulations of a bead-spring (or Rouse) chain with parameters $x_0 = 5l_R$ and $V = 30x_0$. In c) and d) the factor $1/\kappa$ was removed so that the scaling from Eq. (3.69) is the leading contribution of reactivity.

τ_1 is still of order one, but τ_κ , still of order $\kappa^{-\frac{1}{1-H}}$, now goes to zero instead of infinity: the reactivity modifies $\mu(t)$ at very small times only, with the longer times being dominated by the behaviour of the perfect case.

We assume that the scaling laws for $\mu(t)$ are

$$\mu(t) \underset{\kappa \rightarrow 0}{\sim} \begin{cases} \kappa^{-\alpha} h(t/\tau_\kappa) & \text{for } t \sim \tau_\kappa \\ \mu_P(t) & \text{for } t \sim 1 \end{cases}, \quad (3.71)$$

or, reestablishing homogeneity,

$$\mu(t) \underset{\kappa \rightarrow 0}{\sim} \begin{cases} x_0^{1+\alpha} \tau_1^{-\alpha} \kappa^{-\alpha} h(t/\tau_\kappa) & \text{for } t \sim \tau_\kappa \\ x_0 \mu_P(t/\tau_1) & \text{for } t \sim \tau_1 \end{cases}, \quad (3.72)$$

where $h(\tau)$ is a function independent of κ , the exponent α is expected to be positive, and $\mu_P(\tau)$, which does not depend on κ , x_0 or K , is the dimensionless solution of the perfect case,

thus obeying the equation:

$$0 = \int_0^\infty \frac{dt}{\sqrt{2\pi t^H}} \left[(\mu_P(t+\tau) - \mu_P(t)M(t,\tau))e^{-\frac{\mu_P^2(t)}{2t^{2H}}} - (1 - M(t,\tau))e^{-\frac{1}{2t^{2H}}} \right]. \quad (3.73)$$

Introducing Eq. (3.73) into the integral equation for $\mu(t)$, Eq. (3.28), one can remove the terms that do not depend on $\mu(t)$ or $\mu_P(t)$:

$$0 = \frac{\mu(\tau)}{\kappa} + \int_0^\infty \frac{dt}{\sqrt{2\pi t^H}} \left[(\mu(t+\tau) - \mu(t)M(t,\tau))e^{-\frac{\mu^2(t)}{2t^{2H}}} - (\mu_P(t+\tau) - \mu_P(t)M(t,\tau))e^{-\frac{\mu_P^2(t)}{2t^{2H}}} \right]. \quad (3.74)$$

From the study of the perfect case, one can assume that the short time behaviour of $\mu_P(t)$ is given by

$$\mu_P(t) \underset{t \rightarrow 0}{\sim} \mu_0 t^H. \quad (3.75)$$

Though this behaviour is only an assumption, it holds at perturbative order for weakly non-Markovian processes, see Eq. (3.52), and for the case of a Rouse chain, with $H = 1/4$ (Guérin et al., 2013). Matching the behaviour of $\mu_P(t)$ and $h(t/\tau_\kappa)$ for $\tau_\kappa \ll t \ll 1$, one realizes that $h(t \gg 1) \sim t^H$. Therefore, using the scaling laws of Eq. (3.71) one can obtain the exponent α ,

$$\kappa^{-\alpha} h\left(\frac{t}{\tau_\kappa} \gg 1\right) \sim \kappa^{-\alpha} t^H \kappa^{\frac{H}{1-H}} \sim \mu_P(t \ll 1) \sim t^H \quad \Rightarrow \quad \alpha = \frac{H}{1-H}. \quad (3.76)$$

Note that, here, there are no different exponent laws for different Hurst exponents. Therefore, in principle, there should not be significant differences in the mean reaction time for different Hurst exponents, contrary to what we found in the weakly reactive case where the mean reaction time displays two different behaviours, one for $H < 1/3$ and another for $H > 1/3$.

The new found exponent α allows us to expand the integral equation in Eq. (3.74) for times $\tau = v\tau_\kappa$ where v is fixed as $\kappa \rightarrow \infty$:

$$0 = \kappa^{-\frac{H}{1-H}} h(v) + \kappa^{-\frac{H}{1-H}} \int_0^{\chi/\tau_\kappa} \frac{du}{\sqrt{2\pi u^H}} (h(u+v) - h(u)M(u,v))e^{-\frac{h^2(u)}{2u^{2H}}} - \int_0^{\chi/\tau_\kappa} \frac{du}{\sqrt{2\pi u^H}} (\mu_P((u+v)\tau_\kappa) - \mu_P(u\tau_\kappa)M(u,v))e^{-\frac{\mu_P^2(u\tau_\kappa)}{2u^{2H}} \kappa^{\frac{2H}{1-H}}}, \quad (3.77)$$

where χ is an intermediate time, such that $\tau_\kappa \ll \chi \ll 1$. The integral was split, at time χ , into the integrals that remained in Eq. (3.77) and one integral, from χ to ∞ , where the integrand is zero due to the fact that $\mu(t > \chi) \sim \mu_P(t)$. If one now notices that, for $u \sim 1$,

$\mu_P(u\tau_\kappa) \approx \mu_0 \kappa^{-\frac{H}{1-H}} u^H$, one finds the final integral equation for $h(v)$:

$$0 = h(v) + \int_0^\infty \frac{du}{\sqrt{2\pi}u^H} \left[(h(u+v) - h(u)M(u,v))e^{-\frac{h^2(u)}{2u^{2H}}} - \mu_0 \left((u+v)^H - u^H M(u,v) \right) e^{-\frac{\mu_0^2}{2}} \right], \quad (3.78)$$

where, due to the fact that both terms in the integral go to infinity in the same way, the limit $\chi/\tau_\kappa \rightarrow \infty$ was safely taken. Since we can find a defined equation for $h(t)$ it is reasonable to assume that the initial assumption: $h(t \gg 1) \sim t^H$ is correct. Combining this result with the asymptotes found in Section 3.2 one obtains the full behaviours of $h(t)$ and $\mu_P(t)$, summarized in Table 3.3.

	$h(\tau \ll 1)$	$h(\tau \gg 1) \sim \mu_P(\tau \ll 1)$	$\mu_P(\tau \gg 1)$
$H < 1/2$	τ^{2H}	τ^H	$1 - A\tau^{2H-1}$
$H > 1/2$	τ		

Table 3.3: **Asymptotic behaviour of the scaling functions $h(\tau)$ and $\mu_P(\tau)$.** These functions are connected to $\mu(t)$ by the scaling law in Eq. (3.71).

Reestablishing the units in the scaling laws for $\mu(t)$, Eq. (3.71), and introducing the asymptotic behaviours from Table 3.3, it is possible to obtain the full behaviour of $\mu(t)$ for strongly reactive targets as a function of x_0, K and κ , as shown in Table 3.4.

$\mu(t) \underset{\kappa \rightarrow \infty}{\sim}$	$t \ll \tau_\kappa$	$\tau_\kappa \ll t \ll \tau_1$	$t \gg \tau_1$
$H < 1/2$	$K^{\frac{1-2H}{2-2H}} \kappa^{\frac{H}{1-H}} t^{2H}$	$\sqrt{K}t^H$	$1 - AK^{\frac{2H-1}{2H}} x_0^{\frac{1-H}{H}} t^{2H-1}$
$H > 1/2$	κt		$AK^{\frac{2H-1}{2H}} x_0^{\frac{1-H}{H}} t^{2H-1}$

Table 3.4: **Typical behaviour of the mean trajectory after reaction for $\kappa \rightarrow \infty$.**

Let us now look for the effect that these scaling laws have on the mean reaction time. We go back to Eq. (3.16) and introduce the scaling laws

$$\frac{\langle \text{RT} \rangle}{V} \underset{\kappa \rightarrow \infty}{\sim} \frac{1}{\kappa} + \int_0^\infty \frac{dt}{\sqrt{2\pi}t^H} \left(e^{-\frac{\mu_P^2(t)}{2t^{2H}}} - e^{-\frac{1}{2t^{2H}}} \right) + \frac{1}{\kappa} \int_0^{\chi/\tau_\kappa} \frac{dt}{\sqrt{2\pi}t^H} \left(e^{-\frac{h^2(t)}{2t^{2H}}} - e^{-\frac{\mu_P^2(t\tau_\kappa)}{2t^{2H}} \kappa^{\frac{2H}{1-H}}} \right), \quad (3.79)$$

where one identifies in the second term the mean first passage time, i.e., the mean reaction time in the perfect case, which is naturally the limit of $\langle \text{RT} \rangle$ for $\kappa \rightarrow \infty$. The leading contribution of reactivity, in $\sim \kappa^{-1}$, can further be simplified by using $\mu_P(t \ll 1) \sim \mu_0 t^H$ and, with this simplification it becomes clear that the integral converges when χ/τ_κ is taken to ∞ . Therefore, the mean reaction time for strongly reactive targets can be written as

$$\frac{\langle \text{RT} \rangle}{V} \underset{\kappa \rightarrow \infty}{\sim} \frac{\langle \text{T} \rangle}{V} + \frac{1}{\kappa} \left[1 + \int_0^\infty \frac{dt}{\sqrt{2\pi}t^H} \left(e^{-\frac{h^2(t)}{2t^{2H}}} - e^{-\frac{\mu_0^2}{2}} \right) \right]. \quad (3.80)$$

To find the sign of the integral in Eq. (3.80), one can start by realising that $|\mu(t)|$ is a (monotonically) increasing function and, therefore, $|\kappa^{-\frac{H}{1-H}} h(t/\tau_\kappa)| \leq |\mu_0 t^H|$. If one now introduces a time u such that $t = u\tau_\kappa$, the previous inequality can be written as $|h(u)| \leq |\mu_0 u^H|$. Thus proving that the integrand of Eq. (3.80) is always positive.

The fact that the integral correction to the term $\sim \kappa^{-1}$ is positive means that, when there is memory, the correction for light imperfectness of the target (as is the case in almost perfect targets) is larger than the one expected if there was no memory, thus making reactions slower for non-Markovian processes.

3.5 | Conclusion

In this chapter we have developed a theory that quantitatively predicts the mean reaction time for a Gaussian non-Markovian random walker that reacts at a target with reactive rate $k(x) = \kappa\delta(x)$. The first result of our theory is that for non-Markovian processes one cannot treat the problem of imperfect reactions as the sum of two first passage problems. We have found the long and short time behaviours of the mean trajectory after reaction and prove that, for long time subdiffusive processes, the memory of the initial conditions will remain infinitely long in the system. Then, we have explored the limiting case of weakly non-Markovian processes, where we have seen that a small perturbation to Markovianity does not influence the mean reaction time in a non-trivial way, i.e., pseudo-Markovian approaches would be enough to predict the mean reaction time. In this case, we have seen that a new intrinsic time scale appears in the behaviour of $\mu(t)$, that is due to reactivity. Additionally, we have explored the two limiting cases of reactivity for the fractional Brownian motion. In the weakly reactive case, where the target is almost inert, we found that the mean reaction time displays a non-trivial, divergent, dependence with reactivity beyond the traditional reaction controlled time, which means that memory makes reactions much slower when reactions are already rare. In the strongly reactive limit, the almost perfect target, we see that the mean reaction time is typically slower than one would predict with a “mixed-Markovian” approach, where transport (the first passage) would be computed for a non-Markovian walker but the reaction step would simply be considered by adding the reaction controlled term, $\sim 1/\kappa$.

IMPERFECT REACTIONS FOR GATED REACTIONS, FINITE TARGETS AND HIGHER DIMENSIONS

4.1	The mechanism of gated reactions.	54
4.1.1	Dynamics of the target activity.	54
4.1.2	Mean reaction time to an intermittent target.	55
4.2	One-dimensional extended targets	57
4.3	Imperfect reactions in two dimensions.	61
4.4	Conclusion	66

In Chapter 3, we have developed a theory that provides the mean reaction time for a Gaussian random walker moving in a confinement volume. However, this theory is only a first step in the study of imperfect reactions, as it is limited to the mechanism of sink reactivity, one dimension and localized (point-like) target. Given these limitations, one would like to use the insights obtained from this theory to study more general situations.

One important class of imperfect reactions that cannot be studied with the theory of Chapter 3 is the case of semi-reflective targets (Grebekov, 2019). In this case, if a reaction does not happen, then, the particle is reflected. This means that the motion of the particle is still changed by an encounter with the target even if there is no reaction, which is clearly not the case in the theory previously developed. To deal with these targets, one has to find a way of introducing a semi-reflective interface in a non-Markovian system. However, the introduction of interfaces in non-Markovian system is a problem that has not yet been solved, with the best result being the introduction of a reflective wall by numerically solving a generalized Langevin equation (Vojta et al., 2019). There is, then, not much hope to solve the problem of semi-reflective interfaces before theoretically solving the reflective wall. Here, we do not focus on this problem, and, therefore, will not deal with this category of imperfect reactions.

Another mechanism of imperfect reactivity, that is not included in the theory of Chapter 3, is the mechanism of gated reactions, where, in addition to an imperfect target, the target

might randomly switch to an inactive state, where no reaction can happen. By introducing an extra process for the dynamics of the target, it is possible to adapt the theory developed before to study the mechanism of gated reactions. Then, we can also study the case of targets with finite extensions, where one can also allow for space dependent reactivities. It is important to understand the relevance of these targets when trying to extend one-dimensional theories to higher dimensions. In fact, in two dimensions it is virtually impossible for a random walker that diffuses to find an infinitesimal target, see the Markovian mean reaction time in Section 2.1.4. Therefore, if one wants to study the problem of sink reactivity in two dimensions, it is useful to first understand how extended targets can be treated in one dimension.

In the present chapter, we develop three extensions of the non-Markovian theory for imperfect reactions. First, in Section 4.1, we study one-dimensional gated reactions. Then, in Section 4.2, we expand the previous theory to extended targets, where $k(x)$ is no longer a delta function. Particularly, we study the case of Gaussian-shaped reaction rates. Finally, in Section 4.3, we obtain the equations that give us the mean reaction time for a two-dimensional random walker to react at a Gaussian-shaped target.

4.1 | The mechanism of gated reactions.

4.1.1 | Dynamics of the target activity.

Let us start by characterizing the target. The principle of gated reactions is that the target has two possible states, active (a) and inactive (i). If the target is inactive, then no reactions are possible $k(x, i) = 0$; contrarily, if the target is active, then reactions are possible and the reaction rate is $k(x, a) = \kappa_a \delta(x)$. Note that, here, the target is considered to be point-like and the random walker is one-dimensional.

We assume that the target switches from the active to the inactive state with rate ω_i , and from inactive to active state with rate ω_a . Additionally, we also assume that these transitions can be described as a Markov process that is independent of the position $x(t)$, so that

$$\partial_t q(a, t) = -\omega_i q(a, t) + \omega_a (1 - q(a, t)), \quad (4.1)$$

where $q(a, t)$ represents the probability to observe the active state at time t , and we have used $q(a, t) + q(i, t) = 1$, with $q(i, t)$ the probability of the inactive state. Let us call $q_s(a)$ the stationary probability to observe an active state, and $q(a, t|a, 0)$ the probability that the target is active at t , given that it was active at $t = 0$. Then,

$$q(a, t|a, 0) = q_s(a) + (1 - q_s(a))e^{-(\omega_a + \omega_i)t} \quad \text{with} \quad q_s(a) = \frac{\omega_a}{\omega_a + \omega_i} = q_s. \quad (4.2)$$

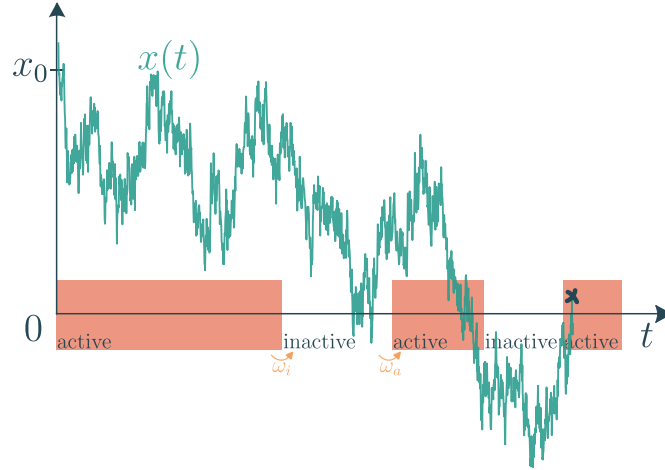


Figure 4.1: **Representation of gated reactions.** A random walker $x(t)$ is searching for an imperfect target, at the origin of the positions, that switches between active and inactive. When active, the target is imperfect.

4.1.2 | Mean reaction time to an intermittent target.

Let us now derive the equations that will give access to the mean reaction time. For simplicity we assume that at $t = 0$ the probability to start in the active state is stationary (this hypothesis will only be used only in the final steps of the derivation and would be very easy to relax). The generalization of Eq. (3.17) is

$$p(0, a, t; x_1, t + t_1) = p(0, a, t; x_1, t + t_1; \text{RT} > t) + \int_0^t d\tau p(0, a, t; x_1, t + t_1 | \text{RT} = \tau) F(\tau), \quad (4.3)$$

where $p(0, a, t; x_1, t + t_1)$ is the joint probability density to observe $x(t) = 0$, with the target active, a , at time t , and $x(t + t_1) = x_1$. Writing the joint probability to have a reaction at time t and to obtain $x(t + t_1) = x_1$, we obtain the generalization of (3.23):

$$\kappa_a p(0, a, t; x_1, t + t_1; \text{RT} > t) = p(x_1, t + t_1 | \text{RT} = t) F(t). \quad (4.4)$$

Using these relations, and repeating exactly the same calculation steps as in Section 3.1, we find that the generalization of Eq. (3.18) to gated reactions is

$$p_s(0, a; x_1, t_1) \langle \text{RT} \rangle = \frac{p_\pi(x_1, t_1)}{\kappa_a} + \int_0^\infty dt [p_\pi(0, a, t; x_1, t + t_1) - p(0, a, t; x_1, t + t_1)], \quad (4.5)$$

where $p_s(0, a; x_1, t_1) = \lim_{t \rightarrow \infty} p(0, a, t; x_1, t + t_1)$ is the stationary probability of finding the particle at an active target and finding it at x_1 after time t_1 .

Next, the joint probability distribution function of the position and state can be evaluated by using our approximation of independence between the switching dynamics of the target

and the position $x(t)$. Indeed, we can write:

$$p_\pi(0, a, t; x_1, t + t_1) = p_\pi(0, t; x_1, t + t_1) q(a, t|a, 0), \quad (4.6)$$

$$p(0, a, t; x_1, t + t_1) = p(0, t; x_1, t + t_1) q_s(a), \quad (4.7)$$

where in the last equality we have used our hypothesis that the probability to start in the active state is $q_s(a)$. With these simplifications, the expression of the mean reaction time in the non-Markovian theory for gated reactions become

$$\frac{\langle \text{RT} \rangle}{V} q_s = \frac{1}{\kappa_a} + \int_0^\infty dt [p_\pi(0, t) q(a, t|a, 0) - p(0, t) q_s], \quad (4.8)$$

and, using the usual Gaussian approximations for the trajectories after reaction, the integral equation for $\mu(t)$ becomes

$$\begin{aligned} \frac{\mu(\tau)}{\kappa_a} + \int_0^\infty \frac{dt}{\sqrt{2\pi\psi(t)}} \left\{ \left[\mu(t + \tau) - \mu(t) \frac{\sigma(t + \tau, t)}{\psi(t)} \right] e^{-\frac{\mu(t)^2}{2\psi(t)}} q(a, t|a, 0) \right. \\ \left. - x_0 \left[1 - \frac{\sigma(t + \tau, t)}{\psi(t)} \right] e^{-\frac{x_0^2}{2\psi(t)}} q_s \right\} = 0. \end{aligned} \quad (4.9)$$

Note that, since $\lim_{\tau \rightarrow \infty} q(a, \tau|a, 0) = q_s$, then the long time behaviour of $\mu(t)$ is not changed and Eq. (3.40) is still true.

We also note that this result, Eqs. (4.8) and (4.9), generalize to the case of non-Markovian random walkers the results of (Spouge et al., 1996), specifically Eq. (19) in this reference, obtained for Markovian random walkers searching for an imperfect gated target.

Let us now look at one limit often studied in the case of gated reactions, the limit of low switch rates, $\omega = \omega_a + \omega_i \rightarrow 0$, when q_s is kept constant. In this limit, one can write the mean reaction time as

$$\frac{\langle \text{RT} \rangle}{V} = \frac{\omega}{\kappa_a \omega_a} + \int_0^\infty \frac{d\tau/\omega}{\sqrt{2\pi\psi(\tau/\omega)}} \left[\left(1 + \frac{1 - q_s}{q_s} e^{-\tau} \right) e^{-\frac{\mu^2(\tau/\omega)}{2\psi(\tau/\omega)}} - e^{-\frac{x_0^2}{2\psi(\tau/\omega)}} \right] \quad (4.10)$$

$$= \frac{\omega}{\kappa_a \omega_a} + \frac{1}{\omega^{1-H}} \int_0^\infty \frac{d\tau}{\sqrt{2\pi K}} \frac{1 - q_s e^{-\tau}}{q_s \tau^H}, \quad (4.11)$$

where the arguments in the exponentials go to zero with $\omega \rightarrow 0$. Therefore, in the low switch rate limit, reactions become rare and one can write

$$\frac{\langle \text{RT} \rangle}{V} \underset{\omega \rightarrow 0}{\sim} \frac{1}{\kappa_{\text{eff}}}, \quad \kappa_{\text{eff}} = \omega^{1-H} \frac{q_s}{1 - q_s} \frac{\sqrt{2\pi K}}{\Gamma(1 - H)}, \quad (4.12)$$

where κ_{eff} is an effective reaction rate that generalizes the result obtained in Eq. (23) of (Mercado-Vásquez and Boyer, 2019) where the authors studied this problem in the diffusive, i.e., Markovian ($H = 1/2$), regime.

In Figure 4.2, we compare the results of simulations¹ to the theoretical predictions. Our theoretical predictions slightly overestimate the mean reaction times, but, even with this systematic error, one can consider that our theory provides good predictions of the mean reaction times in the case of gated reactions with $H = 0.34$. The predictions are particularly good when compared to the previous best predictions, the pseudo-Markovian ones, that overestimates the mean reaction times with a factor of almost 10. We also note that the low switch rate prediction, found in Eq. (4.12), is verified by the simulations and does not change with the “real” reactivity of the target, κ_a .

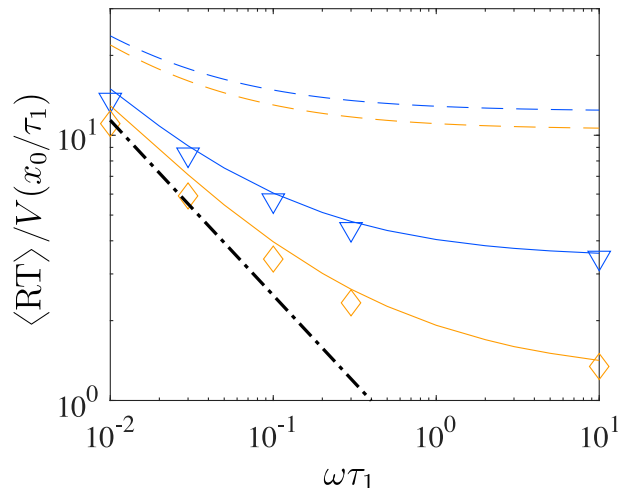


Figure 4.2: **Testing the validity of our theory for gated reactions.** Theory (continuous lines) and simulations (symbols, $V = 30x_0$) of gated reactions for the fractional Brownian motion on a ring with $H = 0.34$ for $q_s = 0.5$. The time unit τ_1 is defined as $\tau_1 = (x_0^2/K)^{1/2H}$. The orange (lower) line is for $\kappa_a \tau_1 / x_0 = 1$ and the blue (upper) line is for $\kappa_a \tau_1 / x_0 = 10$. The dashed lines represent the pseudo-Markovian approximation and the dashed-dot line is the asymptotic prediction in Eq. (4.12).

4.2 | One-dimensional extended targets

Let us now study the case of an extended target, with reaction rate $k(x)$. In a latter stage, we choose to study Gaussian-shaped targets. However, for the sake of generality, we start with a general reaction rate, localized in the region \mathcal{R} , the reactive region. We assume that the reaction rate is normalized, $\kappa = \int_{\mathcal{R}} dx k(x)$, and that it is symmetric and centered at zero, $\int_{\mathcal{R}} dx xk(x) = 0$. We start by generalizing the renewal equation:

$$p(x, t; x_1, t + t_1) = p(x, t; x_1, t + t_1; \text{RT} > t) + \int_0^\infty d\tau p(x, t; x_1, t + t_1; \text{RT} = \tau), \quad (4.13)$$

where we have already used the joint probabilities knowing that it will be relevant for the calculation of $\mu(t)$.

Since the target is no longer point-like one has to use the reaction probability distribution

¹The simulations are performed with the methods described in Section 3.1.3

function, $f(x, t)$, i.e., the probability density for the reaction to happen at x at time t , instead of only the reaction time density, $F(t) = \int_{\mathcal{R}} dx f(x, t)$. It is then possible to adapt Eq. (3.23) to the case of extended targets by noticing that, if P is the probability

$$P = \mathbb{P}\left(x(t) \in [x, x + dx[; x(t + t_1) \in [x_1, x_1 + dx_1[\text{ and } \text{RT} \in [t, t + dt[\right), \quad \forall x \in \mathcal{R}, \quad (4.14)$$

then P can also be written in two different ways. One way is using the reaction probability distribution function, $f(x, t)$,

$$P = \left(f(x, t) dx dt \right) \left(p(x_1, t + t_1 | x, t; \text{RT} = t) dx_1 \right), \quad (4.15)$$

where $f(x, t)$ takes into account the probability to reach the position x and react at x . Another way to write P is by using the reaction rate, $k(x)$,

$$P = \left(k(x) dt \right) \left(p(x, t; x_1, t + t_1; \text{RT} > t) dx dx_1 \right), \quad (4.16)$$

where the second propagator takes into account reaching the position x with no previous reaction and then going to x_1 at $t + t_1$. Note that, since we multiply this propagator by the probability of reaction at position x , this is equivalent to the probability that $\text{RT} = t$, with $x(\text{RT}) = x$. Therefore, the argument in Eq. (3.23) is extended as

$$p(x, t; x_1, t + t_1; \text{RT} > t) k(x) = f(x, t) p(x_1, t + t_1 | x, t; \text{RT} = t). \quad (4.17)$$

Following the steps of Section 3.1 one obtains:

$$k(x) p_s(x_1, t | x) \frac{\langle \text{RT} \rangle}{V} = p_\pi(x, 0; x_1, t_1) + k(x) \int_0^\infty dt \left[p_\pi(x, t; x_1, t + t_1) - p(x, t; x_1, t + t_1) \right], \quad (4.18)$$

where $p_\pi(x, t; x_1, t + t_1)$ has the same meaning as in Chapter 3, but a slightly different definition:

$$p_\pi(x, t; x_1, t + t_1) = \int_0^\infty d\tau \int_{\mathcal{R}} d\chi f(\chi, \tau) p(x, \tau + t; x_1, \tau + t + t_1 | \chi, \tau; \text{RT} = \tau). \quad (4.19)$$

Note that, using this definition, $p_\pi(x, 0)$ can be written as

$$p_\pi(x, 0) = \int_0^\infty d\tau \int_{\mathcal{R}} d\chi f(\chi, \tau) p(x, \tau | \chi, \tau; \text{RT} = \tau) \quad (4.20)$$

$$= \int_0^\infty d\tau \int_{\mathcal{R}} d\chi f(\chi, \tau) \delta(x - \chi) \quad (4.21)$$

$$= \int_0^\infty d\tau f(x, \tau) \equiv \pi(x), \quad (4.22)$$

and therefore $p_\pi(x, 0) dx = \pi(x) dx$ is the probability that the reaction happens in the space interval $[x, x + dx[$. This probability is also known as the splitting probability.

From Eq. (4.18) one obtains the mean reaction time by integrating over x_1 and x ,

$$\frac{\langle \text{RT} \rangle}{V} = \frac{1}{\kappa} + \int_{\mathcal{R}} dx \frac{k(x)}{\kappa} \int_0^\infty dt \left[p_\pi(x, t) - p(x, t) \right]. \quad (4.23)$$

This is an exact result that is valid for any process $x(t)$ and reaction rate $k(x)$. Additionally, one can obtain another equation by first multiplying Eq. (4.18) by x_1 and then integrating over x_1

$$k(x) \langle x(t_1)|x \rangle_s \frac{\langle \text{RT} \rangle}{V} = \langle x(t_1)|x, 0 \rangle_\pi \pi(x) + k(x) \int_0^\infty dt \left[\langle x(t+t_1)|x, t \rangle_\pi p_\pi(x, t) - \langle x(t+t_1)|x, t \rangle p(x, t) \right], \quad (4.24)$$

where we recall that $\langle x(t_1)|x, 0 \rangle_\pi$ is the mean position at time t_1 after the reaction given that the reaction happened at x (at time 0), $\langle x(t+t_1)|x, t \rangle_\pi$ is the mean value of $x_\pi(t+t_1)$ given that $x_\pi(t) = x$, $\langle x(t+t_1)|x, t \rangle$ is the mean value of $x(t+t_1)$ given that $x(t) = x$ and $\langle x(t_1)|x \rangle_s$ is the mean position at time t_1 in the stationary limit given that at time 0 the random walker is at position x .

To proceed further, we have to find an explicit form for $p_\pi(x, t)$, the probability after reaction. In the extended case reactions might happen at any $x \in \mathcal{R}$ with probability density $\pi(x) = p_\pi(x, 0)$. An integral equation for $\pi(x)$ can be found from Eq. (4.18), by integrating over x_1 :

$$0 = \pi(x) + k(x) \left\{ -\frac{1}{\kappa} + \int_0^\infty dt \int_{\mathcal{R}} dy \left[\left(\delta(x-y) - \frac{k(y)}{\kappa} \right) p_\pi(y, t) - \left(\delta(x-y) - \frac{k(y)}{\kappa} \right) p(y, t) \right] \right\}. \quad (4.25)$$

In principle, one could solve this integral equation coupled with Eq. (4.24). However, these equations are highly non trivial and even numerically it would be hard to solve them. Given this difficulty, we have to choose an ansatz for the splitting probability, $\pi(x)$, which (at this point) can only be done for a class of reactivities at a time². We choose to proceed with reactivity rates that can be described by Gaussians: $k(x) = \kappa e^{-x^2/2\delta} / \sqrt{2\pi\delta}$, where $\delta^{1/2}$ is the typical size of the target. With this choice, after performing preliminary simulations, one is led to believe that a reasonable ansatz for $\pi(x)$ would also be a Gaussian with two new parameters: α , the mean position where reactions happen, and β , the variance of this reaction coordinate. Moreover, following the Gaussian approximations used in the previous chapter, we approximate $p_\pi(x, t|x_\pi, 0)$ by a Gaussian with mean $\mu(t) + x_\pi$, where $\mu(t)$ is independent of x_π , and covariance $\text{Cov}_\pi(x(t+\tau), x(t)|x_\pi, 0) = \sigma(t+\tau, t)$, which is verified by the preliminary simulations. Using these approximations one can write the full distribution $p_\pi(x, t)$ as

$$p_\pi(x, t) = \int_{\mathcal{R}} dx_\pi p_\pi(x, t|x_\pi, 0) \pi(x_\pi) = \frac{1}{\sqrt{2\pi(\beta + \psi(t))}} \exp \left(-\frac{(x - [\alpha + \mu(t)])^2}{2(\beta + \psi(t))} \right). \quad (4.26)$$

²Take, for example, $k_a(x) \sim 1 - \Theta(|x| - a)$ and $k_b(x) \sim e^{-x^2}$, the distribution of reaction coordinates is intuitively different for each of these reactivities.

Additionally, these approximations allow us to explicitly write the means in Eq. (4.24),

$$\langle x(\tau)|x \rangle_s = x, \quad (4.27)$$

$$\langle x(\tau)|x, 0 \rangle_\pi = x + \mu(\tau), \quad (4.28)$$

$$\langle x(t + \tau)|x, t \rangle_\pi = \mu(t + \tau) + \alpha - \frac{\sigma(t + \tau, t) + \beta}{\psi(t) + \beta}(\mu(t) + \alpha - x), \quad (4.29)$$

$$\langle x(t + \tau)|x, t \rangle = x_0 - \frac{\sigma(t + \tau, t) + \beta}{\psi(t) + \beta}(x_0 - x). \quad (4.30)$$

Using these means in Eq. (4.24) we obtain

$$0 = \alpha + \mu(\tau) + \int_{\mathcal{R}} dx k(x) \int_0^\infty dt \left[\left(\mu(t + \tau) + \alpha - (\mu(t) + \alpha - x) \frac{\sigma(t + \tau, t) + \beta}{\psi(t) + \beta} \right) p_\pi(x, t) - \left(x_0 - (x_0 - x) \frac{\sigma(t + \tau, t)}{\psi(t)} \right) p(x, t) \right], \quad (4.31)$$

where we have integrated x and used the facts that $\pi(x)$ is normalized and that $k(x)$ has zero mean. The equations for α and β can be obtained from Eq.(4.25):

$$0 = \alpha + \int_{\mathcal{R}} dx x k(x) \int_0^\infty dt [p_\pi(x, t) - p(x, t)], \quad (4.32)$$

which is obtained by multiplying x and then integrating over the same variable and, finally,

$$0 = \beta + \alpha^2 + \int_{\mathcal{R}} dx x^2 k(x) \left\{ -\frac{1}{\kappa} + \int_0^\infty dt \int_{\mathcal{R}} dy \left[\left(\delta(x - y) - \frac{k(y)}{\kappa} \right) p_\pi(y, t) - \left(\delta(x - y) - \frac{k(y)}{\kappa} \right) p(y, t) \right] \right\}, \quad (4.33)$$

obtained by multiplying x^2 and integrating. To finalize this extension to the case of extended (Gaussian) targets, we introduce the expression of reactivity and perform the remaining spatial integrals in Eqs. (4.31),(4.32) and (4.33):

$$0 = \alpha + \mu(\tau) + \kappa \int_0^\infty \frac{dt}{\sqrt{2\pi}} \left[\left(\mu(t + \tau) + \alpha - (\mu(t) + \alpha) \frac{\sigma(t + \tau, t) + \beta}{\delta + \psi(t) + \beta} \right) \frac{e^{-\frac{(\alpha + \mu(t))^2}{2(\delta + \beta + \psi(t))}}}{\sqrt{\delta + \beta + \psi(t)}} - x_0 \left(1 - \frac{\sigma(t + \tau, t)}{\delta + \psi(t)} \right) \frac{e^{-\frac{x_0^2}{2(\delta + \psi(t))}}}{\sqrt{\delta + \psi(t)}} \right], \quad (4.34)$$

$$0 = \alpha + \kappa \delta \int_0^\infty \frac{dt}{\sqrt{2\pi}} \left[\frac{\alpha + \mu(t)}{\delta + \beta + \psi(t)} \frac{e^{-\frac{(\alpha + \mu(t))^2}{2(\delta + \beta + \psi(t))}}}{\sqrt{\delta + \beta + \psi(t)}} - \frac{x_0}{\delta + \psi(t)} \frac{e^{-\frac{x_0^2}{2(\delta + \psi(t))}}}{\sqrt{\delta + \psi(t)}} \right], \quad (4.35)$$

and

$$0 = \beta + \alpha^2 - \delta + \kappa\delta^2 \int_0^\infty \frac{dt}{\sqrt{2\pi}} \left[\frac{(\alpha + \mu(t))^2 - (\delta + \beta + \psi(t))}{(\delta + \beta + \psi(t))^2} \frac{e^{-\frac{(\alpha + \mu(t))^2}{2(\delta + \beta + \psi(t))}}}{\sqrt{\delta + \beta + \psi(t)}} - \frac{x_0^2 - (\delta + \psi(t))}{(\delta + \psi(t))^2} \frac{e^{-\frac{x_0^2}{2(\delta + \psi(t))}}}{\sqrt{\delta + \psi(t)}} \right]. \quad (4.36)$$

Thus forming a set of closed equations for α, β and $\mu(t)$, which, when solved numerically, are all the variables needed to find the mean reaction time, given by

$$\frac{\langle \text{RT} \rangle}{V} = \frac{1}{\kappa} + \int_0^\infty \frac{dt}{\sqrt{2\pi}} \left(\frac{e^{-\frac{(\alpha + \mu(t))^2}{2(\delta + \beta + \psi(t))}}}{\sqrt{\delta + \beta + \psi(t)}} - \frac{e^{-\frac{x_0^2}{2(\delta + \psi(t))}}}{\sqrt{\delta + \psi(t)}} \right). \quad (4.37)$$

4.3 | Imperfect reactions in two dimensions.

Here, we present the extension of our formalism to the two-dimensional case. We assume that the process $\mathbf{r}(t) = (x(t), y(t))$ is a two-dimensional stochastic process for which each coordinate, in absence of confinement, satisfies the hypotheses assumed for one-dimensional processes. We focus on isotropic walks, so that, in free space, there are no correlations between the directions x and y :

$$\text{Cov}(x_i(t), x_j(t')) = \delta_{ij} \sigma(t, t'), \quad (4.38)$$

where i and j label spatial coordinates and $\sigma(t, t')$ is given by Eq. (3.1). Similarly to the case studied in the previous section, we focus on Gaussian targets, with a reaction rate

$$k(\mathbf{r}) = k(r = |\mathbf{r}|) = \kappa \frac{e^{-\frac{r^2}{2\delta}}}{2\pi\delta}. \quad (4.39)$$

It is easy to show that the development leading to Eq. (4.18) in the previous section for one-dimensional extended targets still holds in two dimensions by replacing x by \mathbf{r}_* and x_1 by \mathbf{r}_1 :

$$k(\mathbf{r}_*) p_s(\mathbf{r}_1, t | \mathbf{r}_*) \frac{\langle \text{RT} \rangle}{V} = p_\pi(\mathbf{r}_*, 0; \mathbf{r}_1, t_1) + k(\mathbf{r}_*) \int_0^\infty dt \left[p_\pi(\mathbf{r}_*, t; \mathbf{r}_1, t + t_1) - p(\mathbf{r}_*, t; \mathbf{r}_1, t + t_1) \right], \quad (4.40)$$

where $p_\pi(\mathbf{r}_*, t; \mathbf{r}_1, t + 1)$ is the joint probability distribution function of $\mathbf{r}(\text{RT} + t) = \mathbf{r}_*$ and $\mathbf{r}(\text{RT} + t + t_1) = \mathbf{r}_1$. Integrating (4.40) over \mathbf{r}_1 and \mathbf{r}_* leads to the expression of the mean

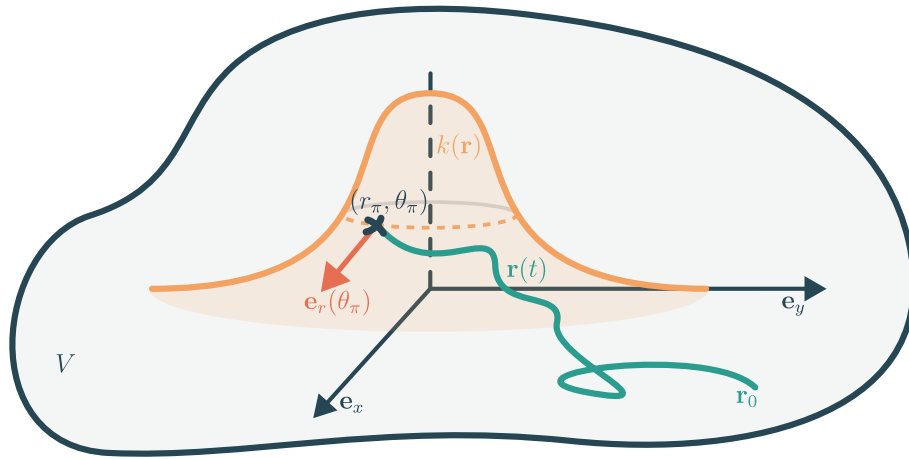


Figure 4.3: **Schematic representation of a two-dimensional imperfect reaction with sink reactivity.** A random walker $\mathbf{r}(t)$ that moves inside a confinement of volume V is searching for a reaction at a target centered at the origin of coordinates with a Gaussian-shaped reaction rate, $k(\mathbf{r})$.

reaction time:

$$\frac{\langle \text{RT} \rangle}{V} = \frac{1}{\kappa} + \int_0^\infty dt \int d\mathbf{r}_* \frac{k(\mathbf{r}_*)}{\kappa} [p_\pi(\mathbf{r}_*, t) - p(\mathbf{r}_*, t)]. \quad (4.41)$$

Note that this expression is, once again, exact and valid for any reaction rate $k(\mathbf{r}_*)$ and process $\mathbf{r}(t)$, not necessarily Gaussian.

Let us now give explicit expressions for Gaussian processes. Let us define the center of the target as the origin of space. Since, for large volumes, the mean reaction time should not depend on the initial angle θ_0 between the vector $\mathbf{r}_0 = \mathbf{r}(0)$ and the x -axis, we assume that the initial position is uniformly distributed around the target, with a fixed distance r_0 . In two dimensions, the probability distribution function of initial angles is therefore $p(\theta_0) = 1/2\pi$. With this choice of initial condition, if \mathbf{r}_π is the position of the random walker at the instant of reaction, the probability distribution function of the angle θ_π between \mathbf{r}_π and the x -axis is also uniform. We define $\rho(r_\pi)$ the probability distribution function of the distance r_π to the target center at the reaction time.

As in the one-dimensional case, we assume that the trajectories in the future of the reaction, given that the reaction happens at polar coordinate (r_π, θ_π) , display Gaussian statistics. Additionally, we assume that the mean square displacement of these trajectories after reaction is the same as the mean square displacement of the original process, and that the average trajectory is oriented in the direction $\mathbf{e}_r(\theta_\pi)$ (defined as the unit vector in the direction θ_π , see Fig. 4.3):

$$\langle \mathbf{r}(\text{RT} + t) | \text{reaction at } (r_\pi, \theta_\pi) \rangle = \langle \mathbf{r}(t) | r_\pi, \theta_\pi, 0 \rangle_\pi = [r_\pi + \mu(t)] \mathbf{e}_r(\theta_\pi), \quad (4.42)$$

where $\mu(t)$ does not depend on r_π and θ_π . We also assume, as in the one-dimensional case, that all propagators appearing in (4.40) can be evaluated in free space (except for $p_s(\mathbf{r}_*) = 1/V$). We note that $p_\pi(\mathbf{r}, 0)$, just like before, is the splitting probability, $\pi(\mathbf{r})$. Using

the above notations, we obtain

$$p_\pi(\mathbf{r}, 0) = \pi(\mathbf{r}) = \frac{\rho(r)}{2\pi r}, \quad (4.43)$$

with $r = |\mathbf{r}|$. Without loss of generality, we consider a position $\mathbf{r}_* = x_*\mathbf{e}_x$ along the x -axis, and Eq. (4.40), after integration of \mathbf{r}_1 , becomes

$$\begin{aligned} \frac{\langle \text{RT} \rangle}{V} k(x_*) &= \frac{\rho(x_*)}{2\pi x_*} + k(x_*) \int_0^\infty dt \left[\int_0^{2\pi} \frac{d\theta_\pi}{2\pi} \int_0^\infty dr_\pi \rho(r_\pi) p_\pi(x_*\mathbf{e}_x, t|r_\pi, \theta_\pi, 0) \right. \\ &\quad \left. - \int_0^{2\pi} \frac{d\theta_0}{2\pi} p(x_*\mathbf{e}_x, t|r_0, \theta_0, 0) \right], \end{aligned} \quad (4.44)$$

where $p_\pi(\mathbf{r}, t|r_\pi, \theta_\pi, 0)$ is the probability distribution function of $\mathbf{r}(\text{RT} + t)$ given that the reaction occurs at a distance r_π from the target center, with an angle θ_π , and $p(\mathbf{r}, t|r_0, \theta_0, 0)$ is the probability distribution function of positions at t given that the initial angle is θ_0 . With our hypotheses, these conditional probability distribution functions can be written as

$$p_\pi(x_*\mathbf{e}_x, t|r_\pi, \theta, 0) = \frac{1}{2\pi\psi(t)} \exp\left(-\frac{x_*^2 + [r_\pi + \mu(t)]^2 - 2x_*[r_\pi + \mu(t)] \cos \theta}{2\psi(t)}\right), \quad (4.45)$$

$$p(x_*\mathbf{e}_x, t|r_0, \theta, 0) = \frac{1}{2\pi\psi(t)} \exp\left(-\frac{x_*^2 + r_0^2 - 2x_*r_0 \cos \theta}{2\psi(t)}\right). \quad (4.46)$$

To obtain an explicit expression for the mean RT, we multiply (4.44) by x_* and integrate over positive x_* . Using the above equation, and the expression (4.39) of $k(x_*)$, the integrals over x_* and θ_π, θ_0 can be performed, leading to

$$\frac{\langle \text{RT} \rangle}{V} = \frac{1}{\kappa} + \int_0^\infty \frac{dt}{2\pi(\delta + \psi(t))} \left(\int_0^\infty dr \rho(r) e^{-\frac{(r+\mu(t))^2}{2(\delta+\psi(t))}} - e^{-\frac{r_0^2}{2(\delta+\psi(t))}} \right). \quad (4.47)$$

Next, let us identify the self-consistent equations for $\mu(t)$. We write Eq. (4.40) for $\mathbf{r}_* = x_*\mathbf{e}_x$, with $x_* > 0$, multiply it by x_1 and integrate over all values of \mathbf{r}_1 , leading to

$$\begin{aligned} k(x_*) \frac{\langle \text{RT} \rangle}{V} \langle x(t)|x_*\mathbf{e}_x \rangle_s &= \frac{\rho(x_*)}{2\pi x_*} \langle x(t_1)|x_*\mathbf{e}_x, 0 \rangle_\pi \\ &+ k(x_*) \int_0^\infty dt \int_0^{2\pi} \frac{d\theta}{2\pi} \left[\int_0^\infty dr_\pi \rho(r_\pi) \langle x(t+t_1)|x_*\mathbf{e}_x, t; r_\pi, \theta, 0 \rangle_\pi p_\pi(x_*\mathbf{e}_x, t|r_\pi, \theta, 0) \right. \\ &\quad \left. - \langle x(t+t_1)|x_*\mathbf{e}_x, t; r_0, \theta, 0 \rangle p(x_*\mathbf{e}_x, t|r_0, \theta, 0) \right]. \end{aligned} \quad (4.48)$$

Using the isotropy condition, the conditional averages read, see Appendix A,

$$\langle x(t+t_1)|x_*\mathbf{e}_x, t; r_\pi, \theta, 0 \rangle_\pi = [r_\pi + \mu(t+t_1)] \cos \theta - \frac{\sigma(t+t_1, t)}{\sigma(t, t)} ([r_\pi + \mu(t)] \cos \theta - x_*), \quad (4.49)$$

$$\langle x(t+t_1) | x_* \mathbf{e}_x, t; r_0, \theta, 0 \rangle = r_0 \cos \theta - \frac{\sigma(t+t_1, t)}{\sigma(t, t)} (r_0 \cos \theta - x_*). \quad (4.50)$$

To find a self-consistent integral equation for $\mu(t)$, we multiply (4.48) by $2\pi x_*^2$ and integrate over positive values of x_* . Using the above formulas, the integration over θ and x_* can be performed analytically, leading to the result

$$\begin{aligned} \frac{\kappa\delta}{2\pi} \int_0^\infty dt \left\{ \int_0^\infty dr \rho(r) \frac{e^{-\frac{(r+\mu(t))^2}{2(\delta+\psi(t))}}}{\delta+\psi(t)} \left[\frac{(r+\mu(t))^2}{\delta+\psi(t)} \left(\frac{r+\mu(t+t_1)}{r+\mu(t)} - M_\delta(t_1, t) \right) + 2(M_\delta(t_1, t) - 1) \right] \right. \\ \left. - \frac{e^{-\frac{r_0^2}{2(\delta+\psi(t))}}}{\delta+\psi(t)} \left[\frac{r_0^2}{\delta+\psi(t)} [1 - M_\delta(t_1, t)] + 2(M_\delta(t_1, t) - 1) \right] \right\} + \mu(t_1)\alpha = 0, \quad (4.51) \end{aligned}$$

where

$$M_\delta(t_1, t) = \frac{\delta + \sigma(t+t_1, t)}{\delta + \sigma(t, t)}, \quad (4.52)$$

α is the mean radius at the reaction time, $\alpha \equiv \int_0^\infty dr_\pi r_\pi \rho(r_\pi)$ and we have used (4.44) to eliminate $\langle \text{RT} \rangle / V$.

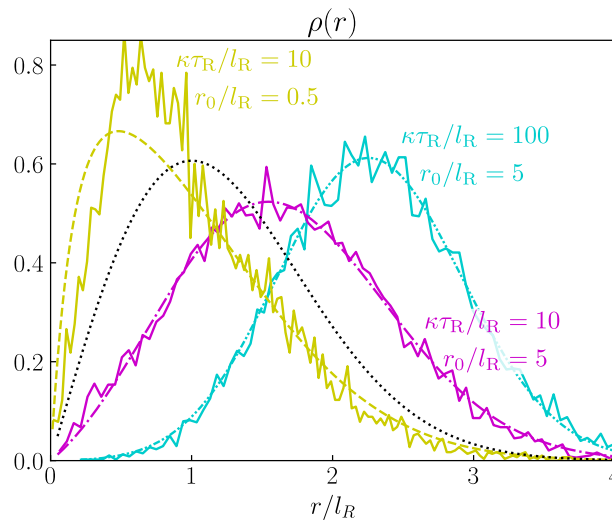


Figure 4.4: **Distribution of the reaction distance to the center of the target, $\rho(r)$.** The simulations were performed for a Rouse chain with 40 monomers with a target size $\delta = l_R$. The simulation results are shown by continuous lines. Then, fits were made with the function in Eq. (4.53): the dashed line is the fit of the simulations with $\kappa\tau_R/l_R = 10$ and $r_0 = 0.5l_R$; the dashed-dot line is the fit with $\kappa\tau_R/l_R = 100$ and $r_0 = 5l_R$; the dashed-dot-dot line is the fit with $\kappa\tau_R/l_R = 10$ and $r_0 = 5l_R$; and the equivalent pseudo-Markovian result is shown with a dotted line, $2\pi r k(r)/\kappa$. We use the natural units of the Rouse chain model: l_R is the typical size of a bond, τ_R is the relaxation time of one monomer.

The last step of the theory consists in characterizing the distribution of the radius at the reaction time, see Fig. 4.4. In principle one could use Eq. (4.44) as an integral equation that, coupled with Eq. (4.51), would give us $\rho(r)$. However, this is a very difficult procedure to solve, even if one solves the equations with numerical methods. Therefore, we will set an

ansatz for $\rho(r_\pi)$:

$$\rho(r_\pi) = \frac{1 - e^{-\frac{r_\pi}{a}} e^{-\frac{(r_\pi - a)^2}{2b}}}{Z \sqrt{2\pi b}}, \quad (4.53)$$

where Z is a normalization constant and two new parameters, a and b , have been added to the problem, thus creating the need for two new independent equations. To find these two equations, first one multiplies Eq. (4.44) by $2\pi x_*^3$ and integrate over positive x_* :

$$\kappa\delta^2 \int_0^\infty dt \left[\int_0^\infty dr \rho(r) \frac{e^{-\frac{(r+\mu(t))^2}{2(\delta+\psi(t))}}}{2\pi(\delta+\psi(t))} \frac{(r+\mu(t))^2 - 2(\delta+\psi(t))}{(\delta+\psi(t))^2} - \frac{e^{-\frac{r_0^2}{2(\delta+\psi(t))}}}{2\pi(\delta+\psi(t))} \frac{r_0^2 - 2(\delta+\psi(t))}{(\delta+\psi(t))^2} \right] + \beta + \alpha^2 - 2\delta = 0, \quad (4.54)$$

where $\beta = -\alpha^2 + \int_0^\infty dx x^2 \rho(x)$ is the variance of the reaction distance to the origin. For the second equation, one can multiply by x_*^5 (instead of $2\pi x_*^3$) and integrating over x_* , with the resulting equation:

$$8\kappa\delta^3 \int_0^\infty dt \left[\int_0^\infty dr \rho(r) \frac{e^{-\frac{(r+\mu(t))^2}{2\psi_\delta(t)}}}{2\pi\psi_\delta(t)} \frac{\frac{\delta}{8}[r+\mu(t)]^4 + \psi(t)\psi_\delta(t)[r+\mu(t)]^2 - \psi_\delta^2(t)[\psi_\delta(t) + \psi(t)]}{\psi_\delta^4(t)}, - \frac{e^{-\frac{r_0^2}{2\psi_\delta(t)}}}{2\pi\psi_\delta(t)} \frac{\frac{\delta}{8}r_0^4 + \psi(t)\psi_\delta(t)r_0^2 - \psi_\delta^2(t)[\psi_\delta(t) + \psi(t)]}{\psi_\delta^4(t)} \right] + \int_0^\infty dr r^4 \rho(r) = 8\delta^2, \quad (4.55)$$

where $\psi_\delta(t) = \delta + \psi(t)$ is introduced to improve readability.

We have now a set of 3 coupled equations that characterize $\mu(t)$, Eq. (4.51), a , Eq. (4.54), and b , Eq. (4.55). With the solutions of these equations we can use Eq. (4.47) to find the mean reaction time. After this development it is quite natural to see that a generalization to three dimensions is possible and no new argument has to be added.

Let us first analyze our predictions of the reaction coordinate distribution, $\rho(r)$. In Figure 4.4, we represent the distribution of r at the reaction time for three sets of reactivity and initial positions. We see that $\rho(r)$ can in fact be approximated by the ansatz in Eq. (4.53). Additionally, for large reactivity, we see that the position where reactions are most probable is clearly not the center of the target and, in fact, almost no reactions happen at the center of the target, where the reaction rate is largest, see the cyan curve in Figure 4.4. In the cases, $r_0 = 0.5l_R$, we find that the ansatz is not a good fit to the simulation data at all regimes, predicting quite well the large r behaviour. As a consequence of this less than ideal match between the simulation and the ansatz, we do not expect our theory to work for small initial distances with large reactivities. We note, however, that this was already expected for particles that start “inside” the target ($r_0 < \sqrt{\delta}$).

In Figure 4.5 one can see that our theoretical predictions are a very good match to the simulation results. When analyzing the pseudo-Markovian predictions (e.g., the mean reaction time for $\kappa\tau_R/l_R = 10$ and $r_0/l_R = 1$ is predicted to be negative), it becomes clear that, to predict the mean reaction times in two dimensions, it is essential to develop non-Markovian theories that do not rely on pseudo-Markovian approaches. We note that, for small r_0 and large κ (blue curve), we do not represent the theoretical prediction because the numerical scheme to solve the integral equations does not converge (at least in the set of parameters we tested), which was expected as we had already shown in Figure 4.4 that this situation is problematic in our theory. However, when $\kappa \rightarrow \infty$ and the particles is started inside the target the mean reaction time becomes very small and estimating it does not represent the most important goal of the theory. Outside this region of initial conditions the predictions are much better.

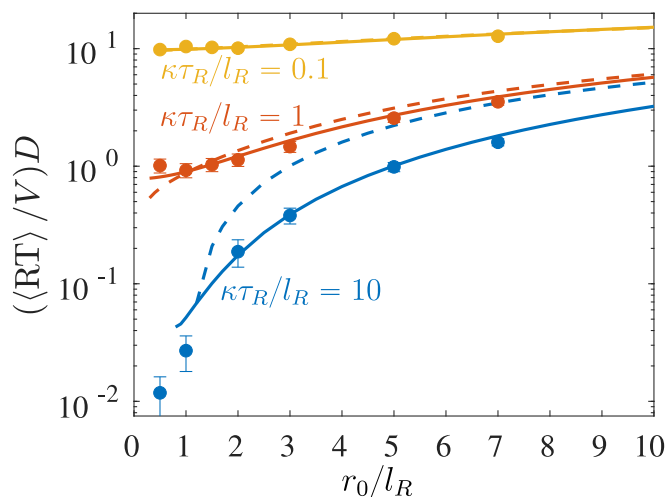


Figure 4.5: **Verification that our theoretical predictions match simulations in two dimensions.** With continuous lines we represent our theoretical prediction for the mean reaction time in two dimensions. The mean reaction time obtained from the simulations of a Rouse chain with 40 monomers in two dimensions are represented by the symbols with corresponding uncertainties. With dashed lines we represent the predictions obtained using a pseudo-Markovian approach. The parameters of the simulation have been controlled so that a convergent limit is reached. When the pseudo-Markovian approach is not shown is because it would predict negative mean reaction times (except for $\kappa\tau_R/l_R = 0.1$, where the pseudo-Markovian is hidden behind the non-Markovian one). In this case $D = l_R^2/\tau_R$ is the diffusion constant of a single monomer, l_R is the typical size of a bond, τ_R is the relaxation time of one monomer and the target size is $\delta = l_R$.

4.4 | Conclusion

In this chapter, we have developed three new theories describing the kinetics of imperfect reactions. First, we have extended the one-dimensional case to include gated reactions, where a target that is imperfect might be active or inactive. We have found the equations that enable the calculation of the mean reaction time and verified that our theory incorporates the previous results for Markovian processes. Then, we have studied the case of extended

targets, particularly the case of the Gaussian-shaped ones. Finally, we studied the case of two-dimensional imperfect reactions with Gaussian-shaped targets. We found equations that lead to the mean reaction time, the space distribution of the reactions and the mean trajectory after a reaction. Using simulations we have shown that the theory is correct when the particles are initially outside the target. The fact that the theory in two dimensions is correct when compared to simulations serves a strong suggestion that the one-dimensional theory for extended targets is similarly correct, even though we have not performed any simulations in that case. Moreover, we believe that the two-dimensional approach can easily be extended to three dimensions, as no new arguments have to be made in the three dimensions.

COMPETITIVE FIRST PASSAGE EVENTS IN VISCOELASTIC FLUIDS AND CONFRONTATION WITH EXPERIMENTS

5.1	Non-Markovian motion in viscoelastic fluids and the generalized Langevin equation	72
5.1.1	The Generalized Langevin Equation for a Rouse Chain	72
5.1.2	Calculation of the mean square displacement	75
5.1.3	Developing an experiment to see non-Markovian effects	77
5.2	Predicting the splitting probabilities for Gaussian random walkers	82
5.3	Testing the theory with experiments	86
5.3.1	Choosing appropriate experimental parameters	86
5.3.2	Experimental mean trajectories after reaction	87
5.3.3	Experimental Splitting Probabilities	88
5.4	Conclusion	89

Up to now, the work presented in this thesis is only theoretical. The question arises if the impact of memory on first passage events can be observed in an experimental setup. Though many physical processes are non-Markovian, experiments are usually restricted to the observation of the mean square displacement and do not explore the first passage quantities (Mason et al., 1997; Wei et al., 2000). Experimental observations of first passage quantities in non-Markovian processes are scarce, limited to the persistence exponents (Bray et al., 2013; Wong et al., 2001) or the barrier crossing problem (Ferrer et al., 2021; Ginot et al., 2022). In this chapter, we aim to observe and describe how memory influences competitive first passage events in viscoelastic fluids.

Viscoelastic fluids are materials that exhibit a combination of viscous and elastic behaviors, blurring the line between solids and liquids (Denn, 1990; Lin et al., 2005). Their distinctive characteristics include both resistance to flow under shear stress (viscous behavior) and the ability to store and release energy during deformation (elastic behavior). These fluids display time-dependent responses that can be seen as a memory storage: deformations to

the fluid will be remembered for some time until the fluid finally relaxes back to equilibrium. Through the use of microrheology, an experimental method that is usually used to infer the rheological properties of a fluid (Mason and Weitz, 1995), it has been observed that the movement of beads in (sufficiently) viscoelastic fluids displays anomalous diffusion (Mason et al., 1997). Microrheology implicitly assumes that the observed processes are Gaussian, which combined with the observed subdiffusion (and stationary increments) suggests that the process is non-Markovian, see Section 2.2.1. Therefore, one can use the movement of beads in viscoelastic fluids to test first passage theories and find first passage properties in real non-Markovian systems.

There are many first passage properties that one could study. Here, we focus on competitive events. In a general formulation, a competitive event is when there are (at least) two possible outcomes of a first passage problem and one wants to know the probability of each. Competitive events are the natural choice if one wants to observe first passage properties in experiments, see Figure 5.1. This is because, experimentally, one typically has a particle moving in a frame that is smaller than the physical confining volume. Let us assume that we want to observe a first passage to one target. If the particle leaves the frame while it is searching for the target, then, we lose it and, even if it comes back inside the frame, one cannot be sure that it is the same particle. In contrast, for competitive events, one can place a target at each exit of the frame, meaning that, before a particle leaves the frame (and we lose it), it has already performed a first passage to one of the targets.

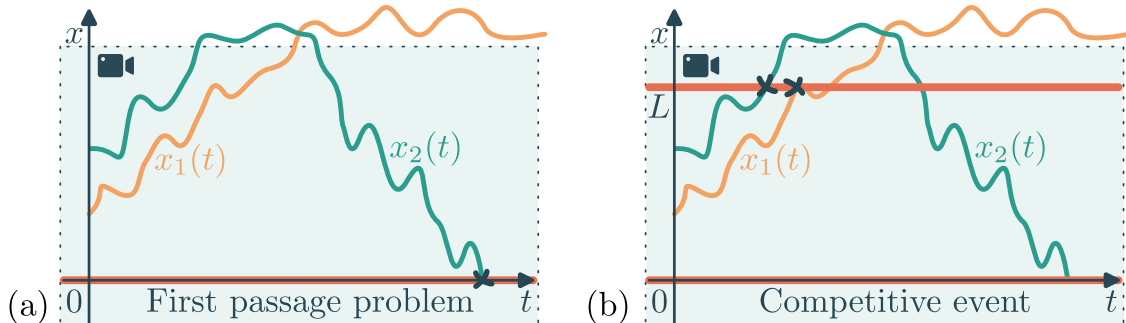


Figure 5.1: **Experimental difference between observing first passage to one target and competitive events.** Experimentally, the trajectories $x_1(t)$ and $x_2(t)$ that are searching for the red targets can only be seen inside the dotted region (corresponding to the space that is recorded by the camera). In the case of a first passage to one target, (a), many trajectories are lost. In the case of competitive events, (b), it is not possible to lose particles from the recorded region, as trajectories must touch one of the targets before leaving this region.

In addition to being suitable to experimental observation of first passage events, the problem of competitive targets is relevant in various domains. An historical example would be the “gambler’s ruin problem”, in which one wishes to know the risk for a gambler to get ruined before achieving a given profit, clearly a relevant problem in financial mathematics (Bouchaud et al., 2018). Other examples appear in chemical (Espenson, 1981), biochemical (Hansen et al., 2019) and photochemical (Motti et al., 2019) reactions. The key quantity characterizing competitive events is the *splitting probability*, which is the probability for a random process to realize an event before the other one. Contrary to the case of non-

Markovian processes, for Markovian (memoryless) processes, splitting probabilities are well-characterized (Dobramysl and Holcman, 2020; Cheviakov and Ward, 2011; Bressloff, 2020, 2021; Condamin et al., 2008; Bénichou and Voituriez, 2014).

However, memory effects are essential in complex systems (Mason et al., 1997; Squires and Mason, 2010; Furst and Squires, 2017). Despite their relevance, a general quantitative theory of competitive events for non-Markovian processes is lacking. For such non-Markovian processes, first passage theories have mainly been limited to the case of single targets (Guérin et al., 2016; Bray et al., 2013; Levernier et al., 2019; Dolgushev et al., 2015; Delorme and Wiese, 2015; Sadhu et al., 2018; Levernier et al., 2022; Walter et al., 2021; Levernier et al., 2020). For the two-target problem, the prediction of splitting probabilities is limited to one dimensional processes, in a few specific examples (Masoliver et al., 1986; Bicout and Burkhardt, 2000) or for scale invariant processes using scaling arguments (Majumdar et al., 2010) or perturbative methods (Wiese, 2019). The question naturally arises as to whether one could predict the outcome of competitive events for non-scale invariant stochastic processes, as in the case of viscoelastic fluids.

Here, we describe an experimental setup that enables us to obtain the movement of beads in a viscoelastic fluid and obtain some characteristic properties movement. Then, we build a non-perturbative theory that gives us the splitting probabilities with the intent of testing it with our experiment. The theory developed here is valid for Gaussian non-Markovian processes. We experimentally show that, in viscoelastic polymer fluids, memory leads to an increase of the probability to hit the closest target, which is quantitatively predicted by our theory. Moreover, our observations provide the first experimental proof that the state of the system (of the random walker and the additional degrees of freedom, that are at the origin of memory) at the first passage event is not an equilibrium state. As a consequence of this non-equilibrium feature, the trajectories after the first passage are biased on average, which our theory shows is the key to correctly predict splitting probabilities.

The outline of the chapter is as follows. First, in Section 5.1.1, we give a short derivation of the generalized Langevin equation (a “Langevin” equation that allows for memory), and then, in Section 5.1.2, we use this equation to find the mean square displacement of different memory kernels. In Section 5.1.3, we describe an experimental setup that enables the acquisition of non-Markovian trajectories and characterize these trajectories. Then, in Section 5.2, we derive the equations that enable us to calculate the splitting probabilities. Finally, in Section 5.3, we analyze the experimental data to obtain the first passage properties and compare them to the predictions of our theory.

5.1 | Non-Markovian motion in viscoelastic fluids and the generalized Langevin equation

In this section, we study how non-Markovian motion can be described in a viscoelastic fluid. First, we present a short derivation of the generalized Langevin equation, essential to mathematically describe motion with memory. We do this derivation for the particular case of a spring-bead (Rouse) chain. Then, we explore some memory kernels (a function that describes the delayed response of the fluid) and obtain the corresponding mean square displacements. To finish the section, we analyze an experimental setup that allows us to see non-Markovian walks in viscoelastic fluids.

5.1.1 | The Generalized Langevin Equation for a Rouse Chain

The derivation of the generalized Langevin equation typically requires the consideration of a thermal bath that is linearly coupled to the variables of interest (Zwanzig, 2001; Pavliotis, 2014). Here, for simplicity, we derive the equation in the specific case of a N monomer spring-bead (Rouse) chain. However, it must be noted that our formalism also allows for other types of chains and, in a more general way, any combination of N coupled degrees of freedom. Our derivation is slightly different from the one presented by Panja (2010).

Let us start with a polymer chain with N monomers connected by springs. The position of each monomer is x_i , with i from 1 to N . The objective here, is to find an equation for the position of the i_0 th monomer, $y(t) = x_{i_0}(t)$, so that all other monomers are hidden in some effective functions. We allow for an external force that is only applied to the i_0 th monomer, $F(y(t))$. The connectivity matrix, M , is a matrix that describes how monomers are connected to each other. The dynamics of each monomer (in natural units $l_R = 1 = \tau_R$, where l_R is the typical length of one bond and τ_R is the relaxation time of one monomer, see Section 3.1.3 for a small introduction of the Rouse chain) can be described by the following Langevin equations,

$$\dot{x}_i(t) = - \sum_{j=1}^N M_{ij} x_j(t) + f_i(t) + \delta_{i_0 i} F(y(t)), \quad \forall_i, \quad (5.1)$$

where we have added two fictive monomers $x_0(t) = x_1(t)$ and $x_{N+1}(t) = x_N(t)$ for Eq. (5.1) to be valid for all i and introduced the thermal noise (white Gaussian) $f_i(t)$, with mean zero and covariance

$$\langle f_i(t) f_j(t') \rangle = 2\delta_{ij} \delta(t - t'). \quad (5.2)$$

The connectivity matrix, M , is defined by setting $M_{ij} = -1$ if the monomer i is connected to the monomer j and M_{ii} equal to the number of connections to the monomer i . This matrix is clearly symmetric, which means that it can be diagonalized with the matrix of eigenvectors

P and its transpose P^T :

$$P^T M P = D = \text{diag}(\lambda_1, \dots, \lambda_N), \quad (5.3)$$

where $P^T = P^{-1}$, due to the symmetry of M . The diagonal matrix, D , is a matrix with the eigenvalues, λ_i , in the diagonal. Using the matrix P one can define a new coordinate system, $a_i = \sum_j P_{ji} x_j$, that decouples the Langevin equations:

$$\dot{a}_i = -\lambda_i a_i + g_i + G_i(y(t)), \quad (5.4)$$

where $g_i = \sum_j P_{ji} f_j$ and $G_i(y(t)) = P_{i_0 i} F(y(t)) = b_i F(y(t))$ with $b_i \equiv P_{i_0 i}$. Due to the fact that $P^{-1} = P^T$, the new noise term, g_i , is still Gaussian with mean zero and covariance $\langle g_i(t) g_j(t') \rangle = 2\delta_{ij} \delta(t - t')$. The new coordinate system is called the normal mode space, where the a_i s are called the normal modes (or just modes). The solution of Eq. (5.4) reads

$$a_i(t) = a_i(0) e^{-\lambda_i t} + \int_0^t dt' e^{-\lambda_i(t-t')} [g_i(t') + G_i(y(t))]. \quad (5.5)$$

The first mode, a_1 , is typically related to the position of the center of mass of the polymer. If the polymer is free to move (no monomers are fixed at a position), then, when there is no external force F , the position of the center of mass should diffuse. In Eq. (5.4), it is clear that the only way for a_1 to be diffusive is if $\lambda_1 = 0$. This is true for any connectivity matrix M that represents a set of degrees of freedom not attached.

The equation for the monomer of interest, $y(t) = x_{i_0}(t)$, can also be written with the help of these modes,

$$\dot{y}(t) = -\sum_{i=2}^N b_i \lambda_i a_i + f_{i_0} + F(y(t)), \quad (5.6)$$

where the $i = 1$ term of the sum is zero because $\lambda_1 = 0$. Using the solutions obtained for the modes $a_i(t)$, one can write

$$\dot{y}(t) = -\sum_{i=2}^N b_i \lambda_i \left(a_i(0) e^{-\lambda_i t} + \int_0^t dt' e^{-\lambda_i(t-t')} [g_i(t') + b_i F(y(t))] \right) + f_{i_0} + F(y(t)), \quad (5.7)$$

where we identify two functions

$$h(t) = f_{i_0}(t) - \sum_{i=2}^N b_i \lambda_i \left(a_i(0) e^{-\lambda_i t} + \int_0^t dt' e^{-\lambda_i(t-t')} g_i(t') \right), \quad (5.8)$$

$$\chi(t) = \delta(t) - \sum_{i=2}^N b_i^2 \lambda_i e^{-\lambda_i t}. \quad (5.9)$$

With these functions it is possible to rewrite the equation for $y(t)$ as

$$\dot{y}(t) = h(t) + \int_0^t dt' \chi(t-t') F(y(t')). \quad (5.10)$$

This is one form of the overdamped generalized Langevin equation. Analyzing Eq. (5.10),

one might think that when there is no external force the memory effects disappear due to the fact that the equation is reduced to $\dot{y}(t) = h(t)$. However, the noise term, $h(t)$, is clearly time-correlated (not white) and it depends on the (initial) conformations of the polymer. One can, as an example of this dependence, compute the mean of $h(t)$,

$$\langle h(t) \rangle = \sum_{i=2}^N b_i \lambda_i \langle a_i(t) \rangle = \sum_{i=2}^N b_i \lambda_i e^{-\lambda_i t} \langle a_i(0) \rangle. \quad (5.11)$$

Let us now assume that the initial configuration is the equilibrium one conditioned to $y(0) = y_0$. This would be equivalent to finding the stationary limit of Eq. (5.4). The initial conditions on the modes are¹, therefore,

$$\begin{aligned} \langle a_i(0) \rangle &= 0, \\ \langle a_i(0) a_j(0) \rangle &= \delta_{ij} / \lambda_i, \quad \text{for } i, j \geq 2, \end{aligned} \quad (5.12)$$

even if there is an external force. Since $\lambda_1 = 0$ for a free polymer, one cannot extend Eq. (5.12) to $i, j = 1$. This is not a problem here because one can always write the modes with index one as a function of the other modes and the position of the monomer of interest, $y(t)$.

From the definitions of $h(t)$ and $\chi(t)$, Eqs. (5.8) and (5.9), using the initial conditions for $a_i(0)$, one can observe that the fluctuation dissipation theorem is still true

$$\langle h(t) h(t') \rangle = \chi(|t - t'|). \quad (5.13)$$

where, once again, it is made clear that, even if the system is started at equilibrium ($\langle a_i(0) \rangle = 0$), the effective ‘‘thermal’’ noise remains correlated.

Another form of the generalized Langevin equation is obtained by using the Laplace transform² to invert Eq. (5.10):

$$\int_0^t dt' K(t - t') \dot{y}(t') = \xi(t) + F(y(t)), \quad (5.14)$$

where $K(t) = \mathcal{L}^{-1}[1/\tilde{\chi}(s)](t)$ is the memory (friction) kernel and $\xi(t) = \mathcal{L}^{-1}[\tilde{h}(s)/\tilde{\chi}(s)](t)$ is a random force that, in general, is not white. Note that the fluctuation dissipation theorem is also verified for $\xi(t)$ and $K(t)$,

$$\langle \xi(t) \xi(t') \rangle = k_B T K(|t - t'|), \quad (5.15)$$

where we have reestablished the factor $k_B T$, with k_B the Boltzmann constant and T the temperature, that is necessary for homogeneity. Further discussion on the memory kernel is

¹In fact, one can write $p_s(a_i(0)|y(0) = y_0) \propto e^{-V(y_0) - \sum_i \lambda_i a_i^2}$, with $F(y) = -V'(y)$, which means that the statistics of $a_i(0)$ conditioned to the fact that $y(0) = y_0$ does not depend on the value of y_0 , nor the external force.

²we recall that the Laplace transform of $f(t)$ is $\tilde{f}(s) = \mathcal{L}[f(t)](s) = \int_0^\infty dt e^{-st} f(t)$

given in the end of the next section.

5.1.2 | Calculation of the mean square displacement

One of the first results one can obtain from the generalized Langevin equation is the mean square displacement of the process $y(t)$ in the absence of an external forces. Let us assume here that the origin of the coordinate system is at $y(0) = 0$ and that there are no external forces. From Eq. (5.10) it is possible to obtain

$$\langle \tilde{y}(s)\tilde{y}(s') \rangle = \frac{1}{ss'} \langle \tilde{h}(s)\tilde{h}(s') \rangle = k_B T \frac{\tilde{\chi}(s) + \tilde{\chi}(s')}{(s + s')ss'}, \quad (5.16)$$

where we have used the fact that, when $\langle f(t)f(t') \rangle = g(|t - t'|)$, the double Laplace transform of $\langle f(t)f(t') \rangle$ is given by $\langle \tilde{f}(s)\tilde{f}(s') \rangle = \frac{\tilde{g}(s) + \tilde{g}(s')}{(s + s')}$.

If one assumes that the Gaussian process being studied displays stationary increments, then, the covariance of this process must be

$$\langle y(t)y(t') \rangle = \frac{1}{2} (\psi(t) + \psi(t') - \psi(|t - t'|)), \quad (5.17)$$

where $\psi(t)$ is the mean square displacement, see Section 2.2.1 for the proof. Performing the double Laplace transform on $\langle y(t)y(t') \rangle$ on obtains

$$\langle \tilde{y}(s)\tilde{y}(s') \rangle = \frac{1}{2} \left(\frac{\tilde{\psi}(s)}{s'} + \frac{\tilde{\psi}(s')}{s} - \frac{\tilde{\psi}(s) + \tilde{\psi}(s')}{s + s'} \right) = \frac{s^2\tilde{\psi}(s) + s'^2\tilde{\psi}(s')}{2(s + s')ss'}. \quad (5.18)$$

Combining Eqs. (5.16) and (5.18), it is clear that the mean square displacement is given by

$$\psi(t) = 2k_B T I(t), \quad \text{with} \quad I(t) = \mathcal{L}^{-1} \left[\frac{\tilde{\chi}(s)}{s^2} \right] (t) = \mathcal{L}^{-1} \left[\frac{1}{s^2 \tilde{K}(s)} \right] (t). \quad (5.19)$$

Let us now study some memory kernels. The first result from Eq. (5.19), is that, if $K(t)$ is integrable, i.e., $\int_0^\infty dt K(t) = \tilde{K}(0)$ exists, then, the long time behaviour is known:

$$\lim_{t \rightarrow \infty} \psi(t) = \mathcal{L}^{-1} \left[\lim_{s \rightarrow 0} \frac{2k_B T}{s^2 \tilde{K}(s)} \right] (t) = \mathcal{L}^{-1} \left[\lim_{s \rightarrow 0} \frac{2k_B T}{s^2 \tilde{K}(0)} \right] (t) \sim \frac{2k_B T}{\tilde{K}(0)} t. \quad (5.20)$$

Therefore, if the memory kernel is integrable, then, the long time behaviour of the random walker is diffusive. It comes as no surprise that when the memory kernel is a Dirac delta function, the mean square displacement is diffusive at all times, as memory is instantaneously lost and the system is Markovian. Alternatively, diffusion can still be reached if the memory kernel decays exponentially. In that case the system is non-Markovian but eventually becomes diffusive.

Moreover, let us look for one case where the long time behaviour is not diffusive. One can, for example, choose the memory kernel

$$K_\infty = \frac{\alpha_\infty}{t^{2H}}, \quad \text{with } H > 0, \quad (5.21)$$

that is not integrable. This kernel corresponds to memory that decays as a power law, and, therefore, memory is long lasting. The resulting mean square displacement is

$$\psi(t) = \frac{k_B T \sin(2\pi H)}{\pi H \alpha_\infty} t^{2H}, \quad \text{for } H < \frac{1}{2}, \quad (5.22)$$

corresponding to a subdiffusive fractional Brownian motion, with Hurst exponent H .

Furthermore, we would like to find a memory kernel that is subdiffusive at short times and becomes diffusive after some crossover time. This is motivated by the study of beads moving inside polymer solution, where this behaviour is found (Mason et al., 1997). To this end, we choose a memory kernel that displays a power law decay up to some typical time τ_0 and an exponential decay after. The motivation is to create a subdiffusive regime up to τ_0 and a diffusive one after. We propose:

$$K(t) = \frac{\gamma_0}{\tau_0} f_{H_v} \left(\frac{t}{\tau_0} \right), \quad f_{H_v}(x) = \frac{1}{\Gamma(1 - 2H_v)} \frac{e^{-x}}{x^{2H_v}}, \quad \text{for } H_v < \frac{1}{2}, \quad (5.23)$$

where $\gamma_0 = \int_0^\infty K(t) dt$ is the long time friction coefficient (this will become evident when the long time behaviour is analyzed), τ_0 is the crossover time from subdiffusion to diffusion and $H_v < 1/2$ is the (short time) Hurst exponent of the viscoelastic fluid. Introducing this kernel into Eq. (5.19), one obtains

$$\psi(t) = \frac{2\tau_0 k_B T}{\gamma_0} \frac{1}{\Gamma(2H_v)} \left[\left(\frac{t}{\tau_0} - 2H_v + 1 \right) \gamma \left(2H_v, \frac{t}{\tau_0} \right) + \left(\frac{t}{\tau_0} \right)^{2H_v} e^{-t/\tau_0} \right], \quad (5.24)$$

where $\gamma(\alpha, x) = \int_0^x t^{\alpha-1} e^{-t} dt$ is the lower incomplete gamma function. Analyzing the asymptotic behaviour of the mean square displacement, one can find that for short times,

$$\psi(t) \underset{t \ll \tau_0}{\sim} \frac{2\tau_0 k_B T}{\gamma_0 \tau_0^{2H_v} \Gamma(1 + 2H_v)} t^{2H_v}, \quad (5.25)$$

we do find subdiffusion and for long times,

$$\psi(t) \underset{t \gg \tau_0}{\sim} 2 \frac{k_B T}{\gamma_0} t, \quad (5.26)$$

we find regular diffusion with a diffusion coefficient $D = k_B T / \gamma_0$. In the next section, we analyze experimental trajectories that are obtained from the tracking of beads in a viscoelastic fluid. Then, we check if the mean square displacement obtained here matches the experimental one.

5.1.3 | Developing an experiment to see non-Markovian effects

In this section, we briefly describe one experimental framework where non-Markovian effects can be observed. Then, we study the corresponding trajectories and obtain their mean square displacement. The experiments described in this section have been performed by B. Gorin, K. Xie and H. Kellay, our experimental colleagues at LOMA, from which we obtained the trajectories of non-Markovian walkers, that we have further analysed.

5.1.3.1 | Experimental setup and first limitations

With the hope of creating a viscoelastic fluid where memory effects are visible, a solution of NaCl and polyacrylamide in water is prepared. Polyacrylamide has a long linear chain structure that, when hydrated, creates gels. Tuning the concentration of polyacrylamide one can tune the viscoelastic properties of the solution. Now that a complex (viscoelastic) fluid is prepared, one can immerse acrylic³ fluorescent microspheres in the solution. These are glass-like spheres with $1\mu\text{m}$ diameter that emit light and therefore, using a microscope, it is possible to record their positions. Then, fitting Gaussians to the bright spots on each frame, it is possible to obtain the trajectories $x(t_i)$ for each particle in the frame.

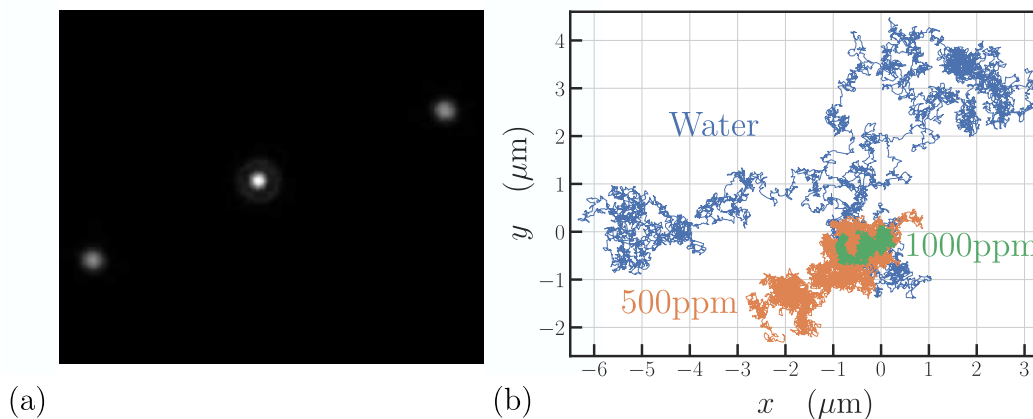


Figure 5.2: **The movement of acrylic beads in a viscoelastic solution.** (a) Intensity map obtained from the microscope. (b) Three examples of bead trajectories in solutions with different concentrations of polymers.

Note that, recording images from a microscope requires the storage of N frames with $m \times n$ pixels. This means that, even though we only want a trajectory, i.e., a list $(t_i, x_i) \forall_{i=1, \dots, N}$, we have to store a lot of data that is mostly useless to our analysis, thus limiting the amount of statistics that is reasonably obtainable. To maximize the statistics obtained one can reduce the size of each frame, however, one has to be careful to not reduce the frame size too much making it easier to have particles that leave the frame. Alternatively, one could increase the number of particles in the fluid, thus including more information in one frame. However, this would mean that particles would interact with each other and we do not want to study particle interactions here.

³Poly(methyl methacrylate)

5.1.3.2 | Characterization of the experimental trajectories

Let us now analyze the trajectories obtained from the experiments described before. We have prepared four different polymer solutions with the hope of producing different ranges of non-Markovian effects. One solution has no long polymers (water), for control, and the three others have polymer concentrations of 500ppm, 1000ppm and 2000ppm, where we hope to see increasing memory effects.

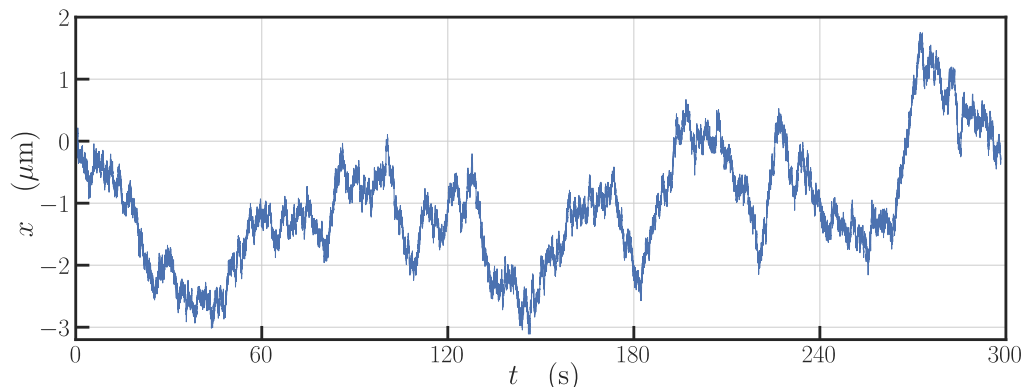


Figure 5.3: **Example of a trajectory obtained from the experiments.** Trajectory obtained by tracking the bright spots in the videos. Here, the acrylic bead is moving in a solution with concentration 500ppm of polymers. The frame rate is 500 frames per second.

From Figure 5.3 some characteristics of the underlying stochastic process become evident. At first observation, it is clear that the trajectories can be seen as non-smooth, $\langle \dot{x}^2(t) \rangle = \infty$, just like in the case of Brownian motion. This means that, in fact, one can ignore the inertia of the bead in comparison to the effect of friction when describing its motion, as expected for micron sized objects in fluids more viscous than water. One can then use the overdamped dynamics that is assumed in Section 5.1.1.

One can also check if these trajectories display stationary increments. In fact, plotting $\Delta_\tau(t) = x(t + \tau) - x(t)$ as a function of t (see Figure 5.4), we see that $\Delta_\tau(t)$ does not depend on t and, therefore, the trajectories display stationary increments.

Then, one can also check that the process is Gaussian. In Figure 5.5, we represent the statistics of the normalized steps, $(x(t + \tau) - x(t)) / \sqrt{\text{Var}(x(t + \tau) - x(t))}$, for different elapsed times, τ . It can be seen that the statistics of the steps in the four solutions studied is Gaussian. Therefore, since the process also displays stationary increments, the covariance of these trajectories, $\sigma(t, t')$, can be written as

$$\sigma(t, t') = \frac{\psi(t) + \psi(t') - \psi(|t - t'|)}{2}, \quad (5.27)$$

where $\psi(t)$ is the mean square displacement, see Section 2.2.1.

Let us now look for the mean square displacement of these trajectories. For this we create

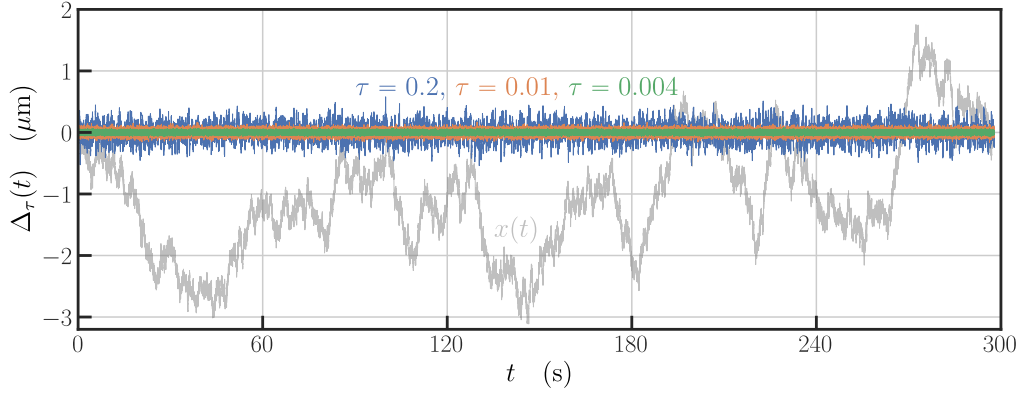


Figure 5.4: **Verification that the trajectories display stationary increments.** Representation of the increments $\Delta_\tau(t) = x(t + \tau) - x(t)$ for three different times τ . It is clear that there is no t dependence in $\Delta_\tau(t)$ showing that the trajectory $x(t)$ is of stationary increments. The trajectory used is represented in grey and was obtained for a solution of concentration 500ppm with a frame rate of 500 frames per second.

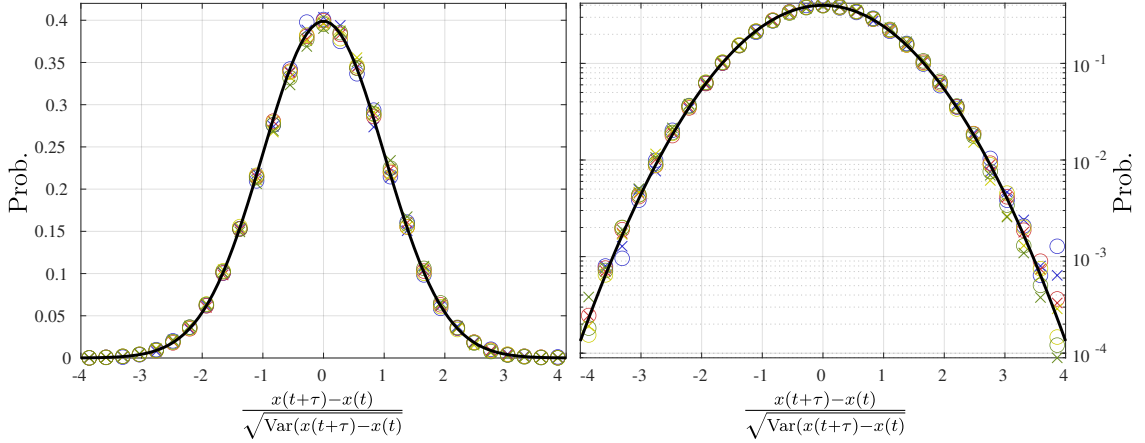


Figure 5.5: **Verification that the distribution of the steps is Gaussian for each solution.** Normalized histograms (linear and semi-log) of the increments $x(t + \tau) - x(t)$ for water (in blue), 500ppm (in green), 1000ppm (in yellow) and 2000ppm (in red). Two different elapse times, τ , are represented: the crosses correspond to $\tau = \tau_0$ (the memory time obtained from the fit to Eq. (5.19), see figure 5.7) and the circles correspond to $\tau = \tau_0/2$.

the estimator

$$\delta^2(\tau, T) = \frac{1}{T - \tau} \int_0^{T-\tau} dt [x(t + \tau) - x(t)]^2, \quad (5.28)$$

where T is the time length of the trajectory. The mean value of this estimator is the mean square displacement, $\langle \delta^2(\tau, T) \rangle = \psi(\tau)$, and its variance can be written as

$$\text{Var}(\delta^2(\tau, T)) = \left\langle \left(\delta^2(\tau, T) - \psi(\tau) \right)^2 \right\rangle = \int_0^{T-\tau} dt \frac{T - \tau - t}{(T - \tau)^2} \left[\psi(t + \tau) + \psi(|t - \tau|) - 2\psi(t) \right]^2. \quad (5.29)$$

In Figure 5.6 we, represent the estimator $\delta^2(\tau, T)$ to $N_{\text{traj}} = 59$ trajectories tracked in a solution with concentration 500ppm. The mean of this estimator, equivalent to the mean

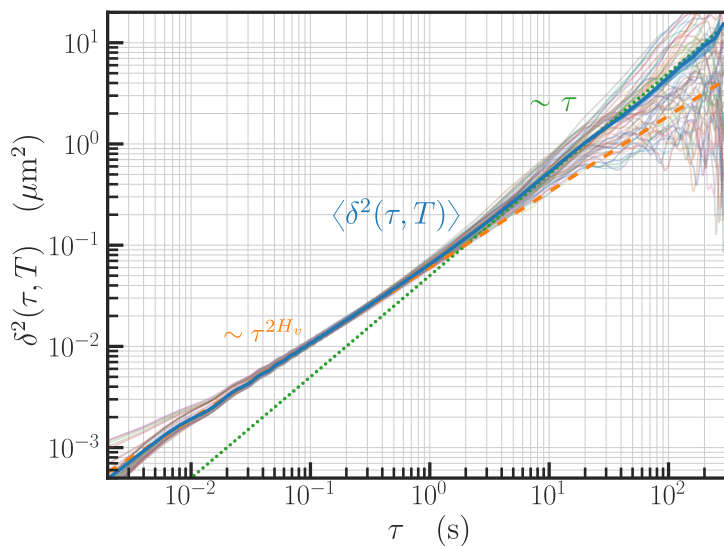


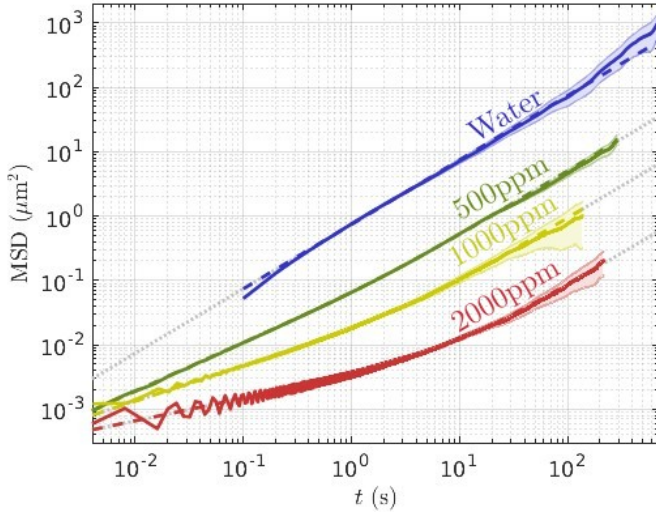
Figure 5.6: **Graph of the estimator $\delta^2(\tau, T)$ for a solution of concentration 500ppm.** In partially transparent lines, $\delta^2(\tau, T)$ is plotted for each of the $N_{\text{traj}} = 59$ tracked trajectories. The mean value, $\langle \delta^2(\tau, T) \rangle$, and corresponding uncertainty, $\sqrt{\text{Var}(\delta^2(\tau, T))/N_{\text{traj}}}$, are shown in a blue thick line and a (small) shaded region of the same color. Two asymptotic lines are drawn: the dotted line, that represents a fit to the diffusive behaviour (for long times), and the dashed line, representing the fit to the subdiffusive behaviour with $H_v < 1/2$. These trajectories were obtained from a solution of concentration 500ppm (of long polymers) with a frame rate of 500 frames per second.

square displacement, is also represented. In the figure, one can see that for large times the mean square displacement is linear and, therefore, for large times, the movement of the bead becomes diffusive. However, for short times, one can see that the mean square displacement is no longer linear and is in fact subdiffusive (with $H_v < 1/2$). This suggests that the mean square displacement in Eq. (5.24), obtained with the memory kernel $K(t) \sim e^{-t}/t^{2H_v}$, might be a good fit to the experimental data. In Figure 5.7, we represent the results of this fit to the mean square displacement of each solution prepared. There, analyzing H_v as a function of concentration, it is clear that memory effects increase with concentration.

Combining the facts that the trajectories are Gaussian, with stationary increments and display subdiffusion, and after checking the properties for the other concentrations, one can say that the process underlying the movement of beads in viscoelastic fluids is non-Markovian. This is a consequence of an extension of Doob's Theorem, see Section 2.2.1.

In order to use these experiments to verify non-Markovian theories, one has to check if the trajectories are subjected to drift, that is usually a consequence of residual currents in the fluid. This is important because, up to now, there are no theories studying first passage events for non-Markovian random walkers that are subjected to drifts. Therefore, one must first verify that there is no drift. To do this, we build the estimator:

$$m(\tau, T) = \frac{1}{T - \tau} \int_0^{T-\tau} dt (x(t + \tau) - x(t)), \quad (5.30)$$



Water	
D	$0.37 \mu\text{m}^2/\text{s}$
500ppm	
$\gamma_0/k_B T$	$40 \text{ s}/\mu\text{m}^2$
τ_0	1.48 s
H_v	0.375
1000ppm	
$\gamma_0/k_B T$	$217.5 \text{ s}/\mu\text{m}^2$
τ_0	2.9 s
H_v	0.275
2000ppm	
$\gamma_0/k_B T$	$2415 \text{ s}/\mu\text{m}^2$
τ_0	7 s
H_v	0.175

Figure 5.7: **Mean square displacement of an acrylic bead moving in different viscoelastic solutions.** We represent, in continuous lines the mean square displacement corresponding to the four different solutions, obtained from $\delta^2(\tau, T)$, and corresponding uncertainty represented as a shaded region around $\psi(t)$. The fit of Eq. (5.24) to the data is represented with dashed lines and the extension outside the time range of the fit is represented with a grey dotted lines. The parameters of the fit are given in the table on the right.

where one analyzes the time averaged increments. Assuming that the system is ergodic, the estimator $m(\tau, T)$ is equivalent to $\langle x(t + \tau) - x(t) \rangle$. If there is no drift, then $\langle x(t) \rangle$ must be constant, and, therefore, the no-drift hypothesis is equivalent to saying that one must observe $\langle m(\tau, T) \rangle = 0, \forall \tau$. The variance of this estimator is

$$\text{Var}(m(\tau, T)) = \langle m^2(\tau, T) \rangle = \int_0^{T-\tau} dt \frac{T-\tau-t}{(T-\tau)^2} [\psi(t+\tau) + \psi(|t-\tau|) - 2\psi(t)], \quad (5.31)$$

which is calculated under the hypothesis of no drift. With this estimator, one can check if the no-drift hypothesis is valid. For this we compute the estimator $m(\tau, T)$ for every trajectory observed and verify if the estimator leaves the region $0 \pm 2\sigma_m = \pm 2\sqrt{\text{Var}(m(\tau, T))}$. If there is no drift, then 95% of the trajectories should fall inside this region for all τ . In Figure 5.8-(a) we show how this test is performed. We take the trajectories of beads in a 500ppm solution and compute $m(\tau, T)$ for each trajectory. One can see that ≈ 15 trajectories go outside the region $\pm\sigma_m$, corresponding to 74% of all trajectories and ≈ 2 trajectories leave the region $\pm 2\sigma_m$, corresponding to 3%. One can see from Figure 5.8 that the four solutions prepared before verify the no-drift hypothesis.

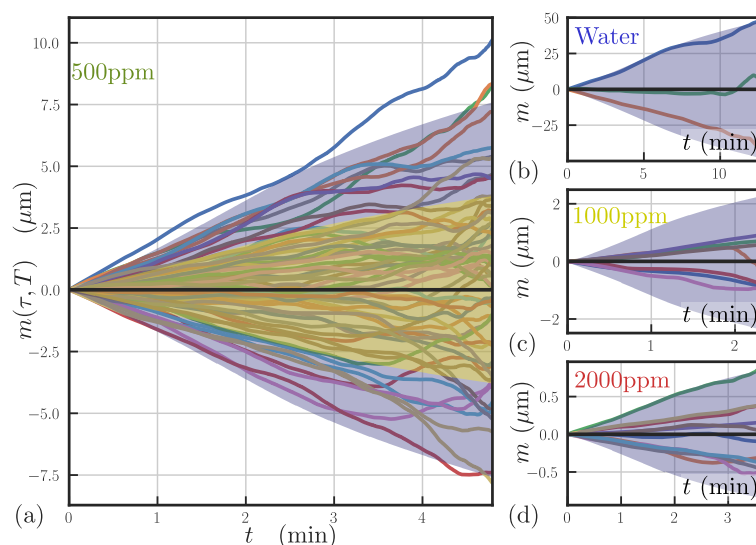


Figure 5.8: **Verification that the no-drift hypothesis is valid.** Representation of the estimator $m(\tau, T)$, defined in Eq. (5.30), for every trajectory in every solution studied. If there is no drift, then the estimators $m(\tau, T)$ (one for each trajectory recorded) should land inside the region in purple, $\pm 2\sqrt{\text{Var}(m(\tau, T))}$, with 95% probability. In (a), one additional region is represented, $\pm\sqrt{\text{Var}(m(\tau, T))}$, where trajectories should land with probability 74%. (a) Solution with 500ppm of long polymers recorded at 500 frames per second; (b) Water solution recorded at 10 frames per second; (c) 1000ppm at 245 frames per second; (d) 2000ppm at 250 frames per second.

5.2 | Predicting the splitting probabilities for Gaussian random walkers

Now that we have an experimental setup that produces real non-Markovian trajectories, one can use these trajectories to prove (or disprove) non-Markovian theoretical predictions. In this section, we develop a theory that enables us to calculate the splitting probabilities for Gaussian non-Markovian random walkers and test it against experimental results for four different viscoelastic fluids.

Let us start by assuming that a free random walker $x(t)$, started at $x_0 > 0$, moves in the search of two targets, one at $x_1 = 0$ and one at $x_2 = L > x_0$. Here, we derive the equations that provide the probabilities of touching the left target before the right one, π_1 (π_2 is the opposite). To this end, some properties of the random walker must be assumed. We assume that the random walker is non-biased (there is no drift), non-smooth ($\langle \dot{x}^2(t) \rangle = \infty$) and Gaussian with covariance $\sigma(t, t')$ and stationary steps. Due to these assumptions one can write the covariance as

$$\sigma(t, t') = \frac{1}{2}(\psi(t) + \psi(t') - \psi(|t - t'|)), \quad (5.32)$$

where $\psi(t)$ is the mean square displacement⁴. One also assumes, for generality, that the

⁴see Section 2.2.1

long time behaviour of the mean square displacement is a fractional Brownian motion, $\psi(t) \underset{t \rightarrow \infty}{\sim} Kt^{2H}$, with $0 < H < 1$ the Hurst exponent, which includes the particular case of long time diffusion (as seen in the previous experimental results). Note that $H = 1/2$ does not correspond to $H_v = 1/2$, as H_v corresponds to the subdiffusion that happens at short time scales. In fact, these assumptions “create” trajectories similar to those of the experiments, i.e., non-biased (no drift), non-smooth, with stationary increments and long time Brownian motion (if the theory is applied to the case of $H = 1/2$), see Section 5.1.3.2. With these assumptions one can write a renewal equation,

$$p(\chi, t) = p(\chi, t; \text{FPT} > t) + p(\chi, t; \text{FPT} \leq t), \quad (5.33)$$

where $p(\chi, t)$, corresponding to the probability distribution function to find $x(t) = \chi$, is split into two ways of reaching that point. The first term in the right hand side corresponds to the trajectories that reach the position χ at time t without touching any of the target ($\text{FPT} > t$), $p(\chi, t; \text{FPT} > t)$. The second term corresponds to the (joint) probability of touching one of the targets for the first time (the first passage time, FPT) before t and then reaching the position χ at time t , $p(\chi, t; \text{FPT} \leq t)$. Using the probability distribution function of touching one of the targets for the first time at time t , $F(t)$, one can further develop Eq. (5.33),

$$p(\chi, t) = \int_t^\infty d\tau F(\tau) p(\chi, t | \text{FPT} = \tau) + \int_0^t d\tau F(\tau) p(\chi, t | \text{FPT} = \tau). \quad (5.34)$$

If one now multiplies Eq. (5.34) by χ and integrates over the same variable, one obtains

$$x_0 = \int_t^\infty d\tau F(\tau) \mathbb{E}[x(t) | \text{FPT} = \tau] + \int_0^t d\tau F(\tau) \mathbb{E}[x(t) | \text{FPT} = \tau], \quad (5.35)$$

where $\mathbb{E}[x(t) | \text{FPT} = \tau]$ is the mean position of the random walker $x(t)$ given that, at time τ , the random walker touched one of the targets for the first time.

Let us now define a new process, the one describing the movement after the random walker touches one of the targets for the first time, $x_\pi(t) = x(t + \text{FPT})$. We assume that this process has mean $\mu(t)$, that can be written as

$$\mu(t) = \mathbb{E}[x(t + \text{FPT})] = \int_0^\infty d\tau F(\tau) \mathbb{E}[x(t + \tau) | \text{FPT} = \tau]. \quad (5.36)$$

Let us now introduce one variable A , that will later be taken to infinity, and integrate the function $g(t) = \int_0^t d\tau f(t, \tau)$ from 0 to A :

$$\begin{aligned} \int_0^A dt \int_0^t d\tau f(t, \tau) &= \int_0^A d\tau \int_t^A dt f(t, \tau) = \int_0^A d\tau \int_0^{A-\tau} du f(u + \tau, \tau) \\ &= \int_0^A du \int_0^{A-u} d\tau f(u + \tau, \tau). \end{aligned} \quad (5.37)$$

Using Eq. (5.37) with Eqs. (5.35) and (5.36), one can write

$$\begin{aligned} & \int_0^A dt \left(\mu(t) - x_0 + \int_t^\infty d\tau F(\tau) \mathbb{E}[x(t)|\text{FPT} = \tau] \right) \\ &= \int_0^A du \int_{A-u}^\infty d\tau F(\tau) \mathbb{E}[x(t+\tau)|\text{FPT} = \tau] \equiv Q(A). \end{aligned} \quad (5.38)$$

If we can show that $Q'(A)$ goes to zero for large A , then, the integrand of the left hand side of Eq. (5.38) must also go to zero for large t . Using the change of variables $u \rightarrow v = A - u$ one can rewrite $Q(A)$ as

$$Q(A) = \int_0^A dv \int_v^\infty d\tau F(\tau) \mathbb{E}[x(\tau + A - v)|\text{FPT} = \tau]. \quad (5.39)$$

We now argue that, whatever the conditions imposed on the past trajectory, the mean of the process at long times cannot travel a bigger distance than the square root of the mean square displacement, $\sim K_1 t^H$. Hence, one can assume that, for large A ,

$$|\mathbb{E}[x(\tau + A - v)|\text{FPT} = \tau]| < K_1 A^H, \quad (5.40)$$

where $K_1 > 0$ is arbitrary. Using Eq. (5.40) and the survival probability⁵, $S(v) = \int_v^\infty dt F(t) > 0$, one can find an upper bound for $Q(A)$:

$$|Q(A)| < K_1 A^H \int_0^A dv \int_v^\infty d\tau F(\tau) = K_1 A^H \int_0^A dv S(v) < K_1 A^H \int_0^\infty dv S(v) = K_1 A^H \langle T \rangle, \quad (5.41)$$

where $\langle T \rangle = \int_0^\infty dv S(v)$ is the mean first passage time, which is finite in our case because, for times larger than $(L^2/K)^{1/2H}$ the random walker is almost sure to have reached one of the targets⁶. With this, we have shown that $Q'(A) \sim 1/A^{1-H}$, with $H < 1$, goes to zero and, therefore, the integrand in the left hand side of Eq.(5.38) must also go to zero:

$$\lim_{t \rightarrow \infty} \left(\mu(t) - x_0 + \int_t^\infty d\tau F(\tau) \mathbb{E}[x(t)|\text{FPT} = \tau] \right) = 0. \quad (5.42)$$

If one now notices that the trajectories that have not yet reacted must be inside the region $x(t) \in]0, L[$, it becomes clear that, for $\tau > t$, $0 \leq \mathbb{E}[x(t)|\text{FPT} = \tau] \leq L$. It is then possible to find the upper and lower bounds of the third term of Eq. (5.42):

$$0 \leq \lim_{t \rightarrow \infty} \int_t^\infty d\tau F(\tau) \mathbb{E}[x(t)|\text{FPT} = \tau] \leq L \lim_{t \rightarrow \infty} \int_t^\infty d\tau F(\tau) = 0, \quad (5.43)$$

which means that this term is equal to zero and one can write

$$\lim_{t \rightarrow \infty} \mu(t) = x_0. \quad (5.44)$$

⁵The survival probability, $S(t)$, is defined as the probability of not touching any target before time t . It is naturally equal to the probability of touching a target for the first time at a time larger than t . Therefore, $S(t) = \int_t^\infty d\tau F(\tau)$.

⁶This time is such that $\psi(t) \sim L^2$.

Finally, by splitting $\mu(t)$ into the trajectories that touched the left target first, with probability π_1 and mean trajectory $\mu_1(t)$, and the trajectories that touched the right target, with probability π_2 and mean $\mu_2(t)$, one can write

$$x_0 = \lim_{t \rightarrow \infty} [\pi_1 \mu_1(t) + \pi_2 \mu_2(t)]. \quad (5.45)$$

In principle, Eq. (5.45) enables us to obtain π_1 by using the fact that $\pi_1 + \pi_2 = 1$ ⁷. However, we are still required to find the long time limit of $\mu_1(t)$ and $\mu_2(t)$. To find the mean trajectories after reaction⁸, one can write a new renewal equation describing the movement after one of the targets (at $x_1 = 0$ or $x_2 = L$) is met,

$$p(x_i, t; y, t + \tau) = \int_0^t dt' F(t') p(x_i, t; y, t + \tau | \text{FPT} = t'), \quad (5.46)$$

where y is an arbitrary position that is reached a time $\tau > 0$ after touching one target at time t . Developing Eq. (5.46) in a way that is described in Appendix D, one can write:

$$\int_0^\infty dt \left(\mathbb{E}[x_\pi(t + \tau) | x_\pi(t) = x_i] p_\pi(x_i, t) - \mathbb{E}[x(t + \tau) | x(t) = x_i] p(x_i, t) \right) = 0, \quad (5.47)$$

where $\mathbb{E}[x_\pi(t + \tau) | x_\pi(t) = x_i]$ is the mean position of the process $x_\pi(t)$ at time $t + \tau$ given that it was at the x_i at time t (after it reacted at time “zero”) and $\mathbb{E}[x(t + \tau) | x(t) = x_i]$ is the mean of the process $x(t)$ at time $t + \tau$ given that it was at x_i at time t .

Since the joint probability distribution after reaction, $p_\pi(x_i, t; y, t + \tau)$, can be split into reactions that happened at the left or right targets, one can write

$$p_\pi(x_i, t; y, t + \tau) = \sum_{j=1,2} \pi_j q_j(x_i, t; y, t + \tau), \quad (5.48)$$

where $q_j(x_i, t; y, t + \tau)$ is the joint probability distribution function to find $x_{\pi_j}(t) \equiv x(t + \text{FPT}_j) = x_i$ and $x_{\pi_j}(t + \tau) = y$ with $x_{\pi_j}(t)$ the process that describes the movement of the particle after it touched (for the first time, at time FPT_j) the target at position x_j before touching the other target. Using this decomposition one can write

$$\mathbb{E}[x_\pi(t + \tau) | x_\pi(t) = x_i] p_\pi(x_i, t) = \sum_{j=1,2} \pi_j \mathbb{E}[x_{\pi_j}(t + \tau) | x_{\pi_j}(t) = x_i] q_j(x_i, t), \quad (5.49)$$

and, therefore, Eq. (5.47) can be rewritten as

$$\int_0^\infty dt \left[\sum_{j=1,2} \pi_j q_j(x_i, t) \mathbb{E}_{\pi_j}(x_{\pi_j}(t + \tau) | x_{\pi_j}(t) = x_i) - p(x_i, t) \mathbb{E}(x(t + \tau) | x(t) = x_i) \right] = 0. \quad (5.50)$$

Then, since we do not know the functions q_j , we assume that the process $x_{\pi_j}(t)$ is

⁷This is true because, one of the assumptions is that $\psi(t) \sim Kt^{2H}$ for large t with $H > 0$

⁸Here, a reaction is when the random walker touches for the first time one of the targets.

(approximately) Gaussian with mean $\mu_j(t)$ and covariance $\sigma(t, t')$. Thus enabling us to use the projection law (described in Appendix A) to explicitly write the conditioned means. Using the fact that $q_j(x_i, t)$ (and $p(x_i, t)$) is Gaussian with mean $\mu_j(t)$ (mean x_0) and covariance $\sigma(t, t')$, one can write two integral closed equations for $\mu_1(t)$ and $\mu_2(t)$:

$$\int_0^\infty \frac{dt}{\sqrt{\psi(t)}} \left(\sum_{j=1,2} \pi_j \left[\mu_j(t + \tau) - (\mu_j(t) - x_i) \frac{\sigma(t + \tau, t)}{\psi(t)} \right] \exp\left(-\frac{(x_i - \mu_j(t))^2}{2\psi(t)}\right) - \left[x_0 - (x_0 - x_i) \frac{\sigma(t + \tau, t)}{\psi(t)} \right] \exp\left(-\frac{(x_i - x_0)^2}{2\psi(t)}\right) \right) = 0, \quad \forall_{i=1,2}, \quad (5.51)$$

We have now two coupled integral equations that can be numerically integrated to find the limits of $\mu_1(t)$ and $\mu_2(t)$ at large times. With these limits, the splitting probability can be found from Eq. (5.45). Now that we have a theory for competitive events, we can test it with the experiments described in the Section 5.1.3.

5.3 | Testing the theory with experiments

5.3.1 | Choosing appropriate experimental parameters

As mentioned in Section 5.1.3.1, our experimental setup produces a large amount of data that is irrelevant if one only wants to store the trajectories of different particles. This is due to the fact that one has to store a video instead of the trajectories, and only after one can analyze the video to extract the trajectories of the particles. This by it self is the biggest constraint to the amount of data one can obtain. However, there are other particularities of the setup that one has to tune to obtain usable data.

As we intend to study first passage events it is important to be sure that, when we detect such an event it is in fact close to *the* first passage event. This problem arises from the fact that, when recording the videos, we have to choose one frame rate f , i.e., the time in between frames of the video, and this will directly influence the time definition of our trajectories. If the frame rate is low, then, the particles might realize first passage events in between frames and we will measure first passage quantities that are incorrect. We call this artifact a border effect: when the frame rate is too low, $\pi_2(x_0)$ is overestimated for $x_0 \rightarrow 0$ and underestimated for $x_0 \rightarrow L$.

The solution is then to choose a high frame rate. However, as mentioned before, storing all this frames is expensive and eventually one does meet a maximum number of frames, N_{frames} , that can be stored (in our case, $\sim 1TB$). This limits the observation time to N/f . Naturally, if one increases the frame rate the recording time is reduced and, consequently, the distance travelled by the particles during the video is smaller. This is a problem because

we are looking for memory effects that macroscopically influence movement, meaning that, ideally, we would like to see $\pi(x_0) \neq x_0/L$ (the Markovian prediction) for large L , or at least of the order of the radius of the particles.

Therefore, one has to find a balance between a high frame rate where border effects are small and low frame rate where one can see longer trajectories and consequently measure the memory effect at larger scales.

5.3.2 | Experimental mean trajectories after reaction

Applying the fit parameters, obtained from Figure 5.7, in the Eq. (5.51) one can obtain the theoretical prediction of the mean trajectory after touching one of the targets for the first time, $\mu_1(t)$ and $\mu_2(t)$. This theoretical prediction is obtained by following a numerical scheme similar to that of Section 3.1.3. Then, we can compare these theoretical predictions to the mean trajectories measured from the experiments.

To obtain $\mu_1(t)$ and $\mu_2(t)$ from the experiments, we take one experimental trajectory $x(t)$ and look for the moment it touches one of the targets for the first time. Say, for example, that the first target touched is the target at x_i and it is touched at time FPT_i . Then, one stores the rest of the trajectory, $x(t + \text{FPT}_i)$, with $0 < t < T_{\text{obs}}$ where T_{obs} is the observation time⁹. With the stored trajectories after reaction one computes $\mu_i(t) = \langle x(t + \text{FPT}_i) \rangle$. To maximize the statistics, one can use the same trajectory multiple times. However, one must take measures to ensure that the sample is not correlated. To this end, we start at $t = 0$ and look for a first passage that happens at the time FPT_i , then, we redefine the trajectory as $x(t) = x_0 + x(t + T_{\text{sample}}) - x(T_{\text{sample}})$, where the delay $T_{\text{sample}} = 2\tau_0$ is added to ensure that the new starting point of this trajectory has no memory of the previous one, by forcing a time gap of two memory times (τ_0 from Figure 5.7).

In Figure 5.9, we present the mean trajectories after reaction that we have obtained for the four solutions prepared. One can see that the theoretical predictions quantitatively match the direct experimental observations, thus verifying the accuracy of our theory¹⁰. The physical intuition of subdiffusion, where particles tend to return to their previous positions (due to the delayed response forces exerted by the fluid on the particles), is clearly shown in this figure. This observation is a clear experimental evidence that, right after a first passage event, the motion of the particle is effectively biased, demonstrating that the supplementary degrees of freedom (where memory is “stored”) are in a non-equilibrium state at the moment of the first passage. We note that, in the control case (water), this effects does not happen, and the trajectory after reaction is in fact unbiased.

⁹The observation time, T_{obs} , is the time range of our measurements of $\mu(t)$

¹⁰Note that in Figure 5.9 (d) the measured means are constantly jumping, suggesting that the spatial resolution is poor and the error bars are highly underestimated.

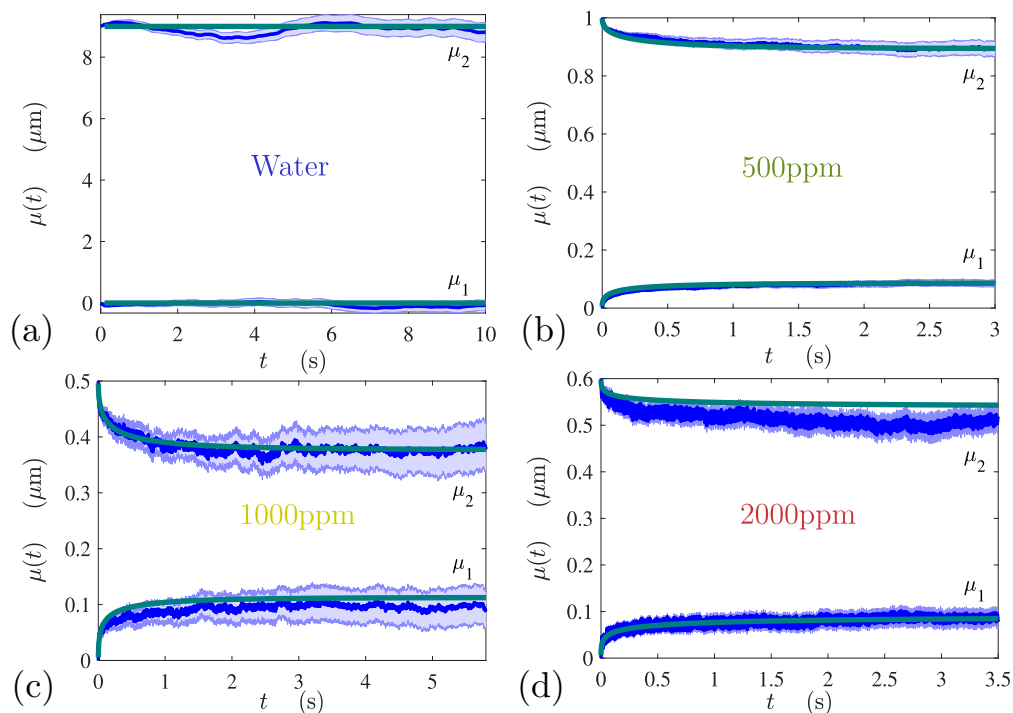


Figure 5.9: **Experimental mean trajectory after one of the targets is touched.** In green we represent the theoretical prediction of $\mu_i(t)$ and, in blue (with the respective 95% errorbars), we represent the experimental analogous. The positions of the targets are $x_1 = 0$ and $x_2 = L$. (a) is obtained in water with a $L = 9\mu\text{m}$ and $x_0 = 2\mu\text{m}$. (b) is obtained in the solution with 500ppm concentration for $L = 1\mu\text{m}$ and $x_0 = 0.2\mu\text{m}$. (c) 1000ppm solution with $L = 0.5\mu\text{m}$ and $x_0 = 0.2\mu\text{m}$. (d) 2000ppm solution with $L = 0.6\mu\text{m}$ and $x_0 = 0.2\mu\text{m}$.

5.3.3 | Experimental Splitting Probabilities

With the theoretical (numerical) prediction of $\mu_i(t)$, one can use Eq. (5.45) to obtain the theoretical predictions of the splitting probabilities π_i . Experimentally, it is easier to obtain the splitting probabilities π_i than $\mu_i(t)$. This is due to the fact that one only has to store if a first passage event happened or not at x_i , and not the full trajectory after it happened, thus allowing for better statistics. In this case, it is also possible to obtain more statistics from one trajectory.

In Figure 5.10, we see that the theory (green curves) matches the experiments (in blue) and predict the correct shapes of $\pi_2(x_0)$. This is particularly relevant because the previous best theoretical estimation of the full $\pi_2(x_0)$ is the Markovian one (red dashed line), $\pi_2(x_0) = x_0/L$, which does not take into account memory and is clearly not a good prediction for viscoelastic fluids. Analyzing the curves of the splitting probabilities for non-Markovian processes it becomes clear that the effect of memory is to favor the first passage to happen at the closest target to the initial position. This effect was already qualitatively predicted by the analysis of scale invariant processes (Majumdar et al., 2010) and is quantitatively predicted by our theory for non-scale invariant processes.

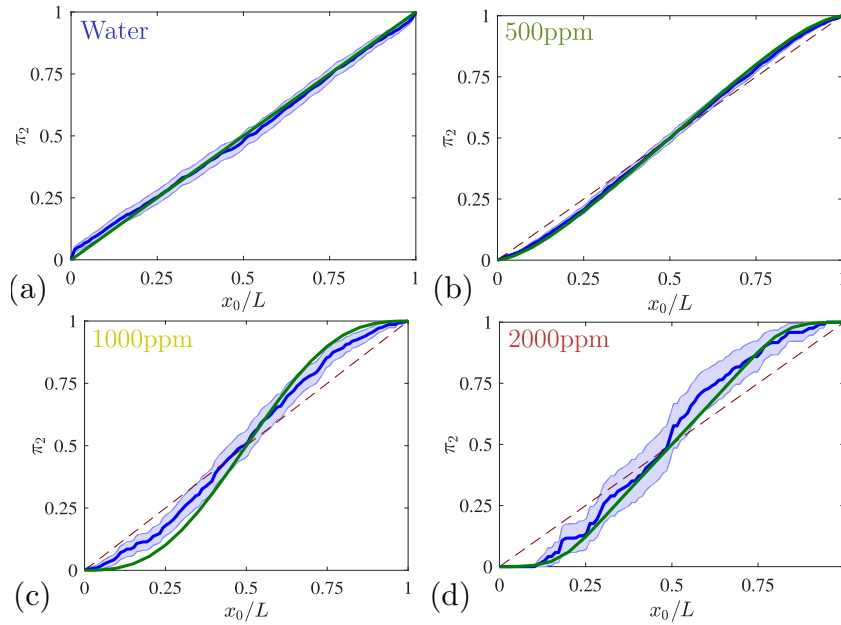


Figure 5.10: **Experimentally measured splitting probability π_2 and respective theoretical prediction for four different solutions.** In green we represent the theoretical prediction of π_2 and, in blue (with the respective 95% errorbars), we represent the experimental analogous. The Markovian prediction is represented with a red dashed line. (a) is obtained in water with a $L = 9\mu\text{m}$. (b) is obtained in the solution with 500ppm concentration for $L = 1\mu\text{m}$. (c) 1000ppm solution with $L = 0.5\mu\text{m}$. (d) 2000ppm solution with $L = 0.6\mu\text{m}$.

5.4 | Conclusion

In this chapter, we have described an experimental setup where one can track acrylic beads that are randomly moving in a viscoelastic fluid of long polymers. We have verified that the trajectories are Gaussian, with stationary increments. Additionally, we have verified that one does not need to introduce drift forces (fluid flows) to explain the movement of the beads. This was important because a theory of how non-Markovian particles move when subjected to drift forces is lacking. When measuring the mean square displacement we found that there are two regimes of movement, one, for short times subdiffusive and another, for longer times, diffusive. It follows, from an extension of Doob's theorem (see Section 2.2.1), that the trajectories we have observed in viscoelastic fluids are non-Markovian. Four different viscoelastic solutions have been studied, with different levels of memory, in water there is no memory (as expected), but, in the other solutions, we have found that the typical memory times of these viscoelastic fluids can be of order 1 to 10s, meaning that the effect of memory is relevant at macroscopic scales.

Then, we have presented a general theory that predicts the effect of memory on the outcome of competitive events, quantified by the splitting probability to reach one target before the other for Gaussian stochastic processes. The theoretical predictions for the splitting probability were tested against the experiments. This test showed that our theory quantitatively describes the effects of memory in the splitting probabilities. In particular, we

showed that, in the context of splitting probabilities, memory makes targets that are close from the initial condition effectively closer and easier to reach, which is characterized by the tilted S-shapes in $\pi_2(x_0)$. We note that this effect is significantly different from the case where subdiffusion arises from random jumps with heavy-tailed distributed waiting times, since the distribution of waiting times does not influence splitting probabilities (Condamine et al., 2008). By testing the theory against the experiments we have also found the first direct experimental evidence that, at first passage, the system is not at an equilibrium state, as seen from the biased trajectories that particles take after the first passage event.

FIRST PASSAGE IN COMPLEX COMPARTMENTALIZED MEDIA

6.1	Theory of diffusion in fractals	93
6.2	Transport in a medium with a fractal compartment	96
6.2.1	Dynamics in free (infinite) space	96
6.2.2	Introduction of a confining volume: the stationary distribution	97
6.3	Calculation of the mean first passage time	98
6.4	The bond-percolation network and simulations	101
6.4.1	Parameters of the fractal	102
6.4.2	Simulation scheme	104
6.4.3	Simulation results	105
6.5	Does the compartment facilitate reactions?	107
6.5.1	Compartment with no energetic bonding	108
6.5.2	Compartment with energetic bonding	108
6.5.3	Is optimization still possible in two-dimensional space?	109
6.6	Conclusion	110

In this chapter, we study the properties of first passage events when the target is embedded in a compartment where transport is complex. This study is motivated by the observation of such compartments in biological cells, where membraneless organelles play crucial roles in cellular processes (Zhao and Zhang, 2020). These organelles lack a surrounding membrane, and their formation is driven by liquid-liquid phase separation (Hyman et al., 2014; Brangwynne et al., 2015; Perry, 2019). Membraneless organelles have been found to be involved in numerous cellular functions, including RNA processing (Hirose et al., 2023), signal transduction (Zhang and Herman, 2020), and stress response (Gavrilova et al., 2023). While their diverse roles have been extensively studied, recent research suggests that these organelles may also be important for regulating reactivity within the cell (Nakashima et al., 2019; O’Flynn and Mittag, 2021).

One notable characteristic of membraneless organelles is their high density and viscosity, which give rise to their viscoelastic properties that have been observed in Elbaum-Garfinkle

et al. (2015). The viscoelastic behavior is observed through the subdiffusive motion (for short times) of large beads within these compartments, obtained via microrheology. Subdiffusion refers to a slower-than-normal diffusion process, often resulting from hindered movement due to crowding or viscoelasticity.

Given the presence of membraneless organelles and their viscoelastic nature, an intriguing question arises: can reaction times be optimized by the presence of subdiffusive compartments? The optimization of reaction times is of significant importance in cellular processes, as it directly affects the efficiency and speed of molecular interactions and signaling cascades. Previous studies on first passage problems in heterogeneous media with compartments have focused on diffusive processes (Vaccario et al., 2015; dos Santos et al., 2022). However, the incorporation of subdiffusion within these compartments to predict first passage properties remains unexplored.

Addressing the question of optimization mediated by subdiffusive compartments is not straightforward, as multiple factors come into play. On one hand, in 3-dimensional space, diffusive walks face difficulty in reaching very small targets, whereas point-like targets (infinitesimal) can be reached in finite time for subdiffusive walks, particularly when they are compact (Condamine et al., 2007). Notably, optimization strategies based on dimensional changes have been discovered for surface-mediated diffusion (Bénichou et al., 2010) and DNA search processes (Berg and von Hippel, 1985; Coppey et al., 2004). On the other hand, subdiffusion in compartments can also arise due to crowding and viscoelasticity of the medium, which inherently slows down the motion and is expected to increase the first passage times.

To determine if the speed-up, due to the change of dimensionality, or the slow-down, due to subdiffusion, dominates, and to explore the potential optimization of mean first passage times, a theoretical framework is required. There are three main theoretical origins for subdiffusion. First, one can consider continuous time random walks with long waiting times, where the random walker waits for a random time between jumps (Metzler and Klafter, 2000). However, these walks typically need infinite (mean) time to find targets, which is naturally not suitable for optimisation of reaction rates. The second option to create subdiffusive medium is viscoelasticity, i.e., developing a full non-Markovian description of the compartment. This is for now impossible as the theoretical framework of non-Markovian walks does not allow us to incorporate interfaces. There are few results for non-Markovian walks close to interfaces, notably, for the case of a walk close to a reflective wall, the only results available are obtained from simulations (Vojta et al., 2019). The last theoretical “option” is the use of fractal networks, where, due to crowding (characterized by lower connectivity between sites), subdiffusion might happen (O’Shaughnessy and Procaccia, 1985). Since one can write differential equations that describe the dynamics of diffusive particles in a fractal, this seems a promising first approach to the study of interfaces between subdiffusive and regularly diffusive mediums. Therefore, in this chapter, we choose to investigate media with fractal compartments. Generalization to non-Markovian processes will be postponed due to the complexity of the problem. However, we note that scaling laws for non-Markovian processes with stationary increments are often the same as their Markovian counterparts. \sphericalangle

In this chapter, we aim to uncover insights into the optimization of reaction times mediated by subdiffusive compartments described by fractal networks. With this objective, we first describe how random walkers move in fractals, finding the corresponding Fokker-Planck equation in Section 6.1. Then, we analyze how the existence of a fractal compartment inside a regularly diffusive confining volume can be described with a Markovian framework (Section 6.2). We derive the equation providing the mean first passage time for random walkers to find a target in the center of the compartment (Section 6.3). Then, in Section 6.4, to test the validity of our theory, we perform simulations in a bond-percolation network and compare the simulations to the theoretical predictions. To complete the discussion, we study the possible optimisations of the mean first passage time that the compartment allows (Section 6.5). There, in Section 6.5, we show that if there is no accumulation (or deficiency) of stationary probability inside the compartment, it is possible to improve the mean first passage time even when movement inside the compartment is slower than outside (under some conditions which we identify).

6.1 | Theory of diffusion in fractals

Let us first remind the features of dynamics in fractals, in a way that can be generalized to describe compartments. A simple theory for transport in such environments was developed in O’Shaughnessy and Procaccia (1985), who adopted an effective, coarse grained description of the dynamics. In what follows, we briefly derive the equation that describes the evolution of the probability distribution function of the position of a random walker that moves in a fractal network centered at the origin of our coordinate system. The origin of space is assumed to be one of the sites of the fractal.

Assume a continuous time random walker, $r(t)$, where r is the distance to the origin, that moves in a fractal network of dimension d_f , in a bath of temperature T . As an addition to the original theory, we allow for the existence of a radial force, $F(r)$, which is not present in (O’Shaughnessy and Procaccia, 1985) but will be useful for the next sections. The probability of finding the random walker in a spherical shell between r and $r + dr$ at time t is given by $q(r, t)dr$ and it is assumed to follow a continuous (no jumps) Markovian dynamics, so that it satisfies a Fokker-Planck equation, which can be written as

$$\partial_t q(r, t) = \partial_r \left(\chi(r) \left[\beta \phi'(r) q(r, t) + \partial_r q(r, t) \right] \right), \quad (6.1)$$

without loss of generality. In Eq. (6.1), $\phi'(r) = \partial_r \phi(r)$ is the derivative of the free energy, $\phi(r)$, related to the entropic cost of moving inside the fractal (equivalent to an effective potential), $\chi(r)$ is a space dependent effective diffusivity and $\beta = 1/k_B T$, with k_B the Boltzmann constant. Note that, in the stationary state, one recovers $q_s(r) \equiv \lim_{t \rightarrow \infty} q(r, t) \sim e^{-\beta \phi(r)}$.

Since $\phi(r)$ is a free energy, it is related to the entropy of the fractal, $S(r) = k_B \ln \Omega(r)$, where $\Omega(r)$ is the number of possible configurations in a spherical shell of radius r to $r + dr$,

by the thermodynamic formula

$$\phi(r) = U(r) - TS(r) = U(r) - \beta^{-1} \ln \Omega(r). \quad (6.2)$$

Note that we have also allowed for an energetic potential, $U(r)$, to exist, such that there is a radial force $F(r) = -\partial_r U(r)$. From the definition of the fractal dimension, one knows that inside a volume of radius R the number of sites grows as $\sim R^{d_f}$ (Bunde and Havlin, 1996). It is then natural to see that in a spherical shell of radius r , the number of configurations, can be written as

$$\Omega(r) \sim r^{d_f-1}, \quad (6.3)$$

up to an unimportant¹ spatial cutoff related to the microscopic scale of the sites. Therefore, using Eq. (6.2),

$$\beta\phi'(r) = -\beta F(r) - \frac{d_f - 1}{r}. \quad (6.4)$$

For the effective diffusivity, $\chi(r)$, one assumes that it is a power law, $\chi(r) = Kr^{2-d_w}$, where d_w is known as the walk dimension and is defined in this way so that $\langle r^2(t) \rangle \sim t^{2/d_w}$. Note that, in a more natural approach, one could just use $\chi(r) = Kr^\alpha$ with a general exponent α . Then, when computing $\langle r^2(t) \rangle$, choose $\alpha = 2 - d_w$ so that $\langle r^2(t) \rangle \sim t^{2/d_w}$ and identifying the walk dimension.

The evolution of the propagator $q(r, t)$ can then be written as

$$\partial_t q(r, t) = \partial_r \left[Kr^{2-d_w} \left(-\beta F(r)q(r, t) - \frac{d_f - 1}{r}q(r, t) + \partial_r q(r, t) \right) \right], \quad (6.5)$$

where the entropic term, $-\frac{d_f-1}{r}q(r, t)$, can be absorbed into the derivative:

$$\partial_t q(r, t) = \partial_r \left[Kr^{2-d_w} \left(-\beta F(r)q(r, t) + r^{d_f-1} \partial_r \left(\frac{q(r, t)}{r^{d_f-1}} \right) \right) \right]. \quad (6.6)$$

However, in O'Shaughnessy and Procaccia (1985), the results are obtained for the propagator $p(\mathbf{r}, t)$ ², corresponding to the probability distribution function of the position \mathbf{r} , i.e., $p(\mathbf{r}, t)d\mathbf{r}$ is the probability that the random walker is inside a volume element $d\mathbf{r}$ centered at the position \mathbf{r} . If one assumes that there is spherical symmetry, which is often the case in self similar fractal networks, then, the angular coordinates can be integrated. In that case, one can think in terms of $p(r = |\mathbf{r}|, t)$, the propagator of one specific position \mathbf{r} , that is equal to all the other sites at distance r . One can connect the propagators by the following relation

$$q(r, t)dr = \int d\mathbf{r}' p(\mathbf{r}', t)\delta(|\mathbf{r}'| - r) = \Omega_{d_f} r^{d_f-1} p(r = |\mathbf{r}|, t)dr, \quad \forall \mathbf{r}: |\mathbf{r}|=r, \quad (6.7)$$

where $\Omega_{d_f} = 2\pi^{d_f/2}/\Gamma(d_f/2)$ is the surface area of the unitary sphere in a space of fractal

¹Unimportant because we take the derivative of $\ln \Omega(r)$, thus removing this dependency with the cutoff.

²The use of vectors as an identifier for a site is a clear abuse of notation, however, it gives an interesting (physical way) of interpreting fractal spaces

dimension. Note that $\Omega_n r^{n-1}$ is the Jacobian determinant in a n -dimensional space with spherical symmetry. Hereafter, for simplicity, we use the form $p(r, t)$ for $p(r = \mathbf{r}, t)$. Using the propagator $p(r, t)$, and ignoring the potential $U(r)$, one obtains

$$\partial_t p(r, t) = \frac{1}{r^{d_f-1}} \partial_r \left(r^{d_f-1} K r^{2-d_w} \partial_r p(r, t) \right). \quad (6.8)$$

This is the result of (O'Shaughnessy and Procaccia, 1985), that can be interpreted as a generalization of the Fokker-Planck equation to fractal spaces. It is possible to solve this differential equation and obtain $p(r, t|0, 0)$, i.e., the probability $p(r, t)$ given that the random walker starts at the origin:

$$p(r, t|0, 0) = \frac{d_w}{\Omega_{d_f} \Gamma(d_f/d_w)} \frac{1}{(K d_w^2 t)^{d_f/d_w}} \exp \left(-\frac{r^{d_w}}{K d_w^2 t} \right), \quad (6.9)$$

where the normalization $\int dr (\Omega_{d_f} r^{d_f-1}) p(r, t) = 1$ was used and $\Gamma(x)$ is the gamma function. This propagator has been analyzed and compared to simulations for the case of Sierpinski gaskets in (Klafter et al., 1991). There, the authors found that, for finite $\xi = r/t^{1/d_w}$ (corresponding to not too large jumps), the propagator is in good agreement with simulations and that, for large ξ (big jumps), there is no agreement. However, it must be noted that small jumps are the most common realizations of the process and Eq. (6.9) is a reasonable description of motion in a fractal network, at least as first approximation. Now that the propagator in a fractal is found one can find the moments of the random walker position, for example the second moment

$$\langle r^2(t) \rangle = \left(K d_w^2 \right)^{2/d_w} \frac{\Gamma((d_f + 2)/d_w)}{\Gamma(d_f/d_w)} t^{2/d_w}, \quad (6.10)$$

and so we confirm that d_w , is in fact the walk dimension. Here, d_w is the parameter indicating that there is anomalous diffusion, which is the case when $d_w \neq 2$.

Finally, for later use, we note that using the Chapman-Kolmogorov equation,

$$q(r, t|r_0, t_0) = \int_0^\infty dr' q(r, t|r', t') q(r', t'|r_0, t_0), \quad \text{with } t_0 < t' < t, \quad (6.11)$$

and deriving the variable t' , it is possible to obtain the backwards version of the O'Shaughnessy-Procaccia equation, i.e., how the propagator evolves when r_0 is varied (Gardiner, 1985):

$$\partial_t q(r, t|r_0, 0) = \frac{1}{r_0^{d_f-1}} \partial_{r_0} \left[r_0^{d_f-1} K r_0^{2-d_w} \partial_{r_0} q(r, t|r_0, 0) \right] + \beta F(r_0) K r_0^{2-d_w} \partial_{r_0} q(r, t|r_0, 0). \quad (6.12)$$

6.2 | Transport in a medium with a fractal compartment

In this section, we explain the interplay between the compartment and the rest of the d -dimensional confining space. As explained in the introduction, we use compartments of fractal dimension, $d_f < d$, to model the membraneless organelles, where diffusion happens according to the last section due to the complex interior. These compartments are embedded in an arbitrarily shaped confining space (the “cell”) of volume V , where normal diffusion happens in d -dimensional space. We allow for an energetic gain inside the compartment by setting the potential $U(r) = -E_0 < 0$ for $r < R$ and zero outside. This potential could come, for example, from the interaction between random walkers and the polymer matrix inside compartments; E_0 controls the stationary probability for the reactants to be inside the compartment. See Figure 6.1 for a scheme of the problem studied here.

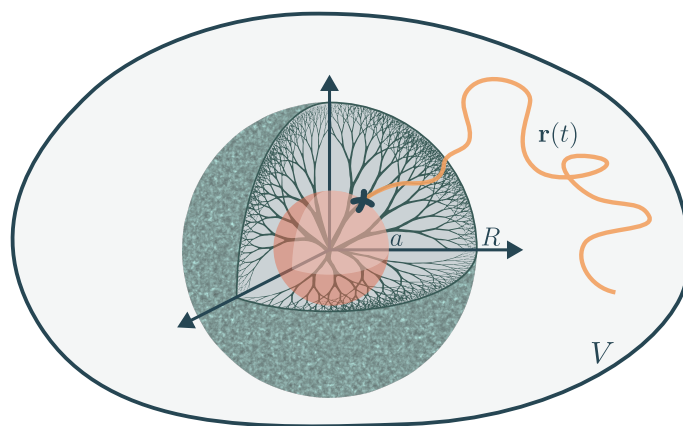


Figure 6.1: **Scheme of the problem studied in this chapter.** A random walker $r(t)$, started at $\mathbf{r}_0 = \mathbf{r}(0)$, moves in a confining volume, V , searching for a target of radius a inside a fractal compartment of radius R .

6.2.1 | Dynamics in free (infinite) space

Let us start by describing how one can introduce a compartment in free (infinite) space, i.e., when there is no confining volume. To facilitate the study, we chose to have a spherical compartment, and to treat the problem in the radial direction, so that the only relevant propagator is the radial probability distribution function, $q(r, t)$. In Section 6.3, we prove that this is in fact the only relevant propagator to find the mean first passage time when there is an external confinement. Using Eq. (6.6), one can write the dynamics inside and outside the compartment as

$$\partial_t q(r, t|r_0) = \partial_r \left(r^{d-1} D \partial_r \frac{q(r, t|r_0)}{r^{d-1}} \right) \quad \text{for } r > R, \quad (6.13)$$

$$\partial_t q(r, t|r_0) = \partial_r \left(r^{d_f-1} K r^{2-d_w} \partial_r \frac{q(r, t|r_0)}{r^{d_f-1}} \right) \quad \text{for } r < R, \quad (6.14)$$

where we note that, since the potential $U(r)$ is constant both inside and outside the compartment, it does not intervene in the dynamic equations. In fact, this energetic gain inside the compartment is only visible in the free energy, $\phi(r)$, as previously seen in Eq. (6.2). Using the general equation for Markovian dynamics, Eq. (6.1), it is possible to combine Eqs. (6.13) and (6.14)

$$\partial_t q(r, t|r_0) = \partial_r \left(\chi_e(r) \partial_r q(r, t|r_0) + \beta \phi'_e(r) \chi_e(r) q(r, t|r_0) \right) = \mathcal{P}_r q(r, t|r_0), \quad (6.15)$$

where we introduce the Fokker-Planck operator, \mathcal{P}_r and two new effective functions

$$\beta \phi_e(r) = \begin{cases} -(d-1) \ln r & , r > R \\ -(d_f - 1) \ln r - C - \beta E_0 & , r < R \end{cases} \quad \text{and} \quad \chi_e(r) = \begin{cases} D & , r > R \\ K r^{2-d_w} & , r < R \end{cases}. \quad (6.16)$$

The constant C is added for generality, since $\phi_e(r)$ appears only as a derivative. Note that these expressions are valid in the limit of large volumes when r is fixed, i.e., r is far from the confining boundaries.

In search problems, the target position is typically fixed and our objective is to determine the probability of reaching this point from an initial position r_0 . In such cases, it can be beneficial to model the dynamics of $q(r, t|r_0)$ using backward Fokker-Planck equations (Gardiner, 1985). Using the Chapman-Kolmogorov equation, Eq. (6.11), it is possible to obtain the backwards version of Eq. (6.15):

$$\partial_t q(r, t|r_0) = \partial_{r_0} \left(\chi_e(r_0) \partial_{r_0} q(r, t|r_0) \right) - \beta \phi'_e(r_0) \chi_e(r_0) \partial_{r_0} q(r, t|r_0) \equiv \mathcal{P}_{r_0}^\dagger q(r, t|r_0), \quad (6.17)$$

where the operator $\mathcal{P}_{r_0}^\dagger$ is the adjoint of \mathcal{P}_r at r_0 .

6.2.2 | Introduction of a confining volume: the stationary distribution

Let us now introduce a confining volume V , of arbitrary shape in the external domain. If one considers that the confining volume is large, it is natural to assume that, far from the confinement, the dynamics is the same as in the unconfined case. Then, close to confining boundaries, the dynamic must change. However, if the volume is large, the regions close to the boundaries become small in comparison to the volume and one can neglect their effects.

As a first result from this formalism let us find the stationary probability distribution function, $q_s(r)$. To do so, we state that, when r is far from the confinement, $q_s(r)$ must satisfy Eq. (6.15) in the stationary limit, i.e., $\partial_t q_s(r) = 0$. This is equivalent to say that the current $J_{\mathcal{P}_s}(r)$ must be constant, and, due to the confinement (where there is no current), it must be equal to zero. This leads to

$$q_s(r) = \frac{e^{-\beta \phi_e(r)}}{Z}, \quad (6.18)$$

where Z is a normalization constant. To find Z , we look at the stationary probability $p_s(\mathbf{r})$, previously defined as the probability distribution function of a position \mathbf{r} with $r = |\mathbf{r}|$. This function must be constant outside the compartment, $p_s(\mathbf{r}) = A/V$, with A a constant. If one assumes that the confining volume is large in comparison to the compartment, then A must be equal to unity. Using Eq. (6.7), we obtain

$$q_s(r) = \Omega_d r^{d-1}/V, \text{ for } r > R, \quad (6.19)$$

thus giving us $Z = V/\Omega_d$ when comparing with Eq. (6.18). Therefore, far from the confinement boundaries, the stationary probability, $q_s(r)$, is given by

$$q_s(r) = \frac{\Omega_d}{V} e^{-\beta\phi_e(r)} = \frac{\Omega_d}{V} \begin{cases} r^{d-1} & , r > R \\ r^{d_f-1} e^C e^{\beta E_0} & , r < R \end{cases}. \quad (6.20)$$

One interesting question is what is the probability to find the random walker inside the compartment in the stationary regime, P_s^{in} . By definition, we know that the available volume inside a fractal is ηR^{d_f} , where η is a parameter of the specific fractal used, and, therefore, adding the contribution of the energetic gain inside the compartment, E_0 , one has

$$P_s^{\text{in}} = e^{\beta E_0} \frac{\eta R^{d_f}}{V}. \quad (6.21)$$

Alternatively, one can use the stationary radial distribution from Eq. (6.20):

$$P_s^{\text{in}} = \int_0^R dr q_s(r) = \left(\frac{\Omega_d}{d_f} e^C \right) e^{\beta E_0} \frac{R^{d_f}}{V}. \quad (6.22)$$

Combining these two ways of writing P_s^{in} allows us to obtain C , and its relation to the fractal specific parameter η :

$$C = \ln \frac{d_f \eta}{\Omega_d}. \quad (6.23)$$

6.3 | Calculation of the mean first passage time

Now that the probability distribution function is well defined inside and outside the compartment one can find the mean first passage time, $\langle T \rangle$, for a particle that is started outside the compartment to reach a target of radius a inside the compartment.

First, inspired by (Condamin et al., 2007), we would like to find an expression for $\langle T \rangle$ as a function of the radial distribution function, $q(r, \Theta, t | r_0, \Theta)$, where we have added the angular components, Θ , to allow for arbitrary shapes of the confinement volume. We start

by writing a renewal equation

$$q(a, \Theta, t|r_0, \Theta_0) = \int_0^t d\tau \int d\Theta' q(a, \Theta, t - \tau|a, \Theta') f(\tau, \Theta'), \quad (6.24)$$

where $f(\tau, \Theta)$ is the probability distribution function that the first passage happens at time τ with angular coordinates Θ . One can also introduce $F(\tau) = \int d\Theta f(\tau, \Theta)$, the probability distribution function of the first passage time. If one subtracts $q_s(a, \Theta)$ on both sides of Eq. (6.24) and integrates over t from 0 to ∞ , we obtain

$$\begin{aligned} & \int_0^\infty dt [q(a, \Theta, t|r_0, \Theta_0) - q_s(a, \Theta)] \\ &= \int_0^\infty dt \int_0^t d\tau \int d\Theta' f(\tau, \Theta') [q(a, \Theta, t - \tau|a, \Theta') - q_s(a, \Theta)] - q_s(a, \Theta) \int_0^\infty dt \int_t^\infty d\tau F(\tau) \end{aligned} \quad (6.25)$$

$$= \int_0^\infty d\tau \int_\tau^\infty dt \int d\Theta' f(\tau, \Theta') [q(a, \Theta, t - \tau|a, \Theta') - q_s(a, \Theta)] - q_s(a, \Theta) \int_0^\infty d\tau \int_0^\tau dt F(\tau) \quad (6.26)$$

$$= \int d\Theta' \int_0^\infty d\tau f(\tau, \Theta') \int_0^\infty du [q(a, \Theta, u|a, \Theta') - q_s(a, \Theta)] - q_s(a, \Theta) \int_0^\infty d\tau \tau F(\tau) \quad (6.27)$$

$$= \int_0^\infty du \int d\Theta' \pi(\Theta') [q(a, \Theta, u|a, \Theta') - q_s(a, \Theta)] - q_s(a, \Theta) \langle T \rangle, \quad (6.28)$$

where the calculation steps are as follows: *i*) to obtain Eq. (6.25), one uses the fact that $1 = \int_0^\infty d\tau F(\tau) = \int_0^\infty d\tau \int d\Theta f(\tau, \Theta)$; *ii*) to obtain Eq. (6.26), the time integration order was reversed; *iii*) to obtain Eq. (6.27), the change of variables $t \rightarrow u = t - \tau$ was performed; *iv*) and, to obtain Eq. (6.28), we have introduced the splitting probability $\pi(\Theta) = \int_0^\infty d\tau f(\tau, \Theta)$, the probability that the first passage happens with angular coordinates Θ . Therefore the mean first passage time can be written as

$$q_s(a, \Theta) \langle T \rangle (a|r_0) = \int_0^\infty dt \left(\int d\Theta' \pi(\Theta') q(a, \Theta, t|a, \Theta') - q(a, \Theta, t|r_0, \Theta_0) \right), \quad (6.29)$$

To proceed further, we consider the large volume limit: we approximate $q(r, \Theta, t|r_0, \Theta_0)$, which in general depends on the shape of the confining volume, by its unconfined form, $q_\infty(r, \Theta, t|r_0, \Theta_0)$:

$$q_s(a, \Theta) \langle T \rangle (a|r_0) = \int_0^\infty dt \left(\int d\Theta' \pi(\Theta') q_\infty(a, \Theta, t|a, \Theta') - q_\infty(a, \Theta, t|r_0, \Theta_0) \right). \quad (6.30)$$

Note that, even though we approximate q by the unconfined q_∞ , the stationary probability $q_s(a, \Theta)$ is maintained as the confined one, and, in fact, it is the only contribution of the confinement to this equation. This result is true for any Θ , therefore, one can integrate over Θ and obtain

$$q_s(a) \langle T \rangle (a|r_0) = \int_0^\infty dt \left(\int d\Theta' \pi(\Theta') q_\infty(a, t|a, \Theta') - q_\infty(a, t|r_0, \Theta_0) \right). \quad (6.31)$$

Since $q_\infty(a, t|a, \Theta')$ is the propagator in unconfined space there is no reason for $q_\infty(a, t|r_0, \Theta_0)$ to depend in Θ_0 . Hence, the angular dependences can be omitted and, due to the nor-

malization of $\pi(\Theta)$, one obtains the final form of the equation for the mean first passage time

$$\bar{T}(a|r_0) \equiv q_s(a) \langle T \rangle (a|r_0) = \int_0^\infty dt (q_\infty(a, t|a) - q_\infty(a, t|r_0)), \quad (6.32)$$

where \bar{T} is the mean first passage times rescaled by the factor $q_s(a)$. Note that, even though the propagators in Eq. (6.32) only depend on the radial coordinates, we have just shown that this expression is true for any shape of the (exterior) confining volume V .

Applying the adjoint Fokker-Planck operator, $\mathcal{P}_{r_0}^\dagger$, defined in Eq. (6.17), to Eq. (6.32) one obtains

$$\mathcal{P}_{r_0}^\dagger \bar{T}(a|r_0) = \int_0^\infty dt (0 - \mathcal{P}_{r_0}^\dagger q_\infty(a, t|r_0)) = \delta(r_0 - a), \quad (6.33)$$

where we have used Eq. (6.15) and realized that $\lim_{t \rightarrow \infty} q_\infty(r, t|r_0) \rightarrow 0$. Therefore, the equation that we have to solve to find the mean first passage time is

$$\partial_{r_0} (\chi_e(r_0) \partial_{r_0} \bar{T}(a|r_0)) - \beta \phi'_e(r_0) \chi_e(r_0) \partial_{r_0} \bar{T}(a|r_0) = \delta(r_0 - a). \quad (6.34)$$

Let us start by finding the behaviour of \bar{T} close to the target. We realize that Eq. (6.34) can be rewritten as

$$\partial_{r_0} (e^{-\beta \phi_e(r_0)} \chi_e(r_0) \partial_{r_0} \bar{T}(a|r_0)) = e^{-\beta \phi_e(r_0)} \delta(r_0 - a), \quad (6.35)$$

which one can integrate from a^- to a^+ , i.e., from $a - \varepsilon$ to $a + \varepsilon$ with $0 < \varepsilon \rightarrow 0$, giving us the first boundary condition on the mean first passage time

$$\chi_e(a) \partial_{r_0} \bar{T}(a|r_0) \Big|_{r_0=a^+} = 1. \quad (6.36)$$

Note that, to find this result, we have used the fact that inside the target ($r < a$) the mean first passage time is trivially zero, and therefore the derivative, $\partial_{r_0} \bar{T}$, is also zero. A similar boundary condition was obtained for the case of narrow escape problem in (Bénichou and Voituriez, 2008), here, we have generalized it to compartmentalized media.

For $r_0 > a$, the delta term in Eq. (6.35) is zero, and one can write

$$\chi_e(r) \partial_r \bar{T}(a|r) = B e^{\beta \phi_e(r)}, \quad (6.37)$$

where $B = e^{-\beta \phi_e(a)}$ is an integration constant that can be obtained from the boundary condition at the target, Eq. (6.36). Integrating Eq. (6.37) over r from a to r_0 we obtain

$$\bar{T}(a|r_0) = \int_a^{r_0} dr \frac{e^{\beta \phi_e(r) - \beta \phi_e(a)}}{\chi_e(r)}, \quad \text{for } r_0 > a, \quad (6.38)$$

where we have used the fact that $\bar{T}(a|r)$ must be continuous. As we are interested in random walkers that start outside the compartment we have to find the solution for $r_0 > R$. By

substituting $\phi_e(r)$ and $\chi_e(r)$, one obtains

$$\bar{T}(a|r_0) = \frac{a^{d_f-1}}{K} \int_a^{R^-} dr r^{d_w-d_f-1} + \int_{R^-}^{R^+} dr \frac{e^{\beta\phi_e(r)-\beta\phi_e(a)}}{\chi_e(r)} + \frac{a^{d_f-1}e^C e^{\beta E_0}}{D} \int_{R^+}^{r_0} dr 1/r^{d-1}, \quad (6.39)$$

where the integral from R^- to R^+ is equal to zero due to the continuity of the mean first passage time³. Therefore, using the stationary probability $q_s(a) = d_f \eta a^{d_f-1} e^{\beta E_0} / V$ from Eq. (6.20), one obtains

$$\frac{\langle T \rangle (a|r_0 > R)}{V} = \frac{e^{-\beta E_0} R^{d_w-d_f} - a^{d_w-d_f}}{\eta d_f K} + \frac{1}{\Omega_d D} \int_R^{r_0} dr 1/r^{d-1}. \quad (6.40)$$

In particular, for a confining space of 3 dimensions one can write

$$\frac{\langle T \rangle (a|r_0 > R)}{V} = \frac{e^{-\beta E_0} R^{d_w-d_f} - a^{d_w-d_f}}{\eta d_f K} + \frac{1}{4\pi D} \left(\frac{1}{R} - \frac{1}{r_0} \right), \quad (6.41)$$

and, for a 2 dimensional confinement,

$$\frac{\langle T \rangle (a|r_0 > R)}{V} = \frac{e^{-\beta E_0} R^{d_w-d_f} - a^{d_w-d_f}}{\eta d_f K} + \frac{1}{2\pi D} \ln \left(\frac{r_0}{R} \right). \quad (6.42)$$

Additionally, one can also write the mean first passage time by integrating Eq. (6.38) for $r_0 < R$:

$$\frac{\langle T \rangle (a|r_0 < R)}{V} = \frac{e^{-\beta E_0} r_0^{d_w-d_f} - a^{d_w-d_f}}{\eta d_f K}. \quad (6.43)$$

We thus have a theoretical framework to predict the mean first passage time in compartmentalized media. In the next two sections, we evaluate the validity of this theory and question if the compartment can optimize the mean first passage time.

6.4 | The bond-percolation network and simulations

In this section we focus on the specific case of two-dimensional circular bond-percolation networks and use them as an example of a fractal compartment. The main goal of this section is to control the validity of our theory, which is easier in two dimensions than in three, due to the added complexity of the three dimensional simulations. First, we describe the bond-percolation networks:

- We create a square lattice of size L and spacing $\ell = 1$, which is the confining volume.
- Inside a circle of radius R , we remove bonds with probability p , close to the critical value $p_c = 0.5$.

³ $\int_{R^-}^{R^+} dr \frac{e^{\beta\phi_e(r)-\beta\phi_e(a)}}{\chi_e(r)} = \bar{T}(a|R^+) - \bar{T}(a|R^-) = 0$.

- For each simulation a new bond-percolation network is created so that one averages over the disorder.

Then, we develop a simulation scheme for the random walker:

- At each step, the random walker is moved to one of its z neighbours.
- The residence time at each site is τ_0/z , with $\tau_0 = 1$ defining the time units.
- If the random walker reaches the confinement, then, the step is ignored.
- The target is a circle of radius a , if the random walker enters this circle we say that there was a reaction.

Finally, we show the simulation results and compare them to the predictions of our theory.

6.4.1 | Parameters of the fractal

There are many examples of fractals that one could study to verify the veracity of our theory, which should be valid for any fractal medium compartment. Here, we will use the example of a bond-percolation network. To create the compartment, we take a lattice (in our case a square lattice with spacing $\ell = 1$) and then, with probability p , one goes over all bonds inside a centered circle of radius R (the compartment) and decides if the bond is removed or not. This process creates isolated clusters, i.e., sets of sites that are connected by bonds. The biggest of these clusters can be considered a fractal, when p is equal to the critical value, in this case $p = p_c = 0.5$ (Bunde and Havlin, 1996). In Figure 6.2 one can see how the connectivity of each node of the network changes when p increases. We chose this example of fractal because, as explained before, it is very natural to embed such a compartment in a larger square lattice.

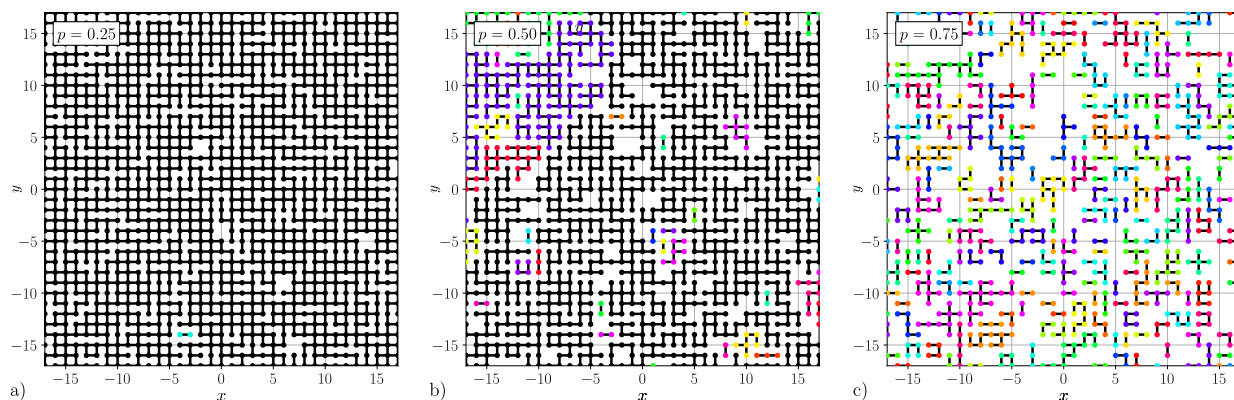


Figure 6.2: **Three realizations of a bond percolation network.** The different colors represent different clusters, i.e., groups of nodes that are connected by bonds. The biggest cluster is always represented in black. The order parameter is: a) $p = 0.25$; b) $p = 0.5$; c) $p = 0.75$.

When dealing with percolation networks, one usually considers the largest cluster to be the most relevant and the study is based on this cluster. However, in the case of crowded compartments, the full network is important and not only the biggest cluster. This is due to the possibility of a random walker to leave the fractal and reenter it from another cluster,

which would not be possible if the network was not connected to the exterior medium, since different clusters have no connecting paths. It is then easy to understand that, at critical order parameter, the total number of accessible sites in the fractal, N , is much higher than the one expected by traditional percolation theory, N_B , which would be the number of sites in the biggest cluster. This is clearly visible in Figure 6.3, where the biggest cluster (the one in black) has only 4419 sites, corresponding to 20% of all accessible sites, defined as the sites connected to the exterior medium. By counting the sites that are connected to the exterior of the percolation network, one can see that the existence of the percolation network does decrease the available space in the compartment, in the case of Figure 6.3, the number of accessible sites is $\approx 70\%$ of the total number of sites in the compartment.

In Figure 6.3 it is also possible to see that some big regions of the network might be ignored due to the fact that they are not connected to the exterior. For example the cluster in green, close to the center of the circle, is never visited by a random walker that is started outside this cluster. A discussion of the effect of these clusters in the simulation results will be given in Section 6.4.2.

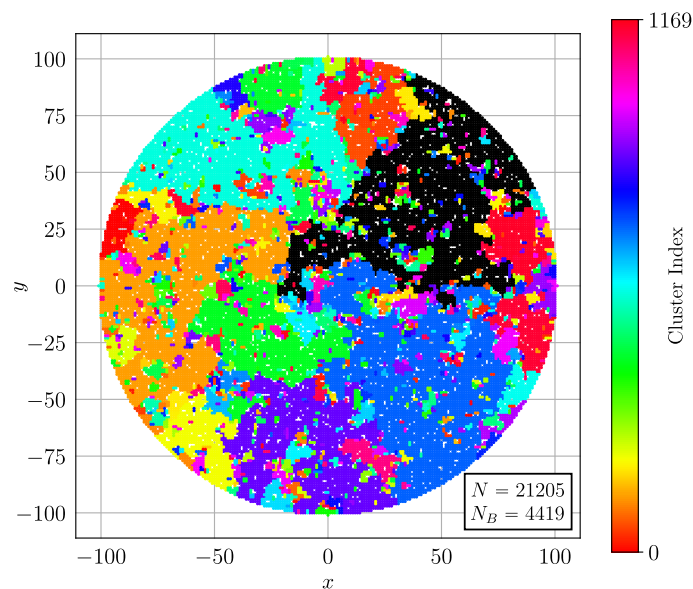


Figure 6.3: Realization of a circular bond percolation network at critical order parameter. Each bond at distance $r = \sqrt{x^2 + y^2} < R = 100$ is deleted with probability $p = 0.5$. Different colors represent different clusters. Each cluster is assigned an index, there are 1170 different clusters in this figure. The total number of accessible sites is $N = 21205$ and the number of sites in the biggest cluster is $N_B = 4419$.

The fractals created by bond-percolation networks have been extensively studied, (Bunde and Havlin, 1996). It has been found that the fractal dimension of the biggest cluster is exactly $d_f = 91/48$. Here, we will approximate the fractal dimension of the total compartment (with all accessible sites) to the one for the biggest cluster, so that $N(R) \approx \eta R^{d_f}$. In Figure 6.4 a fit is performed to obtain the parameter $\eta \approx 5.18$. Note that the real fractal dimension of the full compartment is larger than $d_f = 91/48$, as suggested by the faster growth of N as a function of R , however, the fit is still good and, as long as we stay in the range used for the fit, the results of the theory should still be valid.

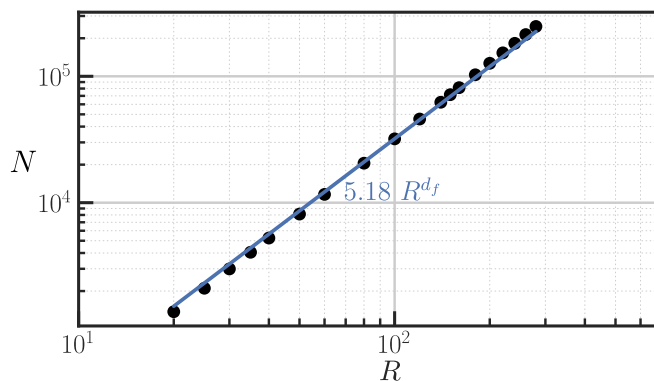


Figure 6.4: **Number of accessible sites as a function of the compartment radius.** Simulations results are shown as black circles and the fit, with $\eta \approx 5.18$ and $d_f = 91/48$, is represented by the continuous line.

6.4.2 | Simulation scheme

In this section, we discuss the simulation scheme used and its limitations. Simulations are started by creating a bond percolation network where one removes bonds inside the compartment of radius R with probability p . All bonds connecting to the exterior of the compartment ($r \geq R$) are kept in place so that connectivity between the two media is perfect. The exterior volume is simulated as a square lattice. After creating the circular network we start our random walker at a distance r_0 from the center of the fractal, which might land inside or outside the compartment. For each simulation a new fractal is created, thus eliminating the angular dependence of the simulation, i.e., the simulation can always be started in the x axis, without loss of generality. Then, as shown in Figure 6.5, the random walker moves to one of its z neighbours with uniform probability. This step takes a time τ_0/z , where we set $\tau_0 = 1$ defining the time units. This choice ensures that the stationary probability distribution function at each site, $p_s(\mathbf{r}_i) = 1/N$, is uniform; it is called the “edge centric dynamics” in (Masuda et al., 2017). Note that, at the confining boundary, we ignore steps that leave the confining volume, which is not compatible with the “edge centric dynamics”. However, as these events are rare (due to the simulations being performed at large volumes), one can still be confident that the stationary distribution remains uniform at every site in the bulk. Simulations end when the random walker reaches a target of radius a concentric with the compartment.

This simulation scheme has two main limitations. First, the random walker might start at a node that does not have any neighbours, in which case the simulation is aborted and ignored. The second problematic case is the one where the random walker is started inside a cluster that is not connected to the exterior, see Figure 6.3. This case is clearly impossible in the real system we want to model because random walkers are usually started outside the compartment and therefore cannot access this position. Two results can come out of this case: first, the simulation might never finish due to the fact that the random walker is trapped. In this case, the maximum time of the simulation is reached without a reaction and the simulation is ignored; then, the other possible outcome, is if the disconnected cluster

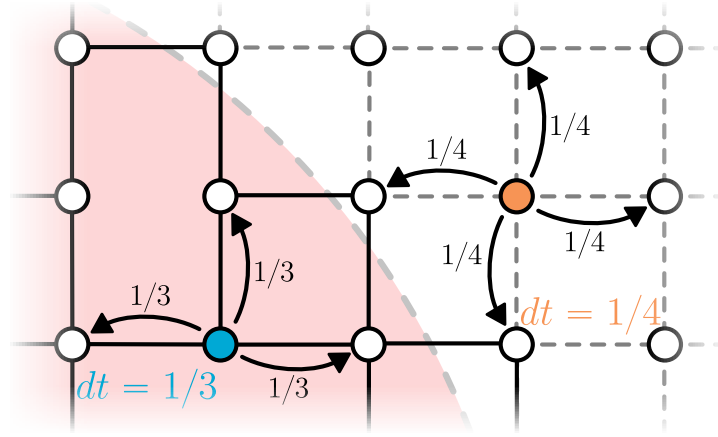


Figure 6.5: **Simulation scheme used inside and outside the compartment.** Two situations are represented, when a random walker moves inside the fractal compartment (blue node), and when it is outside the compartment (orange node). The waiting time dt at each site is also indicated.

intercepts the target. In that case a reaction might happen, giving us a misleading result from a system that is equivalent to a simple confinement with volume that is much smaller than V . We do not have a way of identifying this last case, thus making our simulations not perfect. However, as discussed before, these clusters only account for $\approx 30\%$ of the total number of sites and most do not intercept with the target, thus making us believe that the simulation results are still reasonable. Moreover, this problem does not appear when the random walker is started outside the compartment, which is the relevant region here, as we want to optimize reactions by coating a target with a subdiffusive compartment.

6.4.3 | Simulation results

Now that the fractal has been thoroughly characterized and the simulation scheme has been defined, it becomes possible to simulate random walks and measure the dynamic parameters. The first three parameters of interest are the walk dimension, d_w , the fractal diffusion constant, K , and the diffusion constant, D .

The walk dimension, d_w , has already been investigated in the literature and determined to be $d_w = 2.87(2)$ using the method of exact enumeration of random walks, (Majid et al., 1984). To determine the values of the diffusion constants, we conduct simulations of random walks that starts at the center of the circular compartment. These walks evolve to explore the entire confining volume, allowing us to measure the mean square radial position, see Figure 6.6. To identify the values of K and D , we employ Eq. (6.10)⁴. From Figure 6.6, we find that $K \approx 0.56$ and $D = 1$, which is the exact result for diffusion on a square lattice.

It is worth noting that the method used to determine these dynamic parameters may fail when the random walk is started within one of the disconnected clusters, effectively

⁴To find D one uses $d_f = 2$ and $d_w = 2$, resulting in $\langle r^2(t) \rangle = 4Dt$.

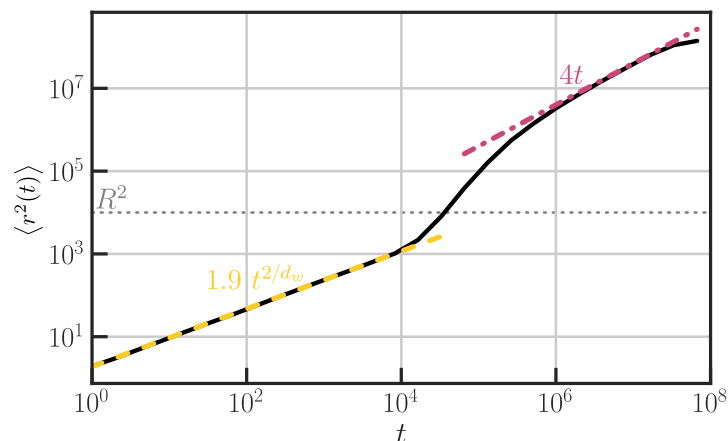


Figure 6.6: **Simulated $\langle r^2(t) \rangle$ for diffusion in a square confinement with a bond-percolation compartment.** Simulation results of a random walker that is started at the center of a random circular bond-percolation network connected to the exterior lattice. Here, $R = 100$, $V = 9 \cdot 10^8$ and $p = 0.5$.

trapping the walk inside the compartment. To circumvent this issue, we discard any random walks that have never exited the compartment. This is possible because the probability of remaining inside the cluster decreases exponentially. Therefore, by employing a sufficiently large maximum simulation time, the random walkers are virtually guaranteed to leave the compartment.

d_f	91/48
η	5.18
d_w	2.87(2)
K	0.56
D	1
E_0	0

Table 6.1: **Summary of the values identified by the simulations that are used to obtain our theoretical predictions.** The values shown in this table are written in natural units $l = 1 = \tau_0$, where l is the space between nodes and τ_0/z is the residence time on a node with z neighbours.

We are now in a position where the theory can be tested by comparison to simulations. A summary of the values used in our theory is given in Table 6.1. In Figure 6.7 it is possible to see that the theory matches the simulation results. Even though the result is not quantitatively perfect, it correctly describes the variation of the mean first passage time with the initial position r_0 and the compartment radius, R . Note that, even though the O’Shaughnessy-Procaccia theory (on which our analysis relies) is not an exact theory, the average precision of our theory (in the example of Figure 6.7) is around 10%. This is obtained without any fitting parameters, as a direct consequence of the slower, fractal, subdiffusion inside the compartment, and validates our formula for $\langle T \rangle$.

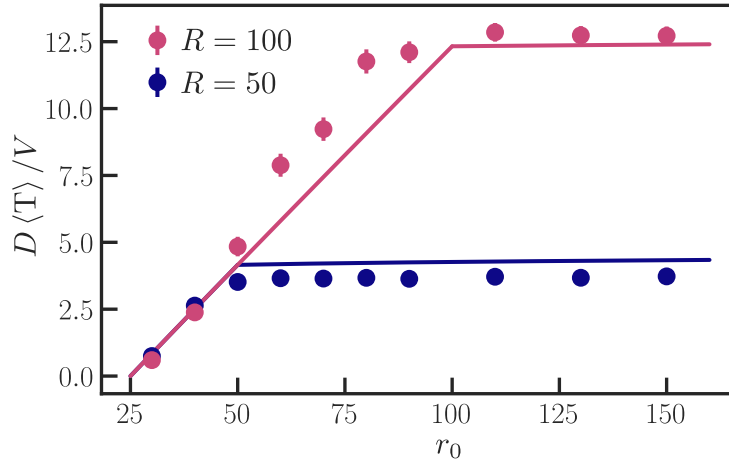


Figure 6.7: **Theoretical predictions and simulations results of the mean first passage time.** Theoretical prediction, Eq. (6.43) for $r_0 < R$ and Eq. (6.42) for $r_0 > R$, represented with continuous lines and simulation results with circles. Simulations were performed in a square confining volume with $V = 2.5 \cdot 10^5$, a circular compartment of radius $R = 50$ (lower line) and $R = 100$ (higher line) at critical order parameter, $p = 0.5$.

6.5 | Does the compartment facilitate reactions?

Now that we have a valid model for how a compartment influences the mean first passage time, one might ask if this compartment facilitates reactions, by decreasing the time that it takes for a reactant to find the target. First, we study the case where the external medium is of dimension $d = 3$ and then, if we find an optimization scheme, try to apply it to $d = 2$ for completeness. Let us assume that the random walker starts far from the compartment ($r_0 \gg R$), as would be the case in the biological problem, so that

$$\frac{\langle T \rangle_\infty}{V} = \frac{e^{-\beta E_0}}{\eta d_f K} \frac{R^{d_w - d_f} - a^{d_w - d_f}}{d_w - d_f} + \frac{1}{4\pi D} \frac{1}{R}. \quad (6.44)$$

The idea of this section is to compare $\langle T \rangle_\infty$ to the mean first passage time if there was no compartment, $\langle T \rangle_{\text{NC}}$,

$$\frac{\langle T \rangle_{\text{NC}}}{V} = \frac{1}{4\pi D} \frac{1}{a}, \quad (6.45)$$

equivalent to taking $R \rightarrow a$. Then, we check if the optimisation is possible even though movement is slower (at the target scale) inside the compartment,

$$K a^{2 - d_w} \ll D. \quad (6.46)$$

Note that this slow down is a necessary constraint when anomalous motion comes from crowding ($d_w > 2$), which cannot accelerate the dynamics, see Figure 6.6. Note that, if Eq. (6.46) holds, the dynamics at the scale of the compartment is even slower.

6.5.1 | Compartment with no energetic bonding

Let us start by assuming that there is no energetic incentive to entering the compartment, $E_0 = 0$. For simplicity, we will ignore numerical prefactors when dealing with extreme inequalities, i.e., \ll and \gg . To test if the compartment does facilitate reactions one is interested in having $\langle T \rangle_\infty \ll \langle T \rangle_{\text{NC}}$. Consequently, both terms in Eq. (6.44) must be smaller than $\langle T \rangle_{\text{NC}}/V$, so that

$$\frac{\langle T \rangle_\infty}{V} \ll \frac{\langle T \rangle_{\text{NC}}}{V} \Rightarrow \begin{cases} \frac{1}{DR} \ll \frac{1}{Da} \\ \frac{R^{d_w-d_f}}{\eta K} \ll \frac{1}{Da} \end{cases} \Rightarrow \begin{cases} R \gg a \\ \frac{K}{D} \gg \frac{aR^{d_w-d_f}}{\eta} \end{cases}, \quad (6.47)$$

where we have assumed that $d_w > d_f$, as it is usual for random walks on fractals. The last inequality can be further simplified by noticing that the volume inside a fractal object (with $d_f < 3$) must be smaller than the one inside a 3 dimensional object with the same radius,

$$\eta a^{d_f} < a^3. \quad (6.48)$$

Therefore, the necessary conditions to have optimization of the mean first passage time are

$$R \gg a \quad \text{and} \quad \frac{K a^{2-d_w}}{D} \gg 1, \quad (6.49)$$

which means that diffusion at the scale of the target, a , is faster inside the compartment than outside the compartment. This directly contradicts the condition for movement to be slower inside the compartment, Eq. (6.46). Therefore, the compartment does not allow faster (mean) first passage, even when the targets are small. This is physically due to two constraints of the system. The first is that we force diffusion to be slower, thus making it harder to have faster reactions. The second problem is that entering the compartment requires the passage through an “entropic” barrier, appearing from the crowding inside the compartment, thus decreasing the probability of having particles inside the compartment. We thus conclude that an optimisation is not possible in the absence of an energetic gain inside the compartment. One is then tempted to add an energetic gain to entering the compartment, so that the “entropic” barrier is neutralized. This is what we analyze in the next section.

6.5.2 | Compartment with energetic bonding

Let us now assume that there is an energetic gain, E_0 , when entering the compartment. It is obvious that, for $E_0 \rightarrow \infty$, the mean first passage time vanishes, because reactants become very concentrated near the target. Here, we ask whether one can accelerate a reaction without concentrating the reactants in the compartment, i.e., we choose the energetic gain so that the stationary probability to be inside the compartment is equal to that of being inside a volume (in $d = 3$) of the same radius, R ,

$$\eta R^{d_f} e^{\beta E_0} \sim R^3. \quad (6.50)$$

This is naturally equivalent to say that $q_s(R^-) = q_s(R^+)$. In this case one has

$$\frac{\langle T \rangle_\infty}{V} \sim \frac{R^{d_w-3}}{K} + \frac{1}{DR}, \quad (6.51)$$

where we have assumed that $d_w > d_f$. Comparing $\langle T \rangle_\infty$ to $\langle T \rangle_{\text{NC}}$, one obtains $R \gg a$ and

$$\frac{Ka^{2-d_w}}{D} \gg \left(\frac{R}{a}\right)^{d_w-3} = \left(\frac{a}{R}\right)^{3-d_w}. \quad (6.52)$$

If $d_w < 3$, i.e., the walk inside the compartment is not strongly subdiffusive⁵, this condition is consistent with the condition for slower movement inside the compartment, Eq. (6.46). Therefore, we have found a situation where the compartment facilitates reactions even though movement is slower inside the compartment and reactants are not more concentrated inside the target on average. This can be seen as a situation, $d_f < d_w < 3$, where the dynamical cost is compensated by the reduced space that has to be explored when inside the compartment and by the localization of the random walker close to the compartment and, consequently, the target.

6.5.3 | Is optimization still possible in two-dimensional space?

If one now studies the case of $d = 2$, the mean first passage time to be optimized is the one in Eq. (6.42). With the assumption that the energetic gain, E_0 , is so that the stationary probability to be inside the compartment is equal to that of being inside a volume (in $d = 2$) of the same radius, R ,

$$\eta R^{d_f} e^{\beta E_0} \sim R^2, \quad (6.53)$$

one can rewrite Eq. (6.42) as

$$\frac{\langle T \rangle}{V} \sim \frac{R^{d_w-2}}{K} + \frac{1}{D} \ln\left(\frac{r_0}{R}\right), \quad (6.54)$$

where we have assumed that $d_w > d_f$. The mean first passage time without a compartment is trivially written as

$$\frac{\langle T \rangle_{\text{NC}}}{V} \sim \frac{1}{D} \ln\left(\frac{r_0}{a}\right). \quad (6.55)$$

Stating that the compartment improves the reaction time is equivalent to say that

$$\frac{\langle T \rangle}{V} \ll \frac{\langle T \rangle_{\text{NC}}}{V} \Rightarrow \begin{cases} \frac{1}{D} \ln\left(\frac{r_0}{R}\right) \ll \frac{1}{D} \ln\left(\frac{r_0}{a}\right) \\ \frac{R^{d_w-2}}{\eta K} \ll \frac{1}{D} \ln\left(\frac{r_0}{a}\right) \end{cases} \Rightarrow \begin{cases} R \gg a \\ \frac{Ka^{2-d_w}}{D} \gg \left(\frac{R}{a}\right)^{d_w-2} / \ln\left(\frac{r_0}{a}\right) \end{cases}, \quad (6.56)$$

The last condition has two possible outcomes. If $d_w < 2$, then the compartment is superdif-

⁵We say that a walk is strongly subdiffusive if $d_w > 3$, corresponding to a Hurst exponent of $H < 1/3$ in a fractional Brownian motion.

fusives, which is not compatible with the concept of crowding. In fact, we do not know any fractal displaying superdiffusive transport. If $d_w > 2$ the condition for optimized reaction times is $\frac{Ka^{2-d_w}}{D} \gg \left(\frac{R}{a}\right)^{d_w-2} \gg 1$ which is inconsistent with the condition for slower movement inside the compartment, Eq. (6.46).

Therefore, in two-dimensional space, it is impossible to facilitate reactions with a fractal compartment that slows down movement (at least without overconcentrating the reactants inside the compartment). This was expected since, contrarily to the three-dimensional case, the mean first passage time does not diverge for small targets, see Section 2.1.4. Even if we allow for an energetic gain inside the compartment that forces continuous stationary probability at the interface⁶.

6.6 | Conclusion

In this chapter, we have studied how transport properties are modified in the presence of a fractal compartment embedded in a regular confining volume, where dynamics is described as regular diffusion. In particular, we have found the Fokker-Planck equations that govern the dynamics of the propagators in the compartmentalized space. We have also found the equation connecting the mean first passage to the propagators, which then allow us to find the mean first passage time as a function of the space properties and walk parameters.

Then, we have validated our theory by comparing the theoretical predictions to simulation results. These simulations were performed by introducing a circular compartment with a bond-percolation network of radius R inside the confining volume and allowing a random walker to freely search for a target inside the compartment.

Finally, we have shown that, if there is an energetic gain when entering the compartment (enough so that there is no deficiency of stationary probability inside), then, the mean first passage time can be optimised even when movement inside the compartment is slower. This is achieved when there is an energetic gain $E_0 > 0$ inside the compartment but for values of E_0 that make the stationary probability to be inside the compartment the same as that of being in an equivalent sphere of radius R where pure diffusion happens. This comes from the compact nature of the random walk inside the compartment, so that sites are visited many times before escaping far away in the surrounding volume. Therefore, our study determines in which conditions the change of dimensionality can be used to optimize first passage times for compartments, generalizing other results obtained for surface mediated diffusion or target searches in DNA.

⁶Note that if one takes a large energetic gain, $e^{\beta E_0} \gg R^{d-d_f}/\eta$, the reactants concentrate near the target and it is always possible to optimise $\langle T \rangle$ while keeping diffusion slower inside the compartment.

CONCLUSION AND PERSPECTIVES

In this thesis we have taken some steps towards a better understanding of non-Markovian processes and the effects of their intrinsic memory on the kinetics of different reaction mechanisms. In particular, we have studied three different reaction mechanisms in four cases. First, we have dealt with imperfect reactions that are generated by sink reactivity, where the failure to react does not influence the movement of the searcher. Then, we continued our study of imperfect reactions by studying gated (or intermittent) reactivity, characterized by a target that has two states, active and inactive. In the last two cases studied, we have assumed that reactions happen instantly upon first contact. First, we developed a theory for competitive events and then, outside the realms of non-Markovianity (but still studying subdiffusive motion), we studied the case of compartmentalized media.

In Chapters 3 and 4, we have introduced a formalism to quantify the kinetics of imperfect reactions of non-Markovian random walkers in confinement. Our theory covers the two imperfect reactivity mechanisms of sink reactivity and gated reactions. We have developed the formalism in one and two dimensions, with the eventual adaptation to three dimensions not presenting any new challenges. In the weakly reactive limit, for sufficiently subdiffusive processes, the deviation of the mean reaction time from the reaction controlled time is not equal to the mean first passage time (as expected if one takes a semi-Markovian approach), but diverges as a non-trivial exponent of reactivity that was analytically identified and checked with simulations.

Though we have only found the first moment of the reaction time random variable (the mean), we have reasons to believe that this could lead us to better understand the full distribution of reaction times. In fact, we suspect that the relation between the mean first passage time and the survival probability, obtained for the perfect case (Levernier et al., 2019), can be extended to the case of imperfect reactivity. In that case, one would be able to write

$$S_\kappa(t) \underset{t \rightarrow \infty}{\sim} \frac{\langle \text{RT} \rangle}{V} \frac{1}{t^{1-dH}}, \quad (7.1)$$

where $S_\kappa(t)$ is the survival probability, i.e., the probability density of not reacting before t , in the unconfined case. Since $S_\kappa(t)$ is connected to the distribution of reaction times, $F(t) = -\dot{S}_\kappa(t)$, this could give us an estimate of the probability for a reaction to be slower than expected. Furthermore, one can write the survival probability as the Laplace transform of the distribution of local times, ℓ_t ,

$$S_\kappa(t) = \langle e^{-\kappa \ell_t} \rangle, \quad \text{with} \quad \ell_t \equiv \int_0^t d\tau \delta[x(\tau)], \quad (7.2)$$

where the reactivity κ acts as a Laplace variable. From this relation, one can expect that the study of imperfect reactions could give some insight into the distribution of local times for non-Markovian processes, that are not well characterized (beyond the assessment that they exist). Moreover, one could also extend the study of imperfect reactions to different systems. For instance, we have only studied point-like and Gaussian targets, but what would happen if one considers a one dimensional random walker looking for a reaction at a uniformly reactive thick wall? Would our formalism helps us find the splitting probability, i.e., the distribution of reaction coordinates?

Ideally, one would also like to find a formalism that allows us to deal with partially reflective interfaces, so that the whole class of imperfect reaction can be explored in the non-Markovian regime. However, at this time there is still no clear path to study these problems in the case of non-Markovian processes. Nevertheless, the probability distribution function of $x(t)$ in the presence of a reflecting boundary (roughly) appears to be a truncated Gaussian (Vojta et al., 2019). One could then imagine that our self-consistent Gaussian ansatz could be employed to describe such situations.

Then, in Chapter 5, we have studied the problem of competitive events for non-Markovian processes. In the first part of the chapter, we described an experimental setup that allows us to record non-Markovian trajectories directly from the movement of a bead in a viscoelastic fluid. Then, we derived a theory of non-Markovian competitive events that can be tested with the trajectories obtained from the experiment. When testing the theoretical predictions of the splitting probability and the mean trajectory after reaction we find that the theory quantitatively predicts the correct values for all the viscoelastic solutions tested. Moreover, the experiment that tests the theoretical prediction for the mean trajectory after reaction is the first direct observation that, at the moment of reaction, the system (bead plus viscoelastic fluid) is not at equilibrium.

Though the experimental results are promising, one must mention that the non-Markovian effects are only visible when the distance between the targets is of the order of the size of the bead. This is in big part a problem of the experimental setup. To study these effects at a larger scale one could adapt the experiments in two ways. First, one can use more concentrated solutions, thus creating stronger memory effects that should affect the system at larger scales. Then, one would have to deal with the problem of the efficiency of data acquisition. One solution would be to develop a real-time tracking method that would only store the trajectories (and possibly a compressed version of the video). In this way, longer videos could be taken and with larger frame, thus allowing the beads to explore a bigger portion of space before leaving the frame.

Moreover, one could use also study imperfect reactions with a different experimental setup. By using optical tweezers, one could also create real targets with different reactivities, by changing the strength of the trapping force. First, reactivity could be measured by tracking the movement of beads in water, thus obtaining an accurate curve of reactivity as a function of the trapping force. Then, using different long polymer solutions of different concentrations,

one could create different ranges of memory effect (as in Chapter 5) and test the theories developed in Chapter 4. Furthermore, due to the flexibility of optical tweezers, one could also imagine experiments with more complex targets, such as semi-absorbing walls.

Finally, in Chapter 6, motivated by the existence of membraneless organelles in cells where movement is subdiffusive, we have studied the effect of compartments on first passage properties. Due to the difficulty of implementing interfaces in non-Markovian processes we had to limit our study to the case of Markovian processes. With the intent of creating a crowded environment inside the compartment, we considered that the interior of the compartment is a fractal, of fractal dimension smaller than the space outside the compartment. To treat this problem, we first derived a “diffusion equation” for a random walker that moves in a fractal subject to some external force. Then, by assuming that the compartment is spherical with a smaller spherical target inside, we derived the mean first passage time for random walkers that are started outside the compartment. Using a spherical cut of a bond percolation network, we developed a simulation scheme where one can test the theory previously developed. By comparing the simulations to the theoretical predictions of the mean first passage time, we found that the theory correctly describes the way the mean first passage time depends on the radius of the compartment and initial distance to the target. Moreover, we found that the introduction of a slower compartment might improve the reaction time as long as there is an energetic gain inside the compartment that is enough to force continuous concentration of probability.

The ideal continuation of the study of complex compartments would be to develop a full non-Markovian theory that incorporates interfaces. As mentioned above, one first (possible) step is the study of non-Markovian walks with reflective interfaces, which could later be adapted to introduce coefficients describing the switching dynamics between the two sides of an interface. Next, while staying on the Markovian case, one could also find the full probability distribution function of first passage times that is non-trivial as it incorporates a mixture of compact and non-compact random walks. Alternatively, one can go back to the original motivation to the study of compartmentalized media, and understand that the hypothesis that there is one target in the center of a spherical compartment is not really a good description of what happens inside membraneless organelles. Then, one could develop the theory to incorporate non-spherical compartments and, perhaps more relevant to the study of reaction kinetics in membraneless organelles, one could study the case where targets are uniformly distributed inside the compartments, which would probably change the optimisation conditions that we found in Chapter 6.

CONDITIONED GAUSSIAN PROCESSES AND PROJECTION FORMULAS

Let us assume that X, Y, Z are 3 Gaussian variables, fully described by the probability distribution function

$$p(X, Y, Z_1, \dots, Z_N) = \frac{1}{(2\pi)^{3/2} \sqrt{|\underline{\Sigma}|}} \exp\left(-\frac{1}{2}(\underline{x} - \underline{m})^T \underline{\Sigma}^{-1}(\underline{x} - \underline{m})\right), \quad (\text{A.1})$$

with

$$(\underline{x} - \underline{m}) = \begin{pmatrix} X - \langle X \rangle \\ Y - \langle Y \rangle \\ Z - \langle Z \rangle \end{pmatrix} \quad \text{and} \quad \underline{\Sigma} = \begin{pmatrix} \sigma_{X,X} & \sigma_{X,Y} & \sigma_{X,Z} \\ \sigma_{Y,X} & \sigma_{Y,Y} & \sigma_{Y,Z} \\ \sigma_{Z,X} & \sigma_{Z,Y} & \sigma_{Z,Z} \end{pmatrix}, \quad (\text{A.2})$$

where $\sigma_{A,B} \equiv \text{Cov}(A, B) = \sigma_{B,A}$ for $A, B = X, Y, Z$.

The idea here is to find the statistics of X and Y once Z is known. To this end, one is interested in finding the conditioned probability distribution function $p(X, Y|Z)$, that can be written as

$$p(X, Y|Z = Z_0) = \frac{p(X, Y, Z = Z_0)}{p(Z = Z_0)}, \quad (\text{A.3})$$

where every function is known due to the Gaussian nature of the random variables. It is then possible to calculate $p(X, Y|Z)$ by completing the squares in the exponential argument (Eaton, 2007). The resulting probability density is a bivariate Gaussian with means

$$\langle X|Z \rangle = \langle X \rangle - \frac{\sigma_{X,Z}}{\sigma_{Z,Z}}(\langle Z \rangle - Z_0), \quad (\text{A.4})$$

$$\langle Y|Z \rangle = \langle Y \rangle - \frac{\sigma_{Y,Z}}{\sigma_{Z,Z}}(\langle Z \rangle - Z_0), \quad (\text{A.5})$$

and covariance

$$\text{Cov}(X, Y|Z = Z_0) = \sigma_{X,Y} - \frac{\sigma_{X,Z}\sigma_{Y,Z}}{\sigma_{Z,Z}}. \quad (\text{A.6})$$

We note that the conditioned covariance does not depend on the condition applied, and the only influence of the value of Z_0 comes from the averages of the process.

In our case, these expressions are often useful to compute the mean of a process $x(t)$ given that it has been at some specific point at another time. Assume a Gaussian process with mean $m(t)$ and covariance $\sigma(t, t')$. To apply these equations to this case, one has to study

the conditioned probability distribution $p(x, t; y, t' | z_0, t_0)$. This simplifies the previous results to

$$\langle x(t) | x(t_0) = z_0 \rangle = m(t) - \frac{\sigma(t, t_0)}{\sigma(t_0, t_0)} (m(t_0) - z_0), \quad (\text{A.7})$$

$$\text{Cov}(x(t), x(t') | x(t_0) = z_0) = \sigma(t, t') - \frac{\sigma(t, t_0)\sigma(t_0, t')}{\sigma(t_0, t_0)}. \quad (\text{A.8})$$

We call these three equations the projection formulas.

SOLUTION TO A CLASS OF SECOND KIND VOLTERRA INTEGRAL EQUATIONS

In this appendix, we find the solution of the second kind Volterra Integral Equations of the form:

$$f(\tau) + \int_0^\infty dt K(t)f(t + \tau) = h(\tau), \quad (\text{B.1})$$

where all functions have positive support, i.e., $f(t) = 0 = K(t) = h(t) \forall t < 0$.

To solve this equation we start by considering a special source term, $h(\tau) = h_0(\omega)e^{i\omega\tau}$, and look for solutions of the type $f(\tau) = f_0(\omega)e^{i\omega\tau}$. For this special case the solution reads

$$f_0(\omega) = \frac{h_0(\omega)}{1 + \int_0^{+\infty} dt K(t)e^{i\omega t}}. \quad (\text{B.2})$$

Since Eq. (B.1) is linear, the superposition of solutions is itself a solution and to get a general solution one can just integrate over ω :

$$f(\tau) = \int_{-\infty}^{+\infty} \frac{d\omega}{2\pi} \hat{f}(\omega)e^{i\omega\tau} = \int_{-\infty}^{+\infty} \frac{d\omega}{2\pi} \frac{\hat{h}(\omega)}{1 + \int_0^{+\infty} dt K(t)e^{i\omega t}} e^{i\omega\tau}, \quad (\text{B.3})$$

where $\hat{f}(\omega) = \mathcal{F}[f(t)](\omega) = \int_{-\infty}^\infty dt f(t)e^{-i\omega t}$ is the Fourier transform of $f(t)$. For convenience, let us first analyze the case where $f(t) = y'(t)$. Integrating Eq. (B.3) over τ from 0 to t one obtains:

$$y(t) - y(0) = \int_0^t d\tau \int_{-\infty}^\infty \frac{d\omega}{2\pi} e^{i\omega\tau} \hat{y}'(\omega) \quad (\text{B.4})$$

$$= \int_{-\infty}^\infty \frac{d\omega}{2\pi} \left(\frac{e^{i\omega t} - 1}{i\omega} \right) \frac{1}{1 + \int_0^{+\infty} dt' K(t')e^{i\omega t'}} \left(\int_0^\infty d\zeta h(\zeta)e^{-i\omega\zeta} \right) \quad (\text{B.5})$$

$$= \int_0^\infty d\zeta h(\zeta) \int_{-\infty}^\infty \frac{d\bar{\omega}}{2\pi} e^{i\bar{\omega}\zeta} \frac{1 - e^{-i\bar{\omega}t}}{i\bar{\omega}} \frac{1}{1 + \int_0^{+\infty} dt' K(t')e^{-i\bar{\omega}t'}} \quad (\text{B.6})$$

$$= \int_0^\infty d\zeta h(\zeta) \int_{-\infty}^\infty \frac{d\bar{\omega}}{2\pi} e^{i\bar{\omega}\zeta} (1 - e^{-i\bar{\omega}t}) \widetilde{W}(i\bar{\omega}), \quad (\text{B.7})$$

where $\bar{\omega} = -\omega$ and $\widetilde{W}(s) = \int_0^\infty dt W(t)e^{-st} = 1/s(1 + \widetilde{K}(s))$ that is identified as a Laplace transform taken at the point $s = i\bar{\omega}$. Next, we realize that the integral on $\bar{\omega}$ is actually the Bromwich integral (or the Mellin's inverse formula) that can be used to compute the inverse Laplace transform.

$$y(t) - y(0) = \int_0^\infty d\zeta h(\zeta) \mathcal{L}^{-1} \left[(1 - e^{-st}) \widetilde{W}(s) \right] (\zeta) \quad (\text{B.8})$$

$$= \int_0^{+\infty} d\zeta h(\zeta) [\Theta(\zeta)W(\zeta) - \Theta(\zeta - t)W(\zeta - t)], \quad (\text{B.9})$$

and therefore the $y(t)$ is given by

$$y(t) = y(0) + \int_0^{+\infty} d\zeta W(\zeta) [h(\zeta) - h(\zeta + t)]. \quad (\text{B.10})$$

Therefore, to solve the integral equation one simply has to take the Laplace transform of the function $K(t)$, perform the inverse Laplace transform of $\widetilde{W}(s) = 1/s(1+\widetilde{K}(s))$ and compute the integral in Eq. (B.10). It is quite easy to see that the expression of $f(t) = y'(t)$ is

$$f(t) = - \int_0^\infty d\zeta W(\zeta) h'(\zeta + t). \quad (\text{B.11})$$

ASYMPTOTICS OF THE MEAN TRAJECTORY AFTER REACTION FOR THE FRACTIONAL BROWNIAN MOTION IN THE WEAKLY NON-MARKOVIAN REGIME

In this Appendix, we derive the asymptotic behaviours of the mean trajectory after reaction in the case of almost diffusive fractional Brownian motion. In this case, we write $\psi(t) = t^{2(\frac{1}{2}+\varepsilon)} = t + \varepsilon 2t \ln t$ and $\mu(t) = \varepsilon \mu_1(t)$. In Section 3.3, we have shown that the mean trajectory after reaction can be written as:

$$\mu_1(t) = \frac{x_0 \kappa}{\sqrt{2\pi}} \int_0^{+\infty} d\xi \int_0^{+\infty} d\zeta e^{\frac{1}{2}\kappa^2 \zeta} \operatorname{erfc}\left(\sqrt{\frac{1}{2}\kappa^2 \zeta}\right) \frac{e^{-\frac{x_0^2}{2\xi}}}{\xi^{3/2}} \ln\left(\frac{(\zeta+t+\xi)\zeta}{(\zeta+t)(\zeta+\xi)}\right). \quad (\text{C.1})$$

Let us first analyze the limiting case of high reactivity. Taking the limit $\kappa \rightarrow \infty$ one obtains the equation of the perfect case, previously found in (Guérin et al., 2016),

$$\mu_{1\infty}(t) = \frac{x_0}{\pi} \int_0^{+\infty} d\xi \int_0^{+\infty} d\zeta \frac{e^{-\frac{x_0^2}{2\xi}}}{\xi^{3/2}\sqrt{\zeta}} \ln\left(\frac{(\zeta+t+\xi)\zeta}{(\zeta+t)(\zeta+\xi)}\right), \quad (\text{C.2})$$

$$= -2x_0 \int_0^\infty d\xi e^{-\frac{x_0^2}{2\xi}} \frac{\sqrt{t} + \sqrt{\xi} - \sqrt{t+\xi}}{\xi^{3/2}}. \quad (\text{C.3})$$

Taking the limit $t \rightarrow 0$, one quickly finds that

$$\mu_{1\infty}(t) \xrightarrow[t \rightarrow 0]{} -2\sqrt{2\pi t}. \quad (\text{C.4})$$

However, if one takes the limit $t \rightarrow \infty$ in Eq. (C.3), the integral on ξ becomes divergent for large ξ , which we call an ultra-violet divergence. To solve this problem, we rescale the integration variable $\xi \rightarrow t\chi$ so that the ultra-violet divergence disappears, and the integral converges after taking the limit $t \rightarrow \infty$:

$$\mu_{1\infty}(t) \xrightarrow[t \rightarrow \infty]{} -2x_0 \int_0^\infty d\chi e^{-\frac{x_0^2}{2t\chi}} \frac{1 + \sqrt{\chi} - \sqrt{1+\chi}}{\chi^{3/2}} \xrightarrow[t \rightarrow \infty]{} 2x_0(\gamma - 2 + \ln(2x_0^2)) - 2x_0 \ln t, \quad (\text{C.5})$$

where $\gamma \approx 0.577$ is the Euler γ constant. The integral on χ was performed by Mathematica and only the limit for large time is shown.

One can also analyze the limiting case of low reactivity in Eq. (C.3), where, at first order, one can write:

$$\mu_{10}(t) = \frac{x_0 \kappa}{\sqrt{2\pi}} \int_0^\infty d\xi e^{-\frac{x_0^2}{2\xi} t \ln t + \xi \ln \xi - (\xi + t) \ln(\xi + t)} \frac{1}{\xi^{3/2}}. \quad (\text{C.6})$$

Taking the limit $t \rightarrow 0$ inside the integral one can find

$$\mu_{10}(t) \xrightarrow{t \rightarrow 0} \kappa t \ln t. \quad (\text{C.7})$$

The long time limit is also possible to obtain by rescaling the integration constant $\xi \rightarrow tx$ in Eq. (C.6) and only then, taking the limit $t \rightarrow \infty$

$$\mu_{10}(t) \xrightarrow{t \rightarrow \infty} \frac{\kappa x_0}{\sqrt{2\pi}} \frac{1}{\sqrt{t}} \int_0^\infty d\chi \frac{\chi \ln \chi - (1 + \chi) \ln(1 + \chi)}{\chi^{3/2}} \xrightarrow{t \rightarrow \infty} -2\kappa x_0 \sqrt{2\pi t}. \quad (\text{C.8})$$

We would now like to find the long and short time limits when κ is finite. To do this it is useful to study the derivative of $\mu_1(t)$, since one of the integrals can be performed:

$$\mu_1'(t) = \frac{x_0 \kappa}{\sqrt{2\pi}} \int_0^{+\infty} d\xi \int_0^{+\infty} d\zeta e^{\frac{1}{2}\kappa^2 \zeta} \operatorname{erfc}\left(\sqrt{\frac{1}{2}\kappa^2 \zeta}\right) \frac{e^{-\frac{x_0^2}{2\xi}}}{\xi^{3/2}} \frac{\xi}{(\zeta + t + \xi)(\zeta + t)} \quad (\text{C.9})$$

$$= -x_0 \kappa \sqrt{\frac{\pi}{2}} \int_0^\infty d\zeta e^{\frac{1}{2}\kappa^2 \zeta} \operatorname{erfc}\left(\sqrt{\frac{1}{2}\kappa^2 \zeta}\right) e^{\frac{1}{2}\frac{x_0}{t+\zeta}} \operatorname{erfc}\left(\sqrt{\frac{1}{2}\frac{x_0}{t+\zeta}}\right) \frac{1}{(t+\zeta)^{3/2}}. \quad (\text{C.10})$$

Let us start by looking at the long times limit. If one tries to perform the limit $t \rightarrow \infty$ in Eq. (C.10), the integral becomes ultra-violet divergent. The dependence on $t + \zeta$ of some terms indicates that ζ might scale with t , hence we rescale the integration variable, such that $\zeta \rightarrow tz$. With this change of variables the divergence disappears and, after taking the long time limit, the integral becomes

$$\lim_{t \rightarrow \infty} \mu_1'(t) = - \int_0^\infty dz \frac{x_0}{t \sqrt{z} (1+z)^{3/2}} = -\frac{2x_0}{t}. \quad (\text{C.11})$$

Therefore, the long time behaviour of the mean trajectory after reaction is

$$\mu_1(t) \xrightarrow{t \rightarrow \infty} C - 2x_0 \ln t, \quad (\text{C.12})$$

where C is a constant that can be calculated by looking at the equality $\lim_{t \rightarrow \infty} \int_0^t d\tau \mu_1'(\tau) = C - \lim_{t \rightarrow \infty} 2x_0 \int_1^t d\tau / \tau$.

To find the short time limit in Eq. (C.10), one can take $t \rightarrow 0$ to find that an infra-red divergence emerges due to the fact that the integrand behaves as $\sim \zeta^{-1}$ for small ζ . To

remove this divergence one is tempted to, just like before, rescale $\zeta \rightarrow tz$ and only after performing the limit $t \rightarrow 0$:

$$\mu'_1(t) \xrightarrow{t \rightarrow 0} - \int_0^\infty dz \frac{\kappa}{1+z}. \quad (\text{C.13})$$

However, this integral also displays a divergence, now an ultra-violet divergence. Seeing that the divergences happen in different extremes, one can split the integral in Eq. (C.10) in two different integrals: one, $I_1(t)$, from 0 to $\lambda \gg t$, with the rescaled integration variable; and another, $I_2(t)$, from $\lambda \ll 1$ to ∞ , with the original scaling of ζ . First, we will compute the integral from 0 to $\lambda \gg t$:

$$I_1(t) = - \int_0^{\lambda/t \gg 1} dz \frac{\kappa}{1+z} = - \int_0^1 dz \frac{\kappa}{1+z} - \int_1^{\lambda/t \gg 1} dz \left(\frac{\kappa}{1+z} - \frac{\kappa}{z} + \frac{\kappa}{z} \right) \quad (\text{C.14})$$

$$= -\kappa \ln 2 + \int_1^\infty dz \frac{\kappa}{z+z^2} - \int_1^{\lambda/t \gg 1} dz \frac{\kappa}{z} \quad (\text{C.15})$$

$$= -\kappa \ln \lambda + \kappa \ln t, \quad (\text{C.16})$$

where the first equality is true once one takes the limit $t \rightarrow 0$ after rescaling $\zeta \rightarrow tz$. Then, we subtract the diverging behaviour and add it again. Note that, if the integrand does not diverge for large arguments, then, taking the integral from 1 to $\lambda/t \gg 1$ is the same as integrating from 1 to ∞ . For the second term, the integral from $\lambda \ll 1$ to ∞ , one can use the same method, except that, now, there is no need of rescaling.

$$I_2(t) = -x_0 \kappa \sqrt{\frac{\pi}{2}} \int_{\lambda \ll 1}^\infty \frac{d\zeta}{\zeta^{3/2}} \operatorname{erfcx} \left(\sqrt{\frac{1}{2} \kappa^2 \zeta} \right) \operatorname{erfcx} \left(\sqrt{\frac{1}{2} \frac{x_0}{\zeta}} \right) \quad (\text{C.17})$$

$$= \int_{\lambda \ll 1}^1 d\zeta \frac{\kappa}{\zeta} + \int_0^1 d\zeta \left(\frac{-x_0 \kappa \sqrt{\pi/2}}{\zeta^{3/2}} \operatorname{erfcx} \left(\sqrt{\frac{1}{2} \kappa^2 \zeta} \right) \operatorname{erfcx} \left(\sqrt{\frac{1}{2} \frac{x_0}{\zeta}} \right) - \frac{\kappa}{\zeta} \right) \\ - x_0 \kappa \sqrt{\frac{\pi}{2}} \int_1^\infty \frac{d\zeta}{\zeta^{3/2}} \operatorname{erfcx} \left(\sqrt{\frac{1}{2} \kappa^2 \zeta} \right) \operatorname{erfcx} \left(\sqrt{\frac{1}{2} \frac{x_0}{\zeta}} \right) \quad (\text{C.18})$$

$$= \kappa \ln \lambda + C, \quad (\text{C.19})$$

where $\operatorname{erfcx} x = e^{x^2} \operatorname{erfc} x$ is the scaled complementary error function and C is a sum of two convergent integrals that do not depend on t .

It is then possible to see that, for short times, the mean trajectory after reaction reads

$$\mu_1(t) \xrightarrow{t \rightarrow 0} \kappa t \ln t. \quad (\text{C.20})$$

The fact that the long and short times do not match the ones in the limiting cases of reactivity indicates that there is a time scale, $1/\kappa^\alpha$ with $\alpha > 0$, that is relevant in describing the asymptotic behaviour of $\mu_1(t)$. In Section 3.3, we detail how to find this time scale and how the different behaviours found in this Appendix coexist in distinct time scales.

SELF-CONSISTENT EQUATIONS FOR COMPETITIVE FIRST PASSAGE EVENTS

In this appendix we derive the self-consistent equations that enable the calculation of $\mu_i(t)$. Note that the derivation performed in this appendix is an intermediate step of Section 5.2, where we develop a theory for the splitting probabilities. We then assume that the reader has seen the derivation of Eq. (5.45).

To find the limits of $\mu_i(t)$, we start by writing renewal equation describing the movement of the particle after one of the targets (at $x_1 = 0$ or $x_2 = L$) is met,

$$p(x_i, t; y, t + \tau) = \int_0^t dt' F(t') p(x_i, t; y, t + \tau | \text{FPT} = t'), \quad (\text{D.1})$$

where y is an arbitrary position that is reached a time $\tau > 0$ after meeting the target at t . By the definition of the process after reaction, one can also write

$$p_\pi(x, t; y, t + \tau) \equiv \int_0^\infty dt' F(t') p(x, t + t'; y, \tau + t + t' | \text{FPT} = t'). \quad (\text{D.2})$$

Using Eq. (5.37), $\int_0^A dt \int_0^t d\tau f(t, \tau) = \int_0^A du \int_0^{A-u} d\tau f(u + \tau, \tau)$, for any function $f(t, \tau)$, one can combine Eqs. (D.1) and (D.2) to write

$$\begin{aligned} & \int_0^A dt [p_\pi(x_i, t; y, t + \tau) - p(x_i, t; y, t + \tau)] \\ &= \int_0^A du \int_{A-u}^\infty dt' F(t') p(x_i, u + t'; y, u + t' + \tau | \text{FPT} = t'). \end{aligned} \quad (\text{D.3})$$

Then, multiplying this equation by y and integrating over y ,

$$\begin{aligned} & \int_0^A dt \left(\mathbb{E}[x_\pi(t + \tau) | x_\pi(t) = x_i] p_\pi(x_i, t) - \mathbb{E}[x(t + \tau) | x(t) = x_i] p(x_i, t) \right) \\ &= \int_0^A du \int_{A-u}^\infty dt' F(t') \mathbb{E}[x(u + t' + \tau) | x(u + t') = x_i; \text{FPT} = t'] p(x_i, u + t' | \text{FPT} = t') \\ &\equiv R(A, \tau), \end{aligned} \quad (\text{D.4})$$

where $\mathbb{E}[A | B = b; C = c]$ is the mean value of A given that $B = b$ and $C = c$. Introducing

the change of variables $u \rightarrow v = A - u$, $R(A)$ can be rewritten as

$$R(A, \tau) = \int_0^A dv \int_v^\infty dt' F(t') p(x_i, A - v + t' | \text{FPT} = t') \cdot \mathbb{E}[x(A - v + t' + \tau) | x(A - v + t') = x_i; \text{FPT} = t'] \quad (\text{D.5})$$

Similarly to the argument made to obtain Eq. (5.40), it is reasonable to assume that the mean position of the random walker does not go infinitely far from x_i in a time τ . Therefore, one can assume that there is a function (of only τ) $h(\tau)$ such that:

$$|\mathbb{E}[x(A - v + t' + \tau) | x(A - v + t') = x_i; \text{FPT} = t']| < h(\tau). \quad (\text{D.6})$$

Next, we argue that, for large t ($t \gg \tau$), $p(0, t + \tau | \text{FPT} = \tau) \approx p(0, t)$. And, since the cloud of probability of positions extends over a length t^H , it is natural to assume that $p(0, t) \sim K_0/t^H$. Therefore, for large A , one can write

$$p(x_i, A - v + t' | \text{FPT} = t') \underset{A \rightarrow \infty}{\sim} K_0/A^H. \quad (\text{D.7})$$

Using these two last conditions, Eqs. (D.6) and (D.7), one can write

$$R(A, \tau) < \frac{K_0}{A^H} h(\tau) \int_0^A dv S(v) < \frac{K_0}{A^H} h(\tau) \int_0^\infty dv S(v) = \frac{K_0 h(\tau) \langle T \rangle}{A^H}. \quad (\text{D.8})$$

Hence, for large A , $R(A, \tau)$ vanishes and Eq. (D.4) becomes

$$\int_0^\infty dt \left(\mathbb{E}[x_\pi(t + \tau) | x_\pi(t) = x_i] p_\pi(x_i, t) - \mathbb{E}[x(t + \tau) | x(t) = x_i] p(x_i, t) \right) = 0. \quad (\text{D.9})$$

From here, one can split the process $x_\pi(t)$ in two processes, one that has had the first encounter with the target at the left target, $x_{\pi_1}(t)$, and one at the right target $x_{\pi_2}(t)$. If one assumes that these processes are Gaussian with means $\mu_1(t)$, $\mu_2(t)$ and covariance $\sigma(t, t')$, then using the projection laws described in Appendix A, one can write the final integral equations that provide $\mu_j(t)$:

$$\int_0^\infty \frac{dt}{\sqrt{\psi(t)}} \left(\sum_{j=1,2} \pi_j \left[\mu_j(t + \tau) - (\mu_j(t) - x_i) \frac{\sigma(t + \tau, t)}{\psi(t)} \right] \exp\left(-\frac{(x_i - \mu_j(t))^2}{2\psi(t)}\right) - \left[x_0 - (x_0 - x_i) \frac{\sigma(t + \tau, t)}{\psi(t)} \right] \exp\left(-\frac{(x_i - x_0)^2}{2\psi(t)}\right) \right) = 0, \quad \forall_{i=1,2}, \quad (\text{D.10})$$

BIBLIOGRAPHY

- Bénichou, O., Grebenkov, D., Levitz, P., Loverdo, C., and Voituriez, R. (2010). Optimal reaction time for surface-mediated diffusion. *Phys. Rev. Lett.*, 105:150606.
- Bénichou, O., Moreau, M., and Oshanin, G. (2000). Kinetics of stochastically gated diffusion-limited reactions and geometry of random walk trajectories. *Phys. Rev. E*, 61(4):3388.
- Bénichou, O. and Voituriez, R. (2008). Narrow-Escape Time Problem: Time Needed for a Particle to Exit a Confining Domain through a Small Window. *Physical Review Letters*, 100(16):168105.
- Bénichou, O. and Voituriez, R. (2014). From first-passage times of random walks in confinement to geometry-controlled kinetics. *Phys. Rep.*, 539(4):225–284.
- Berg, H. C. and Purcell, E. M. (1977). Physics of chemoreception. *Biophys J*, 20(2):193–219.
- Berg, O. G. and von Hippel, P. H. (1985). Diffusion-controlled macromolecular interactions. *Annu Rev Biophys Biophys Chem*, 14:131–60.
- Bicout, D. J. and Burkhardt, T. W. (2000). Absorption of a randomly accelerated particle: gambler’s ruin in a different game. *J. Phys. A: Math. Gen.*, 33(39):6835.
- Bouchaud, J.-P., Bonart, J., Donier, J., and Gould, M. (2018). *Trades, Quotes and Prices: Financial Markets Under the Microscope*. Cambridge University Press.
- Brangwynne, C. P., Tompa, P., and Pappu, R. V. (2015). Polymer physics of intracellular phase transitions. *Nature Physics*, 11(11):899–904.
- Bray, A. J., Majumdar, S. N., and Schehr, G. (2013). Persistence and first-passage properties in nonequilibrium systems. *Advances in Physics*, 62:225–361. ADS Bibcode: 2013Ad-Phy..62..225B.
- Bressloff, P. C. (2020). Target competition for resources under multiple search-and-capture events with stochastic resetting. *Proc. Royal Soc. A*, 476(2242):20200475.
- Bressloff, P. C. (2021). First-passage processes and the target-based accumulation of resources. *Phys. Rev. E*, 103(1):012101.
- Bressloff, P. C. (2022). Narrow capture problem: An encounter-based approach to partially reactive targets. *Physical Review E*, 105(3):034141.
- Bressloff, P. C. and Newby, J. M. (2013). Stochastic models of intracellular transport. *Rev. Mod. Phys.*, 85:135–196.
- Bunde, A. and Havlin, S. (1996). *Fractals and disordered systems*. Springer, Berlin (Allemagne), 2nd revised and enlarged edition. edition.

- Burkhardt, T. W. (2000). Dynamics of inelastic collapse. *Physical Review E*, 63(1):011111.
- Chaigneau, A. and Grebenkov, D. S. (2022). First-passage times to anisotropic partially reactive targets. *Phys. Rev. E*, 105:054146.
- Cheviakov, A. F. and Ward, M. J. (2011). Optimizing the principal eigenvalue of the laplacian in a sphere with interior traps. *Math. Comp. Modelling*, 53(7-8):1394–1409.
- Collins, F. C. and Kimball, G. E. (1949). Diffusion-controlled reaction rates. *Journal of Colloid Science*, 4(4):425–437.
- Condamin, S., Bénichou, O., Tejedor, V., Voituriez, R., and Klafter, J. (2007). First-passage times in complex scale-invariant media. *Nature*, 450(7166):77–80.
- Condamin, S., Tejedor, V., Voituriez, R., Bénichou, O., and Klafter, J. (2008). Probing microscopic origins of confined subdiffusion by first-passage observables. *Proc. Natl. Acad. Sci.*, 105(15):5675–5680.
- Coppey, M., Bénichou, O., Voituriez, R., and Moreau, M. (2004). Kinetics of target site localization of a protein on dna: A stochastic approach. *Biophysical Journal*, 87(3):1640–1649.
- Davies, R. B. and Harte, D. S. (1987). Tests for hurst effect. *Biometrika*, 74(1):95–101.
- De Smedt, G., Godreche, C., and Luck, J. (2001). Partial survival and inelastic collapse for a randomly accelerated particle. *Europhys. Lett.*, 53(4):438.
- Delorme, M. and Wiese, K. J. (2015). Maximum of a fractional brownian motion: analytic results from perturbation theory. *Phys. Rev. Lett.*, 115(21):210601.
- Denn, M. M. (1990). Issues in viscoelastic fluid mechanics. *Annual Review of Fluid Mechanics*, 22(1):13–32.
- Dietrich, C. R. and Newsam, G. N. (1997). Fast and exact simulation of stationary gaussian processes through circulant embedding of the covariance matrix. *SIAM Journal on Scientific Computing*, 18(4):1088–1107.
- Dobramysl, U. and Holcman, D. (2020). Triangulation sensing to determine the gradient source from diffusing particles to small cell receptors. *Phys. Rev. Lett.*, 125(14):148102.
- Doi, M. (1975). Theory of diffusion-controlled reaction between non-simple molecules. i. *Chemical Physics*, 11(1):107–113.
- Doi, M. and Edwards, S. (1988). *The Theory of Polymer Dynamics*. International series of monographs on physics. Clarendon Press.
- Dolgushev, M., Guérin, T., Blumen, A., Bénichou, O., and Voituriez, R. (2015). Contact Kinetics in Fractal Macromolecules. *Physical Review Letters*, 115(20):208301.
- Doob, J. L. (1942). The brownian movement and stochastic equations. *Annals of Mathematics*, 43(2):351–369.

- dos Santos, M. A. F., Menon, L., and Anteneodo, C. (2022). Efficiency of random search with space-dependent diffusivity. *Phys. Rev. E*, 106:044113.
- Eaton, M. (2007). *Multivariate Statistics: A Vector Space Approach*. Institute of Mathematical Statistics. Lecture notes-monograph series. Institute of Mathematical Statistics.
- Elbaum-Garfinkle, S., Kim, Y., Szczepaniak, K., Chen, C. C.-H., Eckmann, C. R., Myong, S., and Brangwynne, C. P. (2015). The disordered p granule protein laf-1 drives phase separation into droplets with tunable viscosity and dynamics. *Proceedings of the National Academy of Sciences*, 112(23):7189–7194.
- Espenson, J. H. (1981). *Chemical kinetics and reaction mechanisms*.
- Ferrer, B. R., Gomez-Solano, J. R., and Arzola, A. V. (2021). Fluid viscoelasticity triggers fast transitions of a brownian particle in a double well optical potential. *Phys. Rev. Lett.*, 126(10):108001.
- Furst, E. M. and Squires, T. M. (2017). *Microrheology*. Oxford University Press.
- Gardiner, C. (1985). *Handbook of Stochastic Methods: For Physics, Chemistry and the Natural Sciences*. Lecture Notes in Mathematics. Springer Berlin Heidelberg.
- Gavrilova, A. A., Fefilova, A. S., Vishnyakov, I. E., Kuznetsova, I. M., Turoverov, K. K., Uversky, V. N., and Fonin, A. V. (2023). On the roles of the nuclear non-coding rna-dependent membrane-less organelles in the cellular stress response. *International Journal of Molecular Sciences*, 24(9).
- Ginot, F., Caspers, J., Krüger, M., and Bechinger, C. (2022). Barrier Crossing in a Viscoelastic Bath. *Physical Review Letters*, 128(2):028001.
- Grebenkov, D. S. (2010). Searching for partially reactive sites: Analytical results for spherical targets. *J. Chem. Phys.*, 132(3):01B608.
- Grebenkov, D. S. (2019). Imperfect diffusion-controlled reactions. *Chemical Kinetics: Beyond the Textbook*, pages 191–219.
- Grebenkov, D. S. (2020). Paradigm shift in diffusion-mediated surface phenomena. *Phys. Rev. Lett.*, 125:078102.
- Grebenkov, D. S. (2022). Statistics of diffusive encounters with a small target: three complementary approaches. *Journal of Statistical Mechanics: Theory and Experiment*, 2022(8):083205.
- Grebenkov, D. S., Metzler, R., and Oshanin, G. (2017). Effects of the target aspect ratio and intrinsic reactivity onto diffusive search in bounded domains. *New J Phys*, 19(10):103025.
- Grebenkov, D. S., Metzler, R., and Oshanin, G. (2018a). Strong defocusing of molecular reaction times results from an interplay of geometry and reaction control. *Communications Chemistry*, 1(1):96.

- Grebenkov, D. S., Metzler, R., and Oshanin, G. (2018b). Towards a full quantitative description of single-molecule reaction kinetics in biological cells. *Physical Chemistry Chemical Physics*, 20(24):16393–16401.
- Grebenkov, D. S., Metzler, R., and Oshanin, G. (2019). Full distribution of first exit times in the narrow escape problem. *New Journal of Physics*, 21(12):122001.
- Grebenkov, D. S. and Oshanin, G. (2017). Diffusive escape through a narrow opening: new insights into a classic problem. *Physical Chemistry Chemical Physics*, 19(4):2723–2739.
- Grebenkov, D. S. and Skvortsov, A. T. (2022). Mean first-passage time to a small absorbing target in three-dimensional elongated domains. *Physical Review E*, 105(5):054107.
- Grimm, M., Jeney, S., and Franosch, T. (2011). Brownian motion in a maxwell fluid. *Soft Matt.*, 7(5):2076–2084.
- Guérin, T., Bénichou, O., and Voituriez, R. (2013). Reactive conformations and non-markovian reaction kinetics of a rouse polymer searching for a target in confinement. *Phys. Rev. E*, 87:032601.
- Guérin, T., Dolgushev, M., Bénichou, O., and Voituriez, R. (2021). Universal kinetics of imperfect reactions in confinement. *Communications Chemistry*, 4(157):1–7.
- Guérin, T., Dolgushev, M., Bénichou, O., and Voituriez, R. (2023). Imperfect narrow escape problem. *Phys. Rev. E*, 107:034134.
- Guérin, T., Levernier, N., Bénichou, O., and Voituriez, R. (2016). Mean first-passage times of non-markovian random walkers in confinement. *Nature*, 534(7607):356–359.
- Hansen, S. D., Huang, W. Y. C., Lee, Y. K., Bieling, P., Christensen, S. M., and Groves, J. T. (2019). Stochastic geometry sensing and polarization in a lipid kinase–phosphatase competitive reaction. *Proceedings of the National Academy of Sciences*, 116(30):15013–15022.
- Hirose, T., Ninomiya, K., Nakagawa, S., and Yamazaki, T. (2023). A guide to membraneless organelles and their various roles in gene regulation. *Nature Reviews Molecular Cell Biology*, 24(4):288–304.
- Hyman, A. A., Weber, C. A., and Jülicher, F. (2014). Liquid-liquid phase separation in biology. *Annual Review of Cell and Developmental Biology*, 30(1):39–58. PMID: 25288112.
- Hänggi, P., Talkner, P., and Borkovec, M. (1990). Reaction-rate theory: fifty years after Kramers. *Reviews of Modern Physics*, 62(2):251–341.
- Höfling, F. and Franosch, T. (2013). Anomalous transport in the crowded world of biological cells. *Reports on Progress in Physics*, 76(4):046602.
- Isaacson, S. A., Mauro, A. J., and Newby, J. (2016). Uniform asymptotic approximation of diffusion to a small target: Generalized reaction models. *Phys. Rev. E*, 94(4):042414.

- Khokhlov, A. R. and Grosberg, A. Y. (1994). *Statistical physics of macromolecules*, volume 1. American Institute of Physics.
- Klafter, J., Zumofen, G., and Blumen, A. (1991). On the propagator of sierpinski gaskets. *Journal of Physics A: Mathematical and General*, 24(20):4835.
- Krug, J., Kallabis, H., Majumdar, S. N., Cornell, S. J., Bray, A. J., and Sire, C. (1997). Persistence exponents for fluctuating interfaces. *Physical Review E*, 56(3):2702–2712.
- Levernier, N., Bénichou, O., Voituriez, R., and Guérin, T. (2020). Kinetics of rare events for non-Markovian stationary processes and application to polymer dynamics. *Physical Review Research*, 2(1):012057.
- Levernier, N., Dolgushev, M., Bénichou, O., Voituriez, R., and Guérin, T. (2019). Survival probability of stochastic processes beyond persistence exponents. *Nature Communications*, 10(1):2990.
- Levernier, N., Mendes, T. V., Bénichou, O., Voituriez, R., and Guérin, T. (2022). Everlasting impact of initial perturbations on first-passage times of non-Markovian random walks. *Nature Communications*, 13(1):5319.
- Lin, F.-H., Liu, C., and Zhang, P. (2005). On hydrodynamics of viscoelastic fluids. *Communications on Pure and Applied Mathematics*, 58(11):1437–1471.
- Lindsay, A. E., Bernoff, A. J., and Ward, M. J. (2017). First passage statistics for the capture of a brownian particle by a structured spherical target with multiple surface traps. *Multiscale Modeling & Simulation*, 15(1):74–109.
- Lindsay, A. E., Kolokolnikov, T., and Tzou, J. C. (2015). Narrow escape problem with a mixed trap and the effect of orientation. *Phys. Rev. E*, 91:032111.
- Majid, I., Avraham, D. B., Havlin, S., and Stanley, H. E. (1984). Exact-enumeration approach to random walks on percolation clusters in two dimensions. *Phys. Rev. B*, 30:1626–1628.
- Majumdar, S. N., Rosso, A., and Zoia, A. (2010). Hitting probability for anomalous diffusion processes. *Phys. Rev. Lett.*, 104:020602.
- Masoliver, J., Lindenberg, K., and West, B. J. (1986). First-passage times for non-markovian processes: Correlated impacts on bound processes. *Phys. Rev. A*, 34(3):2351.
- Mason, T. G., Ganesan, K., van Zanten, J. H., Wirtz, D., and Kuo, S. C. (1997). Particle tracking microrheology of complex fluids. *Phys. Rev. Lett.*, 79:3282–3285.
- Mason, T. G. and Weitz, D. A. (1995). Optical measurements of frequency-dependent linear viscoelastic moduli of complex fluids. *Phys. Rev. Lett.*, 74:1250–1253.
- Masuda, N., Porter, M. A., and Lambiotte, R. (2017). Random walks and diffusion on networks. *Physics Reports*, 716-717:1–58.

- Mercado-Vásquez, G. and Boyer, D. (2019). First hitting times to intermittent targets. *Phys. Rev. Lett.*, 123:250603.
- Metzler, R. and Klafter, J. (2000). The random walk’s guide to anomalous diffusion: a fractional dynamics approach. *Physics Reports*, 339(1):1–77.
- Metzler, R., Oshanin, G., and Redner, S. (2014). *First-Passage Phenomena and Their Applications*. WORLD SCIENTIFIC.
- Min, W., Luo, G., Cherayil, B. J., Kou, S. C., and Xie, X. S. (2005). Observation of a power-law memory kernel for fluctuations within a single protein molecule. *Phys. Rev. Lett.*, 94:198302.
- Motti, S. G., Meggiolaro, D., Barker, A. J., Mosconi, E., Perini, C. A. R., Ball, J. M., Gandini, M., Kim, M., De Angelis, F., and Petrozza, A. (2019). Controlling competing photochemical reactions stabilizes perovskite solar cells. *Nature Photonics*, 13(8):532–539.
- Nakashima, K. K., Vibhute, M. A., and Spruijt, E. (2019). Biomolecular chemistry in liquid phase separated compartments. *Frontiers in Molecular Biosciences*, 6.
- O’Flynn, B. G. and Mittag, T. (2021). The role of liquid–liquid phase separation in regulating enzyme activity. *Current Opinion in Cell Biology*, 69:70–79. Cell Signalling.
- O’Shaughnessy, B. and Procaccia, I. (1985). Analytical Solutions for Diffusion on Fractal Objects. *Physical Review Letters*, 54(5):455–458.
- Panja, D. (2010). Anomalous polymer dynamics is non-markovian: memory effects and the generalized langevin equation formulation. *Journal of Statistical Mechanics: Theory and Experiment*, 2010(06):P06011.
- Pavliotis, G. A. (2014). Derivation of the Langevin Equation. Texts in Applied Mathematics, pages 267–282. Springer, New York, NY.
- Perry, S. L. (2019). Phase separation: Bridging polymer physics and biology. *Current Opinion in Colloid & Interface Science*, 39:86–97. Special Topic Section: Outstanding Young Researchers in Colloid and Interface Science.
- Redner, S. (2001). *A guide to First- Passage Processes*. Cambridge University Press, Cambridge, England.
- Reingruber, J. and Holcman, D. (2009). Gated narrow escape time for molecular signaling. *Phys. Rev. Lett.*, 103(14):148102.
- Rice, S. (1985). *Diffusion-Limited Reactions*. Elsevier.
- Sadhu, T., Delorme, M., and Wiese, K. J. (2018). Generalized arcsine laws for fractional brownian motion. *Physical Review Letters*, 120(4):040603.
- Scher, Y., Kumar, A., Santhanam, M., and Reuveni, S. (2022). Continuous gated first-passage processes. *arXiv preprint arXiv:2211.09164*.

- Scher, Y. and Reuveni, S. (2021a). Gated reactions in discrete time and space. *The Journal of Chemical Physics*, 155(23):234112.
- Scher, Y. and Reuveni, S. (2021b). Unified approach to gated reactions on networks. *Physical Review Letters*, 127(1):018301.
- Schmitz, K. S. and Schurr, J. M. (1972). Role of orientation constraints and rotational diffusion in bimolecular solution kinetics. *The Journal of Physical Chemistry*, 76(4):534–545.
- Shoup, D., Lipari, G., and Szabo, A. (1981). Diffusion-controlled bimolecular reaction rates. The effect of rotational diffusion and orientation constraints. *Biophysical Journal*, 36(3):697–714.
- Shoup, D. and Szabo, A. (1982). Role of diffusion in ligand binding to macromolecules and cell-bound receptors. *Biophysical Journal*, 40(1):33–39.
- Sokolov, I. M. (2012). Models of anomalous diffusion in crowded environments. *Soft Matter*, 8(35):9043–9052.
- Spouge, J. L., Szabo, A., and Weiss, G. H. (1996). Single-particle survival in gated trapping. *Phys. Rev. E*, 54:2248–2255.
- Squires, T. M. and Mason, T. G. (2010). Fluid mechanics of microrheology. *Annual review of fluid mechanics*, 42:413–438.
- Vaccario, G., Antoine, C., and Talbot, J. (2015). First-passage times in d -dimensional heterogeneous media. *Phys. Rev. Lett.*, 115:240601.
- Van Kampen, N. (1992). *Stochastic Processes in Physics and Chemistry*. North-Holland Personal Library. Elsevier Science.
- van Kampen, N. G. (1998). Remarks on non-markov processes. *Brazilian Journal of Physics*, 28:90–96.
- Vojta, T., Skinner, S., and Metzler, R. (2019). Probability density of the fractional langevin equation with reflecting walls. *Phys. Rev. E*, 100:042142.
- Walter, B., Pruessner, G., and Salbreux, G. (2021). First passage time distribution of active thermal particles in potentials. *Physical Review Research*, 3(1):013075.
- Wei, Q.-H., Bechinger, C., and Leiderer, P. (2000). Single-file diffusion of colloids in one-dimensional channels. *Science*, 287(5453):625–627.
- Wiese, K. J. (2019). First passage in an interval for fractional brownian motion. *Physical Review E*, 99(3):032106.
- Wilemski, G. and Fixman, M. (1974a). Diffusion-controlled intrachain reactions of polymers. I Theory. *The Journal of Chemical Physics*, 60(3):866–877.

- Wilemski, G. and Fixman, M. (1974b). Diffusion-controlled intrachain reactions of polymers. II Results for a pair of terminal reactive groups. *The Journal of Chemical Physics*, 60(3):878–890.
- Wong, G. P., Mair, R. W., Walsworth, R. L., and Cory, D. G. (2001). Measurement of persistence in 1d diffusion. *Phys. Rev. Lett.*, 86(18):4156.
- Zhang, B. and Herman, P. K. (2020). It is all about the process(ing): P-body granules and the regulation of signal transduction. *Current Genetics*, 66(1):73–77.
- Zhao, Y. G. and Zhang, H. (2020). Phase separation in membrane biology: The interplay between membrane-bound organelles and membraneless condensates. *Developmental Cell*, 55(1):30–44.
- Zhou, H. and Zwanzig, R. (1991). A rate process with an entropy barrier. *The Journal of Chemical Physics*, 94(9):6147–6152.
- Zwanzig, R. (2001). *Nonequilibrium Statistical Mechanics*. Oxford University Press.